

Copyright is owned by the Author of the thesis. Permission is given for a copy to be downloaded by an individual for the purpose of research and private study only. The thesis may not be reproduced elsewhere without the permission of the Author.

PALEOSEISMOLOGY, SEISMIC HAZARD AND VOLCANO-TECTONIC INTERACTIONS IN THE TONGARIRO VOLCANIC CENTRE, NEW ZEALAND

A thesis presented in partial fulfilment of the requirements for the degree of

Doctor of Philosophy

in

Earth Science

at Massey University (Palmerston North, Manawatu)

New Zealand

By

MARTHA GABRIELA GÓMEZ VASCONCELOS

Supervisor: SHANE CRONIN

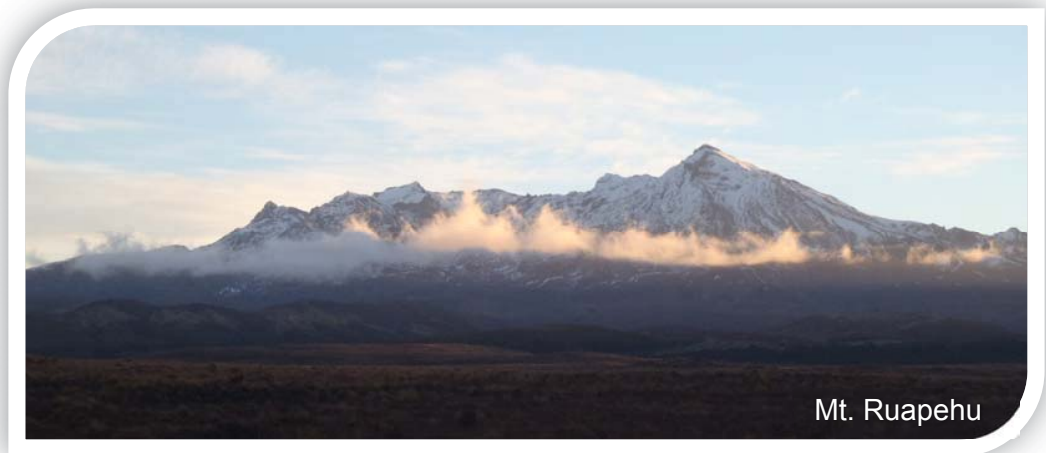
Co-supervisors: PILAR VILLAMOR (GNS Science), ALAN PALMER, JON PROCTER AND BOB STEWART



2017



To my family and Denis Avellán, who stand by me, no matter what.
I love you!



'It is not the mountain we conquer, but ourselves'. Sir Edmund Hillary

With passion, patience and persistence...

Abstract

At the southern part of the Taupo Rift, crustal extension is accommodated by a combination of normal faults and dike intrusions, and the Tongariro Volcanic Centre coexists with faults from the Ruapehu and Tongariro grabens. This close coexistence and volcanic vent alignment parallel to the regional faults has always raised the question of their possible interaction. Further, many periods of high fault slip-rate seem to coincide with explosive volcanic eruptions. For some periods these coincidences are shown to be unrelated; however, it remains important to evaluate the potential link between them. In the Tongariro Graben, the geological extension was quantified and compared to the total geodetic extension, showing that 78 to 95% of the extension was accommodated by tectonic faults and only 5 to 22% by dike intrusions. Within the latter, 4 to 5% was accommodated by volcanic eruptions and 18 to 19% by arrested dike intrusions, with an unknown percentage of hybrid extension. Short-term variations in fault slip-rates and volcanic activity for the last 100 ka in the Tongariro Volcanic Centre may have been influenced by static stress transfer between adjacent faults (within <20 km from the source) and dike intrusions (within <10 km), or by fluctuations in magma input through time. The amount of magma involved in the rifting process will condition the predominant extension mechanism and thus influence the predominant type of volcano-tectonic interaction. A record of volcanic and seismic activity for the last 250 ka was assembled, from new and published studies. This was used to analyse the spatio-temporal associations between volcanic and seismic activity in the southern Taupo Rift. Data on the faulting history, slip-rate variation and seismic hazard of the Upper Waikato Stream, Wahianoa, Waihi and Poutu faults formed the core of the analysis. These faults are capable of producing a M_w 7.2 earthquake with a single-event displacement of 2.9 m, posing an important hazard to the region. Data gathered in this study provides an update to the National Seismic Hazard Model for New Zealand.

Acknowledgments

This thesis is a very special project, accomplished with the help of very special people. I am deeply grateful to all those whose enthusiasm and support helped me get through tough times and make this dream come true.

Special thanks to Pilar Villamor, for her valuable guidance and commitment, for her shared knowledge, friendship and great assistance throughout this process.

Many thanks to my main supervisor, Shane Cronin, for his support and for giving me the opportunity to work in this project, allowing my New Zealand dream to come true.

To my supervision team, for their support throughout this experience: Pilar Villamor, Shane Cronin, Alan Palmer, Jon Procter and Bob Stewart, many thanks for the good times out in the field, for their tireless efforts to improve the manuscript, patience, lessons, discussions, support and friendship.

Thanks to the Volcanic Risk Solutions group and the Institute of Agriculture and Environment in Massey University; and to GNS science staff. To the Department of Conservation, the NZ Forest Trust, the New Zealand National Army at Waiouru and the Tongariro National Park, for allowing access to do field work. Special thanks to Kate Arentsen, Liza Haarhoff and Anja Moebis for her support and for dealing with all the administrative and exhaustive logistic issues. Also, Georg Zellmer, Gert Lube, Clel Wallace, Karoly Nemeth, Mark Bebbington, Maggi Damaschke, Rafael Torres, Szabolcs Kosik, Braden Walsh, Maricar Arpa, Eric Breard, Ermanno Brosch, Adam Neather, Manu Tost, Gabor Kereszturi, Javier Agustin and Natalia Pardo. Thanks to Dougal Townsend and Graham Leonard for providing unpublished stratigraphic data and maps; and to Salman Ashraf for providing the digital surface model.

Thanks to the financial support provided by a Massey University Doctoral Research Scholarship and by a Mexican scholarship from CONACyT. Further field support was

gratefully received via the “Learning to Live with Volcanic Risk” programme within the New Zealand Natural Hazards Research Platform.

Many thanks to my wonderful family; my parents Martha Vasconcelos and Ramón Gómez, who have taught me so much and who awoke in me the passion for volcanoes and nature, for their immense love and unconditional support; to my sisters Adriana and Mariana, my brother in law Sergio and my adorable niece Luisa, for always being so close to me and believing in me, you mean so much to me; and to all my relatives in Mexico, for their love and support.

Thanks to my friends in Palmy, my kiwi family: Javier Agustín, Diana Cabrera, Anita Mar, Patry Rubio, Majela González, Yimi Yapura, Luca Panizzi, Omar Cristobal, Angie Denes, Gabor Kereszturi, Zsuzsa Szmolinka, Szabolcs Kósik, Daniel Salazar, Cindy Chanci, Nura Majzoub, Sole Navarrete, Roberto Calvelo, Marcela Humphrey, Manu Tost, Juliana Velandia, Istvan Hajdu, Paty Alborn, Paty Ham, Mauricio Maldonado, Caro Lozada, Anai Hernandez, Pao Villacis, Kwan Maitrarat, Ceci Falla, Sam McColl, Rafa Torres, Freddy Dondin, Aniek Hilkens, Braden Walsh, Eric Breard, Laila Prae, Lovisa Ekelund, John Quintanilla, Ermanno Brosch, Vilma Rodríguez, German Molano and Alvaro Mehrle. They gave me the energy, empathy and enthusiasm I needed in good and not so good days, they made this experience more enjoyable, I will never forget them!

Thanks to my friends in México: Marthita Cortes, Vivi Ramírez, Ximena Delgado, Magda Velázquez, Susy Osorio, Diana Soria, Idana Trejo, Jennifer Marrón, Teresita Méndez, Fernando Romero, Jaime Tapia, Lucy Tapia, Judith Gasca, Pepe Moreno, Tatty Sanchez, Patty López, Mayra Díaz, Paula Perezgil, Agnes Samper, Mimí Trujillo, Adrián Jiménez, Judith Espino, Ale Huéramo, Lidia Flores, Tete Godínez, Rocy Pedraza, Monica Guizar, Adriana Cerda, Ale Gutiérrez, José Torres, Memo Cisneros, Juan Sánchez, Lupita, María López de Lara, etc.; also to my friends in Nicaragua,

USA, Europe, and other places around the world, for their support and wonderful friendship even through the distance.

Many thanks to Víctor Hugo Garduño and José Luis Macías, my first mentors, who showed me the way to science, volcanoes and faults; for their support and encouragement to discover the mysteries of geosciences.

And last, but not least, to my love, Denis Avellán, for his patience, support, encouragement and immense love he shows me every day in every way.



Table of Contents

ABSTRACT	iii
ACKNOWLEDGMENTS	iv
TABLE OF CONTENTS	vii
LIST OF FIGURES	x
LIST OF TABLES	xvii
LIST OF ABBREVIATIONS	xix
CHAPTER 1. INTRODUCTION	1
1.1 Research problem and motivation	1
1.2 Objectives	5
1.3 Thesis outline	6
CHAPTER 2. LITERATURE REVIEW AND STUDY AREA	9
2.1 Paleoseismology	9
2.2 Volcanic Rifts	10
2.2.1 Morphology of faults in volcanic rifts	10
2.3 Dike Intrusion and emplacement	13
2.3.1 Volcanic load as an influence on fault and dike patterns	16
2.3.2 Seismogenic depth as an influence on dike patterns	17
2.4 Volcano-tectonic interactions	19
2.4.1 Historical examples of volcano-tectonic interactions	22
2.5 The study area: The Tongariro Volcanic Centre	27
2.5.1 Active Tectonics of New Zealand	27
2.5.2 Regional Geology	30
2.5.2.1 The magmatic system of the TgVC	31
2.5.3 Structural Geology	36
2.5.4 Eruptive History	39
2.5.4.1 Stratigraphic summary	44
2.6 Magma-tectonic interactions in the North Island	47
CHAPTER 3. METHODOLOGY	49
3.1 Desk study methods	49
3.2 Fieldwork methods	50
3.3 Data analysis methods	53
CHAPTER 4. RESULTS: Earthquake history at the eastern boundary of south Taupo Volcanic Zone.	57
4.1 Abstract	59
4.2 Introduction	59
4.3 Geological and structural setting	60
4.4 Volcanic history and stratigraphy	62
4.5 Active faulting: the Rangipo and Wahianoa faults	64
4.6 Methods	66
4.7 Results of paleoseismic analysis	71
4.7.1 Upper Waikato Stream Fault	71
4.7.2 Wahianoa Fault	82
4.8 Discussion	84
4.8.1 Is the Upper Waikato Stream Fault part of the Rangipo Fault or part of the Wahianoa Fault?	84
4.8.2 The role of the Wahianoa, Upper Waikato Stream and Rangipo faults in	

the kinematics and evolution of the Taupo Rift	88
4.8.3 Seismic hazard from the Upper Waikato Stream and Wahianoa faults	90
4.8.4 Potential association of volcanism with periods of accelerated seismic activity	93
4.9 Conclusions	94
CHAPTER 5. RESULTS: Earthquake history and Crustal Extension in the Tongariro Graben, New Zealand: Insights into Volcano-tectonic Interactions and Active Deformation in a young Continental Rift.	97
5.1 Abstract	99
5.2 Introduction	100
5.3 Regional Geology	104
5.4 The Tongariro Graben	106
5.5 Methods	108
5.5.1 Fault Mapping and Update of GNS Active Fault Database	109
5.5.2 Fault Geometry and Displacements and Earthquake History	109
5.5.3 Slip-rates and Extension Rates	111
5.6 Results	112
5.6.1 Paleoseismology Analysis	112
5.6.1.1 Rift bounding faults: National Park and Upper Waikato Stream faults	112
5.6.1.2 The Waihi Fault Zone	114
5.6.1.3 The Poutu Fault Zone	115
5.6.2 Fault slip-rates in the Tongariro Graben	117
5.6.3 Dike intrusion rates in the Tongariro Graben	119
5.7 Discussion	120
5.7.1 Is Surface Faulting Associated with Tectonic or Dike Intrusion Processes in the Tongariro Graben?	120
5.7.2 Proportion of Extension Accommodated by Faulting vs. Dike Intrusion	126
5.8 Conclusions	129
CHAPTER 6. RESULTS: Seismic Hazard Analysis of the Tongariro Graben.	131
6.1 Abstract	132
6.2 Introduction	133
6.3 Methods	137
6.4 Results	138
6.4.1 Fault geometry	138
6.4.2 Fault slip-rates	139
6.5 Discussion	141
6.5.1 Fault segmentation	141
6.5.2 Magnitude and recurrence interval of potential earthquakes	147
6.6 Conclusions	148
CHAPTER 7. RESULTS: Spatio-temporal associations between dike intrusions and fault ruptures in the Tongariro Volcanic Centre, New Zealand.	151
7.1 Abstract	152
7.2 Introduction	152
7.3 Tectonic and geological setting	156
7.4 Previously identified volcano-tectonic interactions in the Taupo Rift	157
7.5 Methods	159
7.6 Results	161

7.6.1	Fault slip-rate changes and volcanic activity in the TgVC	161
7.6.2	Eruption volumes	163
7.6.3	Spatio-temporal associations in the TgVC	165
7.6.4	Scenarios for volcano-tectonic interactions in the TgVC	167
7.6.5	Coulomb stress transfer models	169
7.7	Discussion	175
7.7.1	Volcano-tectonic interactions by stress transfer	175
7.7.2	Controlling factors on volcano-tectonic interactions in the TgVC	181
7.7.3	Implications for natural hazards	184
7.7.4	Limitations of this study	184
7.8	Conclusions	186
CHAPTER 8. CONCLUSIONS: Understanding mechanical coupling between volcanic unrest and large earthquakes in the Tongariro Volcanic Centre.		188
8.1	Summary	188
8.2	Tongariro and Ruapehu grabens	191
8.3	Methodologies used: advantages and disadvantages	192
8.4	Fulfilment of study objectives and additional contributions	194
8.5	Future challenges	197
REFERENCES		199
APPENDICES		219
Appendix A. Supplementary data		
A1.	Fault Database and ArcMap shapefile	
A2.	Supplementary figures	
A3.	Supplementary tables	
A4.	Journal publication	
A5.	Extended abstract	
Appendix B. Statements of contribution		

List of Figures

- Figure 1. North Crater and Blue Lake viewed from Red Crater on the Tongariro Crossing Track. (4)
- Figure 2. Main parameters controlling dike emplacement (from Acocella and Neri, 2009). (13)
- Figure 3. Schematic illustration showing the pattern of dike emplacement and type of volcanoes when horizontal tectonic stress is compressional (a) and tensional (b). * (star), depth of brittle-ductile boundary. The shaded parts below the brittle-ductile boundary in 'a' denote magma chambers (Kurokawa et al., 1995). (14)
- Figure 4. Mead's Wall dike (2-4 m wide) at Whakapapa ski field on the northern flanks of Mt. Ruapehu, view looking north at 1678 m elevation. (15)
- Figure 5. Ngāuruhoe volcano and Tongariro Volcanic Complex viewed from Mt. Ruapehu, view approximately to the north. (23)
- Figure 6. Tectonic setting of New Zealand (from Wallace et al., 2004). Yellow dashed line shows the location of the Taupo Volcanic Zone and yellow arrows show the variation of extension rate along the rift, values in mm/yr (Wallace et al., 2004). Black arrows show Pacific/Australia relative motion in New Zealand (DeMets et al., 1994). MFS, Marlborough Fault System; NIDFB, North Island Dextral Fault Belt; TVZ, Taupo Volcanic Zone; BR, Buller regional faults; CEFZ, Cape Egmont Fault Zone. (25)
- Figure 7. Location map of the Tongariro Volcanic Centre (B) as defined by Cole (1978), and its main volcanic structures within the Taupo Volcanic Zone (TVZ) in the central North Island of New Zealand (A), as described by Gregg (1960). SC, Saddle Cone; TL, Tama Lakes; Ng, Ngāuruhoe; Pk, Pukekaikiore; P, Pukeonake; MTg, Mt. Tongariro; RC, Red Crater; TM, Te Maari; NC, North Crater; Mg, Maungakatote; Ku, Kuharua. (29)
- Figure 8. Geological map of the Tongariro Volcanic Centre in New Zealand (modified from QMap; Lee et al., 2011). (30)
- Figure 9. Late Quaternary active fault traces of the Tongariro Volcanic Centre; the northern part delimits the Tongariro Graben and the southern part the Ruapehu Graben (this work; Litchfield et al., 2013; Villamor and Berryman, 2006b). (33)
- Figure 10. General Stratigraphic sequence showing the chronology of the main lahars, tephras and lava flows in the TgVC, and some important rhyolitic stratigraphic markers. (41)
- Figure 11. The Tongariro Volcanic Centre, showing the main faults and volcanic vents, and the four main field sites focused upon for detailed fieldwork within this study. (47)
- Figure 12. Mt. Ruapehu seen from one of the main river exposures in the Upper Waikato Stream, showing a sequence of tephra units and coarse lahar deposits that record the last ~50 ka of deposition (Cronin et al., 1996b). (52)
- Figure 13. A, Tectonic setting of New Zealand. Green rectangle marks location of Figure 1B. B, Location of the Taupo Rift (active faults in red, from Langridge et al., 2016). Yellow rectangle marks location of Figure 1C. C, Location map of the Mt. Ruapehu Graben, Upper Waikato Stream (UWS), Wahianoa and Rangipo faults in the southern part of the Tongariro Volcanic Complex, in the southern Taupo Rift. Potential intersection area marked with a purple rectangle (UWS). (56)

Figure 14. Chronological stratigraphic summary of the laharic and lava formations and andesitic tephtras from the Tongariro Volcanic Centre interbedded with distal rhyolitic tephtras from the Taupo Volcanic Zone calderas. Note the general stratigraphic record for the Upper Waikato Stream and Wahianoa Fault areas at the right. *The oldest laharic formations' ages are based on the Rotoehu ash age (45.16 cal ka BP; Danišik et al., 2012). Ru, Ruapehu; Tg, Tongariro; Ng, Ngāuruhoe; Tp, Taupo; Ok, Okataina, R# corresponds to the lahar episodes as described by Cronin & Neall (1997). (59)

Figure 15. Geological map and general stratigraphy of the SE Mt. Ruapehu area (after Lee et al., 2011; Townsend et al., 2008), showing the location of the study sites (sections 1–3) and active surface fault traces (Langridge et al., 2016). See Figure 14 for detailed stratigraphic record. (61)

Figure 16. Terrestrial laser scanning survey. A, Upper Waikato Stream (UWS) 3D point cloud data. B, Oblique view of the digital outcrop model of the wall 'a' in the Upper Waikato Stream Fault built with 3DReshaper Application. C, Satellite image (using Google Earth images, 2015) showing the scanning locations and river exposures (walls) for the terrestrial laser scanning survey in the Upper Waikato Stream, section 1 (see location on Figure 15). (65)

Figure 17. Location of the main faults in the Upper Waikato Stream area. A, Hillshade map of the Upper Waikato Stream based on 2 m digital surface model showing the studied faults in sections 1 (green rectangle) and 2 (blue dots, blue rectangle). Fault exposures (dots) and fault traces (continuous lines) are differentiated from the inferred faults (discontinuous lines). Faults downthrown to the NW are marked with red lines; faults downthrown to the SE are marked with yellow–brown lines. The fault planes are plotted in stereographic (lower hemisphere) projection and superimposed rose diagrams of fault strike frequency (right-hand rule). B, Section 1 of the Upper Waikato Stream (green rectangle in A) showing the seven main fault traces (purple dots), as well as an extensional fracture and two transects t1 and t2 (white lines) used to sum and calculate the total offset for the Upper Waikato Stream Fault. (71)

Figure 18. Faults in section 1 in the Upper Waikato Stream. A, Wall 'a' main fault exposure, showing fault 1 displacing volcanic deposits older than c. 28 ka (left, field photo; right, interpretation with stratigraphic column). B, Wall 'b' showing the location of fault 2 with a 0.3 m 'fissure fill' (left, field photo; right, interpretation with stratigraphic column). C, Detailed exposure of fault 4 on wall 'b' displacing tephtras older than R11 lahars. The numbers show the elevation in m a.s.l. See Figure 14 for further information about stratigraphic units. (72)

Figure 19. Extensional fractures located on wall 'a' in the Upper Waikato Stream. A, The 12 m long fissure filled with Ōruanui Tephra (white arrow; >25.4 cal ka BP; photo taken by S. Donoghue), cutting older tephtras and lahar deposits. B, Other fissures were measured on the same wall, cutting R11 lahars. C, These fissures do not show any vertical displacement, but record extension. D, The R11 lahar deposits are abruptly truncated at the fissure margins, with no mixed material along fissure sides. The reworked Ōruanui tephtra shows cross-bedding stratified layers. E, All the fissures reflect orthogonal extension and are consistent with the NNE-trending Mt. Ruapehu Graben. Rose diagrams for the measured fissures and faults in the Tongariro Volcanic Centre (TgVC), where strike directions (right-hand rule) are plotted. (74)

Figure 20. Main outcrops of the Upper Waikato Stream Fault in section 2. A, 10/4_2: Normal fault displacing the Papakai Formation. B, 10/4_3: Exposure of fault displacing deposits including R13 and older lahars. (76)

Figure 21. Wahianoa Fault profiles and outcrops. A, Geological map [Leonard et al., 2014] showing the location of the studied field sites along the Wahianoa Fault in section 3; and the 10 topographic profiles (black double-pointed arrows) traced with their corresponding vertical offset

values in meters. The geological map overlies a hillshade created with a 2 m-resolution Digital Surface Model from the SE flank of Mt. Ruapehu. B–C, The two main outcrops of the Wahianoa Fault in section 3 showing displaced tephra (field locations shown on Figure 22A). The fault planes are plotted in stereographic (lower hemisphere) projection and superimposed rose diagrams of fault strike frequency (right-hand rule). Most of the tephra belongs to the Bullock Formation from Mt. Ruapehu (Donoghue and Neall, 2001; Pardo et al., 2012). See Figure 14 for more information about the stratigraphy and Figure 15 for location of section 3. (78)

Figure 22. Fault slip-rate variation from >45 ka to present day for the Rangipo Fault (green square) (Villamor et al., 2007), the Wahianoa Fault (based on profiles, grey circle), and the Upper Waikato Stream Fault (blue circle minimum values and orange circle maximum values). Higher slip-rate periods are coincident with the Bullock Formation, the Pahoka–Mangamate eruptions (PM), the Orange lapilli and marker unit 2 (Elephant surge) from Mt. Ruapehu, and the Ōruanui eruption from Taupo. Taupo pumice (TP) eruption is indicated at 1.72 cal ka BP. Zero (0) indicates the present day. (83)

Figure 23. Potential physical intersections and rupture models of the Upper Waikato Stream Fault with Rangipo and Wahianoa faults. A, Independent ruptures. B, Potential rupture of the Wahianoa (WF) and Upper Waikato Stream (UWS F) faults (27 km). C, Potential rupture of the Rangipo (RF), Upper Waikato Stream and Kaimanawa (Kai F) faults (43 km). (87)

Figure 24. Ngāuruhoe volcano, Pukekaikio and Mt. Ruapehu from the Mangatepopo moraine, view roughly to the south (by Anja Moebis). (92)

Figure 25. Similar geomorphic expression of volcanic rift zones in the Tongariro Graben (A) and the Asal Rift in Djibouti (B), showing parallel normal faults bounding the western and eastern flanks of the volcanic vents (modified from Stein et al., 1991). (96)

Figure 26. A, Location map of the Taupo Rift in the North Island of New Zealand (green rectangle). B, Location of the Tongariro Volcanic Centre (TgVC, yellow rectangle) at the southern part of the Taupo Volcanic Zone. Variation of extension rate along the rift, marked with black arrows, values in mm/yr (Wallace et al., 2004). Large ($M_w > 3$) and shallow (<40 km) earthquakes marked with red circles, compiled from the New Zealand catalogue of earthquakes since the 1930s (extracted from NZ GeoNet database <http://info.geonet.org.nz/display/appdata/Earthquake+Catalogue>). C, Location of the Tongariro Volcanic Complex (TVC) at the Tongariro Graben axis, the Waihi Fault (WF) and the Poutu Fault (PF) zones, Mt. Ruapehu, Ruapehu Graben and the main volcanic vents in the region. The active faults are marked in red (Langridge et al., 2016). Ng, Ngāuruhoe. (100)

Figure 27. Geological map (Leonard et al., 2014) overlain with the faults of the Tongariro Graben; the Waihi and Poutu fault zones in the graben axis area and fault traces (red lines), inferred fault traces (dotted red lines), possible scarps (black lines) and 229 vertical fault displacements (2 northern National Park Fault, 117 Waihi Fault and 110 Poutu Fault; see displacement values in Tables S3 and S4) measured from geomorphic surfaces on transverse profiles across the faults (black and green dots, values in meters). Seventeen transects (T1–T17) are marked with white lines. Field points are marked with purple dots and white numbers (referred to as Tong # in the text and figures, Table S5). (108)

Figure 28. Field outcrops from the Waihi Fault. A, Tong 70: Normal fault (F5a) displacing the Pukekaikio lava flows (190–25 ka; Hobden et al., 1996; Leonard et al., 2014), the Mt. Tongariro lava flows and the Mangatepopo moraine in Mt. Tongariro. B, Tong 78: F4b exposure displacing the Mangatawai tephra (3.52 cal ka BP; Moebis et al., 2011) and the Papakai Formation (11.1–3.7 cal ka BP; Donoghue et al., 1995; Figs. 27 and S5; Tables S5 and S7)(110)

Figure 29. Field outcrops from the Poutu Fault. A, Tong 11: three-step normal fault displacing the Pahoka and Okupata-Pourahu tephras. B, Tong 77: Multiple-step normal fault (F2b) displacing the Okupata-Pourahu tephras (11.77 ± 0.19 cal ka BP; see stratigraphy in Table S10 and locations in Figure 27, and Tables S5 and S9). (111)

Figure 30. Simplified schematic diagrams showing the variety of extension modes in continental rifts. A, Pure tectonic extension by normal faulting (unrelated to volcanism). B, Pure volcanic extension by dike intrusion and eruption (dike reaches the surface). C, Extension through both normal faulting and dike intrusion-eruption. D, Pure volcanic extension by shallow arrested dike-intrusion with associated surficial normal faults (large ground surface displacements are common). E, Hybrid extension through deep dike-intrusion and triggered normal faults (large surface displacements are related to tectonic faulting; if faulting is only related to dike-intrusion ground surface displacements are too small to be observed). F, Extension is a combination of tectonic faulting, dike intrusion-eruptions and arrested dike-intrusion. E, Extension; ET, Tectonic Extension; EV, Volcanic Extension; EAD, Arrested dike extension. (116)

Figure 31. Static displacement caused by an intruding dike projected onto cross sections. A, 1 m-wide dike intruding to the surface and causing no surface deformation; B, 1 m-wide intruding dike at 2 km depth intersecting with 30° dip faults, showing a maximum of 0.5 m of surface deformation. C, 1 m-wide intruding dike at 5 km depth intersecting with 50° dip faults, showing a maximum of 0.25 m of surface displacements. D, 1 m-wide intruding dike at 10-15 km depth intersecting with $60-70^\circ$ dip faults representing the most likely scenario for the Waihi and Poutu faults, showing no surface deformation. NPF, National Park Fault; UWSF, Upper Waikato Stream Fault. E, 20 m-wide dike representing total width of repeated dike intrusions in 20 ka; here the dike is intruding to the surface and causing no surface deformation. F, 20 m-wide intruding dike at 2 km depth intersecting with 30° dip faults, showing a maximum of 6 m of surface deformation. G, 20 m-wide intruding dike at 5 km depth intersecting with 50° dip faults, showing a maximum of 4 m of surface displacement. H, 20 m-wide intruding dike at 10-15 km depth intersecting with $60-70^\circ$ dip faults representing the most likely scenario for the Waihi and Poutu faults, showing 1.5 m of surface deformation. I and J, 1 m-wide dike intruding at 10-15 km depth showing normal stress changes ($\Delta\sigma_n$; bar, unclamping positive) projected onto cross section (A-B) showing positive stress change (red colour) on top of the intruding dike, where the Waihi and Poutu faults are. (120)

Figure 32. Shallow seismicity in New Zealand (GeoNet, <http://info.geonet.org.nz/display/quake/Earthquake>). (125)

Figure 33. A, Location map of the Taupo Rift in the North Island of New Zealand. B, Location of the Tongariro Graben and the Tongariro Volcanic Complex at the southern section of the Taupo Volcanic Zone. 229 vertical fault displacements (2 northern National Park Fault, 117 Waihi Fault and 110 Poutu Fault) measured by geomorphic surfaces on transverse profiles over the faults (values in meters). Seventeen transects marked with white lines (T1-T17). Field points marked with purple dots and white numbers (referred to as Tong # in the text and figures). UWS, Upper Waikato Stream. For more details about displacements, lithology and surface ages see Chapter 5, Tables S3 and S4. (130)

Figure 34. Measured individual fault strand displacements for different age surfaces along the strike of the Waihi and Poutu fault zones. Waihi Fault zone shows greater displacements to the north of the Tongariro Graben. (138)

Figure 35. Potential segment surface-length rupture models for the Waihi and Poutu faults, marked with purple and green lines, respectively. Ng, Ngāuruhoe; RC, Red Crater; NC, North Crater; Ph, Pihanga. (140)

Figure 36. Stormy Point look-out, Manawatu, showing sequences of river terraces from 400 to 12 ka. (145)

Figure 37. A, Location of the Taupo Volcanic Zone in the North Island of New Zealand. B, Tongariro Volcanic Centre in the southern sector of the Taupo Volcanic Zone. Location of the main regional volcanoes and faults (red lines) (Chapter 5; Langridge et al., 2016; Villamor and Berryman, 2006b). Ng, Ngāuruhoe; Tg, Mt. Tongariro; Ot, Oturere; NC, North Crater; UWS, Upper Waikato Stream. (149)

Figure 38. Summed vertical displacements across the Tongariro Graben for the last 100 ka (Waihi and Poutu faults). (156)

Figure 39. Variations in short-term fault slip-rates for various faults in the TgVC from 100 ka to the present-day (zero), showing a temporal association with regional volcanic activity and Taupo caldera eruptions (Hajdas et al., 2006; Hogg et al., 2011; Lowe et al., 2013; Vandergoes et al., 2013; Wilson et al., 2009). UWS, Upper Waikato Stream Fault; TVZ, Taupo Volcanic Zone; PM, Pahoka-Mangamate sequence at ~11 cal ka BP; BF, Bullot Formation; MF, Mangawhero Formation; Tg, Mt. Tongariro; Ot, Oturere lavas. (157)

Figure 40. Eruptive volumes of the main tephras and lava flows in the TgVC (Table S11). Mt. Ruapehu sourced deposits in blue and Tongariro Volcanic Complex in green. Ng, Ngāuruhoe (Moebis et al., 2011); PM, Pahoka-Mangamate sequence (Nairn et al., 1998); WhF, Whakapapa Formation (Conway et al., 2016); BF, Bullot Formation (Pardo et al., 2012); MF, Mangawhero Formation (Conway et al., 2016); TWLF, Te Whaiahu Laharic Formation (Lecointre et al., 2002); WLF, Whangaehu Laharic Formation (Keigler et al., 2011); Tg, Mt. Tongariro (Hobden et al., 1996); Ot, Oturere (Hobden et al., 1996); WF, Wahianoa Formation (Gamble et al., 2003); Pk, Pukekaikiore (Hobden et al., 1996); THF, Te Herenga Formation (Conway et al., 2016); TL, Tama Lakes (Hobden et al., 1996). (158)

Figure 41. Spatio-temporal associations for the Tongariro Volcanic Centre from known paleo-earthquakes (fault slip-rates and events) and volcanic eruptions for six different periods, showing their variation in activity for the last 250 ka. The triangles are the volcanic vents and the lines are the faults. R, Ruapehu; TL, Tama Lakes; Ng, Ngāuruhoe; Tg, Mt. Tongariro; Ot, Oturere; NC, North Crater; TM, Te Maari; Pk, Pukekaikiore; Pn, Pukeonake; P, Pihanga; KT, Kakaramea-Tihia; Hg, Hauhungatahi; OC, Ohakune Craters; HC, Half Cone; NP F, National Park Fault; UWS F, Upper Waikato Stream Fault. At time 4 there was a major caldera forming eruption at Taupo caldera: the Ōruanui ignimbrite at 25.4 cal ka BP (Vandergoes et al., 2013).

(160)

Figure 42. Scenarios for volcano-tectonic, volcano-volcano and fault-fault interactions in the Tongariro Volcanic Centre (marked in red) for six different periods in the last 250 ka based on regional spatio-temporal associations from fault slip-rates and volcanic eruption volume changes (Fig. 41). (162)

Figure 43. Stress change models with different source faults. Red areas are positive, where the stress changes are likely to encourage a fault rupture or a dike intrusion on the receiver fault or dike. Green lines represent faults on surface and red lines represent faults at depth. A, Negative normal stress change on Ngāuruhoe and other dikes in the Tongariro Volcanic Complex, and positive normal stress change on Mt. Ruapehu after a Waihi Fault rupture. B, Negative normal stress change on the Tongariro Volcanic Complex dikes, and positive normal stress change on Mt. Ruapehu after a Poutu Fault rupture. C and D, Positive Coulomb stress change on Rangipo, Upper Waikato Stream (UWS) and Ohakune faults after a Wahianoa Fault rupture. E, Negative normal stress change on Mt. Ruapehu after a Wahianoa Fault rupture. (165)

Figure 44. Stress change models from different source faults. A and B, Positive Coulomb stress change on Wahianoa and Upper Waikato Stream (UWS) faults after a Rangipo Fault rupture. C, Negative normal stress change on Mt. Ruapehu after a Rangipo Fault rupture. D, Positive Coulomb stress change on Wahianoa Fault after an Ohakune Fault rupture. E, Positive Coulomb stress change on the Wahianoa Fault after an Upper Waikato Stream Fault rupture. F, Positive Coulomb stress change on the Rangipo Fault after an UWS Fault rupture. (167)

Figure 45. A, Negative Coulomb stress change on Wahianoa and southern Waihi faults, and positive stress change on southern Poutu Fault and Tama Lakes dikes after a NNE-SSW Ruapehu dike intrusion. B, Positive stress change on southern Waihi and Poutu faults, southern Wahianoa Fault and Tama Lakes dikes, and negative stress change on northern Wahianoa Fault after a N-S Mt. Ruapehu dike intrusion. C, Positive stress change on Poutu Fault and Tama Lakes dikes, and negative stress change on Waihi and Wahianoa faults after an E-W Mt. Ruapehu dike intrusion. D, Positive Coulomb stress change on Waihi and Poutu faults after a NNE-SSW Tongariro Volcanic Complex dike intrusion. E, Positive normal stress change on Ngāuruhoe, Te Maari, Tama Lakes and Ruapehu dikes after a Tongariro Volcanic Complex dike intrusion. (168)

Figure 46. Possible scenarios for dike-fault, dike-dike and fault-fault interactions by stress transfer in the Tongariro Volcanic Centre for the last 250 ka after evaluating the Coulomb and normal stress change models (Figs. 43-45), where the red colour denotes a positive stress change and the blue colour a negative stress change. (169)

Figure 47. Combination of tectonic and magmatic extension in the Tongariro Graben. Fault slip-rate variation could be explained by different tectonic and magmatic input to the total extension. Input can fluctuate through time but total extension remains constant. Magmatic input could vary from 22 to 5% and tectonic input from 95 to 78% of the total extension (Chapter 5). (177)

Figure 48. Mt. Ruapehu volcano from Waihohonu moraine (June 2014 by Agnes Samper). (210)

Supplementary figures

Figure S1. Main river exposures (walls) in the Upper Waikato Stream at section 1 showing the studied faults (red lines). Location of the walls can be seen on Figure 16.

Figure S2. Faults in section 1 in the Upper Waikato Stream. A, Image from Cyclone software showing fault 3 on 'wall b' and its general stratigraphy. B, Fault 3 on 'wall c' showing a three-step fault scarp. C, D & E, Southern corner of 'wall b' showing exposure of fault 4 and general stratigraphy. F, Exposure of fault 5 on 'wall c' showing multiple-step fault on R11 lahars. G, Cyclone measurement of fault 5 on 'wall b' on R11 lahars. H, Exposure of the termination of fault 5 on the Hokey Pokey eruptive period on 'wall c'. I, 'Wall d' with a multiple-step fault (6) cutting through R11 lahars. J, Fault 7 exposure cutting through elephant surge up to R11 lahars with a multiple-event step-fault. See Figure 14 for further information about stratigraphic units.

Figure S3. A, Fault 10/4_1:030/65SE to 055/85NW normal fault, vertical offset ~1 m; and a secondary fault 010/76NW with 0.77 ± 0.16 m of net-slip. The stratigraphic position and the fault termination of this fault are uncertain. B, 10/4_2: normal step-fault cutting through the Papakai Formation. C, 10/4_4b: fault exposure cutting through R13 lahars and older deposits. D, 10/4_4a: Fault exposure 10 m above the river level. E, 10/4_4b: Fault exposure 2 m above the river level cutting through the Okataina sourced Rotoehu Ash (64 ka), R13 lahars, marker unit 3 and R14 lahars. F, 10/4_5: normal fault cutting R15 lahars and older deposits. G: 10/4_6: fault exposure of a normal fault cutting R13 lahars and older deposits. H, 11/4_4 and 11/4_5: faults and fractures that cut through greywackes and younger tephtras, cropping out by the river level.

Figure S4. A, Wahianoa Fault outcrop 'Tong 23' in the Karioi Forest, section 3, showing antithetic faults (field location shown on Figure 21A). The fault planes are plotted in stereographic (lower hemisphere) projection and superimposed rose diagrams of fault strike frequency (right-hand rule). See Figure 14 for more information about the stratigraphy. B, Wahianoa Fault cutting across and andesite lava flow of the Mangawhero Formation.

Figure S5. Waihi Fault main field outcrops. A-D, Field outcrop 'Tong 78' showing displaced tephtra mainly from the Ngāuruhoe Formation (Moebis et al., 2011) cut by fault 5. E-F, Field point outcrop 'Tong 70' showing displaced tephtra mainly from the Bullot Formation from Mt. Ruapehu (Donoghue & Neall, 2001; Pardo et al., 2012) cut by fault 6.

Figure S6. Poutu Fault main field outcrops. A, Field site 'Tong 09' displaced by Poutu Fault strand F7b showing 4 m of deformation since 11 ka. B-C, Field site 'Tong 11' and 'Tong 10' showing ~11 ka displaced tephtras on NE flanks of Mt. Ruapehu. D, Field outcrop 'Tong 50' on F4a Poutu Fault strand.

Figure S7. Poutu Fault main field outcrops. A-B, Field outcrops 'Tong 72' and 'Tong 73' on F1a Poutu Fault strand. C-D, 'Tong 76' and 'Tong 77' field sites showing displaced tephtras between ~14 and 11 ka.

List of Tables

- Table 1. Main morphological structures that evidence a prehistoric earthquake McCalpin, 2009. (8)
- Table 2. Net-slip, single-event displacements, progressive displacements and timing of rupture of the Upper Waikato Stream Fault, at section 1. (68)
- Table 3. Net-slip, single-event displacement and timing of fault rupture of the Upper Waikato Stream Fault, at section 2. (76)
- Table 4. Net-slip, single-event displacements, progressive displacements and timing of rupture of the Wahianoa Fault, at section 3. (78)
- Table 5. Comparison of fault rupture number and timing of the Upper Waikato Stream, Wahianoa and Rangipo faults. (81)
- Table 6. Moment magnitude and single-event displacement for different fault lengths. (87)
- Table 7. Vertical displacements and slip-rates for the Tongariro Graben, from Waihi and Poutu faults transects and rift-bounding faults. (113)
- Table 8. Surface and seismogenic depth extension rates at 20 and 60 ka for the Tongariro Graben. (121)
- Table 9. Vertical displacements and slip-rates summary for the Tongariro Graben, from Waihi and Poutu faults transects and rift-bounding faults. (134)
- Table 10. Moment magnitude and single-event displacement for different fault lengths. (142)

Supplementary tables

Table S1. Net-slip, single-event displacements, progressive displacements and timing of rupture of the Upper Waikato Stream Fault, sections 1 & 2.

Table S2. Net-slip, single-event displacements, progressive displacements and timing of rupture of the Wahianoa Fault, sections 2 & 3, and comparison of fault ruptures of the Upper Waikato Stream, Wahianoa and Rangipo faults.

Table S3. Waihi Fault displacements.

Table S4. Poutu Fault displacements.

Table S5. Field locations.

Table S6. Waihi Fault, geomorphic surface offsets and progressive displacements.

Table S7. Waihi Fault, outcrop offsets and progressive displacements.

Table S8. Poutu Fault, geomorphic surface offsets and progressive displacements.

Table S9. Poutu Fault, outcrop offsets and progressive displacements.

Table S10. Main stratigraphic units.

Table S11. Magma volumes of the Tongariro Volcanic Centre.

Table S12. Co-seismic slip for the southern Taupo Rift faults.

List of abbreviations

BP	Before Present
cal	calibrated
CFC	Coulomb failure criterion
DSM	Digital Surface Model
GIS	Geographic Information System
GNS	Institute of Geological and Nuclear Sciences
GPa	Gigapascal
GPS	Global Positioning System
ka	Thousand years
Ma	Million years
m a.s.l.	Metres above the sea level
Mt.	Mount
M _w	Moment magnitude
PM	Pahoka-Mangamate
RTK	Real Time Kinematic
TgVC	Tongariro Volcanic Centre
TVC	Tongariro Volcanic Complex
TLS	Terrestrial Laser Scanning
TVZ	Taupo Volcanic Zone
UWS	Upper Waikato Stream
VEI	Volcanic Explosivity Index

CHAPTER 1. Introduction

1.1 Research problem and motivation

In volcanic rifts, extension is accommodated by the combination of dike intrusions and normal faulting [McCalpin, 1996], and sometimes, in particular places, they can be related. Large earthquakes, volcanic eruptions and their interaction are important topics to study because they pose important hazards to the population around the world. Volcano-tectonic interactions are complex and demand an interdisciplinary approach. Some research on volcano-tectonic interactions has been done in the central Taupo Volcanic Zone (TVZ), but nothing has been done from this point of view in the Southern TVZ. Therefore, the purpose of this thesis is to study the uncertain interaction between magmatism and fault activity at the Tongariro Volcanic Centre (TgVC).

The TgVC is the southernmost and one of the youngest volcanic provinces within the Taupo Volcanic Zone (TVZ) in the North Island of New Zealand. The TVZ is a NNE-trending continental volcanic arc that was formed ~2 Ma ago in response to the subduction of the Pacific Plate beneath the Australian Plate along the Hikurangi Trench [Wallace *et al.*, 2004]. At the south of the TVZ, the TgVC contains multiple aligned vents, conforming an andesitic to basaltic province that includes five large volcanoes (Kakaramea, Pihanga, Tongariro, Ngāuruhoe and Ruapehu), at least four smaller centres (including Pukeonake, Pukekaikiore, and Maungakatote), several craters and satellite cones (e.g., Saddle Cone), vents, crater lakes (e.g., Tama Lakes, Blue Lake), and associated volcanoclastic deposit aprons or ring-plains [Hackett and Houghton, 1989; Cole, 1990; Hobden *et al.*, 1996; Price *et al.*, 2012] (Fig. 7).

Volcanic activity in the TgVC has been more or less continuous since the middle Pleistocene ~350 ka [Gregg, 1960; Tost *et al.*, 2016], involving various eruption types and the emplacement of lava flows, debris avalanches, debris flows and pyroclastic deposits. Large lahars have been common from all volcanoes, although the Ruapehu-

sourced flows are generally better studied due to their more frequent historical occurrences [Gregg, 1964; Cronin *et al.*, 1997a; Cronin *et al.*, 1997b; Cronin and Neall, 1997]. Ruapehu, Ngāuruhoe and Tongariro have all experienced recent historical eruptions, with the latest activity, a phreatic/hydrothermal eruption, occurring from the upper Te Maari crater on the northern flanks of the Tongariro Volcanic Complex in November 2012 [Procter *et al.*, 2013; Pardo *et al.*, 2014].

The most obvious vent arrangement in the TgVC and the Taupo region to the north is a NNE-SSW alignment of volcanic centres and vents [Nairn *et al.*, 1998]. Three regional active fault sets are present in the area (NE-SW, NNE-SSW and E-W to ESE-WNW) [Villamor and Berryman, 2006b; Townsend *et al.*, 2010], and paleoseismic studies suggest that these faults can produce $M_w > 6.5$ earthquakes [e.g., Villamor *et al.*, 2007] (Fig. 9).

Volcanic eruptions and large earthquakes, and their secondary effects, such as debris flows or debris avalanches, pose important hazards to the region. The permanent population on the slopes of the volcanoes, including several Māori communities, is low due to most of the area being within a National Park. However, there are large seasonal visitor loads, especially during the skiing season on Ruapehu, which contributes greatly to the economy of the region [Jolly *et al.*, 2014]. Furthermore, major transport, power distribution and power generation assets in the area are exposed to volcanic and tectonic hazards. For example, ash fall from even small eruptions (e.g., 1995-96 Ruapehu) generated widespread disruption to air-traffic, electricity generation and distribution and agriculture, with consequent economic impacts exceeding \$NZ100 million in losses [Cronin *et al.*, 1997a; Johnston *et al.*, 2000].

Stratigraphic and volcanic studies in this region have been abundant; however, little attention has been paid to examining the inter-relationship of the volcanic and tectonic processes. The record of explosive eruptions is particularly well studied, with on-going

iterations of research improving the age-constraints and details of the eruption records of the TgVC volcanoes [Topping, 1973; Donoghue *et al.*, 1995; Cronin *et al.*, 1996b; Moebis *et al.*, 2011; Pardo *et al.*, 2012]. However, some faults are still unstudied, and regional or local structural control on vent location, eruption magnitude and recurrence are still unknown.

In addition to the volcanic work, much has been learned about the regional and local tectonic structure of the TVZ [Wallace *et al.*, 2004; Villamor and Berryman, 2006a; Berryman *et al.*, 2008; Langridge *et al.*, 2016], but specific work still has to be carried out on some individual fault systems in the southern TVZ. Changes in fault activity rate have been related to changes in volcanic activity rate [e.g., Villamor *et al.*, 2007]; however, a link between tectonics and volcanism has not been made in the wider context of plate boundary processes [Nairn *et al.*, 1998; Rowland *et al.*, 2010]. Recognising such relationships has been possible at other active volcanic arc systems, e.g., changes in volcanic styles were defined by major changes in local tectonics at Kyushu Island, SE Japan [Mahony *et al.*, 2011]. Understanding the volcano-tectonic relationship in the southern TVZ could provide a major advance in the understanding of volcano-tectonic behaviour and hazards in the region.

A holistic assessment of volcanic activity to evaluate spatio-temporal patterns should consider the creation and activity of volcanic vents, vent location, magma volumes, eruptive styles, frequency and their relationship to the tectonic structure. The location and frequency of dike intrusions and fault movements are ultimately controlled by crustal stress patterns. However, the strength and attributes of the volcano-tectonic relationship are currently unknown, and there are no models that link the observable parameters (e.g., fault rupture and volcanic eruption).

The TgVC is a unique location to study the interplay between volcanic and tectonic activity, because of the backbone of knowledge on its volcanic and seismic activity, and

the geomorphic and geologic expression of volcanism and tectonism [*Hobden et al.*, 1999]. Further, this region contains two major volcanic systems that show contrasting structures; one has a restricted central vent region (Mt. Ruapehu), while its northern neighbour (Tongariro Volcanic Complex) has dispersed and aligned vents. These differences appear to relate to subtle variations in the tectonic regime. The TgVC also occurs at the terminus of a major extensional regime, marking a transition from the caldera systems of the central TVZ to the north [*Ewart et al.*, 1975; *Houghton et al.*, 1995; *Wilson et al.*, 1995] and the stratovolcanoes of the southern TVZ. The evaluation of seismic and volcanic activity in the region is of great relevance for hazard assessment in New Zealand and also helps to elucidate broader convergent margin volcanic processes.

Along the ~30 km axis of the TgVC, many types of interactions between the tectonic structure and volcanism can be found. There is a transitional area of importance at the southern end of the TVZ (south of Ruapehu), where extension gives way to compression [*Villamor and Berryman*, 2006a]. It is crucial to study this and other transitional areas in order to understand how rifts terminate and are replaced by non-volcanic compressional areas.

This thesis studies the faulting history and evaluates the seismic hazard, of some of the main faults in the TgVC, compiles and compares new and existing seismic and volcanic data to address outstanding issues about volcano-tectonic interactions in the Ruapehu and Tongariro grabens. The knowledge gained can help mitigate volcanic and earthquake hazards in the TgVC area, for example through evaluating fault movements through time, their co-seismic displacement, recurrence interval and their potential association to regional dike intrusions.



Figure 1. North Crater and Blue Lake viewed from Red Crater on the Tongariro Crossing Track.

1.2 Objectives

The main aim of this thesis was to determine the spatial and temporal relationships between the volcanic vents and their magmatic activity and the regional and local tectonic structures in the TgVC. To achieve this, the following specific objectives were pursued:

- I. Compile from the literature the volcanic history of the main volcanic vents in the Tongariro Volcanic Centre. Determine the location, age, type, volume and frequency of volcanism.
- II. Review the Quaternary tectonic history of the faults in the southern TVZ. Compile new and existing structural data and try to reconstruct the rupture history of the main faults with (a) paleoseismological and (b) tectonic geomorphology methods. In fault exposures, identify relative timing of deposition of volcanic products (tephrochronology) and fault rupture in the TgVC. Identify temporal variations in fault slip-rates from analysis of geomorphic landforms of different ages. Identify regional faults and fractures

(image analysis and field observations); classify them into the following categories: active, extinct, tectonic, magmatic, or tectonic-magmatic, and describe their main properties including, strike, length, offset, dip, tectonic activity, recurrence, etc.

- III. Compare the seismic and volcanic activities. Determine the relationships between the volcanic and tectonic histories by analysing spatio-temporal associations between fault ruptures and volcanic eruptions. Create integrated models to explain the spatio-temporal volcano-tectonic associations found in the field and use the models to assess the contributions to rifting from the volcano-tectonic interaction models.
- IV. Run static stress transfer models based on the Coulomb failure criterion to assess how volcanic eruptions can change the stresses in the crust around selected faults (in particular testing for time association between a volcanic eruption and fault movement) and vice versa.
- V. Improve the current characterization of the seismic potential of active faults in the region to feed information into future updates of the New Zealand National Seismic Hazard Model. Determine if part of the activity of a fault is volcanic related rather than tectonic and how this should be incorporated (or excluded) from seismic hazard calculations.

1.3 Thesis outline

This thesis comprises eight chapters, references and appendices including specific datasets.

Chapter 1 includes the introduction, aim, research questions and objectives of this study.

Chapter 2 comprises a literature review describing the main concepts of Paleoseismology, volcanic rifts, dike intrusions and volcano-tectonic interactions; as well as the characterization of the study area and previous studies.

Chapter 3 presents the methodology, including a description of the materials and methods used in this study. It is divided into desk study, fieldwork and data analysis methods.

Chapters 4 to 7 report the results. Each chapter is presented in the layout and length requirements of peer-reviewed journals to which work has been or will be submitted for publication.

Chapter 4 is a full-length research article published in the New Zealand Journal of Geology and Geophysics. It analyses the earthquake history at the eastern boundary of the south Taupo Volcanic Zone, evaluating the paleoseismic activity and intersection of the main faults in this area, the Rangipo, Wahianoa and Upper Waikato Stream faults.

Chapter 5 is a research article published in the Geological Society of America Bulletin. It describes the Tongariro Graben, the main faults in this part of the rift (Waihi and Poutu faults) and their relationship with the volcanic activity. This chapter quantifies the geological extension rates in the Tongariro Graben, and discusses the extension mode, as well as the amount of extension accommodated by dike intrusions and normal faults.

Chapter 6 presents a seismic hazard analysis of the Tongariro Graben. A part of this chapter was published as an extended abstract following the 7th International INQUA Meeting on Paleoseismology, Active Tectonics and Archeoseismology, and will be submitted for publication in a scientific journal.

Chapter 7 connects previous sections of the thesis, from Chapter 3 to Chapter 6, presenting spatio-temporal associations for the TgVC volcanic and tectonic activity and

assigning integrated models for potential interactions between fault ruptures and volcanic eruptions. This chapter is also written in the layout of a research article and will be submitted for publication in a scientific journal.

Chapter 8 consists of the conclusions of the thesis. It contains a synthesis of the entire thesis, describes the particular features of the southern Taupo Rift, and analyses the advantages and disadvantages of the methods used in this study. Specific findings addressing the research questions and objectives are mentioned, and some suggestions for future directions of research in the field of volcano-tectonic interactions are provided.

The appendices include supplementary data that are not crucial for this study but may help clarify some ideas, and satisfy curious minds. The appendices consist of the fault database, supplementary figures, supplementary tables, journal publications and statement of contribution.

CHAPTER 2. Literature Review

2.1 Paleoseismology

Paleoseismology is a subdiscipline of Seismicity that studies prehistoric earthquakes through the evaluation of their geologic and geomorphic expression, location, timing and magnitude [Table 1; *McCalpin, 2009*]. When doing a paleoseismic reconstruction, mapping of Quaternary landforms and regional deposits is required to identify the fault. Recognising the geomorphology is also necessary to establish the relative age of a past earthquake. The magnitude of an earthquake will be consistent with a function of the amount of surface deformation, the length and the geometry of the fault.

TABLE 1. GEOMORPHIC EXPRESSION OF FAULTING EVENTS

	COSEISMIC	POSTSEISMIC
PRIMARY EVIDENCE	ON THEFAULT	
	Fault scarp	
	Fissures	
	Striae	Colluvial wedges
	Folds	
	Faceted spurs	
	REGIONAL	
	Tilted blocks	Alluvial terraces
	Coastal cliffs	Fluvial erosion in hanging wall and sedimentation in footwall
	SECONDARY EFFECTS	ON THEFAULT
Sand volcanoes		
Landslides		
Turbidites		Delayed landslides
Tilted trees		
REGIONAL		
Sand volcanoes		Delayed landslides
Fissures		Ground-water flow system affected
Landslides		
Tsunami deposits		
Subsidence		
<p><i>Note:</i> Main morphological structures that evidence a prehistoric earthquake (<i>McCalpin, 2009</i>).</p>		

Paleoseismologists study the deformation of landforms caused by the movement of active faults through time. Earthquake history can be evaluated by the progressive increase in displacements recorded in the sediments or rocks, because cumulative displacements from each seismic event will create a greater displacement on older deposits than on younger ones. Fault slip-rates are used to measure deformation from total displacement within a certain time [McCalpin, 2009].

2.2 Volcanic Rifts

Volcanic rift zones (magmatic rifts) are located in extensional environments where divergent plate motion creates lithospheric dilation, usually accommodated by a combination of normal faulting, extensional fractures and dike intrusions (McCalpin, 2009). In young continental rifts, extension is mostly accommodated (characterised) by normal faulting, while in mature rifts dike intrusions (magmatism) tend to dominate [Biggs *et al.*, 2009; McCalpin, 2009]. In a volcanic rift, inward dipping normal faults create a graben structure, where fractures allow dike intrusions to get to the surface and form volcanoes at the axis of the graben, which is usually aligned to the regional stress pattern [Walter and Troll, 2003].

2.2.1 Morphology of faults in volcanic rifts

In volcanic rift zones it is common to see dike-induced extensional structures, like normal faulting, extensional fractures and graben subsidence at the surface [Rubin, 1992; McCalpin, 2009], which could form seismically or aseismically with low-magnitude earthquake swarms [Michetti, 2002]. Recognition of extensional structures that can produce large earthquakes (e.g., discrimination between dike-induced normal

faults and faults that rupture the whole seismogenic crust) is a great challenge for paleoseismologists.

The combination of magmatic and tectonic processes in continental rifts produces a variety of extension modes that can be defined as pure tectonic, pure magmatic, hybrid or a combination of some of the three modes (Fig. 30). Pure tectonic extension is achieved by normal faulting and it is manifested at the surface as geomorphic fault scarps (Fig. 30A). Pure tectonic faults rupture the entire or most of the seismogenic crust, producing large earthquakes.

Magmatic extension is achieved by dike intrusions, eruptive fissures and extension fractures. In this case three extensional modes are possible: dike intrusion through the whole crust with associated volcanic eruption and no surface faulting (Fig. 30B); dike intrusion through the whole crust with associated volcanic eruption and surface faulting (Fig. 30C); and arrested dike intrusion, i.e. when the dike stops short of the ground surface, and with surface faulting above the dike (Fig. 30D). In the two later cases faults have a very narrow fault width (hundreds of meters to a few kilometers) that are controlled by the depth of the dike. Rupture of such small fault areas will produce small earthquakes.

In the first magmatic case, the dike reaches the surface and creates a volcanic eruption, and no surface faulting occurs on the sides of the dike and the surface expression of extension is usually a series of aligned volcanic cones, fissures or vents in a trend perpendicular to the extension direction [Nakamura, 1977]. Structural analysis of paleo-rift zones suggest that where dikes are common faults are rare, and vice versa [Gudmundsson, 1995]. That implies that normal faulting does not occur in the near proximity to a dike; faulting can occur above the dike but not along its sides.

If dikes are arrested close to the surface, the crustal volume above the tip of the dike may be deformed, usually through normal faulting in the form of a nucleated graben

and extensional fissures [Rubin, 1992]. An example of faulting related to dike intrusions occurred during the Krafla fissure swarm in the Northern Volcanic Zone of Iceland [Paquet et al., 2007], where arrested dike intrusions caused deformation of the brittle crust, forming normal faults and tensile fissures at the surface (Fig. 30C). The width of the produced graben is controlled by the depth of the intruding dike and is usually narrow [e.g., <1 km for dikes intruding to 1 km depth; Rubin, 1992]. In areas where magmatism is the dominant driver of the extension, such as Iceland and Ethiopia divergent margins, faults can be associated to linear volcanic vents. Usually the faults form a few hundred meters away from the extrusion point [Tripanera et al., 2015]. Often these cases involve a horizontally propagating dike. Faulting is usually formed when the dike is propagating horizontally but is still arrested (Fig. 30D). Then extrusion occurs as the magma is abundant and close to the surface.

When dikes are arrested deeply in the crust, they can trigger tectonic faulting at the tip of the dike as it propagates (Fig. 30E). This extension mode is called here “hybrid extension”, because it combines both magmatic and tectonic extension. Deformation of the crust above the dike from dislocation models of deep arrested dikes shows that deformation may not reach the surface, or that displacements may be too small to be detected (Fig. 30D). As this faulting type is tectonic it ruptures most of the seismogenic crust above the deeply arrested dike. The surface expression of the hybrid extension is through geomorphic fault scarps, equal to those of tectonic faulting (unrelated to magmatism). While there is to date no reported examples of hybrid extension worldwide, this mode is similar to some of the cases where nearby faulting was triggered by dike intrusion [e.g., the 1999 eruption in Cerro Negro volcano, related to three MW 5.2 earthquakes; LaFemina et al., 2004]. The peculiarity here is that the fault is above the dike.

Parallel normal faults and tensile fractures are very important paleo-stress indicators because they form perpendicular to the minimum stress, and parallel to the maximum

stress [Nakamura, 1977]. Tension fractures form when the minimum principal compressive stress is low and are thus mostly limited to shallow depths in rift zones [Gudmundsson et al., 2010]. Fractures often form parallel to faults, but sometimes they can be related to volcanic earthquakes, gravitational load or dike emplacement near the surface, representing the local deformation rather than the regional deformation [Guba and Mustafa, 1988].

2.3 Dike intrusion and emplacement

Eruptions in volcanic rifts are normally fed by dike intrusions [Acocella and Neri, 2009]. Magma, which is hotter, less dense and less viscous than the adjacent rock, tends to rise in a dike-fissure as a result of its buoyancy or when the intrusive pressure of the magma exceeds the minimum principal stress and the tensile strength of the surrounding rock [Guba and Mustafa, 1988; Hackett et al., 1996].

Dikes can be very different depending on the regional environment. Average dikes extend down to 10-20 km depth, depending on the regional seismogenic depth. Their length/width ratio is usually 1000 (10 km long dike = 10 m thick), assuming a single dike-intrusion event, although dikes can also be intruded during many events. A single dike can produce many aligned vents (vent clusters) and repetitive dike intrusions can produce dike swarms and complex overlapping deformation features [Gudmundsson, 1983]. Their width can represent the amount of pure extension occurring during their emplacement [Gudmundsson, 2009].

Dike propagation and orientation in rift zones is mainly controlled by regional stresses. The sources of stress capable of driving magma flow in dike intrusions are excess pressure in the magma chamber, magma volatile content and orientation of tectonic stresses [Gudmundsson, 2006]. The orientation of the principal stress direction during dike intrusion controls the orientation of fractures [Magee, 2011]. The propagation

pattern of intrusions at shallow levels within a volcanic edifice depends on the geological, structural and geomorphological characteristics of the volcano and related tectonic stresses [Corazzato *et al.*, 2008]. Magma propagation within the seismogenic crust under a brittle regime involves opening of the fracture ahead of the tip of the dike, leading to propagating fluid and magma flow within the body [Scholz, 2002]. The tensile stress concentration around the dike is greatest at or near its tip; this is why it would easily propagate through the surrounding solidified rock [Gudmundsson *et al.*, 1999].

The main factors that can modify or control the volcano-extensional features are the volcanic mass (volcano load), the local and regional stresses, the depth of the brittle-ductile boundary, and the rheology of the host rock [Acocella and Neri, 2009]. The geometry and depth of the level of neutral buoyancy depend on density gradients within the volcanic edifice. Density is expected to be higher in the core of the edifice and at depth, mainly due to the greater number of intrusions and greater volcanic mass, while it is expected to decrease toward the flanks of the edifice and away from the volcanic centre [Fig. 2; Acocella and Neri, 2009].

Not all dikes make it to the surface and create an eruption. Some energy is used in displacing or breaking through the rocks during its ascent but eventually, as the density contrast between magma and the adjacent rock approaches zero, the magma accumulates and spreads laterally to form a laccolith or a sill and it solidifies [Gudmundsson, 2002]. Soft layers allow dikes to become wider, and weak contacts (e.g., discontinuities, existing normal faults or tensile fractures) suppress dike tensile stress and encourage dike arrest [Gudmundsson and Brenner, 2004]. Dike arrest may also depend on the topography and tectonic setting, which could modify the stress distribution within the rift [Acocella and Neri, 2009]. Usually, arrested buoyancy-driven dikes produce large vertical deformation features above the dike in the form of normal faults or graben subsidence in volcanic rift zones [Rubin, 1992]. Without knowledge of

an arrested dike at depth, surface faults in such situations could be interpreted as purely tectonic, rather than dike-related faults [e.g., *Biggs et al.*, 2009].

A dike intrusion can create a broad zone of uplift up to 10 km wide (swelling), with a narrow zone of subsidence above the propagating dike, where subsidence may be accommodated by normal faulting. The uplift or tilting of the summit area prior to extrusion indicates that the magma accumulates temporarily in a laccolith-like reservoir [*Head et al.*, 1996; *Gudmundsson*, 2011]. The magnitude of the cumulative fault throw at the surface above an intruding dike and the horizontal extension are proportional to the dike width and length, thus basaltic dikes are normally thinner than silicic ones and thicker dikes produce more pronounced grabens and fissures [*Hackett et al.*, 1996; *Head et al.*, 1996].

In a major central volcanic system, magma can be released by a summit eruption, or can migrate along rift zones, producing a flank (fissure) eruption, or both [*Phillips*, 1974]. Explosive gas-expansion driven eruptions are more common from summit craters, while degassed magmas most commonly produce effusive eruptions from flank craters, and the distribution of outer flank craters can reveal the subsurface pattern of dikes [*Nakamura*, 1977]. Dike propagation will depend on the volcanic structure, because it is more difficult for a fracture to propagate through a steep, tall stratovolcano than through a low-sloping basaltic edifice. This might also be related to the difference in slope and to the intrusion frequency [*Gudmundsson*, 2009].

Studying dike emplacement can help establish volcano recurrence intervals and rift extensional rates. Bacon [1982] assumed that the volume of domes erupted at a given volcano during a defined time interval was proportional to the dikes width and therefore to extension during that interval. A second approach to estimate the number of dikes is to estimate the ages, stratigraphy and petrology of exposed domes and lava flows to derive the number of events of dome/lava formation and therefore dike intrusions. If the

domes/lavas have the same age and same chemistry they are assumed to have been fed by the same or linked dikes. If dike intrusion rates are greater than fault slip-rates, dikes are intruding in response to high magmatic pressures or magma chamber inflation, in addition to crustal extension [Bursik and Sieh, 1989].

2.3.1 Volcanic load as an influence on fault and dike patterns

Volcanic mass can load the crust, increasing and reorienting stresses [de Vries and Merle, 1996]. In a rift with aligned volcanoes, added mass leads to increased extension at the volcano, promoting dike intrusions and possibly contributing to voluminous eruptions and less-evolved magmas [de Vries and Merle, 1996]. As the volcanic load increases, the volcanic edifice subsides and creates a compressional stress which inhibits dike intrusions, allowing magmas to evolve or differentiate [Borgia, 1994]. Compressional stress may promote gravitational failure and slumping in weak structures of the volcano flanks [Borgia et al., 1990]. And with greater volcanic load, stresses at the base of the volcano become extensional which allows dike intrusions and may contribute to voluminous eruptions. Those extensional stresses spread to the upper flanks of the volcano and allows less-evolved magmas to erupt [Borgia, 1994].

Volcanic load can also reorient faults or dike intrusions if there is a ductile layer below the volcano [de Vries and Merle, 1996]. Lithostatic load can also concentrate volcanism and narrow the rift. For regional extension without a volcano, the axis of least compressive stress (σ_3) lies in the direction of the extension, the intermediate stress (σ_2) is parallel to it, and the maximum stress (σ_1) is vertical. Faults would form orthogonal to σ_3 and parallel to σ_2 . For regional extension and volcano load, the system will likely show bilateral symmetry, where the least compressive stress orientation will become concentric near the volcano, and parallel at the axis of the rift, where extension should be greatest [Fig. 2; de Vries and Merle, 1996].

I large volcanic edifices with increased lithostatic load gravitational failure and slumping of the flanks of volcanoes can occur.

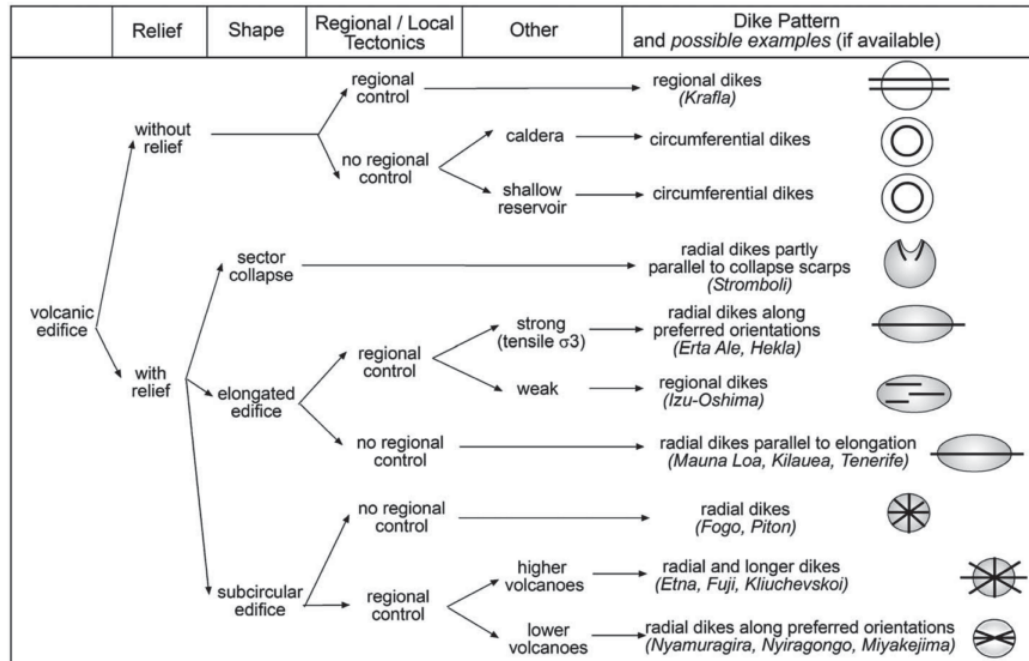


Figure 2. Main parameters controlling dike emplacement [from *Acocella and Neri, 2009*].

2.3.2 Seismogenic depth as an influence on dike patterns

The depth of the brittle-ductile boundary (seismogenic depth) is another factor that can control magma intrusions and the location of volcanic edifices within a volcanic rift zone [*Tibaldi, 1995*]. A compressional regime can lead to the formation of a magma reservoir and bifurcation of dikes above the brittle-ductile boundary, favouring the construction of stratovolcanoes; while an extensional regime could hinder the formation of a central magma reservoir, allowing the bifurcation of magma batches below the boundary and favouring monogenetic volcanoes [Fig. 3; *Kurokawa et al., 1995*].

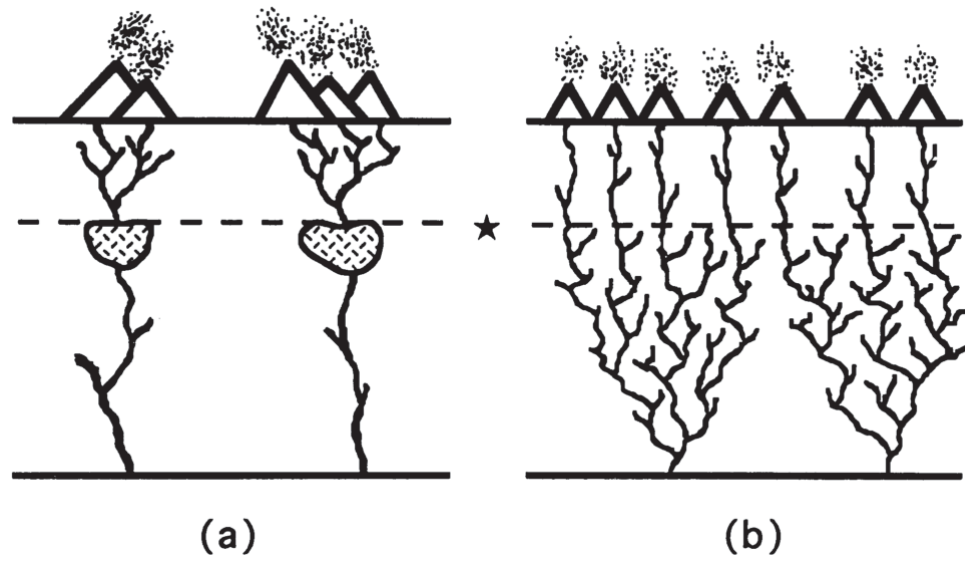


Figure 3. Schematic illustration showing the pattern of dike emplacement and type of volcanoes when horizontal tectonic stress is compressional (a) and tensional (b). * (star) depth of brittle-ductile boundary. The shaded parts below the brittle-ductile boundary in 'a' denote magma chambers [from *Kurokawa et al.*, 1995].



Figure 4. Mead's Wall dike (2-4 m wide) at Whakapapa ski field on the northern flanks of Mt. Ruapehu, view looking north at 1678 m elevation.

2.4 Magma-Tectonic Interactions

Magma-tectonic interactions are the relationships between magma activity and crustal tectonic stress. Magmatic activity refers to the movement of magma within the crust or in a magma reservoir, or through a dike or fracture, which may or may not lead to a volcanic eruption. The forces caused by magma processes (crystallization, magma movement, changes in magma volume, etc.) can influence the state of stress of the crust around the body of magma and may affect nearby tectonic structures [Nostro *et al.*, 1997]. Tectonic forces in the crust, as a consequence of relative movement between the tectonic plates, induce changes in the state of stress in the crust. For instance, a constant build-up of tectonic stresses in association with the forces caused by movement of the tectonic plates can cause the rupture of weak planes within the crust [Stein *et al.*, 1994]. The sudden rupture of faults and fractures creates a tectonic earthquake, and the release of energy during a tectonic earthquake also causes changes in the state of stress of the crust around it and may affect the stress fields around nearby magma chambers and other faults [e.g., King *et al.*, 1994], potentially triggering eruptions and other tectonic earthquakes. The coupling zone where tectonic earthquakes may trigger eruptions and vice versa, occurs only when normal faults are close to Coulomb failure or when magma chambers are near a critical overpressured state [Nostro *et al.*, 2001]. Increasing the Coulomb stress on a fault promotes earthquake failure, and increasing the compressive stress in a magma reservoir at depth and opening its near-surface conduits promotes dike intrusions [Buck *et al.*, 2006; Gudmundsson, 2006]

Stresses arising from tectonic earthquakes can control volcanic unrest. These stresses consist of static (permanent rupture) and dynamic (transient) stress changes [Watt *et al.*, 2009]. Static stress changes seem to be more important for rapidly triggered events within the rupture zone (within hours), because they decay more rapidly with distance from the fault zone than dynamic stresses [Manga and Brodsky, 2006], for example,

the 1960 eruption of Cordón Caulle initiated 38 h after the M_w 9.5 Chilean earthquake [Barrientos, 1994]. This eruption was triggered by magmatic decompression and gas exsolution as a result of strain from extension beneath the volcano [Barrientos, 1994; Manconi *et al.*, 2007]. Conversely, dynamic stress changes are likely to act on longer timescales (within months), even with small stress changes (0.01-0.30 MPa), and on longer distances from the rupture zone (~200–800 km), by promoting vesiculation of rising magma and convection [Manga and Brodsky, 2006; Hill, 2008; Watt *et al.*, 2009], for example, the 1906 eruptions of Chaitén volcano followed the M_w 8.3 Valparaiso earthquake even though it was 450 km beyond the rupture zone [Pallister *et al.*, 2010].

In 2002, Koyama reviewed the possible types of mechanical coupling between volcanic unrest events and large earthquakes: When an earthquake promotes the activation of a volcano (triggering vesiculation of rising magma and convection), there are four mechanisms that explain their coupling: (a) increase in compressional stress, (b) increase in differential stress or magma pressure, (c) increase in tensional stress, and (d) dynamic stress change associated with seismic waves. When a volcano promotes an earthquake (triggers fault rupture), the coupling can be explained (a) by changes in stress produced by dike intrusion, or (b) by pressure changes in the magma chamber [Koyama, 2002].

The interplay between tectonic and volcanic sources is complex. Structures are not always easily differentiated, and magma-induced extensional structures may be misinterpreted as co-seismic tectonic features. The best criteria for identifying volcano-extensional features are their demonstrated relationship to co-genetic volcanic materials, their lack of net vertical displacement across the graben, the small-scale offsets of individual structures, their bilateral symmetry and their association with eruptive fissures along volcanic rift zones [Hackett *et al.*, 1996].

Historic displacements of normal faults that ruptured through the whole crust (or near to it) produce moderate to large earthquakes with well-defined magnitude-displacement empirical scaling relationships [e.g., *Stirling et al.*, 2012]. Conversely, displacements along normal faults associated with shallow arrested dikes (magma-induced normal faults) do not follow these typical empirical scaling relationships because they display relatively large offsets for small earthquakes [e.g., *Rowland et al.*, 2010].

Many volcanic earthquake swarms have been associated in time with eruptions at nearby volcanoes [*Sykes and Sbar*, 1973; *Benoit and McNutt*, 1996]. Four types of earthquakes can occur as an effect of a volcanic eruption: volcano-tectonic earthquakes (VT), low-frequency earthquakes (LP), very low-frequency earthquakes (VLP) and ultra-low frequency earthquakes (ULP, tilt events) [*Ishihara*, 2003; *Roman and Cashman*, 2006]. VT earthquakes are high frequency and short-period earthquakes produced by stress changes in solid rock due to the injection, or withdrawal, of magma or slip on a fault. LP are shallow earthquakes produced by fluid interaction within magma or by the injection of magma into surrounding rock as a result of pressure changes during the unsteady transport of the magma. When magma injection is sustained, a low-magnitude earthquake swarm is produced [*Chouet*, 1996]. VLP earthquakes are very-long-period volcanic earthquakes with a very low frequency. They have been recorded during volcanic eruptions and most likely involve fluid flows, either magma or hydrothermal [*Kumagai et al.*, 2002]. VLP earthquakes can provide insights into conduit geometry and eruption dynamics. ULP earthquakes are ultra-long-period seismic signals that are associated with degassing events during a volcanic eruption and visual observations are thus crucial for understanding the origin of the ULP signals [*Sanderson et al.*, 2010]. These volcanic tremors may occur before, during or after the initial eruption, possibly suggesting mutual triggering relationships [*Nakamura*, 1975; *Hill et al.*, 2002; *Walter and Amelung*, 2006].

The way in which rocks respond to external forces is highly variable, reflecting the type of rock, as well as the properties of the applied force; e.g. a more viscous magma may require a larger magnitude earthquake or a shorter epicentral distance to trigger an eruption [Fujita *et al.*, 2013]. Magma composition, rheology, storage depth, state of volatile saturation, as well as magmatic overpressure, are considered as some of the main factors controlling volcanic eruptions [e.g., Woods and Pyle, 1997; Jellinek and DePaolo, 2003]. Magmatic overpressure is likely to be a key factor determining the time lag before an eruption triggered by tectonic activity [e.g., Blake, 1984; Tait *et al.*, 1989; Manga and Brodsky, 2006].

2.4.1 Historical examples of volcano-tectonic interactions

Identifying comparative examples to the TgVC may help with understanding the possible mechanical coupling in volcano-tectonic interactions. The following are some historical examples of volcanic activity linked to tectonic earthquakes that have been described from around the world.

Fuji, Japan

An example of a tectonic-triggered eruption is the December 1707 explosive eruption (VEI 5) of Mt. Fuji, 49 days after the M_w 8.2 Hiei earthquake [Miyaji *et al.*, 2011]. The strain and dynamic stress changes affected the magma system, resulting in the opening of the dike and ascent of basaltic magma from 20 km into andesitic and dacitic magma chambers located at 8 km depth. The injection of basaltic magma led to magma mixing and a plinian eruption [Chesley *et al.*, 2012].

Bandai, Japan

The great eruption and volcanic collapse in July 1888 at Bandai volcano were promoted by a M_w 5 earthquake 200 km south of the volcano. The seismic shocks and subsequent collapse of the edifice unroofed a pressurised hydrothermal system to cause a sudden expansion and flashing of steam, creating the explosion. Sudden steam production by the release of a confined aquifer can be triggered by reduction of the lithostatic load after a collapse and seismic shocks [Yamamoto *et al.*, 1999].

Kilauea, Hawaii, USA

Kilauea caldera erupted in November 1975, within half an hour of a M_w 7.2 earthquake and large mass movements on the flank of the volcano [Lipman *et al.*, 1985]. At Kilauea the injection of dikes parallel to the SE rift inflates the flank of the volcano, generating flank failures when the over-steepening reaches a critical point. It is uncertain whether the failure actually triggers the eruption, or if the failure is an inevitable consequence of the injection of large amounts of basalt during one of these events, i.e. the dike injection sets the scene for the eruption and the collapse and earthquake are consequential rather than causative.

Karymsky, Kamchatka

A M_w 7.1 tectonic earthquake occurred on Kamchatka peninsula in January 1996 along a SW–NE-trending fracture system. Just two days after the earthquake and at a distance of about 10–20 km to the north, a simultaneous eruption of two separate volcanoes followed: the Karymsky Volcano and Akademia Nauk Volcano. The observations suggest that stress changes related to year-long inflation under the volcanic centres increased the stress to the point where Coulomb failure occurred at

the faults. The earthquake, in turn, promoted dilatation of the magmatic system together with extensional normal stress from intruding N–S trending dikes [*Walter et al.*, 2007].

Shishaldin, Alaska

In March 1999, a shallow M_w 5.2 earthquake occurred beneath Unimak Island in the Aleutian Arc, 10–15 km west of Shishaldin Volcano, a large, frequently active basaltic–andesite stratovolcano. A Strombolian eruption began at Shishaldin roughly 1 month after the main earthquake, culminating in a major explosive eruption in April. Coulomb stress was found to have increased by ~ 0.1 MPa, suggesting that magma intrusion prior to the eruption could have triggered the main earthquake [*Moran et al.*, 2002].

Cerro Negro, Nicaragua

Three M_w 5.2 earthquakes triggered a low-energy (VEI 1) eruption of highly crystalline basalt at Cerro Negro volcano in August 1999. The tectonic earthquakes happened 11 hours before the eruptive activity and within 1 km NW and SE of Cerro Negro, where three new vents formed on the south flank and base of the volcano, promoted by tectonically induced changes in the regional stress field with the accommodation of extensional strain by dike intrusion [*LaFemina et al.*, 2004].

Etna, Italy

The Octobre 2002 eruption at Mt. Etna volcano was preceded by a large tectonic earthquake swarm a month before its onset and accompanied by ground deformation and fracturing from the northeast rift zone. The M_w 5.9 Palermo earthquake occurred

<150 km from Mt. Etna, which eruption was synchronous with the Panarea and Stromboli eruptions [Monaco *et al.*, 2005; Walter *et al.*, 2009].

Merapi, Indonesia

In 2001, a M_w 6.3 tectonic earthquake occurred at 130 km depth and 50 km SW of Mt. Merapi, in conjunction with an increase in fumarole temperature at this volcano. In 2006, another M_w 6.3 tectonic earthquake matching the depth of the subducting slab under this region took place, concomitant with an increase of magma extrusion and pyroclastic flows, possibly affected by seismic dynamic stress changes [Walter *et al.*, 2007].

Sumatra-Andaman Arc, Indonesia

Two volcanic eruptions in the Sumatra-Andaman arc were probably triggered by the M_w 9.3 and 8.7 earthquakes in December 2004 and March 2005, respectively. Talang and Barren Island (India) volcanoes began erupting 12 days and two months, respectively, after the second earthquake, suggesting that abrupt decompression of a magma reservoir and/or its feeding system initiates processes that increase magma overpressure, and can ultimately lead to an eruption [Walter *et al.*, 2007].

Vesuvius, Italy

During the past 1000 years, eruptions of Vesuvius have often coincided with large earthquakes in the Apennines 50–60 km to the northeast. Dynamic stress changes can promote events when the Apennine normal faults and the Vesuvius magma body are close to failure, and oriented normal to the Apennines. A two-way coupling may thus

link earthquakes and Vesuvius eruptions along a 100-km-long set of faults [*Nostro et al.*, 2001].

OI Doinyo Lengai, Tanzania

In the East African Rift, North Tanzania earthquake swarms of $M_w < 5.9$ may have been linked with the 2007 eruptions of the OI Doinyo Lengai volcano. The change of mean stress (~ 0.001 MPa) was induced by the diking and faulting events in July and August 2007, at 5 km and 10 km depth. This suggests that, during the Gelai earthquake swarm, the dynamic effects of seismic waves through the nearby Lengai magma chamber may have promoted the growth and ascent of bubbles in the reservoir [*Baer et al.*, 2008].

Taupo Volcanic Zone, New Zealand

In the central Taupo Rift, volcano-tectonic interactions have been inferred between the rifting and magma movement within the crust. Paleoseismic data from the central Taupo Rift (Ngakuru Graben) suggest that there is a temporal association between eruptions of the Okataina Volcanic Centre and nearby faulting [*Villamor et al.*, 2011]. For example, the 1315 AD rhyolite Kaharoa eruption [*Hogg et al.*, 2003] was primed by a deep basaltic dike [*Nairn et al.*, 2004]. The eruption followed a Ngapouri Fault earthquake but the timing relationship between the earthquake and the initial depth of the basaltic dike is unknown [*Berryman et al.*, 2006]. *Berryman et al.* [2008] and *Villamor et al.* [2011] found geomorphic relationships in paleoseismic trenches that show fault rupture during deposition of volcanic ash on the fault scarp. *Villamor et al.* [2011] suggest that stress transfer could encourage faulting after a dike intrusion and magma chamber inflation or deflation in the Okataina Volcanic Centre.

In the southern Taupo Rift, on the northern Waihi Fault at the south-western edge of Lake Taupo, a M_w 6.3 earthquake in May 1846 was responsible for disastrous landslides [Hegan *et al.*, 2001; Cooper, 2002]. In the same month, an eruption at Ketetahi occurred, suggesting a possible connection with the Waihi Fault earthquake [Scott and Potter, 2014].

2.5 The Study area: The Tongariro Volcanic Centre



Figure 5. Ngāuruhoe volcano and Tongariro Volcanic Complex viewed from Mt. Ruapehu, view approximately to the north.

2.5.1 Active Tectonics of New Zealand

The New Zealand region has undergone several episodes of mountain building and subsidence in a complicated tectonic history, driven by rapid changes in the tectonic setting [Cole, 1990; Wilson *et al.*, 1995]. Alongside the North Island, the Pacific Plate subducts below the Australian Plate [Wallace *et al.*, 2004]. Some parts of the subduction zone (Hikurangi Trench) have been active for the last 40 Ma. They have rotated clockwise at least 60° in the last 20 Ma and are still rotating today [Walcott, 1987; Wallace *et al.*, 2004]. The total displacement across the post-Eocene plate boundary zone is ~ 900 km [Stock and Molnar, 1982] and the total displacement across

the post-Miocene plate boundary zone is ~200 km, obtained from the average rate over the last 5 Ma [Fig. 6; *Walcott*, 1987].

The NNE-SSW Hikurangi Trench, where the Pacific Plate subducts below the Australian Plate, initiated about 15 Ma ago and has progressively propagated southwards with time. Extension is present in a perpendicular direction from the trench, due to the increment of the Pacific Plate subducting angle and slab-rollback. This extension began in Late Miocene or Pliocene times (~5 Ma ago) [*Wallace et al.*, 2004; *Mortimer et al.*, 2007]. The deformation constrained by GPS demonstrates that the North Island rotates clockwise at approximately 0.5–3.8°/Ma relative to the Australian Plate [*Walcott*, 1987]. DeMets et al. [1994] calculated the Pacific/Australia relative motion at 45 mm/yr in the North Island and 35 mm/yr in the South Island (Fig. 6).

The current fore-arc rotation of the Eastern North Island has created an intra-arc extensional regime in the central and northern North Island, leading to formation of the Taupo Volcanic Zone (TVZ). The TVZ exhibits extension rates between 20 mm/yr in the north and 6 mm/yr in the south [*Beanland*, 1995; *Wallace et al.*, 2004]. A change from extension to compression takes place in the southern North Island [*Wallace et al.*, 2004]. This structure means that the central North Island's situation is very complex with many coincident tectonic styles, including intra-arc spreading, continental rifting, transcurrent faulting and fore-arc basin development, involving both extension and folding, as well as volcanic activity.

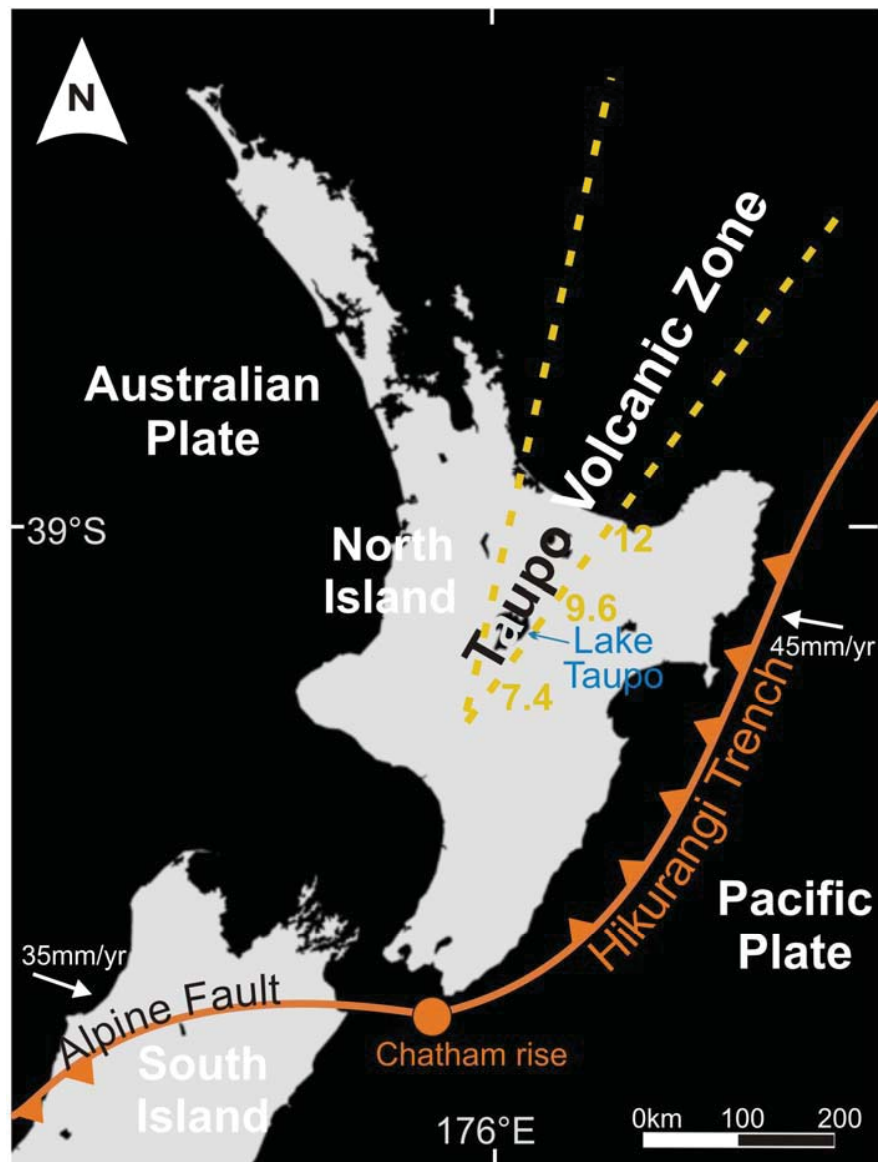


Figure 6. Tectonic setting of New Zealand [from Wallace *et al.*, 2004] displaying the deformation within the plate boundary zone (Hikurangi Trench) and the progressive subduction of the Pacific Plate beneath the Australian Plate. Yellow dashed line shows the location of the Taupo Volcanic Zone and yellow numbers show the variation of extension rate along the rift, values in mm/yr [Wallace *et al.*, 2004]. White arrows show Pacific/Australia relative motion in New Zealand [DeMets *et al.*, 1994].

Compression at the Hikurangi Trench started at 2 Ma at the latest and produces an average uplift rate of 2.5 mm/yr [Walcott, 1987; Nicol and Wallace, 2007], forming the Hikurangi Ranges (Eastern Ranges). The central part of the North Island is a series of mountains, known from north to south as the: Kaimanawa, Ruahine, Tararua and

Orongorongo Ranges, which are a Mesozoic greywacke sequence, with peaks oriented NNE-SSW for 110 km [Lee *et al.*, 2011].

At the southern end of the North Island, the Hikurangi plateau thickens, creating resistance that inhibits subduction. Convergence becomes more oblique to the south and there is more complex partitioning of stress between plate-normal and strike-slip components. More than 1,000 km of lithosphere has been subducted in the northern parts of the Hikurangi Trench, but little or none has been subducted in the south. The rate of present day rotation of the Hikurangi Trench relative to the Pacific Plate is 75 mm/yr at the northern limit, directed perpendicular to the trend of the plate boundary zone. Along the east Pacific coast this direction remains constant but the rate decreases to zero at the southern limit [Nicol and Wallace, 2007].

2.5.2 Regional Geology

The basement geology of New Zealand consists of a number of tectono-stratigraphic terrains and igneous suites that were accreted onto the supercontinent of Gondwana during the late Palaeozoic and Mesozoic era [Mortimer, 2004]. The central North Island lies above the Torlesse and Waipapa Eastern Province terrains, which are dominated by lithic and feldspathic metagreywackes, but also include volcanic, intrusive and ophiolitic assemblages [MacKinnon, 1983; Sutherland, 1999].

The Taupo Volcanic Zone (TVZ) is a NNE-trending Quaternary volcanic arc associated with the subduction of the Pacific Plate below the Australian Plate in the central North Island of New Zealand [Wright, 1993]. The TVZ lies 150 km W from the Hikurangi Trench and is dominated by active rifting [Fig. 7; Acocella *et al.*, 2003]. Extension is created by fore-arc clockwise rotation [Wallace *et al.*, 2004] and slab rollback [Seebeck *et al.*, 2014]. Extension across the rift is associated with a combination of dike intrusion and normal faulting [Rowland *et al.*, 2010; Villamor *et al.*, 2011]. Faults within the

volcanic arc define an intra-arc rift, the Taupo Rift [Rowland and Sibson, 2001; Acocella et al., 2003].

The volcanic arc is known for its rhyolitic calderas, active andesitic stratovolcanoes, parasitic vents, and geothermal and hydrothermal activity within an active fault belt with horst and graben structures [Wilson et al., 2009; Leonard et al., 2010]. The TVZ is also known for having the highest heat flow/km of active arcs [700 mW/m³; Bibby et al., 1995]. It can be divided into three parts: the central part is dominated by eight rhyolitic calderas with >25 caldera-forming eruptions in the last 1.6 Ma [Wilson et al., 2009], while the northern and southern parts comprise andesitic stratovolcanoes [Wilson et al., 1995].

2.5.2.1 The magmatic system of the Tongariro Volcanic Centre

The Tongariro Volcanic Centre (TgVC) forms the southern part of the TVZ. It is a 13 km-long and 5 km-wide basaltic-andesite to dacitic volcano-vent corridor complex [Hackett and Houghton, 1989] within the Mt. Ruapehu and Tongariro grabens [Villamor and Berryman, 2006a]. The TgVC mainly consists of three volcanic complexes (Mt. Ruapehu volcano, the Tongariro Volcanic Complex and the Kakaramea-Tihia massive) and many dispersed vents (Te Tatau, Pukeonake, Maungakatote, Maungaku, Hauhungatahi, Tahurangi Peak, Ohakune craters). Mt. Ruapehu consists of a large andesitic stratovolcano and the Sadde Cone satellite vent. The Tongariro Volcanic Complex consists of two large volcanoes (Mt. Tongariro and Ngāuruhoe) and 12 minor NNE-aligned vents (Upper and Lower Tama Lakes, Pukekaikiore, Oturere Valley Vents, Blue Lake, North Crater, Te Maari Craters, Red Crater, South Crater, Central Crater). The Kakaramea, Tihia and Pihanga form a chain of volcanoes at the northern part of the TgVC [Fig. 7; Hobden et al., 1999].

Mt. Ruapehu is the southernmost and largest volcano in the TgVC and one of the most active volcanoes in New Zealand. It is a complex andesitic stratovolcano with a Crater Lake over its active vent, and is one of the world's most regular producers of lahars [Cronin *et al.*, 1997b; Procter *et al.*, 2010a]. The eastern flanks of Ruapehu, on which flow the Whangaehu River, Mangatoetoenui Stream and Wahianoa River, have been a major pathway for lahars overflowing towards the Desert Road (eastern flanks; state highway 1) since prehistoric times [Lecointre *et al.*, 2004a]. The Whangaehu River drains south to the Whanganui coast, and occasionally lahars overflow into the Tongariro River [Cronin *et al.*, 1997c]. In prehistoric times, lahars may have flowed from the Whangaehu drainage into the Waikato Stream at times, but they also flowed down through Waiouru and Taihape until growth of the Rangipo Fault diverted them down their present course [Procter *et al.*, 2010a].

The TgVC erupts mainly andesitic magmas (Fig. 8). The silica content of erupted magmas ranges between 52.7 and 66.3 wt. % SiO₂. They are mostly medium-K and quartz-hypersthene normative andesites; they exhibit coherent geochemical trends of decreasing Mg, Fe, Ca contents, increasing LILE contents, increasing ⁸⁷Sr/⁸⁶Sr and decreasing Nd with increasing silica [Graham *et al.*, 1995]. All lavas are variably porphyritic (10-40% of phenocrysts) and many contain glomerocrysts, plutonic nodules (gabbro, websterite), and xenoliths from lower, middle and upper crustal levels. Phenocryst assemblages are characterized by plagioclase, orthopyroxene, clinopyroxene, magnetite with accessory chrome spinel, ilmenite and apatite [Gamble *et al.*, 2003; Price *et al.*, 2012].

Andesitic magmas have evolved in a complex system of variable volume reservoirs dispersed throughout the crust with fractional crystallisation, crustal assimilation and magma mixing and mingling being the dominant processes determining whole rock and mineral chemistry and rock textures. Young Ruapehu eruptives (1945–1996) are the end product of a long-lived magmatic system that has reached a steady and mature

The Mt. Ruapehu and the Tongariro Volcanic Complex magmatic systems are different. The Mt. Ruapehu andesitic open-system originated from mantle magmas that infiltrate the lower crust. These magmas stored and evolved in small reservoirs, sills and dikes dispersed in the crust at 5-7 km depth [Nakagawa et al., 1999; Miller and Savage, 2001]. These magmas result in crystal fractionation, crustal assimilation, magma mingling and mixing, which migrate to the surface through a complex plumbing system [Gamble et al., 2003; Price et al., 2005]. In contrast, the Tongariro Volcanic Complex system has remained relatively open with cycles of crustal processing being initiated by periodic influxes of new magma straight from the brittle-ductile boundary at 10-15 km depth [Hayes et al., 2004; Price et al., 2010; Stirling et al., 2012].

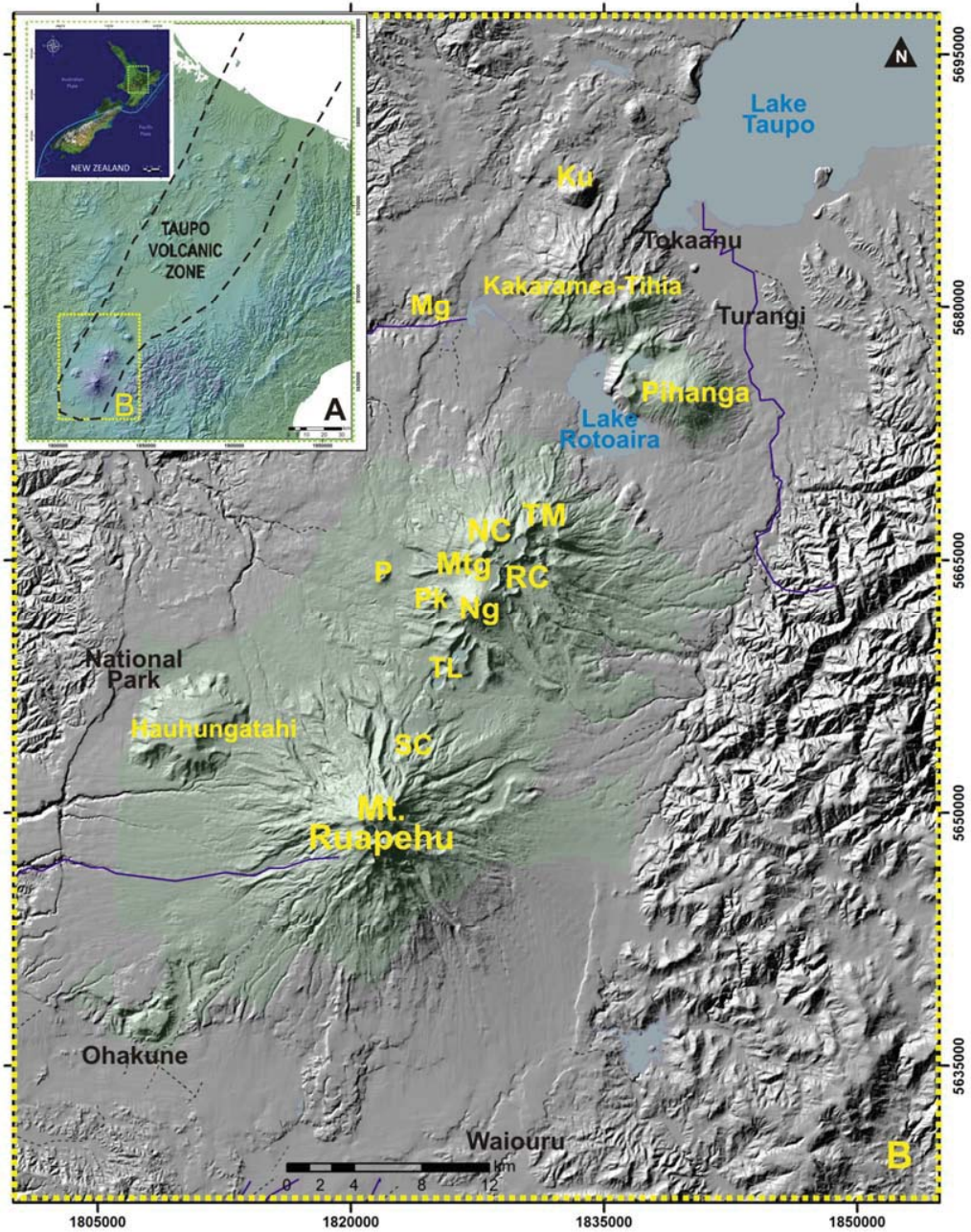


Figure 7. Location map of the Tongariro Volcanic Centre (B) as defined by Cole [1978], and its main volcanic structures within the Taupo Volcanic Zone (TVZ) in the central North Island of New Zealand (A), as described by Gregg [1960]. SC, Saddle Cone; TL, Tama Lakes; Ng, Ngāuruhoe; Pk, Pukekaikiore; P, Pukeonake; MTg, Mt. Tongariro; RC, Red Crater; TM, Te Maari; NC, North Crater; Mg, Maungakatote; Ku, Kuharua.

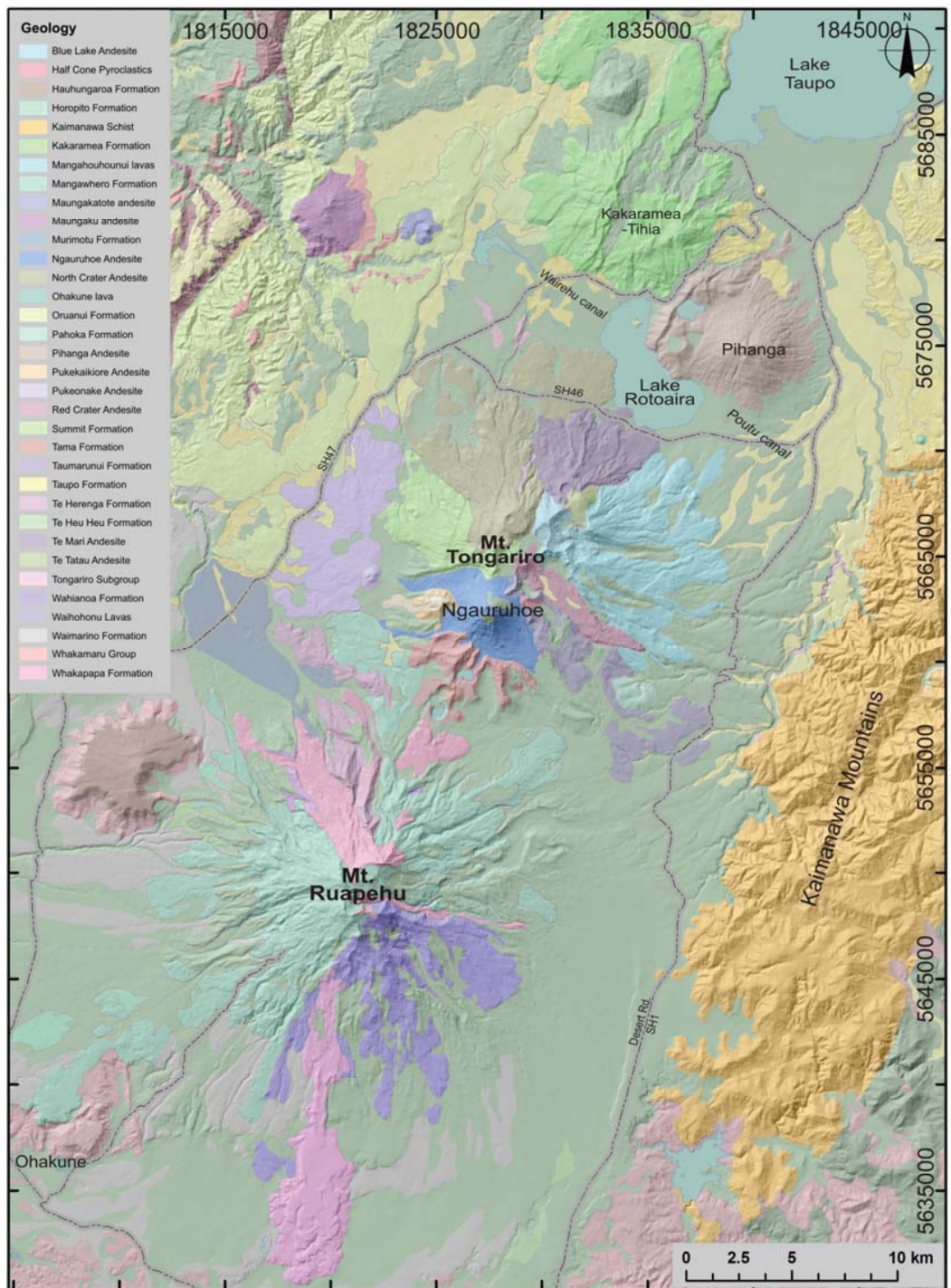


Figure 8. Geological map showing main summary geologic units of the Tongariro Volcanic Centre in New Zealand [modified from QMap; Lee *et al.*, 2011].

2.5.3 Structural Geology

NNE-striking faults delineate the Taupo Rift margins and axis, while E-W and ENE-striking faults delineate the southern termination. Volcanic vents are also NNE-aligned, along the axis of the Mt. Ruapehu and Tongariro grabens [Nairn *et al.*, 1998; Acocella *et al.*, 2003; Villamor and Berryman, 2006b].

Villamor and Berryman [2006a], Langridge *et al.* [2016], Townsend *et al.* [2008] and Lee *et al.* [2011] mapped the active faults and studied some of them at the southern part of the TVZ. Active faults are normal in sense and include three major structures: the NNE-trending Mt. Ruapehu Graben; the E-W to ESE-WNW trending Ohakune-Raetihi fault set; and the NE-trending Karioi fault set (Fig. 9).

The Rangipo Fault is located at the eastern margin of the Ruapehu Graben [Villamor and Berryman, 2006a]. The Rangipo Fault is an active, NNE-striking, normal fault downthrown to the west, and is at least 32 km long with a clear geomorphic expression. To the south, the Rangipo Fault is bounded by the Snowgrass Fault, but its northern extent is still uncertain due to erosion of the scarp by the Whangaehu River and/or by burial with recent lahar deposits. Prior to this study, the fault was mapped only as far north as the intersection with the Wahianoa Fault [Villamor *et al.*, 2007]. Donoghue [1991] estimated 3 mm/yr of displacement, but Villamor *et al.* [2007] calculated from paleoseismic trenches and geomorphic analyses a displacement rate of 1.4 ± 1 mm/yr from 17.7-27 cal ka BP to the present day, and of 0.2 mm/yr from 13.8 cal ka BP to the present day. These data imply an average long-term slip-rate of 1.5 mm/yr for the last c. 65–230 kyr and a period between 13.64 cal ka BP and 17.7–25.4 cal ka BP where slip-rate could have been up to 9 mm/yr. Past earthquakes on the Rangipo Fault have estimated magnitudes between 5.9 and 7.1 with recurrence intervals from 3.4 ka to more than 14 ka, depending on the fault segmentation [Villamor *et al.*, 2007].

The Wahianoa Fault is an ENE-striking normal fault downthrown to the SE, and is the main fault of the Karioi fault set. It has a prominent geomorphic expression for at least 10 km across the SE flanks of Mt. Ruapehu, but the northeastern side of the fault is obscured by younger deposits of lahars and tephra from the TgVC. Preliminary slip-rates were assessed for this fault by Villamor and Berryman [2006a] at 0.3 ± 0.2 mm/yr. It is not certain whether the Wahianoa Fault extends beyond the current mapped trace, as it could be buried under young lahar deposits. Based on the current national Seismic Hazard Model (prior to this study), this fault is capable of producing M_w 6.7 earthquakes based on a 27 km fault length [Stirling *et al.*, 2012; Litchfield *et al.*, 2013].

At the southern termination of the TVZ, there is a co-existence of the three active normal fault sets: the NNE-trending Mt. Ruapehu Graben, the E-W to ESE-WNW-trending Ohakune-Raetihi fault set, and the NE-trending Karioi fault set (Fig. 9). This complex configuration is a consequence of block rotation of the Hikurangi Trench, which may lead to local reorientation of the principal axis of extension (σ_3) (similar to a situation where $\sigma_2 \approx \sigma_3$), possibly causing the abrupt ending of the Taupo Rift [Villamor and Berryman, 2006a].

Normal fault displacements together with fissures and dike intrusions, accommodate extension along the Ruapehu Graben [Rowland *et al.*, 2010]. Mafic dikes feed NNE-trend aligned volcanic vents [Nairn *et al.*, 1998], expressed as a volcanic vent complex emplacing intermediate compositions. Some of the magmatic and tectonic structures within the TVZ are different from the NNE-trend; some of them (NNW-SSE) might represent the southern continuation of the Miocene-Pleistocene Coromandel Volcanic Zone [Skinner, 1986]. Extra-rift volcanic structures are simpler and smaller, represented mostly by monogenetic volcanoes, without significant coupling to active regional faulting. This distinction might demonstrate the role of active tectonics in controlling the location, structure, and development of volcanic systems within the rift zone.

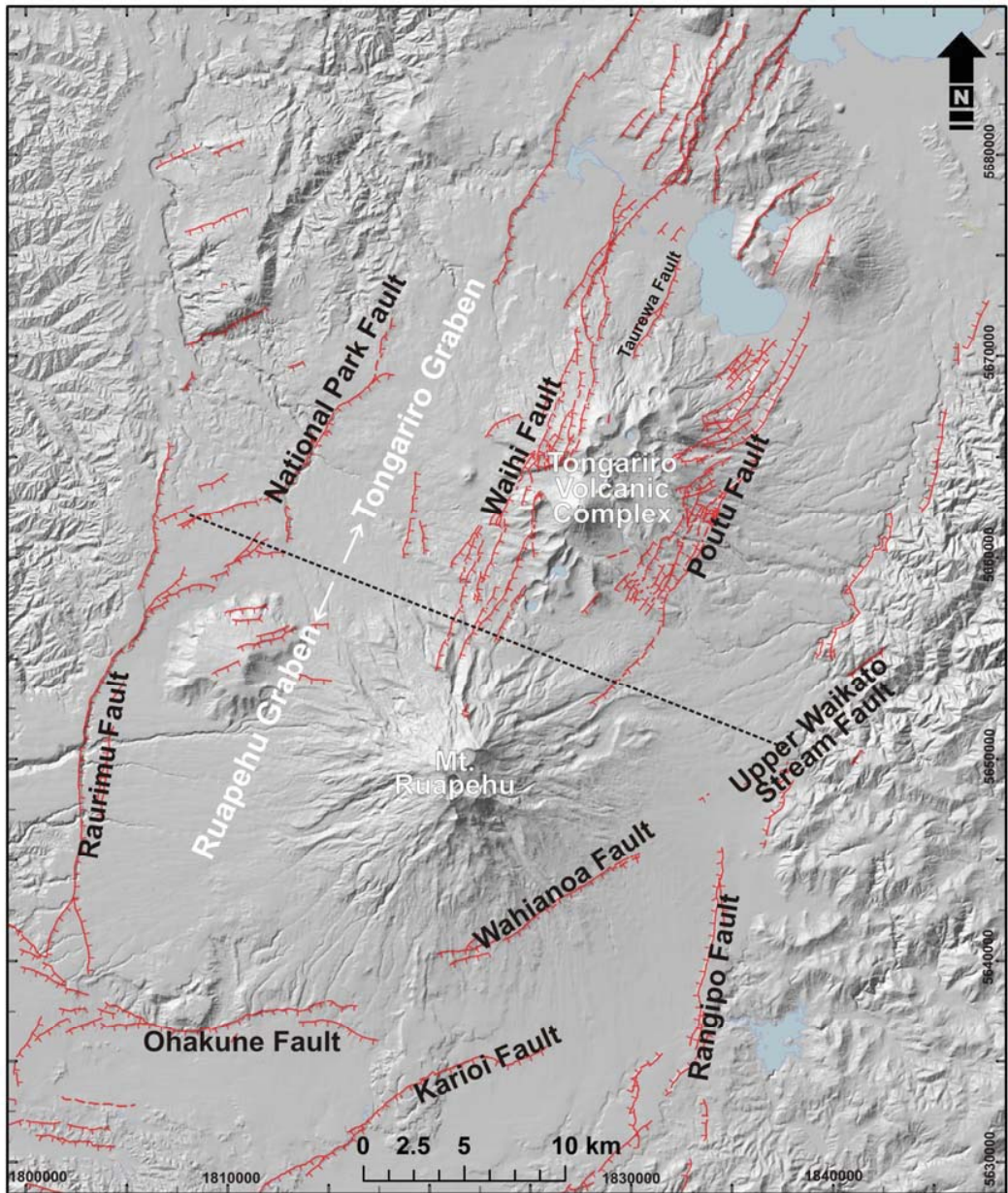


Figure 9. Late Quaternary active fault traces of the Tongariro Volcanic Centre; the northern part delimits the Tongariro Graben and the southern part the Ruapehu Graben [this work; Villamor and Berryman, 2006b; Litchfield et al., 2013].

2.5.4 Eruptive History

The TgVC has had a complex history of volcanic eruptions over the Late Quaternary; some that have been studied and dated reveal important aspects of the evolution of the southern TVZ. Known information about volcanic activity is here mentioned in chronological order:

The maximum age of volcanism in the TgVC is unknown, but Gamble et al. [2003] and Tost et al. [2016] suggest that the activity in this area might have initiated by at least 350 ka (Gamble's estimate was from coastal Whanganui sections, while Tost's was from dated debris avalanche deposits from Ruapehu near Whanganui). The oldest exposed lava flows on the volcano flanks were K–Ar dated at 275 ka [Hobden et al., 1996].

Maungakatote and Maungaku are two andesitic volcanoes located west of Kakaramea; they are thought to be >100 ka and are made up of medium-K pyroxene to hornblende andesite, which overlie the c. 350 ka Whakamaru Group ignimbrite [Cole, 1978; Cashman, 1979; Pillans et al., 1996].

Growth of the TgVC edifices likely began >350 ka, with the earliest lava sequences on the volcanoes dated at 275–215 ka. Hobden et al. [1996] suggest that the lava mainly came from a source at the southern end of the complex. Nairn [1998] proposed that North Crater was already active from ~270 ka.

The Tama Lakes lava flows were also emplaced between 275 and 215 ka [Nairn et al., 1998]. The oldest dated lava flows from the Upper Tama Lake were K–Ar dated at 260 ± 8 ka from a silicic andesite with hornblende [Patterson and Graham, 1988]. The Tama Trig comprises hornblende andesite and basaltic andesite lava flows with associated pyroclastic deposits dated at 210–200 ka. At the same age, a major cone

formed over much of southern Tongariro, with the related central vent somewhere south of the modern summit of Ngāuruhoe [*Hobden et al.*, 1996].

Ruapehu is the largest active andesite volcano in New Zealand; it comprises several overlapping craters, progressively younger towards the south. It has had seven major cone-building episodes over the last 340 ka and these are recognised as Turakina (340–280 ka), Te Herenga (250–180 ka), Oreore (180–160 ka), Wahianoa (180–119 ka), Waimarino (100–55 ka), Mangawhero (50–15 ka) and Whakapapa (<15 ka) formations [*Hackett and Houghton*, 1989; *Lecointre et al.*, 1998; *Price et al.*, 2007; *Tost and Cronin*, 2015; *Conway et al.*, 2016]. The maximum growth of Mt. Ruapehu occurred during the Wahianoa stage [$1 \text{ km}^3/\text{ka}$; *Gamble et al.*, 2003].

Kakaramea is one of the five major andesitic volcanoes of the TgVC; it was K-Ar dated at c. 220–170 ka [*Stipp*, 1968]. Mangahouhounui lavas, older andesitic to basaltic lava flows on the eastern flank of Mt. Tongariro, were emplaced between 250 and 100 ka and associated deposits include pyroclastic deposits and tephra [*Hobden et al.*, 1996; *Leonard et al.*, 2014].

The next group of major cone-building episodes took place between 180 and 70 ka. Over 30 lava flows were extruded, together with the formation of flank scoria cones at northeastern Tongariro (northeastern Oturere vent), principally between 130 and 100 kyrs [*Hobden et al.*, 1996]. Pihanga is a crystal-rich andesitic volcano with abundant plagioclase, pyroxene, some clusters of feldspar and minor olivine [*Cole*, 1978], with its youngest lava flows are about 130 ka [*Hobden*, 1997].

During this time, Pukekaikiore cone grew in the west from a vent in the area now occupied by the northwestern margin of the younger Ngāuruhoe cone [*Hobden et al.*, 1996]. The older Pukekaikiore structure consists of andesite lava flows emplaced between 190 and 120 ka. The Makahikatoa olivine-andesitic lava flow and scoria were

erupted from a scoria cone at the top of Pukekaikiore [Hobden *et al.*, 1996; Nairn *et al.*, 1998]. This youngest Pukekaikiore andesite is interbedded with a 14.7 ka rhyolitic ash [Topping, 1973]. Mangatepopo andesite, Mt. Tongariro sourced, has been K-Ar dated at 100 ± 6 ka [Stipp, 1968]. Tongariro lavas overlap those of Mangatepopo and are therefore less than 100 ka. Between 110 and 65 ka, Tongariro Trig and southeastern Oturere grew; lavas of this age covered an area equivalent to 30% of the total Tongariro Volcanic Complex [Hobden *et al.*, 1996].

For the last c. 60 ka, both large volume and large magnitude explosive eruptions have been frequent at Mt. Ruapehu, with ~1 eruption every 600 years [Wilson *et al.*, 1995; Cronin *et al.*, 1996b; Gamble *et al.*, 2003; Bebbington *et al.*, 2008], along with far more frequent smaller eruptions [e.g., Moebis *et al.*, 2011]. At Ruapehu a period of huge intensity plinian eruptions began at about 50 ka BP [Cronin *et al.*, 1996b], with the latter half of this period known as the Bullot Formation from 25 to 11 cal ka BP [Donoghue *et al.*, 1991; Pardo *et al.*, 2012].

A sequence of six major (each ~1 km³) and several minor pyroclastic eruption episodes occurred in the TgVC during a period of uniquely intense activity at ~11 cal ka BP [Topping, 1973; Nairn *et al.*, 1998]. The Pahoka-Mangamate (PM) sequence is an andesite-dacite sequence with an apparent duration of ~200 to 400 years. The PM vents are located on a 20-km long NNE-trending linear vent zone, lying within a graben-like structure defined by regional fault zones. Some of these faults appear to have ruptured during the eruptive sequence. Juvenile tephra from each of the PM eruptions are chemically and petrographically diverse, indicating that a number of separate magma bodies were tapped during this sequence. The 11 cal ka BP extensional episode was of regional extent with coincident volcanic activity in the Te Maari craters, North Crater, Saddle Cone, proto-Ngāuruhoe, Half Cone, Tama Lakes and Mt. Ruapehu. Rhyolite tephra erupted from Taupo are also interbedded within the PM deposits [Nairn *et al.*, 1998]. Smaller eruptive episodes followed after the 11 ka

burst of activity; North Crater's last volcanic activity was at <11 cal ka BP, when a lava lake formed, erupting Te Rato lapilli [*Hobden et al.*, 1996].

Saddle cone is a small scoria cone at the NNE flank of Mt. Ruapehu; its lavas were erupted from two exposed vents within an older, glacially-modified maar structure [*Topping*, 1973]. The Saddle Cone lavas postdate all Pahoka-Mangamate tephras and are overlain by Papakai Tephra [*Topping*, 1973], constraining its age between 11 and 4 ka [*Donoghue et al.*, 1995].

Red Crater includes basaltic andesite lava flows and scoria. The oldest flows may be <12 cal ka BP and the youngest may be 1 cal ka BP. A scoriaceous basaltic cone surrounds the vent and basaltic andesite dikes are exposed in the crater [*Hobden*, 1997; *Moebis et al.*, 2011].

Ngāuruhoe volcano, Tongariro Volcanic Complex's main active vent and the youngest in the valley area, is a steep andesite stratovolcano, which began erupting about 7 cal ka BP [*Moebis et al.*, 2011]. The exposed Ngāuruhoe lava flows are all younger than 2.5 ka [*Nairn et al.*, 1998]. Its most recent eruptions occurred in 1949, 1954 and 1975. Over 70 ash eruptions occurred between 1839 and 1975, on average one each six years [*Moebis et al.*, 2011]. Eruptions of lava flows are less common than pyroclastic flows; they have been witnessed only in 1870, 1948-9 and 1954 [*Topping*, 1973; *Nairn et al.*, 1998].

Recent magmatic and phreatic activity has occurred at a number of sites in other locations around the Tongariro Volcanic Complex: Te Maari, Tama Lakes, Red Crater, Emerald Lakes, North Crater, Pukekaikiore and Blue Lake crater [*Topping*, 1973], but has been dominated by the rapid growth of Ngāuruhoe cone since 2.5 cal ka BP [*Hobden et al.*, 1996; *Moebis et al.*, 2011].

Early eruptions from lower Te Maari Crater (Sulphur Lagoon) include at least 15 andesite lava flows, pyroclastic flows, and minor dikes. The upper Te Maari crater has erupted multiple times, forming scoria and overlapping olivine andesite lava flows, which are younger than the 1.7 cal ka BP Taupo Pumice [Lube *et al.*, 2014]. Over the last 150 years, Tongariro and Ruapehu have had many eruptions, one of the largest and latest was the explosive eruption from Upper Te Maari crater in December 1896, which deposited up to 5 cm of ash on the Desert Road 10 km to the east [Hurst *et al.*, 2014]. The latest eruption was in August 2012, when Te Maari craters produced violent and widespread pyroclastic density currents [Lube *et al.*, 2014].

Pleistocene volcanic products of Mt. Ruapehu comprise lava flows, fall deposits, pyroclastic density current deposits, debris flows and debris-avalanche deposits [Cronin *et al.*, 1996b; Donoghue and Neall, 2001]. The largest eruptions of Mt. Ruapehu date back to the late Pleistocene [Topping, 1973]. Historical activity has been centred at the South Crater, which is currently occupied by an acidic Crater Lake, and is mainly characterized by lahar generation and small phreatomagmatic eruptions [Kilgour *et al.*, 2010; Procter *et al.*, 2010b]. Recent historic eruptions at Mt. Ruapehu include lahars associated with phreatomagmatic eruptions (1969, 1971, and 1975), lahars associated with lava flows near the lake floor (1968), and pyroclastic surges associated with phreatomagmatic eruptions (1977). The penultimate eruption from the volcano was in 1995-6, during which over 30 major ash-generation events took place, covering >250 km² of the central and eastern North Island with ash [Cronin *et al.*, 2003]. The latest eruption, producing pyroclastic surges and a lahar took place in September 2007 [Lube *et al.*, 2009].

2.5.4.1 Stratigraphic Summary

The late Pleistocene-Holocene stratigraphy consists mainly of andesitic tephtras and lahars from Tongariro and Mt. Ruapehu, interbedded with rhyolitic tephtras and pyroclastic flows from the northern Taupo and Okataina calderas [Fig. 10; *Donoghue*, 1991; *Hodgson*, 1993; *Donoghue et al.*, 1995; *Donoghue and Neall*, 2001].

There are more than 100 different tephtras identified in the TgVC, 13 formations, interbedded with fluvial deposits, hyper-concentrated flows (>35 laharic events) and debris avalanches due to large-scale sector collapses of the SE flanks of Mt. Ruapehu or by snow/ice melt associated with volcanic eruptions or heavy rains. Most of the tephtras represent periods of volcanic subplinian eruptions, with an average eruption interval of approximately one event every 100 - 200 years [*Donoghue*, 1991; *Cronin and Neall*, 1997; *Moebis et al.*, 2011; *Pardo et al.*, 2012].

All tephtras emplaced from the TgVC are grouped into two subgroups: the Tongariro and the Tukino subgroups [*Donoghue et al.*, 1995]. Tephtras identified on the southeastern Mt. Ruapehu ring plain are grouped into seven formations: Ngāuruhoe Formation (c. 1.85 cal ka BP □ present day), Tufa Trig Formation (c. 1.85 cal ka BP □ present day), Mangatawai Tephtra [3.5 cal ka BP; *Moebis et al.*, 2011], Mangamate Tephtra (c. 11 cal ka BP), Pahoka Tephtra (11 cal ka BP), and Bullof Formation [25–11 cal ka BP; *Pardo et al.*, 2012]. Tephtras erupted from Mt. Ruapehu are grouped into the Tufa Trig Formation, Papakai Formation, and Bullof Formation [*Donoghue et al.*, 1995]. Many of these tephtra formations have subsequently proved problematic, because they may contain units from multiple volcanoes [*Moebis et al.*, 2011], or they are defined by stratigraphically convenient breaks (e.g., rhyolitic tephtras) that do not reflect periods of ongoing volcanism [*Cronin et al.*, 1996b; *Cronin et al.*, 1997d].

Ring plain deposits were split up into similar overall deposit formations, including the c. 21 m thick Whangaehu Formation [debris avalanche dated between 180 and 45 ka;

Fleming, 1953; Hodgson, 1993], the >50 m thick Te Heuheu Formation [25.4-17.7 cal ka BP; *Hodgson, 1993*], and younger formations of Tangatu [17.7-5.4 cal ka BP; *Hodgson, 1993*], Murimotu [10.5 cal ka BP; *Palmer and Neall, 1989; Eaves, 2015*], Manutahi [5.4-3.2 cal ka BP; *Lecointre et al., 2004b*], Mangaio [4.6 cal ka BP; *Donoghue and Neall, 2001*], and Onetapu [2-0 cal ka BP; Fig. 10; *Hodgson et al., 2007*].

Lahars on the western and south-western parts of the ring plain have been described and mapped by *Cronin et al. [1997c]* and *Lecointre et al. [2004a]*. Most of the area is covered by lahars from the last glaciation [*Eaves, 2015*], comprising the Tangatu and Te Heuheu Formations. Some areas of Ratan age [Horopito Formation; *Lecointre et al., 1998*] and Porewan age lahars [Waimarino Formation; *Lecointre et al., 1998*] occur at the very western edge of the ring plain. The most recent lahars (Upper Tangatu and Onetapu Formations) occupy parts of the present river beds [Fig. 10; *Neall and Alloway, 2004; Villamor and Berryman, 2006b; Lee et al., 2011*].

Regional stratigraphic markers supporting correlations of andesitic tephtras and lahar units include the rhyolitic Okataina-sourced Okareka Tephra (21.8 cal ka BP), Rerewhakaaitu Tephra 17.7 cal ka BP, and Waiohau Tephra 13.6 cal ka BP [*Shane et al., 2007; Lowe et al., 2008; Shane et al., 2008*]. The most important rhyolitic, Taupo-sourced stratigraphic markers are the Kawakawa/Ōruanui Tephra dated at 25.4 cal ka BP [*Vandergoes et al., 2013*], Hinemaia Tephra dated at 5.2 cal ka BP [*Wilson, 1993*] and the Taupo Pumice dated at 1.7 cal ka BP [Fig. 10; *Hogg et al., 2011*].

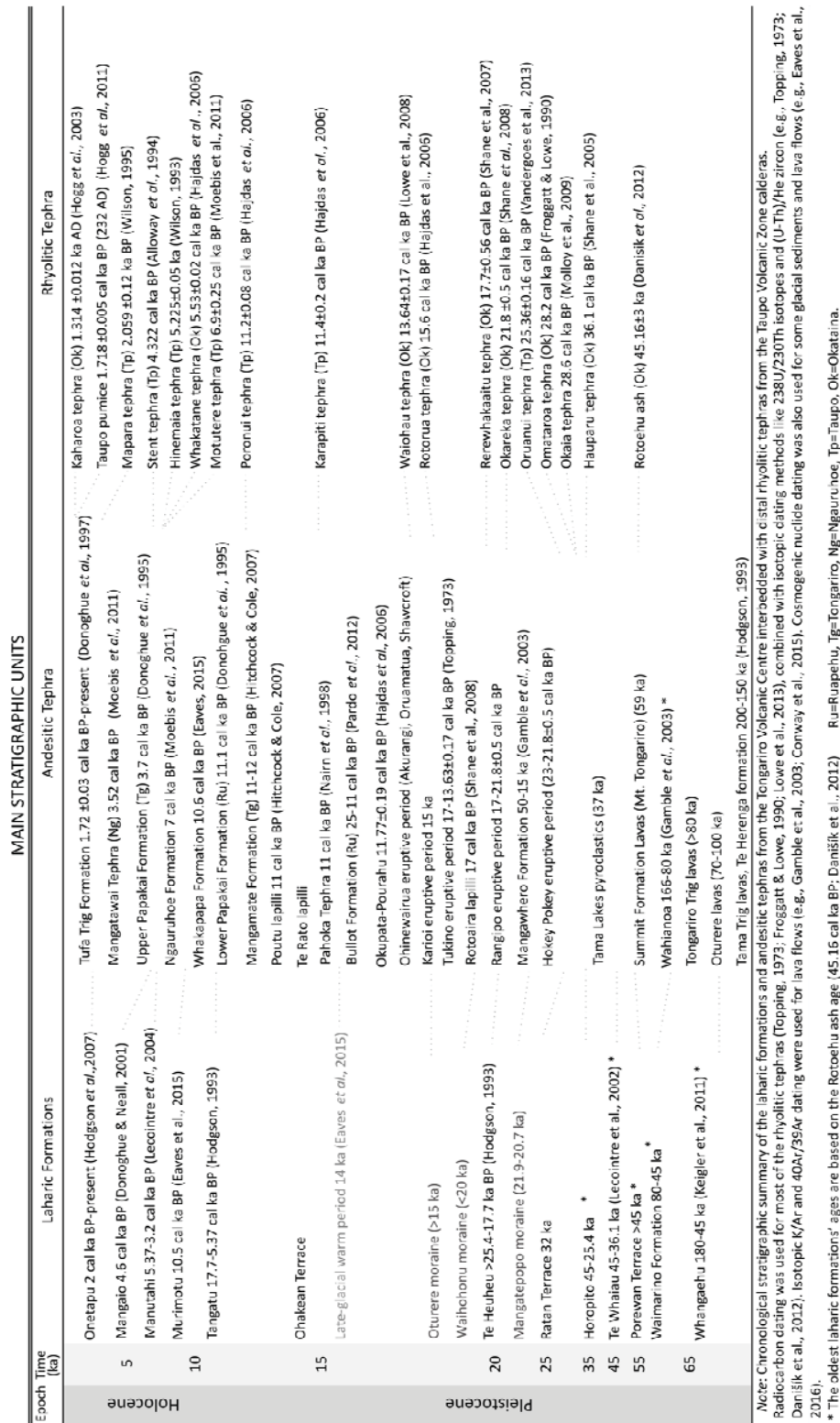


Figure 10. General Stratigraphic sequence showing the chronology of the main lahars, tephras and lava flows in the TgVC, and some important rhyolitic stratigraphic markers.

2.6 Magma-tectonic interactions in the North Island

The first approach to examining structural control on volcanoes in the North Island of New Zealand was made by Kear [1964]; he noticed the alignment of volcanic vents in the Taupo Volcanic Zone and believed that these alignments were related to underlying pre-existing faults that dilated at a point or as a fissure during volcanism. Briggs [1983] studied the Alexandra Volcanic Group, west of the TgVC, and attributed the regional alignments to rising magma that encountered a major fissure at deeper crustal levels, and that the distribution of individual vents at the surface is controlled by recent active faults.

Spinks et al. [2005] proposed a correlation between the amount of extension and the volume and type of volcanism in the TVZ. The segments with the greatest extension appeared to coincide with the highly active Taupo and Okataina calderas, while the segments with lesser extension correspond to lower eruptive volumes and andesitic stratovolcanoes. The correlation between the extension and the eruptive volume/style could be explained as a consequence of the magma storage volumes in the upper crust [*Spinks et al.*, 2005].

Interactions between the rifting and magma movement within the crust in the Taupo Rift were hypothesised by Villamor et al. [2011], and Seebeck et al. [2010]. They suggested that the rift has sections in cold crust where extension is tectonically controlled, while other areas are in thinner, hotter crust, where extension is controlled by dike intrusions. Villamor et al. [2011] compiled paleoseismic data to show the association between fault rupture in cold crust and volcanic activity of neighbouring volcanic sections of the Taupo Rift. They suggested that a crustal stress transfer occurs between faults and magmatic storage zones beneath the volcanic vents, so that close to the volcanoes, faulting may be a direct consequence of dike intrusion or magma chamber deformation.

Nairn et al. [1998] pointed out a time association between faulting and volcanism within the TgVC, by matching a period of accelerated regional extension to multiple vent pyroclastic eruptions. The Pahoka-Mangamate (PM) eruption sequence at 11 cal ka BP was apparently coincident with normal displacements of the graben margin faults and dike intrusions beneath the vent zone on the graben axis [Nairn et al., 1998]. The PM eruptive products are interbedded with two rhyolite Taupo tephras sourced ~50 km to the north, suggesting that the rifting event was of regional extent [Rowland et al., 2010].

Villamor et al. [2007] also found a connection between single fault ruptures and volcanism. Ruapehu volcano was very active from 50 to 11 cal ka BP and high slip-rate periods occurred on the Rangipo Fault at around 25 to 17.6 and 14 cal ka BP, which coincide broadly with voluminous eruptions from Ruapehu [Bullot Formation; Donoghue et al., 1995; Pardo et al., 2012] and a major caldera eruption at Taupo volcano (the 25.4 ka BP Ōruanui event). Similar interactions between a fault and a volcanic eruption have been shown for different volcanic regions in other paleoseismic studies [Nairn et al., 1998; Berryman et al., 2008] and in Coulomb stress studies [Nostro et al., 2001; Hill et al., 2002].

The previous work on TgVC has established a sound framework of the general geology, petrology, geochemistry, volcanic evolution and chronostratigraphy of the TgVC. However, there has been little investigation into the faulting and structural control on volcanic activity in this region. This presents a major opportunity for the research that is the subject of this thesis, to elucidate the nature of volcano-tectonic relationships in the TgVC.

CHAPTER 3. Methodology

This chapter presents the general methods and materials used for the elaboration of this thesis; other specific approaches are also included in the methodology sections of chapters 4 to 7. For simplicity, this chapter is divided in three parts: desk study, fieldwork and data analysis methods.

3.1 Desk study methods

Aside from literature review, other desk-based studies included the development of a 1:5,000 scale fault trace map of the TgVC. This was laid onto a 2 m resolution photogrammetry based Digital Surface Model (DSM) of the region. DSMs and photogrammetry surveys were carried out by Salman Ashraf in 2010 and 2012 as described in Chapter 4. In the present study, surface displacements were calculated from the newly drawn 1:5,000 fault trace map.

Geographic information system (GIS) ArcMap 10.2 software was used to analyse DSMs, four 1:50,000 topographic maps (LINZ, 2009 version) (Raurimu BH34, Turangi BH35, Raetihi BJ33 and Mt. Ruapehu BJ34) and three 1:250,000 geological maps (QMaps) from Taranaki, Rotorua and Hawke's Bay. Grid references on maps are in the NZTM2000 format.

Geomorphologic analysis was carried out in part at GNS (Institute of Geological and Nuclear Sciences) in Lower Hut, Wellington, where aerial photographs were analysed, to identify possible exposures of fault planes in volcanic deposits. The aerial photographs used were from stereoscopic pairs collected in the 1940s and 1960s, at 1:50,000 and 1:16,000 scales, respectively (NZ Aerial Mapping, runs 1727, 1738, 2436, 2564, 2569 and 2572), along with Google Earth images.

Existing faults and geological mapping information were taken from the GNS Active Fault Database [Townsend *et al.*, 2008; Langridge *et al.*, 2016], and from a new geological map of the Tongariro National Park in preparation [Leonard *et al.*, 2014].

3.2 Field methods

Extensive fieldwork was undertaken to complement the GIS and geomorphic analysis. Field work is very important to confirm GIS results, because in some cases geomorphic fault scarps are unlikely to be well-preserved in the landscape. Once blanketed by later eruptive products, or eroded by surface processes, these structures may be unrecognizable at the surface, and thus not detected on aerial photography.

Many fieldwork campaigns were required in order to explore the whole study area and therefore be able to distinguish the best places to perform detailed studies. Four focal sites were chosen for more detailed fieldwork based on the outcrops, fault exposures, volcanic deposits and location within the rift zone. These sites were chosen due to represent a variety of fault structures and landforms and to provide the broad geographic spread needed for this study (Fig. 11).

The first site was the Upper Waikato Stream, at the eastern side of Mt. Ruapehu, beside the Dessert Road (State Highway 1). This is located near the eastern edge of the southern Taupo Rift and includes a zone of distributed deformation several hundred metres wide. At this site the stratigraphic sequence was identified and the Upper Waikato Stream Fault system was studied along the river exposures with extensive fieldwork and Terrestrial Laser Scanning surveys. These data were integrated in order to delimit the fault strands and evaluate their paleoseismic history. Further specific methods used in this site are explained in Chapter 4.

The second field site chosen was the SE flanks of Mt. Ruapehu. The importance of this site is that it contains the NE-striking Wahianoa Fault, one of the main faults that bound the southern end of the TVZ. Fieldwork was undertaken in this site, as well as geomorphic analysis to reconstruct the paleoseismic history of this fault. Further details are described in Chapter 4.

The third field site chosen was the western flank of the Tongariro Volcanic Complex, which contains the Waihi Fault zone. This fault had not been studied before. In order to reconstruct the earthquake history of the Waihi Fault zone, fieldwork was undertaken, as well as real time kinematic GPS, ground penetrating radar and geomorphic analysis with a 2 m resolution digital surface model. Details of these methods are described in Chapter 5.

The fourth field site selected was on the eastern side of the Tongariro Volcanic Complex, within a saddle with many good outcrops containing a wide stratigraphic record and several NNE-trending faults belonging to the Poutu Fault zone. To reconstruct the earthquake history of the Poutu Fault zone. Field exposures were examined, as well as real time kinematic GPS measurements, ground penetrating radar and geomorphic analysis with a 2 m resolution digital surface model. Details of these methods are described in Chapter 5.

At each location, structural field data and observations of presence, or absence and deformed chronological markers were acquired. Structural field data consisted of morphological and geological measurements of various parameters of vents, dikes, fractures, faults, etc. These data were obtained through detailed logging of fault exposures. Existing knowledge on stratigraphic markers (e.g., tephra) in the area were used to assess fault slip timing through detailed analysis of stratigraphic layers in association with fault ruptures.

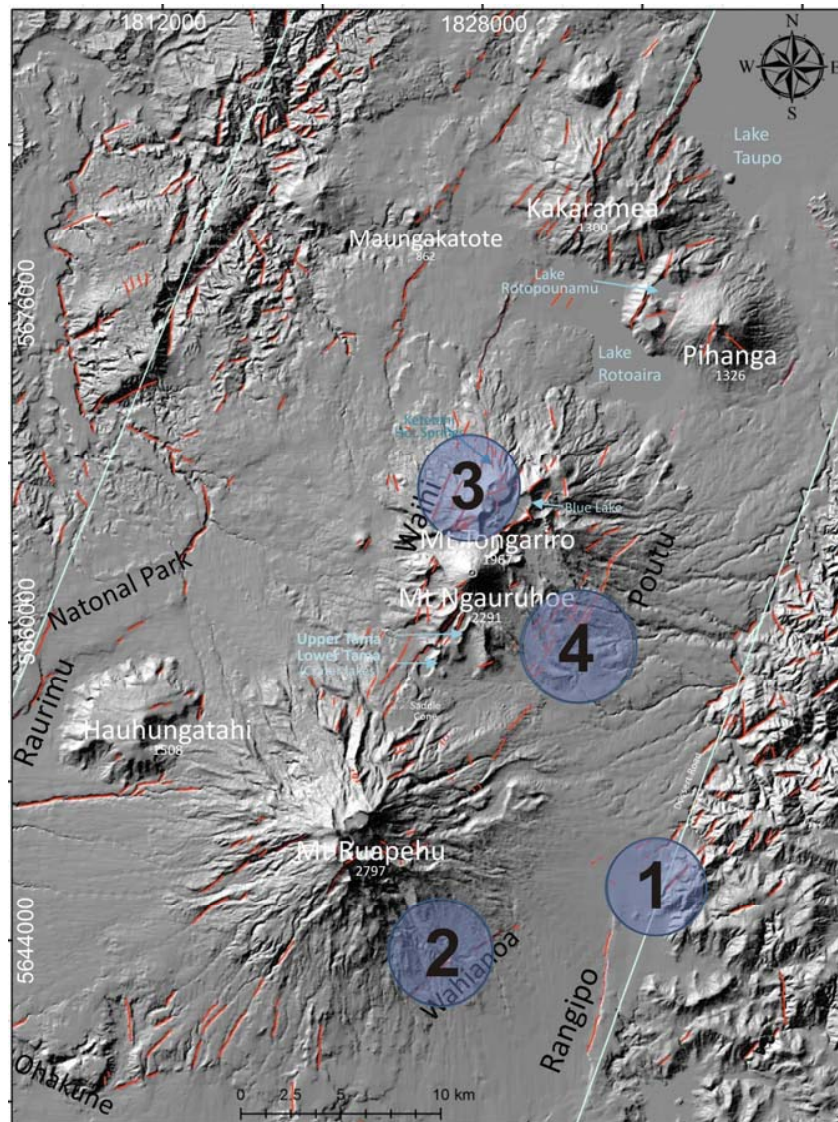


Figure 11. The Tongariro Volcanic Centre, showing the main faults and volcanic vents, and the four main field sites focused upon for detailed fieldwork within this study.

The fault geometry was characterized including trend, dip, movement sense, displacement with field measurements and geomorphic analyses, slope angles, and outcrop face orientation and dip. Fault trend and dip were measured with a geological compass. Displacements were measured with a tape measure, with an error of 0.1 m plus 10% of the measurement. Rozeta 2.0 software was used for plotting the fault planes on the stereographic projection and trend-frequency with rose diagrams. The

Plane Vector Convention was used to report the dips (Dip/Dip Dir.). Some areas (Mangatepopo moraines and along Lake Rotoaira Road) were surveyed with real time kinematic GPS and with an altimeter to measure fault scarp heights. These measurements were compared with the results obtained by surface deformation calculations.

Terrestrial Laser Scanning was applied to the Upper Waikato Stream site. This is a ground-based technique used to measure the position and dimension of objects with a rotating laser beam, where thousands of individual points are acquired (x, y, z). A Leica Nova MS50 MultiStation TLS was used to acquire panorama pictures of the river exposures in conjunction with 3D geo-referenced points, with 2-4 cm spacing of points at ~30 m distances, giving rise to a 0.03 m resolution of the rasterized data. Eight scanning locations were used; each surveyed by a Real-Time Kinematic (RTK) GPS, which was used as a back-sight point during laser scanning. Further details of this method are described in Chapter 4.

3.3 Data analysis methods

Detailed structural data, in conjunction with timing information (e.g., when a fault ruptures or a volcano erupts) may reflect changes on magma pressure and stress fields. Pyroclastic deposits are the most common evidence of volcanic activity in the TgVC, and fault ruptures evidence the earthquakes. Interpretations of the timing of faulting are constrained by the ages of tephra exposed in the outcrops and displaced (or non-displaced) by faults. Well dated tephra are very useful stratigraphic markers to analyse the temporal variation of fault ruptures. Most faults have experienced multiple ruptures, showing more displacement on older tephra than on younger ones. In order to understand these temporal variations the geometry that existed before each rupture on a fault has to be restored. Ideally fault displacement restorations can be easily

undertaken when the geomorphic surface pre-fault movement is sub-horizontal. However, in volcanic environments dominated by fall deposits the original surface is rarely sub-horizontal, fall deposits mantle the existing scarp and the fault deposit boundaries cannot be easily restored to a horizontal line. Therefore, the understanding of how paleosols, debris flows, debris avalanches and pyroclastic deposits form and what architectural shapes they form are important to understand the original shape of the scarp prior to each surface rupture.

The earthquake history was assessed by analyzing progressive displacement of tephra layers of increasing age. The age of stratigraphic markers and geomorphic surfaces constrain the age of a fault movement [e.g., *Villamor et al.*, 2007]. Multiple ruptures on fault strands are identified by progressively larger displacement in older units. Identifying horizons where the total displacement suddenly changes can be used to identify a new faulting event, including its age and offset [*McCalpin*, 1996; *Villamor et al.*, 2007]. Relative timing was obtained for most of the andesitic tephras by the identification of rhyolitic tephra with tephrostratigraphy. Ages of displaced strata were taken from the literature, where ages of the tephras have been estimated by their geochemical correlation to dated units [*Cronin et al.*, 1996a; *Moebis et al.*, 2011], radiocarbon dating [*Topping*, 1973; *Froggatt and Lowe*, 1990; *Lowe et al.*, 2013], combined with isotopic dating methods like $^{238}\text{U}/^{230}\text{Th}$ isotopes and (U-Th)/He zircon [e.g., *Topping*, 1973; *Danišik et al.*, 2012], isotopic K/Ar and $^{40}\text{Ar}/^{39}\text{Ar}$ dating for lava flows [e.g., *Gamble et al.*, 2003; *Conway et al.*, 2015], and cosmogenic nuclide dating for glacial sediments and lava flows [*Eaves*, 2015].

Geomorphic displacements have an uncertainty of 1 m, plus 10% of the scarp height, which represents the uncertainty due to irregularities in the ground surface. For the error propagation, the theory of errors was used [*Taylor*, 1982], as described by *Villamor and Berryman* [2006b]. Anomalous values were avoided, i.e., those that were not consistent with the geomorphic surface age.

To identify the temporal associations between fault rupture and deposition of tephra on the field outcrops, the temporal relationship criterion described by Villamor et al. [2011] was applied:

a) Co-seismic tephra deposition: The tephra was deposited on the fault scarp at the same time as the rupture occurred, and the fault termination is within the tephra. In this case, early deposits of the tephra have larger displacement than those emplaced later. It can be identified when the early tephra deposits of an eruption show displacement after the deformation of the late tephra of the same eruption have been restored, or where scarp-derived colluvial wedge material (derived from the newly formed free-face scarp) is preserved within tephra deposits of the same eruption.

b) Fault rupture immediately pre-tephra deposition: the free face of the surface rupture is preserved intact without erosion, because it was immediately sealed by tephra deposits.

c) Fault rupture immediately post-tephra deposition: The fault exposure shows a colluvial wedge derived from the fault scarp footwall (free face of the scarp erodes). The colluvial wedge deposits overlie the tephra. The absence of a paleosol is a crucial criterion to assign a short time interval between the tephra deposition and the fault rupture.

d) Fault rupture without association to tephra deposition: the colluvial wedge overlies a paleosol, indicating a large time span between fault rupture and the eruption.

To be confident of the absence of volcano-tectonic interaction requires complete preservation of the tephra on both sides of the fault, sufficient layer thickness, and the presence of distinctive beds within the tephra. In sites of thin or distal tephra deposits, deposition may be naturally incomplete, making these methods challenging. Also,

stratigraphic units on the footwall (upthrown side) of normal faults are often eroded from the free face of the scarp as the footwall is uplifted in successive ruptures, and the requisite relationships are not preserved.

To assess the effect of stress changes due to fault rupture or dike intrusion, the *Coulomb 3.1* model [Lin and Stein, 2004; Toda et al., 2005] was used. This is a Matlab application that quantifies the stress changes on a receiver fault or volcano in the surrounding of the fault that experienced the earthquake. A positive stress change implies that the earthquake brought the receiver fault closer to failure, while a negative value indicates a delay of the next earthquake, or the closure of the magmatic conduit. *Coulomb 3.1* calculates the strain field components and the total seismic moment of the sources in the input file, using the fault location, area, slip, dip, Young's modulus, and Poisson's ratio. Details of the parameters used and the method are further described in Chapter 7.

CHAPTER 4. Earthquake history at the southeastern termination of the TVZ.

- 4.1 Abstract
- 4.2 Introduction
- 4.3 Geological and structural setting
- 4.4 Volcanic history and stratigraphy
- 4.5 Active faulting: the Rangipo and Wahianoa faults
- 4.6 Methods
- 4.7 Results of paleoseismic analysis
 - 4.7.1 Upper Waikato Stream Fault
 - 4.7.2 Wahianoa Fault
- 4.8 Discussion
 - 4.8.1 Is the Upper Waikato Stream Fault part of the Rangipo Fault or part of the Wahianoa Fault?
 - 4.8.2 The role of the Wahianoa, Upper Waikato Stream and Rangipo faults in the kinematics and evolution of the Taupo Rift
 - 4.8.3 Seismic hazard from the Upper Waikato Stream and Wahianoa faults
 - 4.8.4 Potential association of volcanism with periods of accelerated seismic activity
- 4.9 Conclusions

Supplementary data (Appendix A)

Table S1. Upper Waikato Stream Fault, sections 1 and 2.

Table S2. Wahianoa Fault and comparison with Upper Waikato Stream and Rangipo faults.

This chapter was published in the New Zealand Journal of Geology and Geophysics.



Figure 12. Mt. Ruapehu seen from one of the main river exposures in the Upper Waikato Stream, showing a sequence of tephra units and coarse lahar deposits that record the last ~50 ka of deposition (Cronin et al., 1996b).

This Chapter is based on a published paper:

Gómez-Vasconcelos, M. G., Villamor, P., Cronin, S. J., Procter, J., Kereszturi, G., Palmer, A., Townsend, D., Leonard, G., Berryman, K., Ashraf, S. 2016. Earthquake history at the eastern boundary of the South Taupo Volcanic Zone, New Zealand. *New Zealand Journal of Geology and Geophysics*. DOI: 10.1080/00288306.2016.1195757.

Participating authors:

Martha Gabriela Gomez-Vasconcelos (undertook the fieldwork, collected and analysed the data, interpreted it and wrote the manuscript)

Pilar Villamor (fieldwork, manuscript editing and discussion)

Shane Cronin (fieldwork, manuscript editing and discussion)

Jon Procter (fieldwork, terrestrial laser scanning survey and data processing)

Gabor Kereszturi (fieldwork, terrestrial laser scanning survey and data processing)

Alan Palmer (fieldwork and manuscript editing)

Dougal Townsend (geological mapping and manuscript editing)

Graham Leonard (geological mapping)

Kelvin Berryman (fieldwork and manuscript editing)

Salman Ashraf (digital surface model)

Journal Publication

<http://www.tandfonline.com/doi/abs/10.1080/00288306.2016.1195757>

RESEARCH ARTICLE

Earthquake history at the eastern boundary of the South Taupo Volcanic Zone, New Zealand

MG Gómez-Vasconcelos^a, P Villamor^b, SJ Cronin^{a,c} , J Procter^a, G Kereszturi^a , A Palmer^a, D Townsend^b, G Leonard^b, K Berryman^b and S Ashraf^b

^aVolcanic Risk Solutions, Institute of Agriculture and Environment, Soil and Earth Sciences, Massey University, Palmerston North, New Zealand; ^bGNS Science/Te Pū Ao, Lower Hutt, New Zealand; ^cSchool of Environment, The University of Auckland, Auckland, New Zealand

ABSTRACT

At the eastern boundary of the south Taupo Rift, the NE-striking, rift-bounding Rangipo and the ENE-striking Wahianoa active normal faults intersect. We investigate their intersection at the Upper Waikato Stream to understand the kinematics of a rift termination in an active volcanic area. The Upper Waikato Stream Fault is a previously unrecognised seismogenic source also at the eastern boundary, capable of producing a M_w 6.5 and up to M_w 7.1 earthquake if it ruptures in conjunction with the Rangipo or Wahianoa faults. We found a minimum of 12 surface-rupturing earthquakes in the last 45.16 ka on the Upper Waikato Stream Fault (mean slip-rate c. 0.5 mm/yr), and a minimum of nine surface-rupturing earthquakes in the last 133 ka on the Wahianoa Fault (mean slip-rate c. 0.2 mm/yr). Periods of highest slip-rate on these faults may coincide in time with Taupo, Ruapehu or Tongariro eruptions, but, despite their intersection, movement was not coincident across all faults. The Upper Waikato Stream Fault responded to a major Taupo Volcano eruption, the Wahianoa to a major eruptive sequence from Mt Tongariro and the Rangipo to major explosive events from Mt Ruapehu.

ARTICLE HISTORY

Received 10 November 2015
Accepted 18 April 2016

KEYWORDS

Paleoseismology; Rangipo Fault; slip-rate; Taupo Rift; Taupo Volcanic Zone; tectonics; Tongariro Volcanic Centre; Upper Waikato Stream Fault; Wahianoa Fault

4.2 Introduction

At the southern end of the Taupo Rift (and Taupo Volcanic Zone) in the Central Plateau of the North Island of New Zealand, local reorientation of the stress tensor axes is responsible for a complex tectonic structure, marking the abrupt closure of the rift [Villamor and Berryman, 2001; Villamor et al., 2007]. Three sets of active normal faults occur in this area, which are highly oblique to each other (Fig. 13).

NE-striking faults delineate the Taupo Rift margins and axis, whereas E–W- and ENE-striking faults delineate the southern termination. At the southernmost part, mapping of active fault scarps has shown E–W and ENE-striking faults hard linked with NE-striking faults. For example, the NE-striking Raurimu Fault intersects the E–W-striking Ohakune Fault in the southwest, and the NE-striking Rangipo Fault intersects the ENE-striking Shawcroft Road Fault in the southeast [Villamor and Berryman, 2006b] (Fig. 13). Along the eastern boundary and north of the intersection between the Rangipo and Shawcroft Road faults, prior studies have identified the Rangipo and Kaimanawa faults

as rift bounding faults between volcanic sediments and the greywacke Kaimanawa Mountains; although only the Rangipo Fault is currently mapped as active [Langridge *et al.*, 2016]. Here, the ENE-striking Wahianoa Fault trend towards the rift boundary but there is no geomorphic expression of intersection with the Rangipo Fault, due to cover by young undisturbed recent sediments. However, active faults do traverse the banks of the Upper Waikato Stream, suggesting that it is very likely that the Rangipo and/or the Wahianoa faults extend northeast, beyond their intersection (Fig. 13).

Understanding the geometry, kinematics and paleoearthquake history of this fault intersection and rift termination may have important implications for seismic hazard assessment in the Tongariro Volcanic Centre (TgVC). In particular, confirming the prolongation of the Rangipo and Wahianoa faults into the Upper Waikato Stream area would increase their potential rupture lengths and thus the associated earthquake magnitudes.

This study characterises the geometry, kinematics and faulting history of the Upper Waikato Stream and Wahianoa faults. Subsequently, their faulting histories were compared with that of the Rangipo Fault [Villamor *et al.*, 2007]. The comparison allows us to assess whether these faults rupture simultaneously or interdependently, and whether their activity is temporally associated with large eruptions from the nearby volcanic centres (Fig. 13).

4.3 Geological and structural setting

The Taupo Volcanic Zone (TVZ) is a NNE-trending Quaternary volcanic arc associated with subduction of the Pacific Plate below the Australian Plate offshore of the North Island of New Zealand along the Hikurangi Trench [Wallace *et al.*, 2004]. The volcanic arc is known for its 25 caldera-forming eruptions in the last 1.6 Ma, active andesitic stratovolcanoes, parasitic vents, such as scoria cones, geothermal and hydrothermal

activity within an active fault belt with horst and graben structures [Wilson *et al.*, 2009; Leonard *et al.*, 2010; Pardo *et al.*, 2014] (Figure 14). Faults within the volcanic arc [Rowland and Sibson, 2001] define an intra-arc rift, the Taupo Rift [Acocella *et al.*, 2003]. Extension is created by fore-arc clockwise rotation [Wallace *et al.*, 2004] and slab rollback [Seebeck *et al.*, 2014]. Extension across the rift is associated with a combination of dike intrusion and normal faulting [Rowland *et al.*, 2010; Villamor *et al.*, 2011].

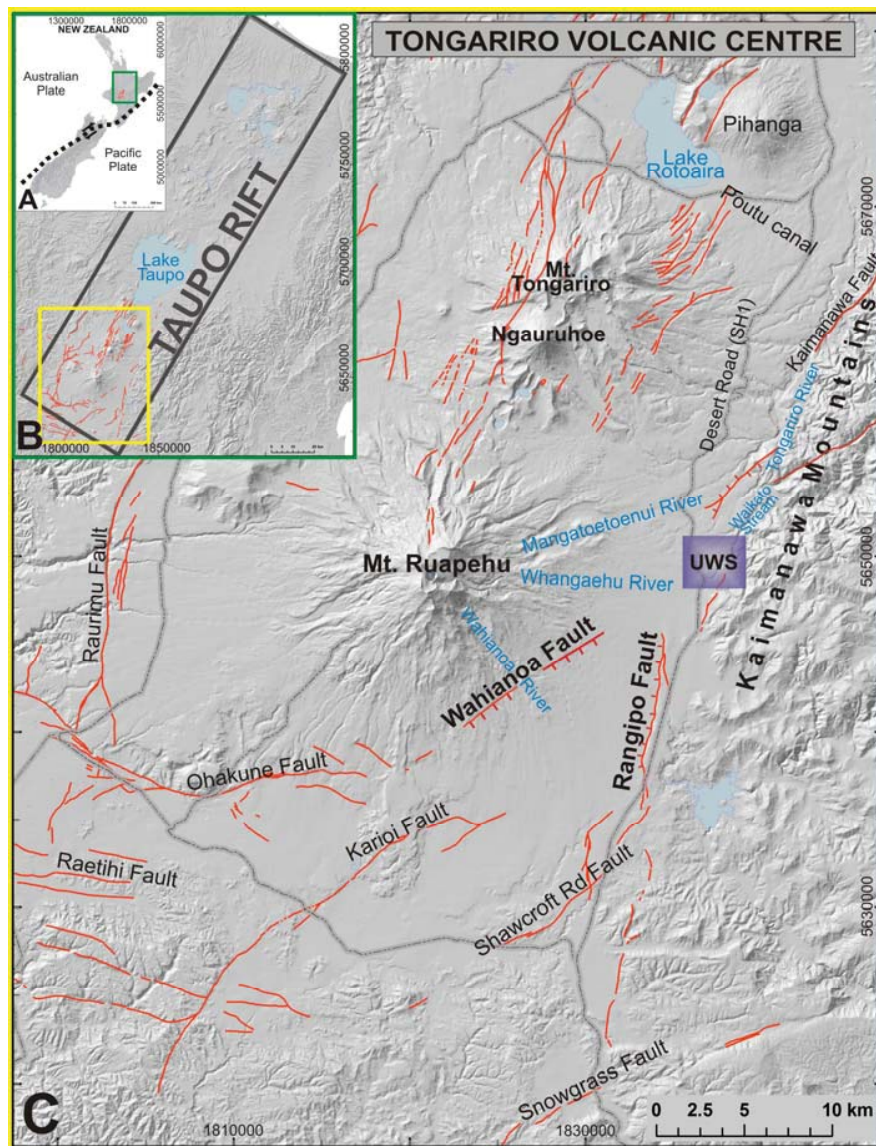


Figure 13. A, Tectonic setting of New Zealand. Green rectangle marks location of Figure 13B. B, Location of the Taupo Rift [active faults in red from *Langridge et al.*, 2016]. Yellow rectangle marks location of Figure 13C. C, Location map of the Mt. Ruapehu Graben, Upper Waikato Stream (UWS), Wahianoa and Rangipo faults in the southern part of the Tongariro Volcanic Complex, in the southern Taupo Rift. Potential intersection area marked with a purple rectangle (UWS).

4.4 Volcanic history and stratigraphy

The TgVC is the southern part of the TVZ. It is a 13 km long and 5 km wide basaltic–andesite to dacitic volcano–vent corridor complex [*Hackett and Houghton*, 1989] within the Mt. Ruapehu Graben [*Villamor and Berryman*, 2006a]. The TgVC includes two major stratovolcano systems, and a number of minor vents. Ruapehu is the southernmost and largest volcano and is one of the most active volcanoes in New Zealand. It is a complex andesitic stratovolcano with a crater lake over its active vent, and is one of the world’s most regular producers of lahars [*Cronin et al.*, 1997a; *Procter et al.*, 2010b]. The eastern flanks of Ruapehu (Whangaehu River, Mangatoetenui Stream and Wahianoa River) have been a major pathway for lahars overflowing towards the Desert Road since prehistoric times [*Lecoindre et al.*, 2004b]. The eastern extent of the Whangaehu River drains into the Upper Waikato Stream and eventually the Tongariro River (Fig. 13).

Detailed studies of the volcanic stratigraphy in this region have provided excellent constraints on the timing of active faulting. Many volcanic deposits provide diachronic chronological markers as they are displaced by different amounts due to repeated fault movement [*Villamor et al.*, 2007]. For this reason, a summary is presented of the chronostratigraphic framework used to assess the paleoearthquake history of the Upper Waikato Stream and Wahianoa faults.

In the Upper Waikato Stream area, 33 andesitic tephrae comprise a comprehensive chronostratigraphic framework [*Topping*, 1973; *Donoghue et al.*, 1995; *Cronin et al.*, 1996a; *Cronin et al.*, 1996b; *Donoghue and Neall*, 2001; *Pardo et al.*, 2012]. These are interbedded with lahar deposits from c. 18 separate events [*Cronin et al.*, 1997a;

Cronin and Neall, 1997; Donoghue and Neall, 2001] and the distal fall deposits of 19 rhyolitic eruptions from Taupo and Okataina volcanic centres [*Froggatt and Lowe, 1990; Wilson et al., 1995; Cronin et al., 1996b; Lowe et al., 2013*] (Fig. 14).

The largest of the TgVC volcanoes, Mt. Ruapehu, has a near-continuous eruptive history from >250 ka to the present [*Hackett and Houghton, 1989; Tost et al., 2015*]. The most complete tephra records of Mt. Ruapehu occur east of the volcano, along the Desert Road. The Upper Waikato Stream includes some of the oldest and deepest outcrops with a continuous record of regional volcanic activity over the past >50 ka [*Cronin et al., 1996a; Cronin and Neall, 1997*], making it an ideal site for this study (Fig. 14). Lahars have been channelled down the Upper Waikato Stream and the Tongariro River several times [*Cronin et al., 1997b*], but since c. 25 ka they stopped flowing this way, due to the formation of a moraine in the upper Whangaehu River during the last glaciation [*Cronin et al., 1997a*] (Fig. 15).

Most of the rhyolitic tephtras are radiocarbon dated [*Topping, 1973; Froggatt and Lowe, 1990; Lowe et al., 2013*], combined with isotopic dating methods such as $^{238}\text{U}/^{230}\text{Th}$ isotopes and (U–Th)/He dating of zircon [*Danišik et al., 2012*]. Identification of the tephra is normally carried out by glass and mineral chemistry using electron microprobe analysis [*Cronin et al., 1996a; Moebis et al., 2011*]. Isotopic K/Ar and $^{40}\text{Ar}/^{39}\text{Ar}$ dating have been used for lava flows [*Gamble et al., 2003; Conway et al., 2015*]. Cosmogenic nuclide dating is also used for glacial sediments [*Eaves, 2015*].

TIME (ka)	LAHARIC, RIVER AND LAVA FORMATIONS	ANDESITIC TEPHRA	RHYOLITIC TEPHRA	
HOLOCENE	Onetapu 2 cal ka BP-present (Hodgson et al. 2007)	Tufa Trig Formation 1.72 ±0.03 cal ka BP-present (Donoghue et al. 1997)	Kaharoa tephra (Ok) 1.314 ± 0.012 ka AD (Hogg et al. 2003)	WAHIAHOA FAULT AREA UPPER WAIKATO STREAM
	Mangaio 4.6 cal ka BP (Donoghue & Neall 2001)	Mangatawai Tephra (Ng) 3.52 cal ka BP (Moebis et al. 2011)	Taupo pumice 1.718 ±0.005 cal ka BP (232 AD) (Hogg et al. 2012)	
	Manutahi 5.37-3.2 cal ka BP (Lecointre et al. 2004)	Ngauruhoe Formation 7 cal ka BP (Moebis et al. 2011)	Mapara tephra (Tp) 2.059 ±0.12 cal ka BP (Wilson 1995)	
	Murimotu 10.5 cal ka BP (Eaves et al. 2015)	Upper Papakai Formation (Tg) 3.7 cal ka BP (Donoghue et al. 1995)	Stent tephra (Tp) 4.322 cal ka BP (Alloway et al. 1994)	
	10	Tangatu 17.7-5.37 cal ka BP (Hodgson 1993)	Lower Papakai Formation (Ru) 11.1 cal ka BP (Donoghue et al. 1995)	
PLEISTOCENE	Whakapapa 10.6 ka (Eaves 2015) (lava)	Mangamate Formation (Tg) 11-12cal ka BP(Hitchcock & Cole 2007)	Whakatane tephra (Ok) 5.53±0.02 cal ka BP (Hajdas et al. 2006)	
	Ohakean Terrace	Poutu lapilli 11 cal ka BP (Hitchcock & Cole 2007)	Motutere tephra (Tp) 6.9±0.25 cal ka BP (Moebis et al. 2011)	
	Late-glacial cold reversal 13-14 ka	Pahoka Tephra 11 cal ka BP (Nairn et al. 1998)	Poronui tephra (Tp) 11.2±0.08 cal ka BP (Hajdas et al. 2006)	
	Late-glacial warm period 14 ka (Eaves et al. 2015)	Bullot Formation (Ru) 25-11 ka (Pardo et al. 2012)	Karapiti tephra (Tp) 11.4±0.2 cal ka BP (Hajdas et al. 2006)	
	15	Okupata-Pourahu 11.77±0.19 cal ka BP (Hajdas et al. 2006)	Waiohau tephra (Ok) 13.64±0.17 cal ka BP (Lowe et al. 2008)	
	Te Heuheu >25.4-17.7 ka BP (Hodgson 1993) (R8)	Ohinewairua eruptive period (Akurangi, Oruamata, Shawcroft)	Rotorua tephra (Ok) 15.6 cal ka BP (Hajdas et al. 2006)	
	Last-glacial maximum >18 ka	Karioi eruptive period 15 ka		
	20	Tukino eruptive period 17-13.63±0.17 cal ka BP (Topping 1973)	Rerewhakaaitu tephra (Ok) 17.7±0.56 cal ka BP (Martin 2005)	
	(R9)	Rotoaira lapilli 17 cal ka BP (Shane et al. 2008)	Okareka tephra (Ok) 21.8 ±0.5 cal ka BP (Shane et al. 2008)	
	Mangawhero 50-20 ka (Gamble et al. 2003) (lava)	Rangipo eruptive period 17-21.8±0.5 cal ka BP	Oruanui tephra (Tp) 25.36±0.16 cal ka BP (Vandergoes et al. 2013)	
25	Hokey Pokey eruptive period 25.4-21.8±0.5 cal ka BP	Okiaia tephra 28.6 cal ka BP (Molloy et al. 2009)		
30	Marker unit 1 (olive tephra) (Cronin 1996)	Omatarao tephra (Ok) 28.2 cal ka BP (Froggatt & Lowe 1990)		
35	Orange lapilli	Hauparu tephra (Ok) 36.1 cal ka BP (Shane et al. 2005)		
45	Elephant surge (marker unit 2) (Cronin 1996)	Rotoehu ash (Ok) 45.16±3 ka (Danisik et al. 2012)		
55	Orange lapilli (marker unit 3) (Cronin 1996)			
65	Whangaehu 180-45 ka (Keigler et al. 2011) (R15)*			
	Wahianoa 134-45 ka (Gamble et al. 2003) (lava)*			
	Porewan Terrace >45 ka *			
	Te Herenga >200 ka (Hodgson et al. 2007) (lava)			

Figure 14. Chronological stratigraphic summary of the laharic and lava formations and andesitic tephras from the Tongariro Volcanic Centre interbedded with distal rhyolitic tephras from the Taupo Volcanic Zone calderas. Note the general stratigraphic record for the Upper Waikato Stream and Wahianoa Fault areas at the right. *The oldest laharic formations' ages are based on the Rotoehu ash age [45.16 cal ka BP; Danišik et al., 2012]. Ru, Ruapehu; Tg, Tongariro; Ng, Ngāuruhoe; Tp, Taupo; Ok, Okataina, R# corresponds to the lahar episodes as described by Cronin & Neall [1997].

4.5 Active faulting: the Rangipo and Wahianoa faults

At the southern termination of the TVZ and the Taupo Rift, radial extension (strain) and local reorientation of the stress axes are responsible for a complex fault pattern around Mt. Ruapehu [Rowland and Sibson, 2001; Villamor and Berryman, 2006b; Villamor et al., 2007]. Three major active fault sets form the southern termination of the rift: (1) the NNE-trending Mt. Ruapehu Graben; (2) the ENE-trending Karioi fault set; and (3) the E–W Raetihi fault set [Villamor and Berryman, 2006b].

Immediately northwards, at the latitude of Tongariro and Ngāuruhoe volcanoes, normal fault displacements together with extensional fissures and dike intrusions accommodate extension along a NNE trend [Rowland and Sibson, 2001]. Volcanic vents are also NNE aligned, along the axis of the Mt. Ruapehu Graben [Nairn et al., 1998; Acocella et al., 2003; Villamor and Berryman, 2006a].

Rangipo Fault is located at the eastern margin of the Mt. Ruapehu Graben [Villamor and Berryman, 2006b]. It is an active, NNE-striking, normal fault downthrown to the west (Fig. 13). The fault is at least 32 km long with a clear fault scarp ranging from a few metres to tens of metres in height. To the south, the Rangipo Fault is bounded by the Snowgrass Fault, but its northern extent remains uncertain due to erosion of the scarp by the Whangaehu River and/or by burial with recent lahar deposits. Prior to this study, the fault was mapped only as far north as the intersection with the Wahianoa Fault [Villamor et al., 2007]. Donoghue et al. [1991] estimated a displacement rate of 3 mm/yr, but Villamor et al. [2007] calculated from paleoseismic trenches and geomorphic analyses a displacement rate of 1.4 ± 1 mm/yr from 17.7–27 cal ka BP to the present day, and of 0.2 mm/yr from 13.8 cal ka BP to the present day. These data imply an average long-term slip-rate of 1.5 mm/yr for the last c. 65–230 kyr and a period between 17.7–25.4 cal ka BP and 13.64 cal ka BP, where slip-rate could have been up to 9 mm/yr. Past earthquakes on the Rangipo Fault had estimated magnitudes of between 5.9 and 7.1 with recurrence intervals from 3.4 ka to >14 ka, depending on whether rupture was segmented or not [Villamor et al., 2007].

The Wahianoa Fault is an ENE-striking normal fault downthrown to the SE, and is the main fault of the Karioi fault set. It has a prominent geomorphic expression for at least 10 km across the SE flanks of Mt. Ruapehu, but the northeastern side of the fault is obscured by younger deposits of lahars and tephra from the TgVC. Preliminary slip-rates were assessed for this fault by Villamor and Berryman [2006a] at 0.3 ± 0.2 mm/yr. It is not certain whether the Wahianoa Fault extends beyond the current mapped trace and it might be buried under young lahar deposits. Based on the current National Seismic Hazard Model, this fault is capable of producing M_w 6.7 earthquakes based on a 27 km fault length [Stirling et al., 2012; Litchfield et al., 2013]. Earthquake magnitude could be considerably more if the fault is, in fact, longer.

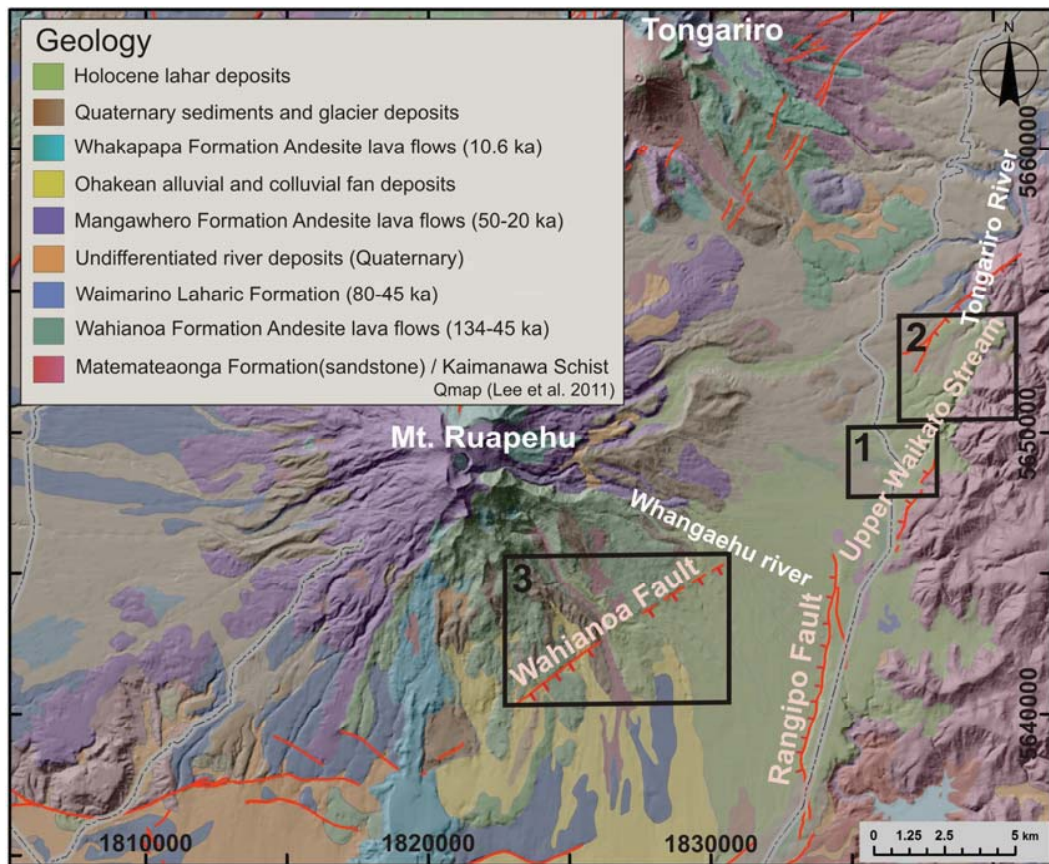


Figure 15. Geological map and general stratigraphy of the SE Mt. Ruapehu area [after Townsend *et al.*, 2008; Lee *et al.*, 2011], showing the location of the study sites (sections 1–3) and active surface fault traces [Langridge *et al.*, 2016]. See Figure 14 for detailed stratigraphic record.

4.6 Methods

To assess the possible connection between the Rangipo and Wahianoa faults in the Upper Waikato Stream area, the current active fault mapping was initially reviewed [Langridge *et al.*, 2016] in the area of intersection, before analysing fault offsets of known stratigraphic units in outcrops, and determining offsets of geomorphic surfaces of known age. The data were used to reconstruct the timing of fault rupture and estimate fault slip-rates, earthquake magnitudes and recurrence intervals for the main structures in this area.

4.6.1 Fault mapping

Fault mapping in the southeastern TVZ was based on aerial photography interpretation from stereoscopic pairs from the 1940s and 1960s, at 1:50,000 and 1:16,000 scales (NZ Aerial Mapping, runs 1727, 1738, 2436, 2564 and 2572) along with Google Earth images. Grid references on maps are in the NZTM2000.

A 2 m resolution photogrammetry-based digital surface model (DSM) was used as a base map for mapping and to calculate surface displacements. The DSM of the entire study area, within the boundary of the Tongariro National Park, was developed from two different aerial surveys conducted in November 2010 and November 2012, respectively, by New Zealand Aerial Mapping Ltd as part of their contract to provide regional aerial coverage to Horizons and Waikato regional councils. The 2010 and 2012 aerial surveys were flown in N–S and E–W orientations, respectively, and captured imagery using VEXCEL UltraCam Xp and UltraCam X large-format digital frame cameras (Microsoft) from a flight height of c. 7200 m a.s.l., which resulted in a ground sampling distance of 40 and 50 cm, respectively. The aerial blocks, consisting of 343 and 68 frames for 2010 and 2012 surveys, respectively, were triangulated using an iterative least-square bundle block adjustment in ERDAS Photogrammetry software.

The extraction of the DSM was conducted using the enhanced Automatic Terrain Extraction (eATE) module of ERDAS Photogrammetry. The algorithm used in eATE applied certain steps to achieve 3D generation from stereo-pairs. The steps encompassed hierarchical image matching, including reverse matching, by the mean of normalised cross correlation and followed by the refinement of matching results using least squares fitting. The eATE method generated a 3D coordinate for every pixel within the overlapped area of each stereo-pair and used maximum three images for simultaneous matching thus generated dense point-cloud data in laser format. These point cloud data from both survey blocks were further processed in LP360 software

using an inverse distance weighted surface algorithm to achieve 2 m resolution DSM. The ground control points used to triangulate the 2010 aerial block contained ellipsoidal heights in NZGD2000 (NZ Geographic Datum 2000) that returned DSM vertical heights different from the 2012 aerial block, which was triangulated using normal-orthometric heights in NZVD2009 (NZ Vertical Datum 2009). The NZ Geoid2009 height model was subtracted from the 2010 DSM that attained its vertical heights compatible with the 2012 DSM. The DSM and a hillshade map were analysed with ArcMap 10.2.1 software (Esri).

Existing fault and geological mapping information were taken from: the GNS Active Fault Database [Langridge *et al.*, 2016]; the 1:250,000 Hawke's Bay geological map [Lee *et al.*, 2011], as well as mapping soon to be completed as part of a new geological map of Tongariro National Park [Leonard *et al.*, 2014].

4.6.2 Fault geometry and displacements

Fault geometry (strike and dip), movement sense and fault displacements (mainly throw but occasionally also net slip) were measured using terrestrial laser scanning (TLS) and geomorphic analysis of the DSM.

Fault strike and dip were measured in the field using a geological compass. Dip-slip offsets were measured with a tape measure. The tape measure error is 0.1 m plus 8.4% of the measurement (equivalent to the highest percentage error using TLS).

TLS is a ground-based technique used to measure the position and dimension of objects with a rotating laser beam in which thousands of individual points are acquired (x, y, z). In the Upper Waikato Stream, a Leica Nova MS50 MultiStation TLS was used to acquire panorama pictures of the river exposures in conjunction with 3D geo-referenced points, with varying spacing between 2 and 4 cm at c. 30 m distance, which

give a 0.03 m resolution on the rasterised data. Eight scanning locations were used; each surveyed by a real-time kinematic GPS, which was used as a back sight point during laser scanning (Fig. 16). The data were processed with Cyclone 8.1 (Leica) and ArcGIS 10.2.1 (Esri) software packages. The merged point cloud data were meshed using the 3DReshaper Application 2014 (Technodigit) to obtain a digital outcrop model of the Upper Waikato Stream in order to measure fault displacements. The reported values (Table 2) are the average of multiple measurements of the offsets in the digital outcrop model.

Displacement measurements for the Wahianoa Fault (section 3) were taken from 10 locations along the fault where a clear scarp displaces geomorphic surfaces of various age. For this, the 2 m resolution DSM was used, leading to an uncertainty of 1 m, plus 10% of the scarp height, due to the irregularity of the ground surface. For error propagation, the theory of errors was used [Taylor, 1982], as described in Villamor and Berryman [2006b].

Stereonet 9.2 software (RW Allmendinger) was used for plotting the fault planes on the stereographic projection and azimuth frequency with rose diagrams. The net displacements measured in the field were converted into vertical offsets; vertical displacements obtained by the TLS were transformed into dip–slip offset using a fault dip range between 50° and 70°, as suggested by other studied faults within the Taupo Rift [Villamor and Berryman, 2001; Nicol *et al.*, 2006; Mouslopoulou *et al.*, 2008]. The Plane Vector Convention was used to report the dips (Dip/Dip Dir.).

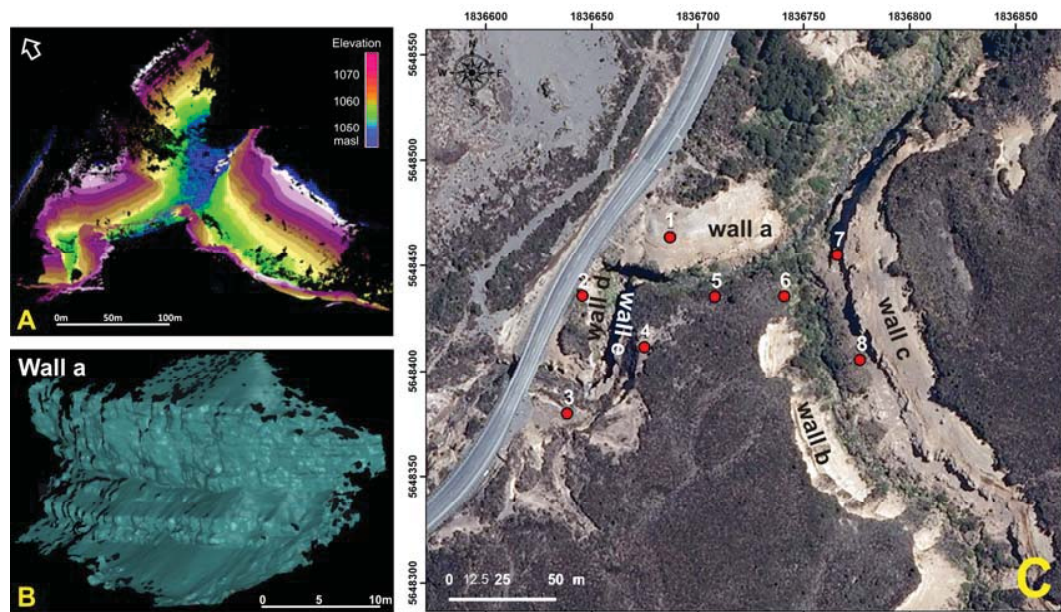


Figure 16. Terrestrial laser scanning survey. A, Upper Waikato Stream (UWS) 3D point cloud data. B, Oblique view of the digital outcrop model of the wall 'a' in the Upper Waikato Stream Fault built with 3DReshaper Application. C, Satellite image (using Google Earth images, 2015) showing the scanning locations and river exposures (walls) for the terrestrial laser scanning survey in the Upper Waikato Stream, section 1 (see location on Figure 15).

4.6.3 Earthquake history and single-event displacement

Paleoseismological investigations provide direct evidence from stratigraphic data to reconstruct the rupture history of the main faults in the Upper Waikato Stream and Wahianoa faults. Earthquake history was assessed by analysing progressive displacement on tephra layers of increasing age. Most faults have produced multiple earthquakes, as evidenced by the increase in fault displacement with increasing age of the tephras. Event horizons were used in association with differential displacements to identify new faulting events [McCalpin, 1996, 1996].

Subtraction of consecutive total displacement values results in an estimate of co-seismic displacement or single-event displacement. This value may correspond to multiple events (progressive displacement) if several fault ruptures have occurred between depositions of horizons of known age.

4.6.4 Slip-rate, earthquake magnitude and recurrence interval

Knowing the fault displacement accrued over a specific period allows calculation of the fault slip-rate. Variations in fault slip-rates over time are used to compare the faulting history of the Upper Waikato Stream Fault with that of the Rangipo and Wahianoa faults, and with periods of enhanced volcanism in the Taupo Rift.

Earthquake moment magnitudes (M_W) are calculated using the fault scaling relationship developed for the TVZ (equation 1) [Villamor *et al.*, 2007; Stirling *et al.*, 2012], based mainly on the surface-rupture length. Fault lengths are based on the findings of this study. The single-event displacement was calculated with subsurface length and event moment magnitude (M_W).

$$M_W = 4.80 + 1.33 \times \log (\text{subsurface rupture length}) \quad (1)$$

Single-event displacements and fault area are used to assess the different fault length scenarios. Also, in conjunction with fault slip-rate, single-event displacements are used to estimate fault rupture recurrence intervals when possible. For fault width, a 15 km thick seismogenic crust is assumed, as suggested by previous seismic studies [Hurst and McGinty, 1999; Hayes *et al.*, 2004; Stirling *et al.*, 2012].

4.7 Results of paleoseismic analysis

4.7.1 Upper Waikato Stream Fault (sections 1 and 2)

The Upper Waikato Stream Fault is located 15.3 km east of Mt. Ruapehu's active Crater Lake (Figs. 13 and 14). It is a low-relief alluvial fan area, representing an important catchment for regional volcanic tephra and Ruapehu-sourced lahars from the last 50 ka to the Late Glacial warm period [Cronin *et al.*, 1996a; Figs. 15 and 17; Lee *et al.*, 2011].

4.7.1.1 Section 1

Section 1 of the Upper Waikato Stream Fault is located immediately adjacent to the Desert Road (State Highway 1) (Figs. 15 and 16) and extends for 0.4 km along the Upper Waikato Stream. Here, five exposures were surveyed with a TLS (Figs. 16, 17 and S1). Wall 'a' is a NE–SW-striking outcrop, 65 m long and 27 m high; walls 'b' and 'c' are parallel, NNW-striking outcrops 155 m long and 22 m high; and walls 'd' and 'e' are parallel, NNE-striking outcrops 62 m long and >13 m high (Figs. 18 and S2). Seven main faults and extensional fractures were analysed in this section (Figure S1).

Several fault traces have been observed (Fig. 17), interpreted as merging into a single fault plane at depth given their close across-strike proximity (e.g. <100 m). These fault traces were linked from outcrop to outcrop, interpreting how they splay and merge. The dip direction of the faults was used to assess their continuity from outcrop to outcrop along strike. Based on this interpretation, it was inferred that the active faulting in the Upper Waikato Stream represents a single fault structure, which is referred to as the Upper Waikato Stream Fault (Fig. 17).

All of the faults studied in section 1 are NE-striking normal faults, dipping to the NW; except for fault 5, which is an antithetic fault and is downthrown to the SE (Table 2 and Fig. 18). Based on the interpretation that these faults coalesce into a single fault at deeper levels, the data were analysed across two transects, which incorporate most deformation accommodated by the Upper Waikato Stream Fault.

TABLE 2. NET-SLIP, SINGLE-EVENT DISPLACEMENTS, PROGRESSIVE DISPLACEMENTS AND TIMING OF RUPTURE OF THE UPPER WAIKATO STREAM FAULT, SECTION 1.

Faults	1		2		3		4		5		Events N event (Total SED/PD; unknown %)
	Net-slip	SED/PD	Net-slip	SED/PD	Net-slip	SED/PD	Net-slip	SED/PD	Net-slip	SED/PD	
Taupo pumice (1.72 ka)	?	?	?	?	?	?	?	?	?	?	?
Pahoka Tephra (11 ka)	?	?	?	?	?	?	?	?	?	?	?
Waiohau Tephra (13.64 ka)	?	?	?	?	?	?	?	?	?	?	?
Rerewhakaaitu Tephra(17.7ka)	?	?	?	?	?	?	?	?	?	?	?
Okareka Tephra (21.9 ka)	?	?	?	?	?	?	?	?	?	?	?
Hokey Pokey eruptive period	?	?	?	?	?	?	?	?	?	?	?
Oruanui Tephra (25.4 ka)	?	1.44±0.24	1.44±0.2 ^b	0.12±0.11	0.12±0.11 ^b	?	?	?	0.01±0.15	0.01±0.15 ^b	9 (0.01±0.2 to 0.09±0.2 m; 90%) ^b
R10 lahars (26.45 ka)	?	3±0.34	1.57±0.41	0.46±0.12	0.35±0.16	?	?	?	0.16±0.24	0.15±0.29	8 (1.71±0.4 to 2.2±0.4 m; 36%)
Marker unit 1 (olive tephra)	?	3.66±0.39	0.65±0.51	0.46±0.12	0±0.17	?	?	?	-	?	7 (1.93±0.4 to 2.73±0.4 [†] m; 29.6%)
R11 lahars (26.45 ka)	0.69±0.22	0.69±0.22 ^b	3.92±0.44	0.26±0.58	0.81±0.23	0.35±0.26	1.73±0.25	1.73±0.3 [†]	-	?	6 (0.65±0.5 to 0.92±0.5 m; 29.6%)
Okaia Tephra (28.6 ka)	-	?	?	?	?	?	?	?	0.43±0.17	0.27±0.3 ^a	5 (1.03±0.7 to 2.76±0.8 [†] m; 0%)
Omataroa Tephra (28.2 ka)	-	?	?	0.92±0.16	0.12±0.28 ^a	2.08±0.36	2.08±0.44 ^a	?	?	?	4 (0.47±0.5 to 1.24±0.5 m; 62.2%) ^a
Orange lapilli	-	?	?	-	?	2.54±0.43	0.46±0.56	?	?	?	3 (0.46±0.6 to 1.79±0.6 m; 74.3%)
Elephant surge (marker unit2)	1.04±0.17	0.35±0.28 ^a	?	1.15±0.25	0.23±0.3	0±0.55	0±0.55	?	?	?	2 (0.58±0.7 to 1.21±0.7 m; 51.94%)
R12 lahars	1.04±0.39	0±0.43	?	?	?	?	?	?	?	?	?
Hauaparua Tephra (36.1 ka)	1.62±0.31	0.58±0.5	?	?	?	?	?	?	?	?	?
Rotoehu Ash (45.16 ka)	?	?	?	?	?	?	?	?	?	?	?
R13 lahars (>45 ka)	?	?	?	?	?	?	?	?	?	?	?
Total	4.39±0.57	4	12±0.71	4	3.93±0.43	6	8.89±0.71	4	0.6±0.33	3	9
Fault observations	Wall a 006-026/75-86NW	R11 lahars	Wall b & c 037/68NW	Wall b & c 029/>80NW	Wall b & c 005-020/81-84NW	Wall b & c 012-043/72-89SE					
Fault termination	R11 lahars	Covered by <17.57±0.6 ka paleo-channel	0.11±0.03 (26.45±1.1ka)	0.02±0.02 (32 ka)	0.07±0.02 (34.05±2.1ka)	0.01±0.01(26.45±1.1ka)	Covered but inferred from fault 5 in 23.6±1.8ka	Hokey Pokey	Unknown	Unknown	Unknown
Mean slip rate (mm/yr) [~]	0.03±0.02 (36.1 ka)	Scarp-derived colluvial wedge >R12 lahars, filled with Hauaparua T. and a grey ash deposit, event shortly after 36.1 ka	0.3 m wide fissure filled with alluvial debris of reworked tephra smeared in fault	Multiple-steps around R11 lahars	1 event just after 36.1 ka, over-thickening layer above Elephant surge (free fault-face eroded). Multiple-steps at Elephant surge	Antithetic normal fault of fault 4				0.07±0.06 (36.1 ka)	
Other comments											

Note: Net-slip=total displacement associated to each chronological marker. SED/PD= single event displacement/progressive displacement. Events: N event= minimum number of rupture events; Total SED/PD= minimum and maximum total progressive displacement; Unknown %= unknown percentage of total PD relative to the 100% displacement measured on R11 lahars. Note that we do not differentiate between single-event displacement or progressive displacement here because of these values could represent one rupture (SED) and more than one rupture event. All the values are in meters. All the ages are cal ka BP. See methods section for data accuracy. Vertical displacements and more detailed description of each fault can be seen in the data supplement (Table S1). ^a Could have happened after this time; ^b Last event known, uncertain timing; - No value; ? Not sure; ___ Fault termination; ~Slip rate based on net-slip; † More than 1 event.

Transect 1 includes faults 1–5 and transect 2 includes faults 2–7 (Fig. 17). Each individual fault is referred as a strand or splay and the sum of fault strand displacement values represents the total fault displacement. For transect 1, fault 5 is antithetic, so its motion was subtracted from the offset sum of faults 1–4.

Based on progressive displacement increments of individual strands, transect 1 shows evidence for at least nine surface-rupture events between 36.1 ka BP (Hauparu Tephra) and 21.9 ka BP (Okareka Tephra) (Table 2). In Table 2, the measured net displacement values are displayed together with the analysis of progressive displacement for each individual fault, as well as summed values for faults within the same transect. Net displacements on the R11 lahar deposits [c. 27 ka; Fig. 14; *Cronin and Neall, 1997*] are used as the best reference to estimate fault slip-rate and to assess distribution of deformation across the transect (across fault strands), because this marker appears in all outcrops. The total displacement across transect 1 ($f_1 + f_2 + f_3 + f_4 - f_5$) on R11 lahars is 6.72 ± 0.62 m (net-slip), and at transect 2 ($f_6 + f_7$; note that offsets for f_2 – f_5 are missing), the offset is 5.43 ± 0.72 m (Table 2). The difference likely reflects the missing f_2 – f_5 measurements on transect 2 (not exposed). Thus transect 1, which strikes perpendicular to the fault strike, is the best representation of the total deformation across the Upper Waikato Stream Fault, whereas along the riverbank to the north, exposures are sub-parallel to the faults and faulting information is probably missing because displacement on some markers could not be measured for all faults. The lack of events on some fault strands is related to two possible causes: (1) the Upper Waikato Stream Fault is comprised of several parallel fault strands at a single location and thus it is possible that not all strands ruptured at once [see e.g. Paeroa Fault, North Taupo Rift, *Berryman et al., 2008*] and not all strands are exposed at each location; (2) not all recognisable horizons were exposed at each of the fault exposures, or they were obscured by vegetation.

The progressive displacement analysis of marker R11 lahar deposits may also help us to assess the amount of deformation that might be missing on other chronological markers. It seems that all fault splays in the Upper Waikato Stream Fault could have ruptured at the same time across transect 1 for some individual surface ruptures because progressive displacement is associated with all strands. Assuming that the summed progressive displacement for R11 lahars in transect 1 is the best representation of the Upper Waikato Stream Fault movement, the percentage of deformation that is accommodated by each individual fault strand can be assessed, namely 10%, 58%, 12%, 26% and -6% (antithetic fault), for faults 1, 2, 3, 4 and 5, respectively. These percentages can be applied to other chronological markers for faults without information in order to assess total deformation at different times. When these percentages are used for other tephra layers, it suggests there may be a loss between 30% and almost 100% of the total progressive displacement on those other markers. With this exercise, it is assumed that all faults always rupture during individual earthquakes. This is a conservative (maximum) approach because it was observed on normal faults that splay into several fault strands at the surface, that surface rupture can occur on different fault splays for different events in a random way [see, e.g. *Berryman et al.*, 2008]. However, this approach allows a conservative estimate for displacement increments that can be compared with the sum values obtained using only the information that was measured on the outcrops (minimum).

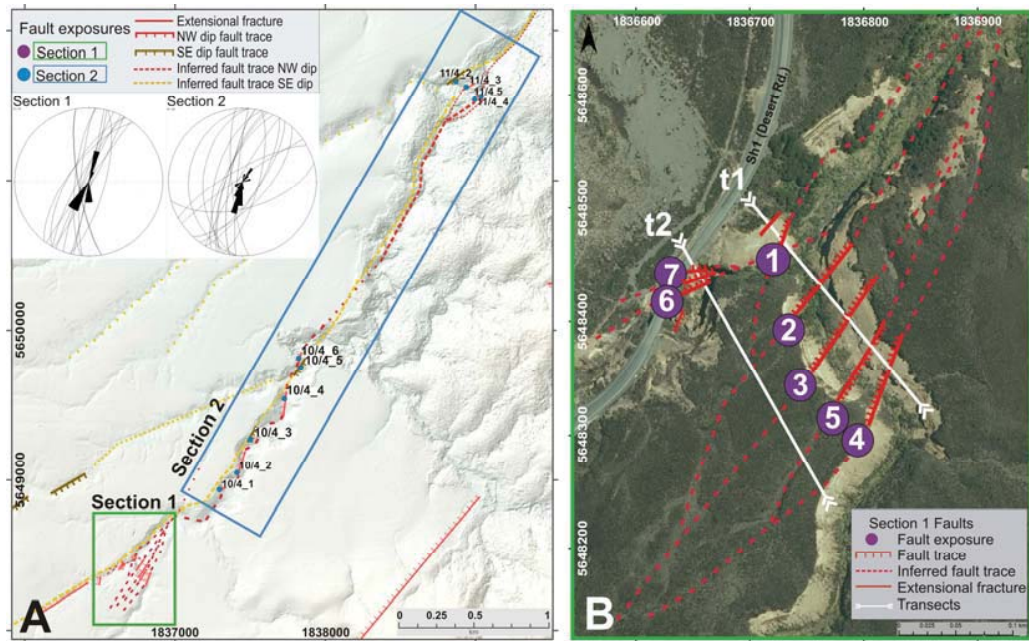


Figure 17. Location of the main faults in the Upper Waikato Stream area. A, Hillshade map of the Upper Waikato Stream based on 2 m DSM showing the studied faults in sections 1 (green rectangle) and 2 (blue dots, blue rectangle). Fault exposures (dots) and fault traces (continuous lines) are differentiated from the inferred faults (discontinuous lines). Faults downthrown to the NW are marked with red lines; faults downthrown to the SE are marked with yellow-brown lines. The fault planes are plotted in stereographic (lower hemisphere) projection and superimposed rose diagrams of fault strike frequency (right-hand rule). B, Section 1 of the Upper Waikato Stream (green rectangle in A) showing the seven main fault traces (purple dots), as well as an extensional fracture and two transects t1 and t2 (white lines) used to sum and calculate the total offset for the Upper Waikato Stream Fault.

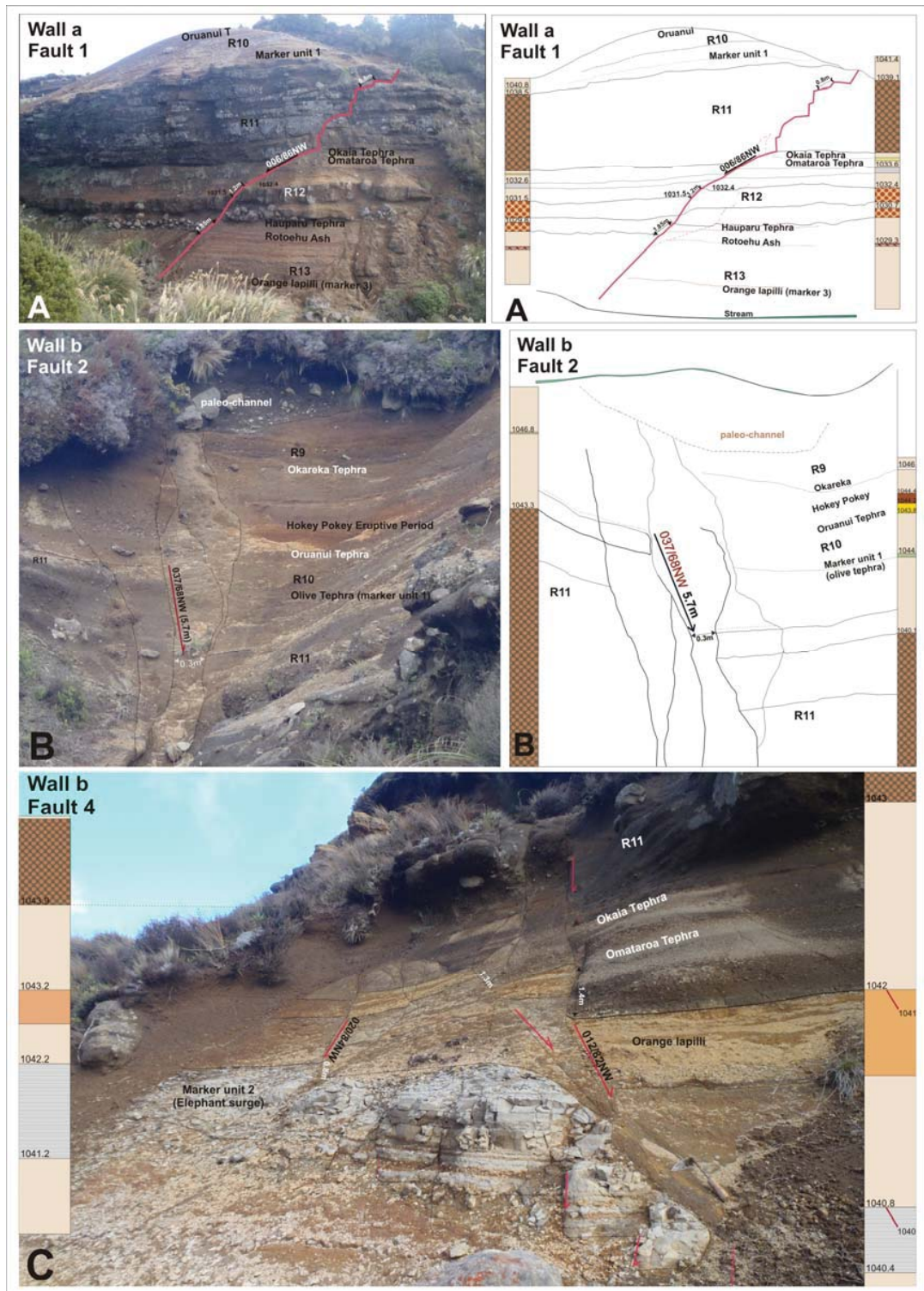


Figure 18. Faults in section 1 in the Upper Waikato Stream. A, Wall 'a' main fault exposure, showing fault 1 displacing volcanic deposits older than c. 28 ka (left, field photo; right, interpretation with stratigraphic column). B, Wall 'b' showing the location of fault 2 with a 0.3 m 'fissure fill' (left, field photo; right, interpretation with stratigraphic column). C, Detailed exposure of fault 4 on wall 'b' displacing tephtras older than R11 lahars. The numbers show the elevation in m a.s.l. See Figure 14 for further information about stratigraphic units.

4.7.1.2 Extensional fractures

In section 1, on the NE side of wall 'a', there is a >12 m long narrow fissure, dipping 030/68NW (Fig. 19) that cuts through tephra and debris flows which are older than 18–16 ka BP. The fissure is 0.05–0.19 m wide and filled with the Taupo-sourced rhyolitic Ōruanui ignimbrite and associated tephra fall [25.4 cal ka BP; *Wilson et al.*, 2006; *Vandergoes et al.*, 2013]. At some levels, the reworked Ōruanui Tephra shows finer grain-size banding and cross-bedding stratified layers, suggesting that water was involved in the transport–depositional process.

Just below this fissure, on the same wall, there are >10 other fissures cutting R11 lahar deposits (27 ka), some also filled with reworked Ōruanui Tephra. They vary slightly in orientation from 350° to 035°, generally matching the preferred direction of the main faults in southern TVZ (027°), downthrown to the NNW with steep dips (80°–90°) [*Rowland and Sibson*, 2001], and similar to the orientations of the faults described here for the Upper Waikato Stream Fault. There is also a normal 170/78W fault that vertically displaces the R11 lahars by 0.18 ± 0.14 m (0.21 ± 0.14 m of net displacement) (Fig. 19).

The main Upper Waikato Stream fissure was noted earlier by Donoghue and Neall [2001], while Topping [1973] described two similar structures in the Poutu canal (Fig. 13) and another section nearby (60H 5678969.46 m S, 385626.35 m E). The sites described by Topping [1973] are no longer exposed, but the fissures were described as relating to the Ōruanui eruption, and are up to 0.52 m wide and striking at 356, cutting through lapilli and tuff deposits older than Ōruanui ignimbrite.



Figure 19. Extensional fractures located on wall 'a' in the Upper Waikato Stream. A, The 12 m long fissure filled with Ōruanui Tephra (white arrow; >25.4 cal ka BP; photo taken by S. Donoghue), cutting older tephra and lahar deposits. B, Other fissures were measured on the same wall, cutting R11 lahars. C, These fissures do not show any vertical displacement, but record extension. D, The R11 lahar deposits are abruptly truncated at the fissure margins, with no mixed material along fissure sides. The reworked Ōruanui tephra shows cross-bedding stratified layers. E, All the fissures reflect orthogonal extension and are consistent with the NNE-trending Mt. Ruapehu Graben. Rose diagrams for the measured fissures and faults in the Tongariro Volcanic Centre (TgVC), where strike directions (right-hand rule) are plotted.

4.7.1.3 Section 2

Section 2 of the Upper Waikato Stream Fault starts 0.5 km downstream (NE) from section 1, and continues for 5 km downstream of the Tongariro River from there (Figs. 15 and 17). Measurements on these faults were made using conventional field techniques, but only the lower few metres of the riverbanks could be reached, the remainder is bush covered or inaccessible. Eleven fault planes were described along this section, which helped assess fault continuity and kinematics, when the results are combined with those of section 1 (Figs. 20 and S3).

4.7.1.4 Earthquake history

A summary of the fault strike and dip, net-slip offsets and progressive displacement analysis is shown in Table 2. Faults 11/4_1, 11/4_2 and 11/4_3 are not included in Table 2 because the stratigraphic position of the deposits that they display is uncertain. These data confirm that the summed values (see below) are minimum offsets because some faults might be missing. Fault 11/4_1 crops out at the Tongariro River and is a 075/60S normal fault that cuts the Mesozoic greywacke sequence in the Kaimanawa Mountains [Lee *et al.*, 2011]. Fault 11/4_2 includes two normal faults: 042/64SE with $>6 \pm 0.3$ m of vertical displacement ($>6.9 \pm 0.96$ m of net-slip); and 035/72SE with 0.5 ± 0.2 m of vertical displacement (0.58 ± 0.22 m of net-slip). Fault 11/4_3 is a small normal fault 060-striking and dipping 76° NW with 0.4 ± 0.2 m of vertical offset (0.46 ± 0.21 m of net-slip). Three faults in section 2 (10/4_3, 10/4_5, 11/4_2; Fig. 17) are dipping to the SE (antithetic).

Based on the analysis of progressive displacement of individual fault strands, a minimum of two events in section 2 are distinguished from 133 to 1.72 cal ka BP. The first event took place between 55 and 11.77 cal ka BP, possibly approximately <25 ka, and the second event <11 cal ka BP; this latter event is additional to those found in section 1. A total of 12 events can be extracted for the information analysed in sections 1 and 2. The data show a gap of seismic activity between 21.9 and 13.64 cal ka BP for the Upper Waikato Stream Fault (Tables 2, 3, 5 and S1).

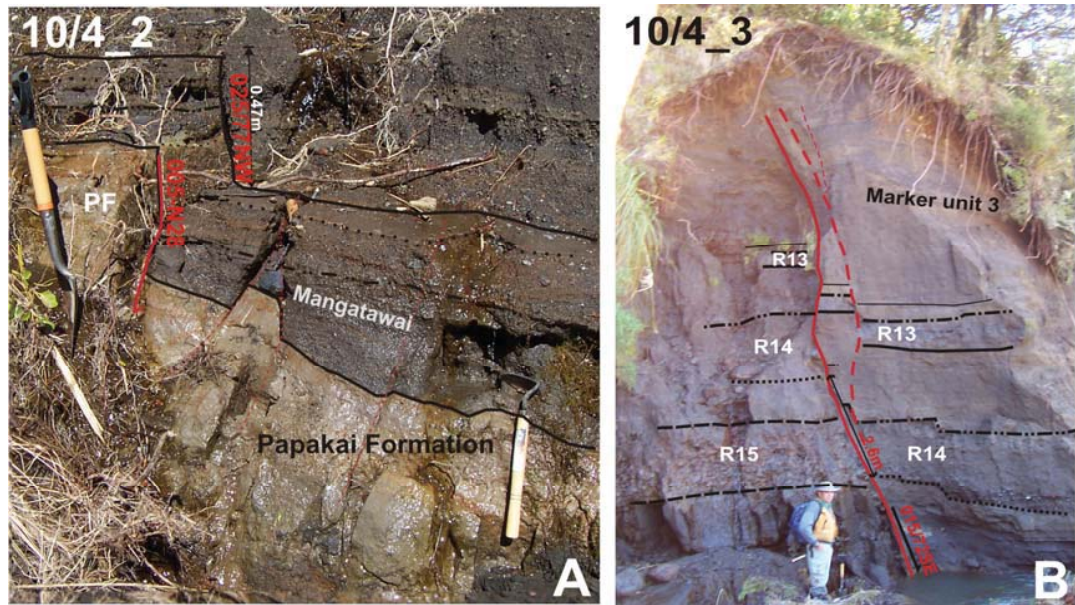


Figure 20. Main outcrops of the Upper Waikato Stream Fault in section 2. A, 10/4_2: Normal fault displacing the Papakai Formation. B, 10/4_3: Exposure of fault displacing deposits including R13 and older lahars.

TABLE 3. NET-SLIP, SINGLE-EVENT DISPLACEMENT AND TIMING OF FAULT RUPTURE OF THE UPPER WAIKATO STREAM FAULT, SECTION 2.							
Faults	10/4_2	10/4_3	10/4_4	10/4_5	10/4_6	11/4_4 & 11/4_5	EVENTS
Offset (m)	Net-slip	Net-slip	Net-slip	Net-slip	Net-slip	Net-slip	(Total SED)
Taupo pumice (1.72 ka)	?						?
Mangatawai Tephra (3.52 ka)	0.54±0.19						?(0.54±0.19 m) ^b
Papakai formation (3-11 ka)	?					?	?
Poutu lapilli (11 ka)			?			0.75±0.21	2 (0.75±0.21 m) ^a
Pahoka Tephra (11 ka)			-			?	?
Okupata (11.77 ka)			2.37±0.42				?(2.37±0.42± m) ^a
Waiohau Tephra (13.64 ka)							?
Karioi eruptive period							?
Rerewhakaaitu Tephra (17.7 ka)							?
Okareka Tephra (21.9 ka)						?	?
Hokey Pokey eruptive period						0.92±0.23	?(0.17±0.31 m) ^a
Oruanui Tephra (25.4 ka)						2.3±0.42	?(1.38±0.48 m)
R10 lahars (26.45 ka)						?	?
Marker unit 1 (olive tephra)							?
R11 lahars (26.45 ka)							?
Okaia Tephra (28.6 ka)							?
Omataroa Tephra (28.2 ka)							?
Orange lapilli							?
Elephant surge (marker unit 2)							?
R12 lahars			?			?	?
Hauparu Tephra (36.1 ka)		?	-			-	?
Rotoehu Ash (45.16 ka)		-	-			-	?
R13 lahars (>45 ka)		-	-			-	?
Marker unit 3		-	-			-	?
R14 lahars (>55 ka)		3±0.52	3.46±0.58	?		1.44±0.3	?(1.44±0.3) ^a
R15 lahars (<133 ka)		?	?	2.43±0.44		?	1 (≥1.1±0.72 m) ^a
TOTAL	0.54±0.19	3±0.35	5.83±0.72	2.43±0.44	1.44±0.3	3.98±0.52	8
Fault observations	005-028/77NW	015/72SE	355-020/46-84NW	030/72SE	015-020/60-72NW	010-025/70-76NW	
Fault termination	uncertain	<45 ka	uncertain (<11 ka)	uncertain	?<36.1 ka	uncertain (<11 ka?)	Unknown
Mean slip rate (mm/yr) [†]	0.21±0.08 (2.54±0.23 ka)	>0.07±0.02 (>45 ka)	0.13±0.04 (55 ka)	>0.02±0.0 (133 ka)	0.02±0.01 (36.1 ka)	0.07±0.03 (25.4±0.2 ka)	0.08±0.07 (133 ka)
Other comments	Multiple-steps at Papakai F.	10 m-high river exposure	Erosive paleo-channel <55 ka	4-step fault at >133 ka	10 m-high exposure 3-step fault >36.1 ka	4 faults & 2 fractures, tilted deposits	

Note: Net-slip=total displacement associated to each chronological maker. SED/PD= single event displacement/progressive displacement. Events: N event= minimum number of rupture events. All the values are in meters. All the ages are cal ka BP. See methods section for data accuracy. Vertical displacements and more detailed description of each fault can be seen in the data supplement (Table S1). ^a Could have happened after this time; ^b Last event known, uncertain timing; - No value; ? Not sure; [†] Slip rate based on net-slip; † More than 1 event.

4.7.2 Wahianoa Fault (section 3)

The Wahianoa Fault clearly displaces lava flows, moraines, tephra and lahar deposits for 10 km along the southeast flanks of Mt. Ruapehu (Figs. 15, 21 and S4). Ten topographic profiles were traced across the fault on geomorphic surfaces of known age in order to assess the fault's earthquake history in section 3. Three outcrops within the Karioi Forest that expose the Wahianoa Fault were also analysed (Fig. 21).

4.7.2.1 Earthquake history

All the Wahianoa Fault planes exposed in the outcrops in section 3 are NE-striking, SE-dipping normal faults. At the 'Tong 23' field site, the faults exposed are antithetic to the main fault (Figs. 21 and S4). Unfortunately, only progressive displacements could be analysed on exposed fault planes for the antithetic faults (Table 4), which help assign timing to some individual rupture events, but not to assess single-event displacements for the main fault. That fault shows that two ruptures occurred between 23 and 11.77 cal ka BP.

Displacements on geomorphic surfaces show different offsets for different ages (Fig. 21). Some measurements give a minimum offset, because the downthrown block is buried by younger deposits. Seven progressive displacement increments for the geomorphic displacements were measured along the fault (profiles in Table 4), suggesting that at least seven events occurred. If the outcrop data is combined with the geomorphic data, two more ruptures can be added (Table 4). However, values of progressive displacement increments for geomorphic data are too large (2–12 m), suggesting that those values are related to several ruptures (see more on single-event displacements below) and that the nine events analysed are a minimum for the last c. 130 kyr.

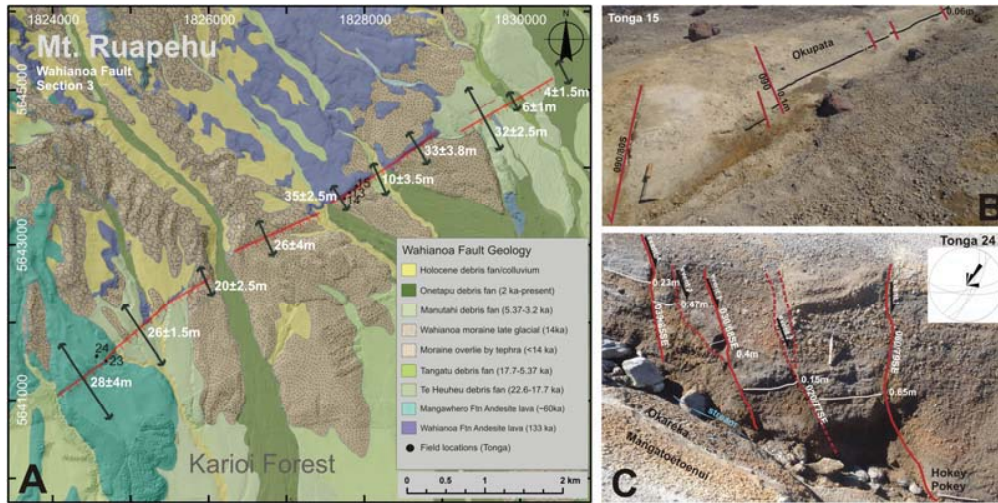


Figure 21. Wahianoa Fault profiles and outcrops. A, Geological map [Leonard *et al.*, 2014] showing the location of the studied field sites along the Wahianoa Fault in section 3; and the 10 topographic profiles (black double-pointed arrows) traced with their corresponding vertical offset values in meters. The geological map overlies a hillshade created with a 2 m-resolution Digital Surface Model from the SE flank of Mt. Ruapehu. B–C, The two main outcrops of the Wahianoa Fault in section 3 showing displaced tephra (field locations shown on Fig. 21A). The fault planes are plotted in stereographic (lower hemisphere) projection and superimposed rose diagrams of fault strike frequency (right-hand rule). Most of the tephra belongs to the Bullot Formation from Mt. Ruapehu [Donoghue and Neall, 2001; Pardo *et al.*, 2012]. See Figure 14 for more information about the stratigraphy and Figure 15 for location of section 3.

TABLE 4. NET-SLIP, SINGLE-EVENT DISPLACEMENTS, PROGRESSIVE DISPLACEMENTS AND TIMING OF RUPTURE OF THE WAHIANOA FAULT, SECTION 3.

Faults	Outcrops			N° event (Total PD)	Profiles		Outcrops + profiles N° event (Total PD)
	Tonga 15 Net-slip	Tonga 23 Net-slip	Tonga 24 Net-slip		Net-slip	PD	
Offset (m)							
Taupo pumice (1.72 ka)				?	?	?	?
Mangatawai Tephra (3.52 ka)		?		?	?	?	?
Papakai formation (3–11 ka)		-		?	?	?	?
Poutu lapilli (11 ka)		-		?	?	?	?
Poronui Tephra (11.2 ka)	?	-		?	6±1.5	6±2.12 ^b	9 (6±2.12†) ^b
Pahoka Tephra (11 ka)	-	-		?	11.5±4	5.5±5.32	8 (5.5±5.32†)
Pourahu member (11.77 ka)	-	-		?	-	-	?
Okupata (11.77 ka)	0.69±0.17	1.07±0.2		2(0.69±0.17) ^b	-	?	7? (0.69±0.17) [*]
Shawcroft Tephra	-	1.44±0.24		?(0.37±0.31)	-	?	(0.37±0.31)
Waiohau Tephra (13.64 ka)	?	1.77±0.27		?(0.32±0.36)	-	?	(0.32±0.36)
Karioi eruptive period (15 ka)		-		?	23±3	12±3.9 [*]	6 (12±3.9†) [*]
Rerewhakaaitu Tephra (17.7 ka)		-		?	30±4.5	7±6	5 (7±6†)
Last glacial maximum (>18 ka)		2.04±0.3	?	?(0.28±0.41) [*]	-	?	?(0.28±0.41) [*]
Hokey Pokey eruptive period		?	2.2±0.32	1(2.2±0.32) [*]	-	?	4? (2.2±0.32) [*]
Oruanui Tephra (25.4 ka)			?	?	-	?	?
R10 lahars (27 ka)					-	?	?
Marker unit 1 (olive tephra)					-	?	?
R11 lahars (27 ka)					-	?	?
Okaia Tephra (28.6 ka)					-	?	?
Orataroa Tephra (28.2 ka)					-	?	?
Orange lapilli					-	?	?
Elephant surge (marker unit 2)					-	?	?
Hauparu Tephra (36.1 ka)					-	?	?
R13 lahars (<45 ka)					32±4.5	2±6 [*]	3 (2±6) [*]
Marker unit 3					-	?	?
R14 lahars (>45 ka)					-	?	?
R15 lahars (<133 ka)					34±3	2±4.24 [*]	2 (2±4.24) [*]
Wahianoa Formation (133 ka)					39±4.5	5±6.36	1 (5±6.36†)
Total	0.69±0.17	6.33±0.51	2.2±0.32	>2	175.51±21.28		>9 events
Fault observations	060-090/80SE	036-098/60-90NNW	020-080/69-85SSE	NE/SE	035-045/SE		NE/SE
Fault termination	Uncertain (<11.77 ka)	Uncertain (<11 ka)	Uncertain (<17.7 ka)	Uncertain (<11.77 ka)	Uncertain (<11 ka)		Uncertain (<11 ka)
Mean slip rate (mm/yr) [~]	0.06±0.02 (11.77 ka)	0.11±0.04 (17.7 ka)	0.09±0.02 (23.6 ka)	0.15±0.31 (>45 ka)	<0.3±1.12 (133 ka)		>0.15±0.31 (133 ka)
Comments	Multiple-step fault	Antithetic faults of Tonga 24	Primary fault of Tonga 23		Good geomorphic expression		

Note: Net-slip=total displacement associated to each chronological marker. SED/PD= single event displacement/progressive displacement. N event= minimum number of rupture events. All the values are in meters. All the ages are cal ka BP. See methods section for data accuracy. Vertical displacements and more detailed description of each fault can be seen in the data supplement (Table S2). ^a Could have happened after this time; ^b Last event known, uncertain timing; - No value; ? Not sure; ~ Fault termination; [~] Slip rate based on net-slip; † More than 1 event.

4.8 Discussion

Based on an analysis of the variation in slip-rate on each fault (Fig. 22) and their paleoseismic histories, the role of each fault in the kinematics of the Taupo Rift, the implications for seismic hazard and their possible association with volcanism can be evaluated.

4.8.1 Is the Upper Waikato Stream Fault part of the Rangipo Fault or part of the Wahianoa Fault?

The location of the study area is at the putative intersection between the Rangipo and the Wahianoa faults, hence whether the Upper Waikato Stream Fault (Figs. 15 and 17) can be associated with one fault or the other can be assessed. This has been evaluated by a comparison of fault geometry, event history and fault slip-rate.

Based on the fault geometry, the extension of the Upper Waikato Stream Fault is interpreted, suggesting that it may have a physical linkage with the Rangipo and the Wahianoa faults (see potential fault linkage models in Figure 23). First, the outcrops of sections 1 and 2 within the Upper Waikato Stream were evaluated. Faults 10/4_2, 10/4_4, 10/4_6, 11/4_3, 11/4_4 and 11/4_5 in section 2 are the same fault, and equivalent to the Upper Waikato Stream Fault of section 1, because they have similar strike and throw sense (NW–W) (Table 2) and are in close proximity, and it can be interpreted that the Upper Waikato Stream Fault extends at least from section 1 to point 11/4_5 (Fig. 17). This suggests that the Upper Waikato Stream Fault is at least 15 km long if it is an independent fault (Fig. 23A).

Second, and with respect to the linkage with the Rangipo Fault, the Stereonet diagrams in Figure 5 show that section 1 of the Upper Waikato Stream Fault, close to the Rangipo Fault, has a strike that varies from 000 to 030°, similar to the Rangipo Fault.

Some of the fault strike measurements from section 2 are also similar to those of the Rangipo Fault and thus it can be considered that Rangipo Fault might extend northwards into section 2 of the Upper Waikato Stream Fault, and perhaps beyond into the Kaimanawa Fault (see further discussion below). This is represented as a fault linkage model in Figure 23C.

Finally, the possible linkage of the Upper Waikato Stream Fault with the Wahianoa Fault is evaluated. Faults 10/4_3, 10/4_5, 11/4_1 and 11/4_2 are downthrown to the S–SE. These may be antithetic faults to the Upper Waikato Stream, but also might be part of, or to some extent controlled by, the Wahianoa Fault (Fig. 17 and Table 3). This might suggest that the Wahianoa Fault extends to point 11/4_2 in Figure 17, and thus a model in which the faults intersect or merge has been developed (Fig. 23B). Section 2 has a greater strike range (000° to 070° E) that can be attributed to the influence of the Wahianoa Fault at that latitude (Fig. 17). If both sections are considered as part of the Wahianoa Fault, they can confirm events 3 and 9 of section 3 (Table 5).

Based on earthquake history and timing of events, the Upper Waikato Stream Fault might have ruptured in conjunction with the Rangipo and Wahianoa faults (Table 5). Comparisons of the rupture history of the Upper Waikato Stream Fault with the Rangipo and Wahianoa faults for the last 11 kyr show that there were two events on the Rangipo (events 4 and 6) and Upper Waikato Stream (events 11 and 12) faults that might overlap in time; one c. 11 cal ka BP and another c. 3.5 cal ka BP. Possibly one event at c. 11 cal ka BP on the Wahianoa Fault (event 8 or 9) also overlaps with the Rangipo and Upper Waikato Stream faults rupture.

TABLE 5 COMPARISON BETWEEN THE UPPER WAIKATO STREAM, THE WAHIANOA AND THE RANGIPO FAULTS.

Fault Section	UWS FAULT Sections 1 & 2	WAHIANOA FAULT Sections 2 & 3 Outcrops + profiles	RANGIPO FAULT Villamor et al. 2007
Offset (m)	N° event (Total PD; unknown %)	N° event (Total PD)	Events (Total SED)
Taupo pumice (1.72 ka)	?	?	7 (0.1 m)
Mangatawai Tephra (3.52 ka)	12? (0.54±0.19 to 0.86±0.19; 37.3%) ^b	?	6 (0.14 m)
Papakai formation (3-11 ka)	?	?	5 (0.8 m)
Poutu lapilli (11 ka)	11 (0.75±0.21 to 1.2±0.21; 37.3%) ^a	?	4 (0.35 m)
Poronui Tephra (11.2 ka)	?	9† (6±2.12 m) ^b	
Pahoka Tephra (11 ka)	?	8† (5.5±5.32 m)	
Pourahu member (11.77 ka)	(2.37±0.42 to 3.78±0.42†; 37.3%) ^a	?	3 (1.2 m) >25 km
Okupata (11.77 ka)		7? (0.69±0.17-1.76±0.26m) ^a	2 (>0.4 m)
Shawcroft Tephra		(0.37±0.31 m)	
Waiohau Tephra (13.64 ka)		(0.32±0.36 m)	1 (32 m)
Karioi eruptive period (15 ka)		6† (12±3.9) ^a	
Rerewhakaaitu Tephra (17.7 ka)		5† (7±6)	
Last glacial maximum (>18 ka)		(0.28±0.41 m) ^a	
Hokey Pokey eruptive period	10 (0.01±0.15 to 0.17±0.15; 99.8%)	4? (2.22±0.32 m) ^a	
Oruanui Tephra (25.4 ka)	9 (1.71±0.39 to 2.2±0.39; 36%)	?	
R10 lahars (27 ka)	8 (1.92±0.44 to 2.73±0.44†; 29.6%)	?	
Marker unit 1 (olive tephra)	7 (0.65±0.54 to 0.92±0.54; 29.6%)	?	
R11 lahars (27 ka)	6 (1.03±0.74 to 2.76±0.77†; 0%)	?	
Okaia Tephra (28.6 ka)	?	?	
Omataroa Tephra (28.2 ka)	5 (0.47±0.52 to 1.24±0.52; 62.2%) ^a	?	
Orange lapilli	4 (0.46±0.56 to 1.79±0.56; 74.3%)	?	
Elephant surge (marker unit 2)	3 (0.58±0.69 to 1.21±0.69; 51.94%)	?	
Hauparu Tephra (36.1 ka)	2 (0.58±0.5 to 5.64±0.5†; 89.7%)	?	
R13 lahars (<45 ka)	?	3 (2±6) ^a	
Marker unit 3	(1.44±0.3 to 2.3±0.3; 37.3%) ^a	?	
R14 lahars (>45 ka)	1 (1.1±0.72 to 1.75±0.72; 37.3%)	?	
R15 lahars (<133 ka)	?	2 (2±4.24) ^a	
Wahianoa Formation (133 ka)		1† (5±6.36)	
Total	>12 events	>9 events	7 events
Fault observations	NE/NW	NE/SE	NNE/NW
Fault termination	Uncertain (<3.52 ka)	Uncertain (<11 ka)	Uncertain (<1.72 ka)
Mean slip rate (mm/yr) [~]	0.5±0.06 (45 ka)	>0.15±0.31 (133 ka)	0.25-0.49 (13.64 ±0.17 ka)

Note: The dark and medium grey-shaded areas show the possible timing for simultaneous rupturing of the Upper Waikato Stream and Wahianoa Faults, while the dark and light grey-shaded areas show possible timing for simultaneous rupturing of the Upper Waikato Stream and Rangipo faults. SED/PD= single event displacement/progressive displacement. N event= minimum number of rupture events. Unknown %= unknown percentage of total PD relative to the 100% displacement measured on R11 lahars. All the values are in meters. All the ages are cal ka BP. See methods section for data accuracy. Vertical displacements and more detailed description of each fault can be seen in the data supplement (Tables S1 & S2). ^a Could have happened after this time; ^b Last event known, uncertain timing; - No value; ? Not sure; ___ Fault termination; [~]Slip rate based on net-slip; † More than 1 event.

Based on a comparison of slip-rate variations in time (Fig. 22), the Upper Waikato Stream Fault has a contrasting pattern to that of the Rangipo and Wahianoa faults. Assuming that the summed progressive displacement for R11 lahars represents all of the Upper Waikato Stream Fault movement, the mean maximum slip-rate over the last 45 ka is 0.63 ± 0.06 mm/yr. With only observed data, the minimum slip-rate is 0.3 ± 0.06 mm/yr (Table 5). From past to present on the Upper Waikato Stream Fault, the slip-rate has changed from 0.45 mm/yr to 1.5 mm/yr and to 0.26 mm/yr for the periods 45–36.1, 36.1– 23.65 and 23.65 cal ka BP to the present, respectively (Fig. 22).

The slip-rate on the Wahianoa Fault varied over time: from 45 to 15 cal ka BP it was <0.1 mm/yr; from 15 to 10 cal ka BP it increased to 5 mm/yr; and from 10 cal ka BP to

the present day it decreased to >0.55 mm/yr (note that the most recent observed data are for 10 cal ka BP, and thus the age of the change in slip-rate and the slip-rate are minimum values). The slip-rate on the Rangipo Fault varied in a different fashion: from >25.4 to 13.6 cal ka BP it was 1.8 mm/yr and from 13.6 cal ka BP to the present day it decreased to 0.24 mm/yr (Fig. 22).

All faults seem to have a period of higher slip-rate, followed by a period of lower slip-rate into the present. However, these periods of higher slip-rate do not coincide with each other: the Rangipo Fault accelerates at 13.6 cal ka BP; the Upper Waikato Stream Fault at 23.65 cal ka BP, although there is a small increase at 11 ka; and the Wahianoa Fault at 10 cal ka BP (or earlier).

From 11 cal ka BP to the present day, all the faults have apparently experienced lower slip-rates, between 0.24 and 0.55 mm/yr, and during this period it was more likely that the Upper Waikato Stream Fault might have ruptured together with either the Rangipo Fault or the Wahianoa Fault. From 11 to 25 ka, the Rangipo Fault had an accelerated period that is not reflected on the Upper Waikato Stream Fault, suggesting that they might have moved independently (Fig. 22).

In summary, the Upper Waikato Stream Fault is a newly discovered and potentially independent seismogenic source in the southern termination of the Taupo Rift, but a fault that could also rupture together with the Rangipo or the Wahianoa faults.

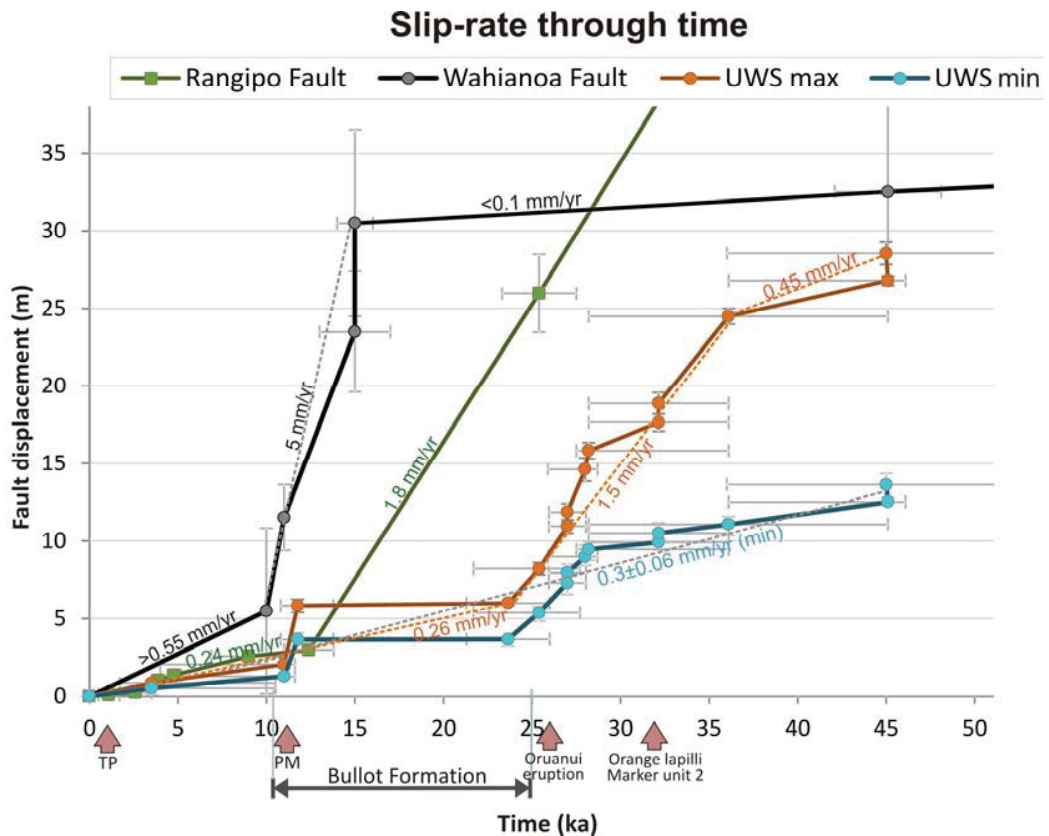


Figure 22. Fault slip-rate variation from >45 ka to present day for the Rangipo Fault (green square) [Villamor *et al.*, 2007], the Wahianoa Fault (based on profiles, grey circle), and the Upper Waikato Stream Fault (blue circle minimum values and orange circle maximum values). Higher slip-rate periods are coincident with the Bullot Formation, the Pahoka–Mangamate eruptions (PM), the Orange lapilli and marker unit 2 (Elephant surge) from Mt. Ruapehu, and the Ōruanui eruption from Taupo. Taupo pumice (TP) eruption is indicated at 1.72 cal ka BP. Zero (0) indicates the present day.

4.8.2 The role of the Wahianoa, Upper Waikato Stream and Rangipo faults in the kinematics and evolution of the Taupo Rift

Since rifting and extensive volcanism started in this area approximately >340 ka ago [Villamor and Berryman, 2001; Gamble *et al.*, 2003], the Wahianoa and Rangipo faults formed, contemporaneously and oblique to each other, playing an important role in the kinematics and evolution of the southern termination of the Taupo Rift.

The orientation of the Upper Waikato Stream and Wahianoa faults were probably inherited from basement faults such as the Oligocene–Miocene Kaimanawa Fault [Fig. 13; Kear, 1993] seen in the Kaimanawa Mountains, east of the Mt. Ruapehu Graben. In

Figure 13 several NE- to ENE-striking lineaments, sub-parallel to the Kaimanawa, Wahianoa and Upper Waikato Stream faults can be observed in the exposed basement in the Kaimanawa Mountains. The strike of the Rangipo Fault does not seem to be represented in the basement lineaments in the Kaimanawa Mountains, but it is possible that the dominant NNE trend of the faults, just north of this area in the Tongariro domain, is forcing the NNE-strike into the Mt. Ruapehu Graben area [Villamor and Berryman, 2006a].

Villamor and Berryman [2006b] suggest that the coexistence of active normal faults with very oblique fault trends in the wider southern Taupo Rift region is likely to be explained by a stress tensor with vertical $|\sigma_1| > |\sigma_2| \approx |\sigma_3|$ that will cause radial extension (radial strain) and where, theoretically, any normal fault direction is possible. Townend et al. [2012] also found several orientations of the azimuth of the maximum horizontal compressive stress (SH_{max}) in their analysis of the shallow focal mechanism in the region of southern Taupo Rift. If radial stresses are affecting the crust in the Mt. Ruapehu area and any fault direction is possible, but still there is a preferred NE orientation, it is possible that the NE and ENE fault trends that dominate in the study area are controlled by pre-existing weaknesses in the basement.

This study shows that in the short-term (few thousands of years), the Wahianoa, Rangipo and Upper Waikato Stream faults have been accommodating extension at the same time, but have taken dominant roles during different periods. The Upper Waikato Stream Fault was dominant from 36.1 to 23.65 cal ka BP (higher slip-rate period), whereas the Rangipo Fault was dominant from >25 to <15 cal ka BP, and the Wahianoa Fault was dominant from 15 to 10 cal ka BP (Fig. 22). These changes in slip-rate over time might represent short periods (c. 5–10 ka) when one extension direction may predominate over others, whereas in the long-term (e.g. since the inception of rifting at >340 ka) the deformation pattern shows extension in different directions. It is also possible that slip variability is simply related to fault interactions

(stress transfer among closely spaced faults) as observed globally for other extensional tectonic regimes [*Weldon et al.*, 2004; *Nicol et al.*, 2006; *Mouslopoulou et al.*, 2009; *Ferry et al.*, 2011; *Cowie et al.*, 2012; *Benedetti et al.*, 2013], or that slip-rate variability is a combination of both processes, fault interactions and short-term changes in the extension direction.

The prominent decrease in slip-rate of the Upper Waikato Stream Fault since c. 24 ka could be used as a sign of rift evolution at this latitude. The Upper Waikato Stream and Rangipo faults represent the east margin of the Taupo Rift, at or very near the major lithological boundary between volcanic rocks and basement greywacke. It is known from the volcanic/greywacke contact that the rift narrows to the north of this area [*Villamor and Berryman*, 2006a]. The decrease in the slip-rate of the Upper Waikato Stream Fault, and the lack of geomorphic expression that suggests low current activity, might be a consequence of the Mt. Ruapehu Graben margin shifting closer to the axis at the Tongariro Graben. However, it is possible that the decrease in slip-rate of the Upper Waikato Stream Fault is a consequence of fault interactions and transfer of motion onto other faults. If so, a rift narrowing at this latitude is not necessary.

4.8.3 Seismic hazard from the Upper Waikato Stream and Wahianoa faults

In this section, seismic hazard is evaluated for the studied faults estimating single-event displacements, earthquake magnitudes and recurrence times for segments of different surface lengths.

Average single-event displacements are derived from fault length using fault-rupture scaling relations (see Methods section) and can be used to assess whether the progressive displacements calculated above represent one or multiple single-event displacements. Fault rupture length is also used to assess future earthquake magnitudes. Several scenarios were considered for rupture of the Upper Waikato

Stream Fault (Fig. 23). The Upper Waikato Stream Fault was mapped for only 5.5 km given the lack of geomorphic expression but it is expected that, as an individual seismogenic source, it may be at least as long as the thickness of the seismogenic crust, that is c. 15 km (Fig. 23A). A combined rupture of the Wahianoa and Upper Waikato Stream faults will produce c. 27 km of rupture (Fig. 23B). Rupture of the Upper Waikato Stream and Rangipo faults was suggested as a possibility by Villamor et al. [2007]. They suggested the potential rupture of the entire Rangipo Fault, including the section between the mapped traces and the Kaimanawa Fault, a section that includes the newly defined Upper Waikato Stream Fault (Fig. 23C). Geomorphic observations support a potential fault rupture of up to 43 km.

For a 27 km long surface rupture (Upper Waikato Stream Fault along with Wahianoa Fault) a M_w 6.8 earthquake is produced with an average single-event displacement of 1.26 m (Table 6). For a 43 km long surface rupture (Upper Waikato Stream Fault along with Rangipo Fault), a M_w 7.1 earthquake is produced with a single-event displacement of 2.4 m. These single-event displacement values represent a total-fault rupture.

Lower single-event displacement values (<1 m) suggest a segmented fault rupture. Based on the estimated average displacements, the maximum progressive displacements for events 1, 3, 4, 5, 9 and 11 on the Upper Waikato Stream Fault could represent a whole-fault rupture, whereas minimum progressive displacements for all the events represent segmented ruptures. Greater values (e.g. 2.73 m on event 8) represent multiple rather than single-event displacements (Tables 2 and 5).

Based on the combined findings, the minimum recurrence interval is estimated for various periods (Table 5). For the Wahianoa Fault, the recurrence interval is 2.4 ka between 25.4 and 11.2 cal ka BP, and 13.6 ka between 133 and 11 cal ka BP (based on sections 2 and 3). For the Upper Waikato Stream Fault, the recurrence interval is

1.6 ka between 36.1 and 21.9 cal ka BP (section 1) and 3.5 ka between 45 and 3.52 cal ka BP (sections 1 and 2).

Earlier studies on the Wahianoa Fault [Villamor and Berryman, 2006b] estimated mean slip-rates of 0.3 mm/yr. Results from this study show that the Wahianoa Fault could have a minimum slip-rate of 0.55 mm/yr from 10 ka to the present day, changing the current seismic hazard. Consequently, this study provides an update to the National Seismic Hazard Model for New Zealand [Stirling et al., 2012; Litchfield et al., 2013]. This study reinforces the segment surface lengths given to the Rangipo [up to 43 km; Villamor et al., 2007] and Wahianoa [27 km; Stirling et al., 2012] faults.

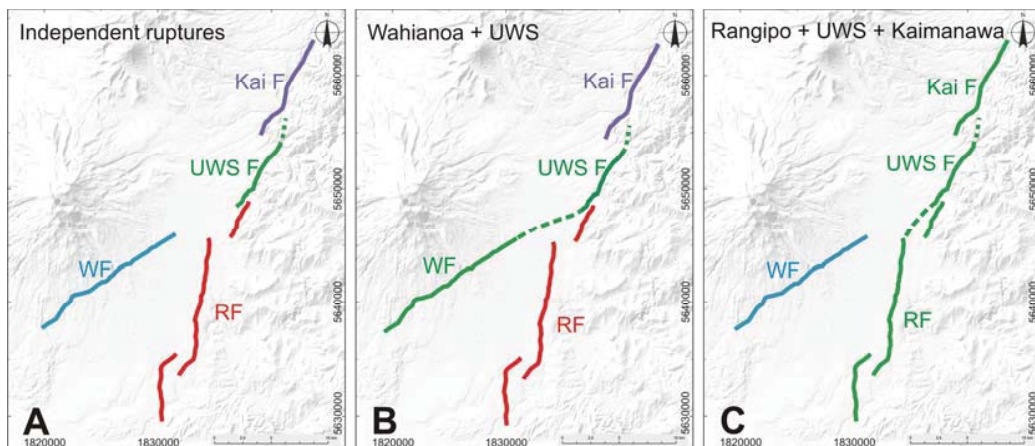


Figure 23. Potential physical intersections and rupture models of the Upper Waikato Stream Fault with Rangipo and Wahianoa faults. A, Independent ruptures. B, Potential rupture of the Wahianoa (WF) and Upper Waikato Stream (UWS F) faults (27 km). C, Potential rupture of the Rangipo (RF), Upper Waikato Stream and Kaimanawa (Kai F) faults (43 km).

TABLE 6. MOMENT MAGNITUDE AND SINGLE-EVENT DISPLACEMENT FOR DIFFERENT FAULT LENGTHS.

Fault	Segment surface length (km)	Average displacement (m)	M_w
UWS ^a	15	0.8	6.5
Wahianoa + UWS	27	1.5	6.8
Rangipo + UWS + Kaimanawa	43	2.4	7.1

Note: Estimated average single-event displacement in meters and earthquake moment magnitude (M_w) based on Webb's equation, for a certain segment surface length (km) and fault area (as described in Villamor et al. 2007; Stirling et al. 2012, see methods section). ^a Note that the Upper Waikato Stream (UWS) Fault individual rupture-length is a minimum value.

4.8.4 Potential association of volcanism with periods of accelerated seismic activity

Fault slip-rate variations appear to be associated with times of enhanced volcanism in the TgVC [Villamor *et al.*, 2007]. Higher slip-rate periods in the Upper Waikato Stream Fault seem to be coincident with the major Ōruanui eruption from the Taupo caldera immediately to the north (25.4 ± 0.2 cal ka BP; vent located 50 km from the fault) at the same time that large extension fissures formed in close proximity to the Upper Waikato Stream Fault (Fig. 19). This eruption was one of the largest known over the last c. 40 ka, producing 530 km³ of erupted magma [Wilson, 2001]. An acceleration of the Upper Waikato Stream Fault movement may also coincide with the eruption of the Orange lapilli (Mt. Ruapehu; vent located 15 km from the fault) and marker unit 2 (probably Mt. Tongariro) at c. 32 ka, as well as with the large Pahoka–Mangamate eruption sequence at c. 11 cal ka BP (vent located 18 km from the fault), an eruptive process during regional extension in the TgVC [Topping, 1973; Nairn *et al.*, 1998]. In the Rangipo Fault, a higher slip-rate period coincides with the eruptions of the Bullot Formation, a period of frequent large plinian eruptions of Mt. Ruapehu from 25 to 11 cal ka BP [Donoghue *et al.*, 1991; Pardo *et al.*, 2012] (vent located 13 km from the Rangipo Fault). In the Wahianoa Fault, a higher slip-rate period coincides with the Pahoka–Mangamate eruption sequence at c. 11 cal ka BP (vent located 18 km from the Wahianoa Fault; Fig. 22).

During these periods of large and explosive volcanic eruptions, the extension across this portion of the rift may be mainly accommodated by dike intrusion, and crustal stresses created by the volcanic intrusions could be influencing the slip-rate changes for some of the faults. The temporal association of Bullot Formation (Mt. Ruapehu) and Pahoka–Mangamate (Ngāuruhoe, Tongariro) eruptions with periods of increased activity on the southern faults (Rangipo and Wahianoa) implies a connection between volcanic and tectonic activity, but the faults did not react in the same way. The Rangipo Fault may have been more connected to the Bullot Formation eruptions from Ruapehu

Volcano and the Wahianoa Fault to the Pahoka–Mangamate eruptions from Tongariro and Ngāuruhoe volcanoes (Fig. 22).

The distance and magnitude of volcanism (e.g. dike opening), together with fault orientations, determine whether the fault will be affected by dike intrusion. The Upper Waikato Stream Fault was strongly affected by the Ōruanui eruption, presenting a higher slip-rate period and extensional fissures. This suggests that Ōruanui eruption was significant enough to alter the crustal stress at distances of >55 km from the caldera, and perhaps change the kinematics of the rift by allowing the activity to shift from the margin of the rift towards the axis.

4.9 Conclusions

This study provides an updated understanding of the eastern boundary of the Taupo Rift close to its termination, extending the mapping of active faults in this area and adding more information on fault characterisation for hazard assessment and suggesting potential volcano–tectonic interactions. The NE-striking Upper Waikato Stream Fault is a newly discovered and potential independent seismogenic earthquake source at the eastern boundary of the rift just north of the NNE-striking Rangipo Fault. Geological evidence suggests that the Upper Waikato Stream Fault might be an independent fault, but might also rupture in conjunction with the Wahianoa and/or Rangipo Fault. The EWE-striking Wahianoa, a known active fault, might be potentially linked with the Upper Waikato Stream Fault, forming a fault intersection pattern similar to those described farther south in the rift.

Paleoseismic and geomorphic analyses demonstrate the occurrence of at least 12 surface-rupturing earthquakes in the last 45 ka on the Upper Waikato Stream Fault, which has a mean slip-rate of 0.3 ± 0.06 to 0.63 ± 0.06 mm/yr. New data on the

Wahianoa Fault suggest at least nine surface-rupturing earthquakes in the last 133 ka, and a long-term mean slip-rate of 0.15 ± 0.31 mm/yr for this fault.

This study provides new data to update the National Seismic Hazard Model [*Stirling et al.*, 2012; *Litchfield et al.*, 2013] for this region. The new seismic source been defined here, the Upper Waikato Stream Fault (M_w 6.5), can be added to the National Seismic Hazard Model. Also, the Wahianoa Fault has a slip-rate of >0.55 mm/yr from 10 cal ka BP to the present day, more rapid than in the current National Seismic Hazard Model. The rupture lengths for the Wahianoa and Rangipo faults were confirmed, the Wahianoa Fault might rupture together with the Upper Waikato Stream Fault (27 km), and the Rangipo Fault might rupture together with the Upper Waikato Stream and Kaimanawa faults, giving a total surface-rupture length of 43 km.

The Rangipo Fault might have ruptured at the same time as the Upper Waikato Stream Fault at c. 11 and 3.52 cal ka BP (Table 5), posing a greater potential seismic hazard. For a 27 km long rupture of the Wahianoa Fault together with the Upper Waikato Stream Fault, the expected earthquake would be M_w 6.8; and for a 43 km long rupture, involving the Rangipo Fault with the Upper Waikato Stream and the Kaimanawa faults, a M_w 7.1 earthquake is expected.

The slip-rate variability of the Upper Waikato Stream and Wahianoa faults estimated here has been compared with existing data on the Rangipo Fault. Tentative explanations of the slip-rate changes on these three faults are: (1) stress transfer interactions among closely space faults, similar to other observations for the Taupo Rift farther north; (2) short-term (few thousands of years) changes in extension direction, with the Wahianoa, Rangipo and Upper Waikato Stream faults taking dominant roles in different periods; (3) higher slip-rate periods coinciding with periods of major explosive volcanism (e.g. the Ōruanui eruption from Taupo caldera at 25.4 ± 0.2 cal ka BP coinciding with higher slip-rates on the Upper Waikato Stream Fault, the Bullot

Formation from Mt. Ruapehu at 25–11 ka with the Rangipo Fault, and the Pahoka–Mangamate eruptions from Tongariro at 11 cal ka BP with the Wahianoa Fault); (4) rift evolution with slip-rate decrease at the rift boundary suggesting shifting of active faulting closer to the rift axis (as has been described farther north); and (5) a combination of all or some of the process above.

CHAPTER 5. Earthquake history and crustal extension in the Tongariro Graben: insights into volcano-tectonic interactions and active deformation in a young continental rift.

- 5.1 Abstract
- 5.2 Introduction
- 5.3 Regional geology
- 5.4 The Tongariro Graben
- 5.5 Methods
 - 5.5.1 Fault mapping and update of GNS Active Fault Database
 - 5.5.2 Fault geometry, displacement values and displacement history
 - 5.5.3 Slip-rates and extension rates from tectonic faulting
 - 5.5.4 Extension rates from dike-intrusion
- 5.6 Results
 - 5.6.1 Paleoseismology analysis
 - 5.6.1.1 Rift bounding faults: National Park and Upper Waikato Stream faults
 - 5.6.1.2 The Waihi Fault zone
 - 5.6.1.3 The Poutu Fault zone
 - 5.6.2 Fault slip-rates in the Tongariro Graben
 - 5.6.3 Dike intrusion rates in the Tongariro Graben
- 5.7 Discussion
 - 5.7.1 Is surface faulting associated with tectonic extension or dike intrusion faulting in the Tongariro Graben?
 - 5.7.2 Proportion of extension accommodated by faulting vs. dike intrusion
- 5.8 Conclusions

Supplementary files (Appendix A)

Table S3. Waihi Fault displacements

Table S4. Poutu Fault displacements

Table S5. Field locations

Table S6. Waihi Fault, geomorphic surface offsets and progressive displacements

Table S7. Waihi Fault, outcrop offsets and progressive displacements

Table S8. Poutu Fault, geomorphic surface offsets and progressive displacements

Table S9. Poutu Fault, outcrop offsets and progressive displacements

Table S10. Main stratigraphic units

Figure S5. Waihi Fault main field outcrops

Figures S6 and S7. Poutu Fault main field outcrops

This chapter has been reviewed and accepted for publication in the Geological Society of America Bulletin.



Figure 24. Ngāuruhoe volcano, Pukekaikiore and Mt. Ruapehu from the Mangatepopo moraine, view roughly to the south (by Anja Moebis).

Participating authors:

Martha Gabriela Gomez-Vasconcelos (undertook the fieldwork, collected and analysed the data, interpreted it and wrote the manuscript)

Pilar Villamor (fieldwork, manuscript editing and discussion)

Shane Cronin (fieldwork, manuscript editing and discussion)

Jon Procter (fieldwork and data processing)

Alan Palmer (fieldwork and manuscript editing)

Dougal Townsend (geological mapping and manuscript editing)

Graham Leonard (geological mapping)

Earthquake history and crustal extension in the Tongariro Graben: insights into volcano-tectonic interactions and active deformation in a young continental rift.

Martha Gabriela Gómez-Vasconcelos, Pilar Villamor, Shane Cronin, Jon Procter, Alan Palmer, Dougal Townsend and Graham Leonard.

5.1 Abstract

In volcanic rift zones surface faulting from tectonic faults or from dike intrusions can be difficult to discriminate because they have similar geomorphic expression. At the Tongariro Graben, near the southern end of the Taupo Rift, New Zealand, crustal extension over the last 350 k.y. has been accommodated by a combination of magma intrusion and tectonic faulting. Normal faults prevail along this 30-km-wide NNE-oriented graben, with vents of the Tongariro Volcanic Complex lying parallel to and overlapping the graben axis. This study quantifies the geological extension at the Tongariro Graben (7 ± 1.2 mm/yr since 20 ka) and the relative contributions from tectonic faulting and dike intrusion. Field observations were used to interpret fault geometry and activity. To discriminate between tectonic faulting and that associated with dike-intrusion (volcano-tectonic), theoretical fault dislocations were modeled from dike intrusion for likely fault-dike spatial relationships, and compared these to measured displacements. Most of the mapped faults are tectonic in origin. The calculations indicate that the rift-bounding normal faults (National Park and Upper Waikato Stream faults) and the intra-rift inward-dipping faults (Waihi and Poutu faults) accommodate 78-95% (5.8-7.0 mm/yr) of the total extension across the graben (tectonic extension), while dike intrusions could accommodate only 5-22% (0.4-1.6 mm/yr; magmatic extension), from which 4-5% is associated with volcanic eruptions and the remainder with deep arrested dikes. These results help to refine the seismic and volcanic hazards of the region and raise questions on the spectrum of volcano-tectonic interactions possible in similar continental rifts worldwide.

5.2 Introduction

It is well known that crustal extension in continental rifts is accommodated by a combination of normal faulting and dike intrusions [McCalpin, 1996]. By contrast, it is difficult to assess the percentage of extension accommodated by each process in such sites [e.g., Biggs *et al.*, 2009; Ebinger *et al.*, 2010]. In some regions, magmatism plays a dominant role in the extension [e.g., Asal Rift in Djibouti; De Chabaliér and Avouac, 1994], while in others tectonic faulting appears to dominate [e.g., Rungwe Volcanic Province in SW Tanzania; Fontijn *et al.*, 2010].

In volcanic environments it can be difficult to distinguish whether ground surface displacements along faults are a result of tectonic faulting, or dike intrusion, or both, because they have similar geomorphic expressions [Gudmundsson and Brenner, 2004; Fig. 25]. Discriminating between the different modes is important, primarily because surface fault displacements are used to calculate future earthquake magnitudes in seismic hazard assessment. Furthermore, volcanic eruption histories and eruption triggering estimates depend on knowing the rates and frequency of magmatic intrusions. Historic displacements of normal faults that ruptured through the whole crust (or near to it) produce moderate to large earthquakes with well-defined magnitude-displacement empirical scaling relationships [e.g., Stirling *et al.*, 2012]. Conversely, displacements along normal faults associated with shallow arrested dikes do not follow these typical empirical scaling relationships because they display relatively large offsets for small earthquakes [e.g., Rowland *et al.*, 2010].

Surface faulting in continental rifts of different tectono-volcanic environments may result in similar geomorphic expressions, despite being controlled by different processes. For example, the Asal Rift (Afar Depression, Djibouti) and the Tongariro Graben are broadly geomorphically similar (Fig. 25), yet the drivers of rifting are different. In both locations, the volcanic deposits are displaced by inward dipping faults,

bounding the aligned active vents and creating a <5 km-wide graben-like structure. In the Asal Rift the most common type of eruption is fissure-forming and eruptive products are basaltic in composition. With rapid extension rates (16 mm/yr), normal faulting in the Asal Rift is the reflection of repeated dike intrusions [Stein *et al.*, 1991]. During a 1978 dike intrusion event, a vertical slip up to 1 m occurred on graben bounding faults within <4 km from the Asal Rift axis, with a related earthquake swarm reaching M_b 4 to 5.3 [Abdallah *et al.*, 1979; Rubin and Pollard, 1988; Stein *et al.*, 1991; Ebinger *et al.*, 2008]. Similarly, during the 2005 Dabbahu rifting episode in the Afar Depression, Ethiopia, a M_b 4.7 earthquake generated 1.5 m of vertical displacement, attributed to a single dike intrusion [Wright *et al.*, 2006].

Using the scaling relationships for the Taupo Volcanic Zone (TVZ), New Zealand [Villamor *et al.*, 2007; Stirling *et al.*, 2012], the above single-event fault displacement of 1.5 m would indicate an earthquake magnitude of up to M_w 6.9. In the northern part of the TVZ, the M_L 6.3 Edgecumbe earthquake in 1987 generated a mean co-seismic vertical displacement of 1 m, attributed to a tectonic fault rupture [Beanland *et al.*, 1989]. This scaling relationship applies, however, in the southern TVZ, especially in the Tongariro Graben. If the fault displacements measured were related to dike intrusion rather than tectonic crustal rupture; seismic hazard would be overestimated when dike intrusion related offsets are used to calculate earthquake magnitudes with the traditional scaling relationships.

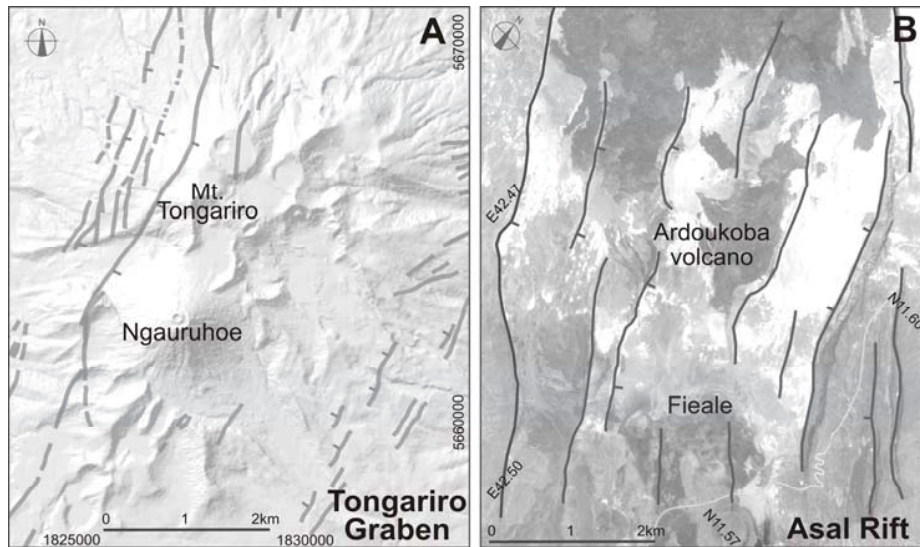


Figure 25. Similar geomorphic expression of volcanic rift zones in the Tongariro Graben (A) and the Asal Rift in Djibouti (B), showing parallel normal faults bounding the western and eastern flanks of the volcanic vents [modified from *Stein et al.*, 1991].

The Tongariro Graben comprises a dense network of NNE-striking active faults, which bound active volcanic vents of the Tongariro Volcanic Complex (Fig. 26). The complex's volcanic activity had begun by ~350 ka ago [*Topping*, 1973; *Cole*, 1978; *Hobden et al.*, 1996; *Gamble et al.*, 2003; *Tost et al.*, 2016] and it has formed a set of eruptive vents that are aligned on trends parallel to the graben axis. Fault strands of the graben displace lava flows, moraines, tephra, and debris fans of the volcanic complex. Their distribution raises the question of mechanisms of interconnection between magmatic and tectonic processes may be. Determining the type and activity of faults present and how they interact with magmatism of the Tongariro Volcanic Complex are the focus of this work. This, in turn, can be used to revise the seismic hazard potential of the area.

Based on morphology and regional studies, *McCalpin* [1996] assumed that all the faults in the Taupo Volcanic Zone were related to dike intrusion. *Cassidy et al.* [2009] applied magnetotelluric and gravity methods in the Tongariro Graben, and suggested that faults provide magma pathways to the surface. Throwing doubt on this, a recent gravity

and magnetic study of the Tongariro Volcanic Complex [Miller and Williams-Jones, 2016], demonstrates the absence of large intrusive bodies within the complex and, rather, modeled faults as deep crustal tectonic structures. Hence further exploration of the drivers of active faulting in the Tongariro Graben is needed. This site also provides an excellent location to study the broader question of interplay between magmatic and tectonic activity. The Tongariro Graben contains a well-studied complex, multi-vent volcanic edifice [Topping, 1973; Cole, 1978; Hobden et al., 1996; Gamble et al., 2003], and a well-exposed set of active fault systems. This region of the Taupo Rift does not have the high volumetric emplacement of magmatism that Iceland, Ethiopia or other well studied rifts have, nor does it experience the same rate of tectonism [De Chabaliere and Avouac, 1994; Biggs et al., 2009]. The record of sporadic medium to large explosive eruptions at Tongariro is dated through a series of studies [Donoghue et al., 1995; Cronin et al., 1996b; Moebis et al., 2011; Pardo et al., 2012].

The principal aim of this work was to define the proportions of faulting in the Tongariro Graben driven by magmatic vs. tectonic processes, and to quantify the magmatic and tectonic contribution to the regional extension. Part of the answer to this was achieved through examining the kinematics of the Tongariro Graben. Analyses of the geometry, faulting history, slip-rate variation through time and extension rates of the Tongariro Graben were completed using paleoseismic methods. Dislocation models were run with Coulomb software [Lin and Stein, 2004; Toda et al., 2005] to estimate deformation at the surface from dike intrusion, and compare values with geological observations. Geologic fault slip-rates were compared with geodetic data to help estimate extension due to dike intrusions and inform possible volcano-tectonic interactions. Understanding the mechanisms and relationship between tectonic faulting and volcanism will improve both seismic and volcanic hazard assessment for this region, which is popular year-round for tourism [Jolly et al., 2014], and a UNESCO World Heritage Area [Rössler,

2006]. This research question is relevant to magmatic-tectonic partitioning of extension and consequent hazard assessment at similar rift systems worldwide.

5.3 Regional geology

The Taupo Volcanic Zone is a NNE-trending Quaternary volcanic arc at the central North Island of New Zealand, where the Pacific Plate subducts below the Australian Plate [Wallace *et al.*, 2004]. An active extensional regime occurs within the arc as a consequence of the current fore arc clockwise rotation [Wallace *et al.*, 2004] and slab rollback [e.g., Seebeck *et al.*, 2014]. Faults within the volcanic arc [Rowland and Sibson, 2001] define the intra-arc Taupo Rift [Fig. 26; Acocella *et al.*, 2003].

The Taupo Rift is defined by a line of shallow seismicity and active faulting [Bibby *et al.*, 1995; Villamor and Berryman, 2001]. Geodynamic modeling of GPS velocities, earthquake focal mechanisms and fault slip-rates across the whole plate boundary suggest that total extension rates decrease from north to south, from 15 mm/yr at the northern part of the Taupo Volcanic Zone to <5 mm/yr at the southern part, where the closure of the rift occurs [Fig. 26; Wallace *et al.*, 2004]. Geological extension rates are estimated at 6.4 mm/yr in the central Taupo Rift [Villamor and Berryman, 2001] and 2.3 mm/yr at the southernmost end [Villamor and Berryman, 2006a].

The Taupo Volcanic Zone is typically divided into three segments: the central portion is dominated by eight rhyolitic calderas with >25 caldera-forming eruptions over the last 1.6 m.y. [Wilson *et al.*, 1984], while the northern and southern parts host andesitic volcanoes [Wilson *et al.*, 1995]. The Tongariro Volcanic Centre represents the southernmost volcanism, including two large volcanic complexes (Ruapehu and Tongariro), and a number of satellite centres of lesser volume. A NNE-aligned volcano-vent corridor occurs along the Ruapehu Graben to the south, passing northward into

the Tongariro Graben [Topping, 1973; Rowland and Sibson, 2001; Villamor and Berryman, 2006a], which is the focus of this study.

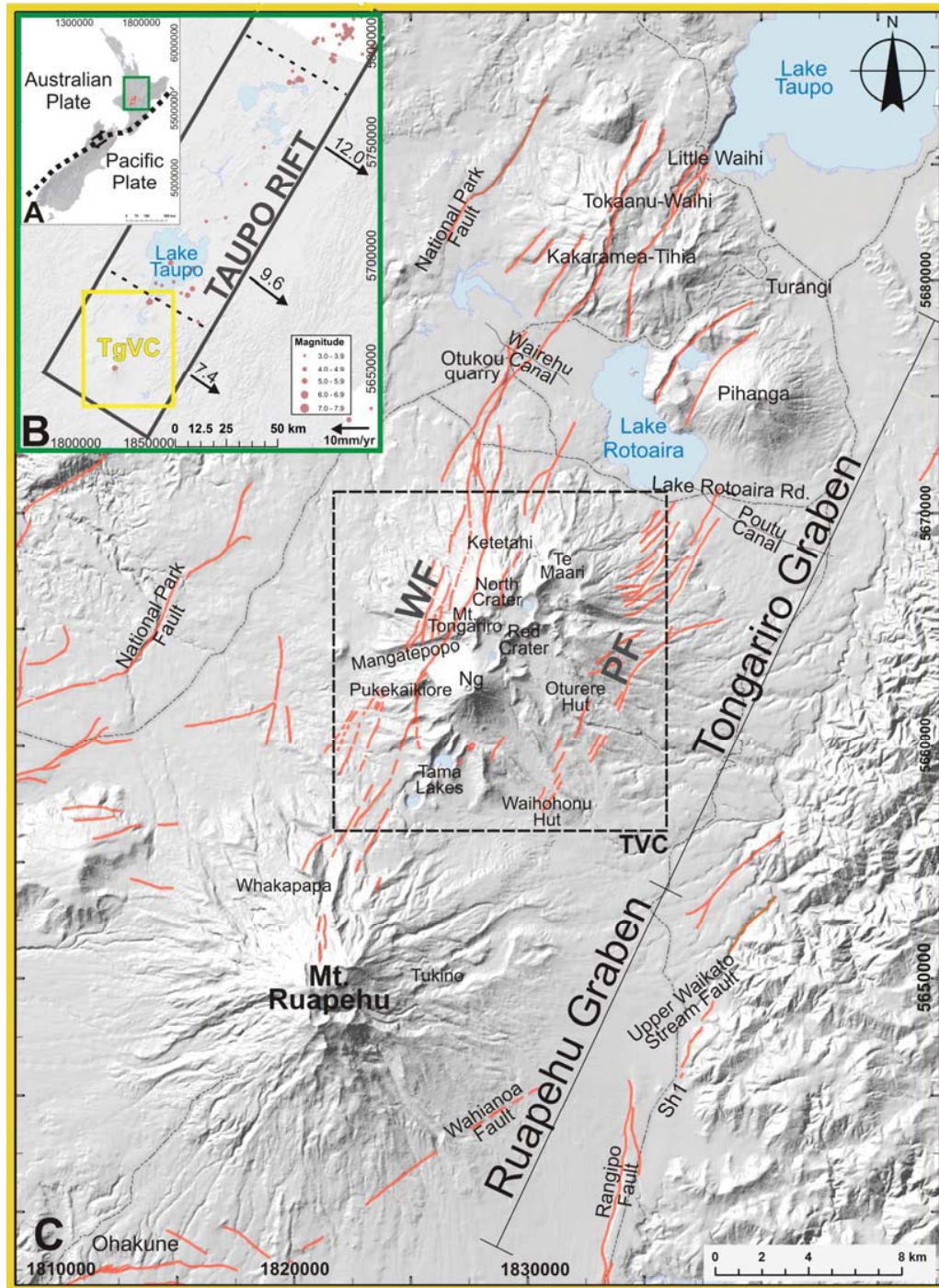


Figure 26. A, Location map of the Taupo Rift in the North Island of New Zealand (green rectangle). B, Location of the Tongariro Volcanic Centre (TgVC, yellow rectangle) at the southern part of the Taupo Volcanic Zone. Variation of extension rate along the rift, marked with black arrows, values in mm/yr [Wallace *et al.*, 2004]. Large ($M_w > 3$) and shallow (< 40 km) earthquakes marked with red circles, compiled from the New Zealand catalogue of earthquakes since the 1930s (extracted from NZ GeoNet database <http://info.geonet.org.nz/display/appdata/Earthquake+Catalogue>). C, Location of the Tongariro Volcanic Complex (TVC) at the Tongariro Graben axis, the Waihi Fault (WF) and the Poutu Fault (PF) zones, Mt. Ruapehu, Ruapehu Graben and the main volcanic vents in the region. The active faults are marked in red [Langridge *et al.*, 2016]. Ng, Ngāuruhoe.

5.4 The Tongariro Graben

Four regional and NNE-striking parallel fault sets comprise the Tongariro Graben: two rift-bounding faults, the National Park Fault [Villamor and Berryman, 2006b] and the Upper Waikato Stream Fault [Chapter 4; Gómez-Vasconcelos *et al.*, 2016]; and two intra-rift faults, the Waihi and the Poutu faults [Fig. 27; Lecointre *et al.*, 2004b; Villamor and Berryman, 2006b; Cassidy *et al.*, 2009]. The National Park Fault [Villamor and Berryman, 2006b] is an active NNE-oriented normal fault that bounds the western Tongariro Graben and is downthrown to the SE. A slip-rate of 0.2 mm/yr was estimated for this fault [Stirling *et al.*, 2012]. The Upper Waikato Stream Fault is an active NE-striking normal fault that bounds the eastern Tongariro Graben and is downthrown to the NW, with a minimum slip-rate of 0.5 mm/yr [Chapter 4; Gómez-Vasconcelos *et al.*, 2016]. The inward-dipping Waihi and Poutu faults define a $\sim 030^\circ$ -trending 8-10-km-wide graben axis and a narrowing of the rift in this area [Fig. 26; Villamor and Berryman, 2006b].

The Waihi Fault zone is an active NNE-oriented normal fault set on the western flanks of the Tongariro Volcanic Complex, downthrown to the SE [Grindley, 1960; Van Dissen *et al.*, 2003]. Lecointre *et al.* [1998] calculated for this fault a 0.9 mm/yr slip-rate for the last 65 ka, while Stirling *et al.* [2012] and Litchfield *et al.* [2013] reported a 1.3 mm/yr slip-rate. The Waihi Fault zone has been associated with historical earthquakes and landslides in the north-western Tongariro Volcanic Centre [Hochstein *et al.*, 1995]. The Hipaua Steaming Cliffs near Little Waihi village (Fig. 27) have produced deadly

landslides in 1846 and 1910, each after magnitude 6.3 earthquakes on the Waihi Fault [Hegan *et al.*, 2001; Cooper, 2002].

The Poutu Fault zone is an active NNE-oriented normal fault set on the eastern flanks of the Tongariro Volcanic Complex [Villamor and Berryman, 2006b], downthrown to the NW with many antithetic faults [Van Dissen *et al.*, 2003]. At the Poutu Canal, east of Lake Rotoaira, Lecointre *et al.* [1998] calculated a 0.14 mm/yr slip-rate between 11 and 7 ka for this fault, while Stirling *et al.* [2012] and Litchfield *et al.* [2013] reported a rate of 1.85 mm/yr. Topping [1973] stated that the Poutu Fault moved subsequently to deposition of the Taupo pumice [1.72 cal ka BP; Hogg *et al.*, 2011]; and that at least one rupture was associated with an eruption from the Ngāuruhoe area at 11-12 ka that resulted in the deposition of the Mangamate Formation [Nairn *et al.*, 1998; Hitchcock and Cole, 2007; Stirling *et al.*, 2012].

Van Dissen *et al.* [2003] calculated a ≤ 2 k.y. recurrence interval for surface rupture of the Waihi and Poutu fault zones based on slip-rates and surface length estimations from faults in the central Taupo Rift [Villamor and Berryman, 2001]. Activity of both fault zones over the last 60 ka has affected patterns of the volcanogenic sedimentation at the northern part of the Tongariro Volcanic Complex and has also influenced the formation of the Lake Rotoaira basin [Lecointre *et al.*, 2004b].

The northern boundary of the Tongariro Graben is the Kakaramea-Tihia volcanic complex, southwest of Lake Taupo, where a major widening of the rift occurs into the calderas of the central North Island. The southern end of the graben abuts the northern slopes of Mt. Ruapehu and is obscured by young volcanic materials. There is no surface expression of these faults south of Mt. Ruapehu crater, but Tejero *et al.* [2004] and Cassidy *et al.* [2009] observed gravity anomalies underneath Mt. Ruapehu that correlate with the Waihi and Poutu faults, suggesting that they may extend south of Mt. Ruapehu crater [Villamor and Berryman, 2006b].

5.5 Methods

To study the faulting history of the Tongariro Graben, various paleoseismic methods were employed. Active fault mapping [e.g., *Leonard et al.*, 2014; *Langridge et al.*, 2016] was analysed and revised by identifying fault offsets of geomorphic surfaces of known age and faulted stratigraphic units in outcrops. These age/offset constraints were used to reconstruct the timing of fault rupture, estimate fault slip-rates and extension rates along the Tongariro Graben. In order to study the extension accommodated by magmatism, eruption rates were compiled and magma intrusion rates estimated from the record of volcanic eruptions.

5.5.1 Fault mapping and update of GNS Active Fault Database

In order to create a 1:5,000 scale fault trace map of the Tongariro Volcanic Centre, a 2 m-resolution photogrammetry based digital surface model (DSM) and aerial photograph interpretation was used to calculate surface displacements. Details of the 2010 and 2012 digital surface model survey development and photogrammetry process are standard and explained more fully in Gómez-Vasconcelos et al. [2016]. The aerial photographs used were stereoscopic pairs from the 1940s and 1960s, at 1:50,000 and 1:16,000 scales, respectively (NZ Aerial Mapping, runs 1727, 1738, 2436, 2564, 2569 and 2572) along with Google Earth images. Grid references on maps are in the New Zealand Transverse Mercator projection. Existing faults and geological mapping information were taken from the GNS Active Fault Database [*Langridge et al.*, 2016], and from the on-going development of a new geological map of Tongariro National Park [e.g., *Leonard et al.*, 2014].

5.5.2 Fault geometry, displacement values and displacement history

Fault geometry in the region was characterized with field measurements of strike, dip, sense of movement and fault displacements (mainly throw but also net-slip). Displacements were measured with a tape measure, with an estimated error of 0.1 m plus 10% of the measurement. Rozeta 2.0 software was used for plotting the faults on stereographic projections (lower hemisphere) and for trend-frequency analysis with rose diagrams. The Plane Vector Convention was used to report the dips (Dip/Dip direction).

The displacement history was assessed by analyzing progressive displacement of tephra layers of increasing age. The age of stratigraphic markers and geomorphic surfaces constrains the age of a fault movement [e.g., *Villamor et al.*, 2007]. Multiple ruptures on fault strands were identified by progressively larger displacement in older units. Identifying horizons where the total displacement suddenly changes can be used to identify a new faulting event, including its age and offset [*McCalpin*, 1996]. Ages of displaced strata were taken from the literature where ages of the andesitic tephra have been established by direct radiocarbon dating and/or by relative stratigraphic position in relation to known rhyolitic tephra [Table S10; *Cronin et al.*, 1996c; *Moebis et al.*, 2011].

Geomorphic analyses along the Tongariro Graben were focused at locations where a clear fault scarp could be identified. Transverse topographic profiles (n=229) were traced at locations where a fault displaces geomorphic surfaces of known ages. Vertical displacements were measured on the 2 m resolution Digital Surface Model using ArcMap GIS software. The mean slope angle was obtained using trigonometric functions. The offsets were measured several times and averaged. Field analyses included calculations of slope angles, outcrop face orientation and displacement. Some areas were also surveyed with real time kinematic (RTK) global positioning system and

with an altimeter to measure fault scarp heights (Mangatepopo, Mt. Tongariro and along Lake Rotoaira Road); measured scarp heights (offsets) were compared with the digital surface model results. These offsets have an estimated uncertainty of 1 m, plus 10% of the scarp height, which represents the uncertainty due to irregularities in the ground surface. For the error propagation, the theory of errors [Taylor, 1982] was used, as described in Villamor and Berryman [2006b].

Subtraction of consecutive total displacement values results in an estimate of co-seismic displacement or single-event displacement (SED). Alternatively, this value may correspond to multiple events (progressive displacement) if several fault ruptures have occurred between deposition of horizons of known age. The total vertical displacement includes offsets of rift-bounding faults and graben-axis faults on 20 and 60 cal ka surfaces [Last Glacial Maximum and Marine Isotope Stage 4; Eaves *et al.*, 2016], for which the data is the most complete, and likely most accurate.

5.5.3 Slip-rates and extension rates from tectonic faulting

In order to calculate the slip-rates and extension rates of the Tongariro Graben, 17 transects were traced across the Waihi and Poutu fault zones, approximately perpendicular to the mean fault trend, (transect azimuth of $\sim 115^\circ$ and between 2.5 and 4.5 km length). Each transect crosses several fault strands, therefore the vertical displacements were summed up across all fault strands to derive the mean vertical slip-rate for the entire fault zone; the vertical slip-rate was subsequently calculated and converted to dip-slip rates at the surface and at seismogenic depth.

Displacements may be underestimated, especially in older deposits, due to footwall erosion or hanging-wall deposition. Because erosion and deposition at the fault scarp are difficult to quantify, locations were chosen along the fault for displacement

calculations corresponding to well preserved surfaces of the same age to minimize that error.

Summed vertical slip-rates were used to quantitatively assess the geological extension at the surface from tectonic faulting, using a 70° average for surface fault dip and 60° at seismogenic depth [suggested by other studied faults within the Taupo Rift; *Villamor and Berryman, 2001; Nicol et al., 2006; Mouslopoulou et al., 2008*]. Measured total surface displacement was multiplied by a factor of 1.6, recognizing that dip-slip motion on a fault in a large earthquake is on average 1.6 times larger than surface displacement [Table 8; *Villamor and Berryman, 2001*]. This corrected dip-slip motion was subsequently multiplied by a factor of 1.33 following the Gutenberg-Richter relation to adjust for extension contribution at depth of small earthquakes that do not produce surface ruptures [Table 8; *Villamor and Berryman, 2001*]. Other uncertainties in extension rate estimates such as fault dip variations at depth and grain-scale deformation could not be clearly defined and are not considered in this study.

5.5.4 Extension rates from dike-intrusion

To discriminate between tectonic faulting and dike-intrusion related faulting, theoretical fault dislocations were modeled from dike intrusion for different fault-dike spatial relationships (geometric models), and modeled displacement values were compared to the measured ones. Cross-sections were drawn with existing surface data using fault and volcanic vent locations, and fault dips. Surface deformation caused by an intruding dike with different widths and depths was modeled with Coulomb 3.3.01 software [*Lin and Stein, 2004; Toda et al., 2005*] to show the amount of surface displacement expected from various geometric models. Coulomb 3.3.01 software uses the formulation of Okada [1992] for the dislocation calculations. Stress changes were also calculated on receiver faults with the same strikes and dips as the mapped faults to

assess interactions between deep arrested dikes and surface faulting. The input values used were: 80 GPa for Young's modulus, 0.25 for Poisson's ratio and 0.4 for the coefficient of friction.

Extension rates from geodynamic modeling [*Wallace et al.*, 2004] were compared with geological rates obtained here to assess contribution to extension from magmatism. In addition, published rates of volcanic eruptions were used to assess dike-intrusion rates. Co-eruptive dike opening values from existing literature and widths of exposed dikes within the area were used to convert dike-intrusion rates to extension rates.

5.6 Results

5.6.1 Paleoseismology analysis

5.6.1.1 Rift-bounding faults: National Park and Upper Waikato Stream faults

On the western boundary of the Tongariro Graben, the geomorphic displacement was estimated on a northern strand of the National Park Fault. Here, 20 ± 3 m of vertical displacement was measured on a ~ 25 ka surface [based on the presence of the 25.4 cal ka BP Ōruanui Ignimbrite; *Vandergoes et al.*, 2013], and 60 ± 7 m of displacement on a 60 ka debris fan surface [age from *Lecointre et al.*, 2004b], with a calculated slip-rate of 1.1 mm/yr over the last 60 ka. For the eastern boundary, existing data from the Upper Waikato Stream Fault were used, where 10 ± 2 m of vertical displacement was found on a 20 ka surface and 30 ± 4 m on a 60 ka surface, derived by extrapolating a 0.5 ± 0.06 mm/yr net slip-rate calculated over the last 45 ka [*Gómez-Vasconcelos et al.*, 2016].

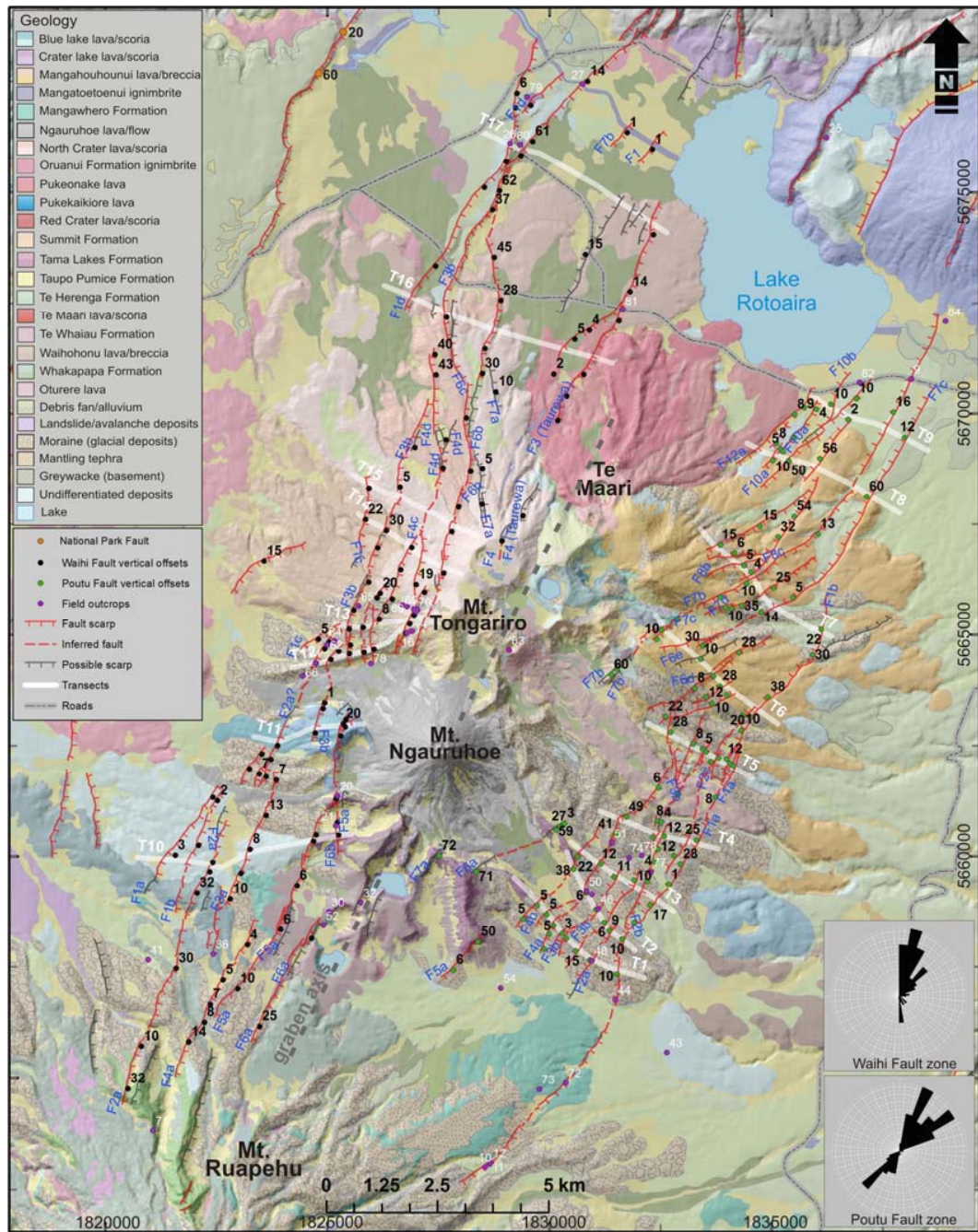


Figure 27. Geological map [Leonard et al., 2014] overlain with the faults of the Tongariro Graben; the Waihi and Poutu fault zones in the graben axis area and fault traces (red lines), inferred fault traces (dotted red lines), possible scarps (black lines) and 229 vertical fault displacements (2 northern National Park Fault, 117 Waihi Fault and 110 Poutu Fault; see displacement values in Tables S3 and S4) measured from geomorphic surfaces on transverse profiles across the faults (black and green dots, values in meters). Seventeen transects (T1-T17) are marked with white lines. Field points are marked with purple dots and white numbers (referred to as Tong # in the text and figures, Table S5).

5.6.1.2 The Waihi Fault zone

The Waihi Fault zone consists of 19 fault strands [Fig. 27; including the Taurewa Fault of *Lecointre et al.*, 2002]. All of these are NNE-oriented normal faults, with 1 antithetic fault (Taurewa). The fault zone width varies between ~1 and 5 km westward of the Tongariro Graben axis. The overall zone is at least 38 km long, between southwestern Lake Taupo and the northwestern slopes of Mt. Ruapehu. The fault zone geometry shows two main directions: the ~025°-trending and the ~000°-trending fault traces. The averaged trend of Waihi Fault zone is 023°. Some fault strands have tilting blocks [e.g., Waihi F3b to the northwest; *Miller and Williams-Jones*, 2016] and have very steep dips (>80°), while others show en-echelon geometry, fault splaying and non-parallel faulting.

Within the ~4 km wide Waihi Fault zone, 117 vertical fault displacements were analyzed by measuring geomorphic surfaces on profiles normal to the overall strike (Tables S3 and S6; Fig. 27) along with examining five fault outcrops (Figs. 27, 28 and S5, Table S7). These data indicate that movement occurred between 200 and 1.72 cal. ka on the fault zone. Displacements range from 1 to 73 m in measured fault scarps, with uncertainties ranging from 1.1 to 8.3 m.

Based on progressive displacement increments within individual strands, at least 17 events (fault surface ruptures) were identified in the last 200 ka, with outcrop data confirming events 15, 16 and 17 and adding at least two further events ca. 4.32 and 1.72 ka (Tables S6 and S7). This number of events is likely to be a minimum, because progressive displacements calculated range from 4 to 91 m, suggesting that several ruptures could have occurred to accumulate the larger values, and expected co-rupture displacement values of 2 m may be produced by earthquakes of up to M_w 7.0 [Table 7; using the Taupo Volcanic Zone fault scaling relationship; *Stirling et al.*, 2012].

Uncertainties for this data set also come from the variable preservation of surfaces and the general paucity of outcrops on the entire fault set. Furthermore, many fault outcrops

show evidence of faulting only for some time intervals, which may reflect that, 1) not all strands ruptured at once [as observed for other normal faults; e.g. Paeroa Fault, North Taupo Rift; *Berryman et al.*, 2008]; or 2) not all time intervals were exposed (or preserved) at each outcrop.

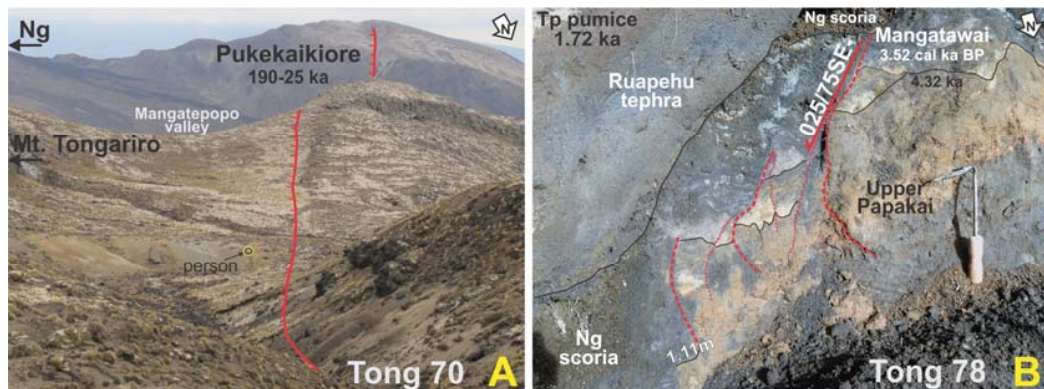


Figure 28. Field outcrops from the Waihi Fault. A, Tong 70: Normal fault (F5a) displacing the Pukekaikiore lava flows [190-25 ka; *Hobden et al.*, 1996; *Leonard et al.*, 2014], the Mt. Tongariro lava flows and the Mangatepopo moraine in Mt. Tongariro. B, Tong 78: F4b exposure displacing the Mangatawai tephras [3.52 cal ka BP; *Moebis et al.*, 2011] and the Papakai Formation [11.1-3.7 cal ka BP; *Donoghue et al.*, 1995; Figs. 27 and S5; Tables S5 and S7].

5.6.1.3 The Poutu Fault zone

The Poutu Fault zone consists of at least 23 sub-parallel NNE-oriented normal fault strands; 11 of them dip to the SE, while the others dip to the NW forming a graben-like structure on the eastern flank of Mt. Tongariro. The zone is ~2 km wide to the east of Mt. Ngāuruhoe and Red Crater vents, and ~6 km wide east of the Tongariro Graben axis (Fig. 27). The fault zone is at least 30 km long, extending from Turangi to the northeast slopes of Mt. Ruapehu. It displays two main faulting directions: 025°-trending and ~060°-trending fault traces. The overall average trend of the fault zone is 040°. Some faults dip at >70° in outcrops; in map view, others show en-echelon geometry, horsetail fault splaying, with soft-linked fault arrays, especially to the north, near Lake Rotoaira (Fig. 27).

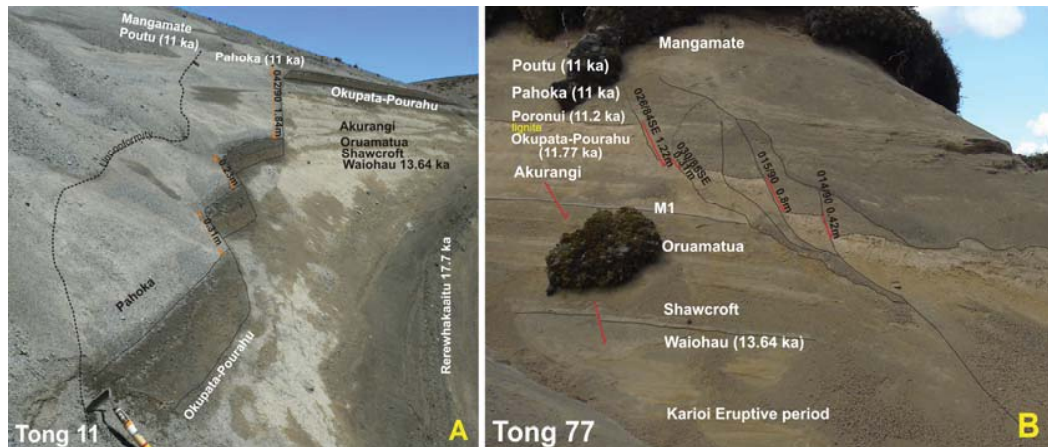


Figure 29. Field outcrops from the Poutu Fault. A, Tong 11: three-step normal fault displacing the Pahoka and Okupata-Pourahu tephras. B, Tong 77: Multiple-step normal fault (F2b) displacing the Okupata-Pourahu tephras (11.77±0.19 cal ka BP; see stratigraphy in Table S10 and locations in Figure 27, and Tables S5 and S9).

Within the ~4 km-wide Poutu Fault zone, 110 fault displacements were measured on dated geomorphic surfaces along transverse profiles (Fig. 27, Tables S4 and S8) and five fault outcrops were studied (Figs. 27, 29, S6 and S7; Table S9). These collectively indicate movement between 200 and <3 cal. ka (Tables S8 and S9). Displacements range from 2 to 72 m in calculated fault scarps, with uncertainties ranging from 1.2 to 8.2 m. Reconstructing progressive displacement of individual fault strands, the geomorphic analysis indicates at least 13 events in this interval, with outcrop data confirming four of these earthquakes (9, 10, 11 and 12), as well as adding two others at 11 and 3.52 cal. ka. Fifteen surface-rupture events in the last 200 ka is likely to be an underestimate, because of the large progressive displacements obtained (1-92 m; Table 7).

5.6.2 Fault slip-rates in the Tongariro Graben

The fault history and slip-rates were evaluated for the last 100 ka in the Tongariro Graben, age of the Mangahouhounui (Oturere) lava flows [Hobden *et al.*, 1996], east of

Red Crater. The spacing between single fault strands within each fault zone is <1 km, and thus they probably merge into a single fault plane at depth, as suggested by Villamor and Berryman [2001] and Nicol et al. [2010] in the central Taupo Volcanic Zone (Fig. 27). If the surface fault strands represent the whole fault, the summation of displacements on all strands will characterize the total deformation of the fault. Eight transects across the Waihi Fault zone and nine across the Poutu Fault zone (Fig. 27) were used to estimate the total deformation accommodated since 100 ka, using the field results integrated with geospatial analysis. For the Waihi Fault this amounted to an average of 28 ± 3.6 m of vertical slip since 20 ka and 173 ± 10.9 m since 60 ka, and for the Poutu Fault, an average of 65 ± 9.3 m since 20 ka and 178 ± 14 m since 60 ka (Table 7). This total displacement provides the basis for slip-rate calculations, leading to mean slip-rates of 2.6 ± 0.8 mm/yr and 2.2 ± 1.9 mm/yr, for the Waihi and Poutu faults, respectively (Table 7). Using available age constraints, rates of 3 ± 0.6 mm/yr on the Waihi Fault occurred between 85 and 40 ka, and 4 ± 0.7 mm/yr thereafter to the present day. For the Poutu Fault the slip-rate was 2.3 ± 0.3 mm/yr from <100 to 40 ka, and 2.2 ± 0.9 mm/yr thereafter to the present day.

Antithetic faults were not included in the above calculations, because the total offsets were not consistent along the Poutu Fault when antithetic fault displacements were subtracted. It is possible that changes in fault dip with depth create space problems during fault movement, requiring internal deformation of fault blocks that is manifest as different slip at surface. This process may exaggerate the tectonic vertical slip, therefore, the total displacement and derived slip-rates are maximum estimates based on the currently observed data (Table 7).

TABLE 7. VERTICAL DISPLACEMENTS AND SLIP-RATES FOR THE TONGARIRO GRABEN, FROM WAIHI AND POUTU FAULTS TRANSECTS AND RIFT-BOUNDING FAULTS

Transect number (age)	Vertical displacement ± error (fault number, age when different from transect age) (m)		Total offset* (synthetic-antithetic) (m)	Total offset* (synthetic+antithetic) (m)	Total offset (only synthetic) (m)	Vertical slip-rate (only synthetic) (mm/yr)	PD* (only synthetic) (m)	Rift- Bounding faults Total offset (m)	West/East Tongariro Graben slip-rate (mm/yr)
	Vertical displacement ± error (m)	Vertical displacement ± error (m)							
Waihi Fault									
T 15 (12 ka)	3±1.3 (1c)	5±1.5 (3b)	11±2.1 (6b)	-	24±3.5	24±0.4	0	-	-
T 10 (20 ka)	3±1.3 (1a)	4±1.4 (1b)	5±1.5 (2a)	8±1.8 (3a)	28±3.6	1.39±0.2	4±5	20±3 [§]	2.4±0.2
T 12 (22 ka)	3±1.3 (2a)	5±1.5 (3b)	15±2.5 (3b)	12±2.2 (4b)	69±5.6	3.12±0.25	37±6.6 ^{Av}	-	-
T 11 (25 ka)	10±2 (2a)	16±2.6 (3b)	20±3 (5a)	15±2.5 (5a)	61±5.1	2.44±0.32	0 ^{Av}	-	-
T 16 (40 ka)	16±2.6 (1d)	45±5.5 (3b)	28±3.8 (6b)	33±4.3 (6c)	160±9.4	4±0.32	91±11 [#]	-	-
T 13 (52.6 ka)	37±4.7 (3b)	5±1.5 (4b)	8±1.8 (4c)	40±5 (5a, 40 ka)	102±8.1	1.95±0.2	37±9.8	-	-
T 14 (59 ka)	22±3.2 (1c)	30±4 (3b)	16±2.6 (4c, 25 ka)	19±2.9 (5b, 25 ka)	173±10.9	3.18±0.3	71±13.6	60±7 [§]	3.9±0.3
T 17 (85 ka)	73±8.3 (1d)	61±7.1 (3b)	15±2.5 (1Tw ^{**} , 25 ka)	14±2.4 (3, 25 ka)	155±11.5	2.47±0.47	33±16.8 [#]	-	-
Mean slip-rate					206±12.8	2.6±0.8			3.2±0.4
Poutu Fault									
T 5 (15 ka) [#]	25±3.5 (1a)	25±3.5 (1b)	12±2.2 (1b)	10±2 (2c ^{**})	48±3.4	5.3±1.8	0 [#]	-	-
T 9 (17.7 ka)	12±2.2 (7c)	16±2.6 (7b)	2±1.2 (9a)	10±2 (10a ^{**})	14±2.6	2.3±0.24	40±4.1	-	-
T 1 (20 ka)	10±2 (1a)	12±2.2 (2a)	15±2.5 (3a)	3±1.3 (3b ^{**})	16±0.9	1.9±0.27	0 [#]	-	-
T 2 (20 ka)	10±2 (1a)	9±1.9 (2a)	6±1.6 (3a)	13±2.3 (3b)	26±2.8	38±3.9	0 [#]	10±2 ^{††}	3.8±0.3
T 3 (20 ka)	17±2.7 (1a)	16±2.6 (2b ^{**})	10±2 (3a)	11±2.1 (3b)	4±1	38±4	0 [#]	-	-
T 7 (20 ka)	22±3.2 (1b, 36.1 ka)	14±2.4 (7c)	10±2 (7d ^{**})	35±4.5 (7b ^{**} , 60 ka)	4±<0	78±5.7	41±4.2	-	-
T 4 (60 ka)	25±3.5 (1a)	27±3.7 (2c)	12±2.2 (2b ^{**})	30±4 (3b)	40±4.6	1.4±0.16	48±7.7 ^{Av}	30±4 ^{††}	3.5±0.2
T 6 (60 ka)	38±4.8 (1b)	29±3.9 (6b)	28±3.8 (6c)	60±7 (6d ^{**})	-42±<0	95±7.3	1.6±0.18	-	-
T 8 (100 ka)	60±7 (7c)	13±2.3 (7b, 17.7 ka)	56±6 (9a)	50±6 (10a ^{**})	71±8.5	1.8±0.22	92±14.2	-	-
Mean slip-rate					291±15	2.2±1.9			3.7±0.4

Note: PD, Progressive displacement from total offset (only nearby transects were used); Tw, Taurewa Fault.

* Displacement values were converted to transect ages when the existing values were of a different age.

† Vertical slip-rate values used for calculating the extension rates in Table 2.

§ National Park Fault.

Av, Averaged progressive displacement with nearby surface offset age

Not used, anomalous data, possibly due to age uncertainties in the offset surfaces.

** Antithetic fault strands.

†† Upper Waikato Stream Fault (Gómez-Vasconcelos et al., 2016).

5.6.3 Dike intrusion rates in the Tongariro Graben

To evaluate the contribution of magmatism to extension, the rates of magmatism in this region were examined and converted into dike intrusion rates. The mean long-term magma extrusion rate in this region since initiation of volcanism (~300 ka) is ~0.8 km³/k.y. (220 km³ derived from a total 350 km³ volcanic volume, minus the volume of overlapping portions of the adjacent Mt. Ruapehu (50 km³) and Tertiary sediment below the volcanics (80 km³) [Miller and Williams-Jones, 2016]. This value is comparable with 1 km³/k.y. estimated by Cronin et al. [1996b] from a 60 ka explosive eruption record of Tongariro Volcanic Centre tephras. An average volume for large pyroclastic eruptions in the Tongariro Volcanic Centre is around 0.2 km³ [Topping, 1973; Hobden et al., 1999; Moebis et al., 2011; Pardo et al., 2012], leading to a rate of ~4 large eruptions per thousand years. Thus even with additional volume from smaller more-frequent eruptions, the bulk volume eruptive rate is dominated by effusive lava-flow eruptions that form the present and paleo-edifice [the latter removed by debris avalanches or remobilized by lahars and fluvial reworking; Cronin et al., 1996b; Lecointre et al., 2002].

In other continental rifts, White et al. [2006] estimated a common ratio of intrusive to extrusive magma volume at 5 to 1. If this is applied to the Tongariro Volcanic Complex, the above ~0.8 km³/ka eruption rate would thus equate to 4 km³/ka of arrested intrusions, and 4 eruptions to 20 arrested intrusions per thousand years.

Historic and prehistoric eruptions have shown distances between co-eruptive vents of no more than 2 km [e.g., Nairn et al., 1998], which can be used to define a conservative estimate of the dike intrusion length. The Tongariro Volcanic Complex extends over 30 km from roughly north to south and thus up to 15 dikes, each 2-km-long would constitute a theoretical feeding system of the whole complex. Not all of these will be open at once, and for example even if up to four large eruptions and 20

arrested dikes occurred every thousand years, then at a single dike location, 0.3 eruptions and 1.3 arrested dikes would occur per ka.

5.7 Discussion

5.7.1 Is surface faulting associated with tectonic or dike intrusion processes in the Tongariro Graben?

The combination of magmatic and tectonic processes in continental rifts produces a variety of extension modes that can be defined as follows: pure tectonic, pure magmatic, hybrid or a combination of some of the three modes (Fig. 30). Pure tectonic extension is achieved by normal faulting and it is manifested at the surface as geomorphic fault scarps (Fig. 30A). Faults here rupture the entire or most of the seismogenic crust, producing large earthquakes.

Magmatic extension is achieved by dike intrusions, eruptive fissures and extension fractures, i.e. fracturing at the tip of the dike and infill of the space with magma. In this case three extensional modes are possible: dike intrusion through the whole crust with associated volcanic eruption and no surface faulting (Fig. 30B), dike intrusion through the whole crust with associated volcanic eruption and surface faulting (Fig. 30C), and arrested dike intrusion, i.e. when the dike stops short of the ground surface and with surface faulting above the dike (Fig. 30D). In the two later cases faults have a very narrow fault width (hundreds of meters to a few kilometers) that are controlled by the depth of the dike. Rupture of such small areas will produce small earthquakes.

In the first magmatic case above the dike reaches the surface and no surface faulting occurs on the sides of the dike and the surface expression of extension is usually a series of aligned volcanic cones, fissures or vents in a trend perpendicular to the extension direction [Nakamura, 1977]. Structural analysis of paleo-rift zones suggest

that where dikes are common faults are rare, and vice versa (Gudmundsson, 1995). That implies that normal faulting does not occur in the near proximity to a dike. Faulting can occur above the dike (see case below) but not along its sides. This later is also supported by the static stress changes on fault planes (parallel and adjacent to the dike). The changes on fault planes will be negative (fault movement is inhibited) due to dike opening (Fig. 31I and 31J). Historic examples such as the 2007 Mt. Ruapehu eruption (Mordret et al., 2010) and the 2012 Te Maari eruption (Jolly et al., 2014) show this extension mode.

If dikes are arrested close to the surface (third magmatic case above; Fig. 30D), the crustal volume above the tip of the dike may be deformed, usually through normal faulting in the form of a nucleated graben and extensional fissures [Rubin, 1992]. An example of faulting related to dike intrusions occurred during the Krafla fissure swarm in the Northern Volcanic Zone of Iceland [Paquet et al., 2007], where arrested dike intrusions caused deformation of the brittle crust, forming normal faults and tensile fissures at the surface. The width of the produced graben is controlled by the depth of the intruding dike and is usually narrow (e.g., <1 km for dikes intruding to 1 km depth; Rubin, 1992).

In areas where magmatism is the dominant driver of the extension, such as Iceland and Ethiopia divergent margins, faults can be associated to linear volcanic vents (Fig. 6C). Usually the faults form a few hundred meters away from the extrusion point (Tripanera et al., 2015). Often these cases involve a horizontally propagating dike. Faulting is usually formed when the dike is propagating horizontally but is still arrested (Fig. 6D). Then extrusion occurs as the magma is abundant and close to the surface.

When dikes are arrested deeply in the crust, they can trigger tectonic faulting at the tip of the dike as it propagates (Fig. 30E). This extension mode is called here “hybrid extension”, because it combines both magmatic and tectonic extension. Deformation of

the crust above the dike from dislocation models of deep arrested dikes shows that deformation may not reach the surface, or that displacements may be too small to be detected (Fig. 31D). However, Coulomb stress on tectonic normal faults with trends and dips similar to those of Waihi and Poutu faults above the dike increases during dike intrusion, and may bring those faults to failure (Fig. 31I and 31J). As this faulting type is tectonic it ruptures most of the seismogenic crust above the deeply arrested dike. The surface expression of the hybrid extension is through geomorphic fault scarps, equal to those of tectonic faulting (unrelated to magmatism). While there is to date no reported examples of hybrid extension worldwide, this mode is similar to some of the cases where nearby faulting was triggered by dike intrusion (e.g., the 1999 eruption in Cerro Negro volcano, related to three M_w 5.2 earthquakes; LaFemima et al., 2004). The peculiarity here is that the fault is above the dike. A combination of some or all of the extension modes defined above is also possible (Fig. 30F).

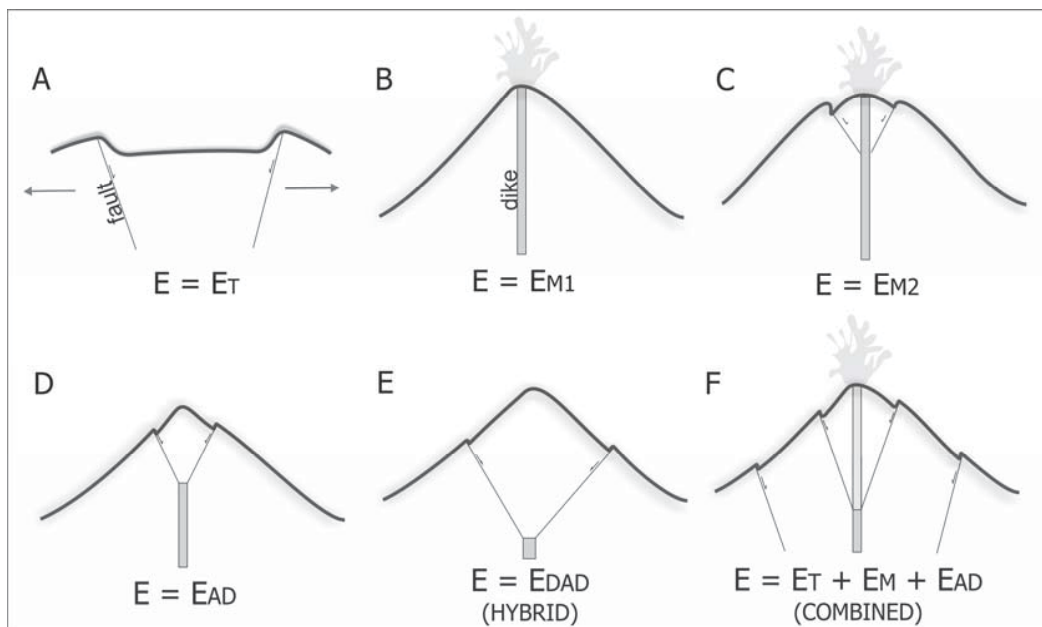


Figure 30. Simplified schematic diagrams showing the variety of extension modes in continental rifts. A, Pure tectonic extension by normal faulting (unrelated to volcanism). B, Pure volcanic extension by dike intrusion and eruption (dike reaches the surface). C, Extension through both normal faulting and dike intrusion-eruption. D, Pure volcanic extension by shallow arrested dike-intrusion with associated surficial normal faults (large ground surface displacements are common). E, Hybrid extension through deep dike-

intrusion and triggered normal faults (large surface displacements are related to tectonic faulting; if faulting is only related to dike-intrusion ground surface displacements are too small to be observed). F, Extension is a combination of tectonic faulting, dike intrusion-eruptions and arrested dike-intrusion. E, Extension; ET, Tectonic Extension; EV, Volcanic Extension; EAD, Arrested dike extension.

Faulting in the central and northern Taupo Rift, where faults and volcanic complexes alternate along the rift, has been described as essentially tectonic [Seebeck and Nicol, 2009; Villamor *et al.*, 2011], but occasionally close to the volcanic vents (<5 km; e.g., Okataina Volcanic Centre), normal faults, or shallow tensile fissures may relate to dike intrusions, or magma chamber inflation/deflation [Villamor *et al.*, 2011; Holden *et al.*, 2015].

In the Tongariro Graben, the morphology suggests a strong interconnection between faults and magma intrusions, because faults spatially coincide with many eruptive vents [Cassidy *et al.*, 2009]. This suggests that surface fault displacements could be associated with shallow arrested dikes [Rowland *et al.*, 2010]. However, Miller and Williams-Jones [2016] hypothesize, alternatively that faults in the Tongariro Graben are of tectonic origin. The later gravity and magnetic studies show that faults are distinct from volcanic vents and that the Waihi and Poutu faults extend into the deep crust and displace the Jurassic basement rocks at depths >2 km, typical of tectonic faults. Therefore, these interactions and the mode of faulting must be re-examined for this area.

It is possible that the Tongariro Graben extension combines several of the extension modes described above (Fig. 30F). Fault traces are absent in the central axis of the Tongariro Volcanic Complex, which may suggest a zone where extension is accommodated by dike intrusion (historic volcanic activity), with no faulting (magmatic case one; Fig. 30B), while outside this area extension is mainly accommodated by normal faulting. The lack of faulting and fissuring along the axis of the graben (5 km

wide axis) suggests that faulting related to shallow dike intrusion (Fig. 30D) or eruption with associated faulting (Fig. 30C) does not occur here.

The rift-bounding faults (National Park and Upper Waikato Stream faults) appear to be driven by pure tectonic extension (Fig. 30A), being >12 km from any volcanic vent. Conversely, Waihi and Poutu faults are more complex in terms of their geometry, and closer to the Mt. Tongariro edifice (<6 km), implying a possible relationship with dike intrusions.

Using the new paleoseismic data, dislocation models were applied to assess whether the Waihi and Poutu faults are of tectonic or magmatic origin. The dislocation models (Fig. 31) indicate the amount of surface deformation caused by dike intrusions. If a dike parallel to the fault reaches the surface it will inhibit deformation of the Waihi and Poutu faults (Fig. 31A and 31E), thus all the offsets seen are either created by arrested dike intrusions, or by pure tectonic faulting.

In the Tongariro Graben, the faults dip >70° at the surface [Rowland and Sibson, 2001], and compilations for the Taupo Rift [Villamor and Berryman, 2001; Lamarche et al., 2006] suggest they dip 60° at depth. Single-event displacements from this study range between 0.4 and 2.4 m. A single dike intrusion in the Tongariro Graben is likely to have widths of 1 to 2 m, based on a summation of field observations in the Tongariro Volcanic Centre and the Taupo Volcanic Zone; e.g., Red Crater dike, Mead's Wall dike, SW Oturere dike and Tarawera dike (Cole and Hunt, 1968; Hobden, 1997). That is our preferred dike width for dislocation modelling. Modeling 1-m-wide dikes intruding to depths of 15 to 10 km does not produce any surface displacement (Fig. 31D). Therefore, surface faulting of Waihi and Poutu faults could either be associated with near-surface arrested dikes (<5 km), or with tectonic faulting (either hybrid or pure tectonic, as described above).

Paleoseismic data may shed further light on arrested-dike vs. tectonic faulting origins. Paleoseismic data show ~28 m of vertical surface offset of Waihi Fault since 20 ka (Table 7). To achieve this amount of deformation from arrested-dike extension, dikes >20 m wide are needed (Fig. 31F to 31H). Models of repeated dike intrusions summing to 20 m wide, at different arresting depths (Fig. 31E to 31H), produce large displacements only when arrest is close to the surface (e.g. Fig. 31F). In this case fault dips are very low (30°); if these faults were extended to the surface the dip value is much lower than those characteristic of this region. Also, normal faults above dikes under Andersonian behavior [Anderson, 1905] would be steeper than 30° and rupture closer to the graben axis than the Poutu and Waihi fault systems. Even in this case, only 6 m of net displacement would result with a 20 m-wide opening at 2 km depth (Fig. 31F), compared to the 28 m vertical displacement observed. Also, there is no evidence of faulting or opening fissures in the 5 km axial zone, therefore there are no grabens associated to shallowly arrested dikes.

Dislocation models presented here are bidimensional, and thus faulting associated to lateral dike intrusion was not considered. However, the lack of faulting within the axial rift suggests that laterally propagating arrested dikes may also be relatively deep (> 5 km) in this area of the rift.

Based on these initial evaluations, long-term surface displacement presented by Waihi and Poutu faults cannot be explained uniquely by shallow arrested dike intrusion and are considered here to be associated with pure tectonic faulting. Tectonic faulting can occur just when stress in the crust leads to normal faulting, without being associated with magmatism. Additionally, dikes intruding at 15 to 10 km depth could also generate positive Coulomb stress changes above them and trigger tectonic faulting on Waihi and Poutu faults (hybrid extension; Figs. 30D, 31I and 31J). Both extension modes result in tectonic faulting (pure and hybrid) and cannot be discriminated with the data used in this study. However, for the purpose of understanding the seismic hazard of the region,

they will be both treated jointly as they both contribute to producing moderate to large earthquakes.

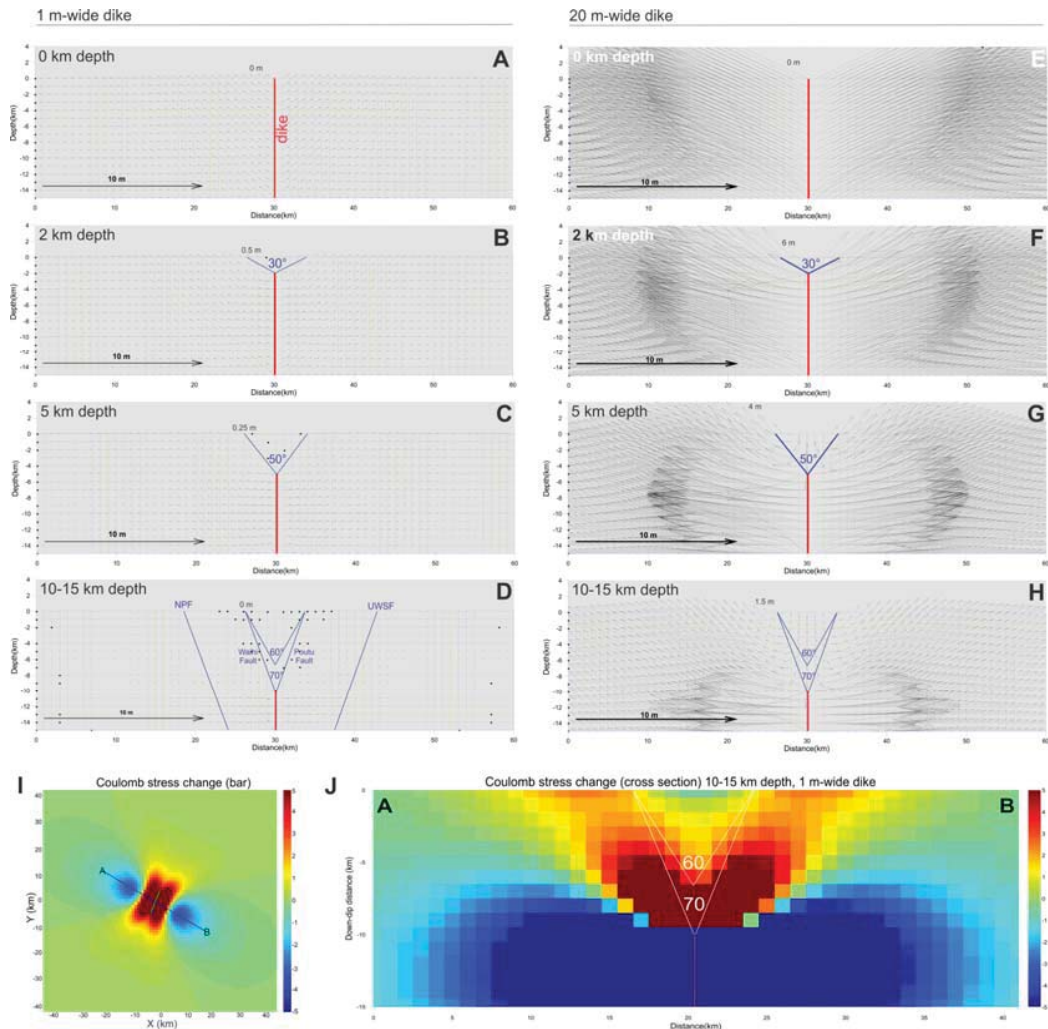


Figure 31. Static displacement caused by an intruding dike projected onto cross sections. A, 1 m-wide dike intruding to the surface and causing no surface deformation; B, 1 m-wide intruding dike at 2 km depth intersecting with 30° dip faults, showing a maximum of 0.5 m of surface deformation. C, 1 m-wide intruding dike at 5 km depth intersecting with 50° dip faults, showing a maximum of 0.25 m of surface displacements. D, 1 m-wide intruding dike at 10-15 km depth intersecting with 60-70° dip faults representing the most likely scenario for the Waihi and Poutu faults, showing no surface deformation. NPF, National Park Fault; UWSF, Upper Waikato Stream Fault. E, 20 m-wide dike representing total width of repeated dike intrusions in 20 ka; here the dike is intruding to the surface and causing no surface deformation. F, 20 m-wide intruding dike at 2 km depth intersecting with 30° dip faults, showing a maximum of 6 m of surface deformation. G, 20 m-wide intruding dike at 5 km depth intersecting with 50° dip faults, showing a maximum of 4 m of surface displacement. H, 20 m-wide intruding dike at 10-15 km depth intersecting with 60-70° dip faults representing the most likely scenario for the Waihi and Poutu faults, showing 1.5 m of surface deformation. I and J, 1 m-wide dike intruding at 10-15 km depth showing normal stress changes ($\Delta\sigma_n$; bar, unclamping positive) projected onto cross section (A-B) showing positive stress change (red color) on top of the intruding dike, where the Waihi and Poutu faults are.

5.7.2 Proportion of extension accommodated by faulting vs. dike intrusion

Fault scarps in the Tongariro Graben are formed by tectonic faulting, as described above, and thus the displacement values can be used to assess the total tectonic extension, following an approach outlined by Villamor and Berryman [Villamor and Berryman, 2001; Villamor and Berryman, 2006b] and Lamarche et al. [2006]. The total vertical displacements of the faults were used to estimate vertical slip-rates and converted to dip-slip rates at surface and at seismogenic depths (Table 8). The extension rates calculated include only moderate to large earthquakes ($M > 5.8$). Small earthquake ruptures do not reach the surface (small-scale faulting), so extension at seismogenic depth was corrected. Table 8 presents the total estimated crustal extension across the whole Tongariro Graben from surface faulting data. This value is calculated from the addition of the extensional component of the slip-rate of all faults in the graben. The total extension rate at seismogenic depth is 7 ± 1.2 mm/yr since 20 ka and 8.4 ± 1.1 mm/yr since 60 ka (Table 8).

TABLE 8. SURFACE AND SEISMOGENIC DEPTH EXTENSION RATES AT 20 AND 60 ka FOR THE TONGARIRO GRABEN

	Age 20 ka	Age 60 ka
(a) Vertical slip-rate at surface (70°)	6.2 ± 0.6	7.4 ± 0.4
(b) Dip-slip rate (DSR) at surface ($a/\sin 70$)	6.6 ± 0.4	7.9 ± 0.3
(c) Extension rate at surface ($b \cdot \cos 70$)	2.3 ± 0.4	2.7 ± 0.3
(c) DSR at seismogenic depth corrected for large Eqs ($b \cdot 1.6$)	10.6 ± 0.9	12.6 ± 0.8
(d) DRS at seismogenic depth corrected for small Eqs ($c \cdot 1.33$)	14 ± 0.9	16.8 ± 0.8
(e) Extension rate at seismogenic depth (corrected) ($d \cdot \cos 60$)	7 ± 1.2	8.4 ± 1.1

Note: Displacement values were all summed for the extension rate estimation, including antithetic faults and outer boundary faults.
Note that this extension rate at seismogenic depth (corrected) considers that all the faults are tectonic.
A best estimate dip of 70° in the surface and 60° at seismogenic depth was used.
All values are in mm/yr.
Eqs, Earthquakes; DSR, dip-slip rate.

These extension rates based on surface geology compare well to the extension rate estimate of 7.4 mm/yr in the Tongariro Volcanic Centre derived independently from geodynamic modeling of the North Island of New Zealand [Wallace et al., 2004]. This

latter estimate is calculated by inverting global positioning system velocities, earthquake slip-vectors and geological fault slip-rates of tectonic blocks driving the Taupo Rift.

Paleoseismic estimates from this study of extension since 20 ka are more directly comparable to recent geodetic measurements (Table 8). These are only 0.4 mm/yr less than geodetic values. This result also strongly suggests that tectonic faulting is accommodating essentially most part of the extension in this region, and the difference between geodetic and geologic rates can be used to assess amount of extension associated with magmatism (~5%).

Another way to assess the percentage of magmatic extension is to use the rates of magmatism and dike intrusion derived above. An average dike intrusion extension, normalized along the graben axis (that is for a single location along the graben), could be ~1.6 mm/yr (22%), assuming intrusion of 1-m-wide dikes and 0.3 eruptions and 1.3 intrusions per thousand year. Therefore ~0.3 mm/yr (4%) of extension is from volcanic eruptions and ~1.3 mm/yr (18%) from arrested dikes (maximum value). Thus the remaining ~5.8 mm/yr (78%) must be accommodated by tectonic faults.

Both methods to assess magmatic extension converge on the same conclusion, that in the Tongariro Graben, 78-95% of the total extension is tectonic and 5-22% is magmatic, from which 4-5% is associated with volcanic eruptions and 18-19% with arrested dikes.

By comparison, at the Snake River Plain volcanic rift in the Basin and Range Province (Idaho, USA), dike intrusions accommodate 5-11% (0.16 to 0.33 mm/yr) of the total extension of 3 mm/yr [Payne *et al.*, 2012]. With over double the extension rate of the Snake River Plain, the Tongariro Graben shows a globally intermediate rate of extension, and also low-to intermediate in the context of the overall Taupo Volcanic Zone continental rift. A similar intermediate rate of extension occurs in the 15 km-wide

south-western part of the Western Volcanic Zone in southern Iceland, with 7.0 mm/yr of extension [LaFemina et al., 2005]. In this case, almost the entire extension is achieved by arrested dike intrusions [Gudmundsson, 2003]. Higher rates of extension than the Tongariro/Snake River Plain scenarios are associated with much higher accommodation of extension by magmatism. For example, at Fieale volcano in the Asal Rift, spreading rates are 17 to 29 mm/yr and dike and fissures accommodate ~90% of the extension [De Chabaliere and Avouac, 1994].

5.8 Conclusions

Waihi and Poutu fault zones create a narrow graben at the axis of the broader Tongariro Graben, bounding the location of vents in the Tongariro Volcanic Complex, hinting at a possible interrelationship between them. This analysis, however, demonstrates that these normal faults are of tectonic (pure tectonic and hybrid) origin and are not driven by magmatic intrusion, despite the geomorphic resemblance of this area to other volcanic rifts where dike intrusion drives the faulting (e.g., Krafla, Asal Rift).

Surface deformation of the Tongariro Graben since 20 ka is resolved on faults with a mean vertical slip-rate of 6.2 ± 0.6 mm/yr and a calculated geological extension rate of 7 ± 1.2 mm/yr based on 70° dipping faults. The extension seen in geodetic measurements (7.4 mm/yr) is thus almost entirely taken up by normal faulting over geological timescales. The normal faults accommodate 78-95% (5.8-7.0 mm/yr) of the total extension and dike intrusions accommodate the remaining 5-22% (0.4-1.6 mm/yr), of which 4-5% may be associated with volcanic eruptions and 18-19% with arrested dike intrusions. An unknown percentage of the tectonic and arrested-dike extension could be of hybrid extension. Therefore, the Tongariro Graben is essentially a tectonic feature where magmatic intrusion plays a secondary role.

Earlier studies on the Waihi and Poutu fault zones [*Lecoinre et al.*, 1998] estimated mean dip-slip-rates of 0.9 and 0.14 mm/yr, respectively. The data presented here show that the mean slip-rate values could be far higher: mean slip-rates could be as much as 2.6 ± 0.8 mm/yr for the Waihi Fault and 2.2 ± 1.9 mm/yr for the Poutu Fault. These new data increase the potential seismic hazard of the region; consequently, the National Seismic Hazard Model for New Zealand [*Stirling et al.*, 2012; *Litchfield et al.*, 2013] should be updated. This also serves as an example for other intermediate to low-rate volcanic rifting areas in the world, where careful attention should be paid to confirm the origin of the faulting whether tectonic or magmatic, as this may affect seismic (and volcanic) hazard evaluations.

CHAPTER 6. Seismic Hazard Assessment in the Tongariro Graben.

6.1 Abstract

6.2 Introduction

6.3 Methods

6.4 Results

6.4.1 Fault geometry

6.4.2 Fault slip-rates

6.5 Discussion

6.5.1 Fault segmentation

6.5.2 Magnitude and recurrence interval of potential earthquakes

6.5.3 Updating fault characterization for seismic hazard assessment in the Tongariro area

6.6 Conclusions

Part of this chapter was published as a conference extended-abstract (PATA days, 2016).

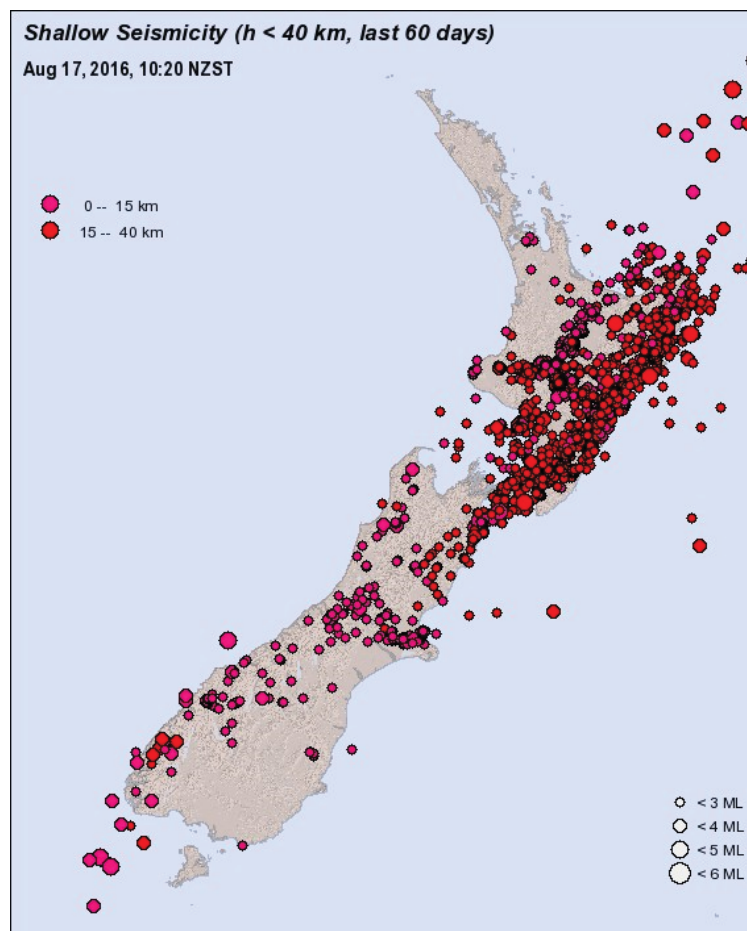


Figure 32. Shallow seismicity in New Zealand (GeoNet, <http://info.geonet.org.nz/display/quake/Earthquake>).



INQUA Focus Group on Paleoseismology and Active Tectonics



paleoseismicity.org

Seismic hazard analysis and active fault slip-rates in the Tongariro Graben, southern Taupo Volcanic Zone, New Zealand.

Martha Gabriela, Gómez-Vasconcelos (1), Pilar, Villamor (2), Jon, Procter (1), Alan, Palmer (1), Shane, Cronin (1,3), Clel, Wallace (1), Dougal, Townsend (2), Graham, Leonard (2).

- (1) Volcanic Risk Solutions, Institute of Agriculture and Environment, Soil and Earth Sciences, Massey University, Private Bag 11 222, Palmerston North 4442, New Zealand. Email: ga8ygomez@yahoo.com
- (2) GNS Science, PO Box 30-368, Lower Hutt, New Zealand.
- (3) School of Environment, The University of Auckland, Private Bag 92019, Auckland 1142, New Zealand.

6.1 Abstract

The Tongariro Graben, southern Taupo Rift, is formed by four regional and parallel NNE-oriented active normal fault sets: the National Park, Waihi, Poutu and Upper Waikato Stream faults. This study presents estimates of displacement and slip-rates associated with the faults in the Tongariro Graben since <100 ka. The time-variant movement associated with these two faults is estimated by measuring vertically displaced geomorphic surfaces over 227 fault traces and field exposures. Fault slip-rates are calculated by summing all displacements across the parallel fault strands that belong to a single fault at depth (the number of parallel surface strands ranges from 3 to 9 across the faults). The summed displacement pattern along each of the faults suggests that they could rupture as a whole. However, the lack of paleoseismic data (trenches) along the faults and the complexity of the fault geometry suggest that the faults could also rupture in shorter segments. The whole Waihi Fault is at least 38 km long, has a slip-rate of 2.6 ± 0.8 mm/yr and is capable of producing a M_w 7.0 earthquake with a recurrence interval of 1 ka. Waihi Fault could be up to 52 km if it extends to the SW boundary of Lake Taupo (M_w 7.2). The Waihi Fault can be divided in two segments: the northern segment is 20 km long (M_w 6.6); and the southern segment is 18 km long (M_w 6.7). The whole Poutu Fault is at least 30 km in length, has a slip-rate

of 2.2 ± 1.9 mm/yr and is capable of producing a M_w 6.9 earthquake with a recurrence interval of 0.9 ka. The Poutu Fault can be divided in two segments: the northern segment is 18 km long (M_w 6.3) and the southern segment is 15 km long (M_w 6.3). Earlier studies on the Waihi and Poutu faults estimated mean slip-rates of 1.1 to 1.85 mm/yr, and M_w of 6.5 to 6.6, respectively. This study yields more rapid slip-rates and greater earthquake magnitudes, increasing the seismic hazard, which can be used to update the National Seismic Hazard Model for New Zealand.

6.2 Introduction

The Taupo Volcanic Zone (TVZ) is the NNE-trending Quaternary volcanic arc associated with the Hikurangi Trench, where the Pacific Plate subducts below the Australian Plate in the North Island of New Zealand. Extension within the arc is caused by the current fore arc clockwise rotation [Wallace *et al.*, 2004] as well as active slab rollback [Seebeck *et al.*, 2014]. Faults within the volcanic arc define the intra-arc Taupo Rift [Acocella *et al.*, 2003; Fig. 33].

The Tongariro Volcanic Complex is a NNE-aligned andesite volcano complex, with vents aligned along the same strike as the Tongariro Graben axis [Topping, 1973; Rowland and Sibson, 2001; Villamor and Berryman, 2006b]. Four NNE-striking parallel faults make up the Tongariro Graben: two rift-bounding faults: the National Park Fault and the Upper Waikato Stream Fault, and two intra-rift faults: the Waihi and the Poutu faults [Chapter 5; Van Dissen *et al.*, 2003; Lecointre *et al.*, 2004b; Villamor and Berryman, 2006b; Cassidy *et al.*, 2009]. The National Park Fault is an active NNE-oriented normal fault that bounds the western Tongariro Graben and is downthrown to the SE. Ruptures along this fault have been characterised as producing M_w 6.1 earthquakes every 0.4 ka [Stirling *et al.*, 2012]. The Upper Waikato Stream Fault is an active NE-striking normal fault that bounds the eastern Tongariro Graben and is

downthrown to the NW, with a minimum slip-rate of 0.5 mm/yr over the last 45 ka [Chapter 4; *Gómez-Vasconcelos et al.*, 2016]. This fault can produce M_w 6.5 earthquakes every >1.6 ka if it ruptures by itself, and M_w 7.1 if it ruptures together with Rangipo and Kaimanawa faults [*Gómez-Vasconcelos et al.*, 2016].

The Waihi Fault zone is an active NNE-oriented normal fault set on the western flanks of the Tongariro Volcanic Complex, downthrown to the SE [*Grindley et al.*, 1961; *Van Dissen et al.*, 2003]. The Waihi Fault zone has been associated with historical earthquakes and landslides in the north-western TgVC [*Hochstein*, 1995]. The Hipaua Steaming Cliffs near Little Waihi village have suffered devastating landslides in 1846 and 1910, each after M_w 6.3 earthquakes on the Waihi Fault [*Hegan et al.*, 2001; *Cooper*, 2002]. *Stirling et al.* [2012] associate ruptures along this fault with M_w 6.5 earthquakes every 1 ka.

The Poutu Fault zone is an active NNE-oriented normal fault set on the eastern flanks of the Tongariro Volcanic Complex [*Villamor and Berryman*, 2006b], downthrown both to the SE and to the NW. At the Poutu Canal, east of Lake Rotoaira, *Van Dissen et al.* [2003] calculated a ≤ 2 ka recurrence interval for surface rupture of the Waihi and Poutu fault zones based on slip-rates and surface length estimations from faults in an area 85 km north within the Taupo Rift. *Stirling et al.* [2012] associate ruptures along this fault with M_w 6.6 earthquakes every 1 ka.

Both fault zones have affected patterns of the volcanogenic sedimentation at the northern part of the Tongariro Volcanic Complex for the last 60 ka and have influenced the formation of the Lake Rotoaira basin [*Lecointre et al.*, 2004b].

Extension (strain) direction in the Tongariro area has an ESE-WNW direction (ca. 110°), as suggested by the trend of active faults and dikes [*Rowland and Sibson*, 2001], earthquake focal mechanisms [*Townend et al.*, 2012] and geodynamic modelling [*Wallace et al.*, 2004]. The total geodetic crustal extension at seismogenic

depth in the Tongariro Graben is 7.4 mm/yr [Wallace *et al.*, 2004]. From the total extension, tectonic faults accommodate 78-95% across the graben (tectonic extension) and dike intrusions accommodate the remaining 5-22% (volcanic extension); from which 4-5% is associated with volcanic eruptions and 18-19% with arrested dikes (Chapter 5).

The seismic hazard potential for the Tongariro Graben has not been defined. Evaluating the fault geometry, slip-rates and segmentation in the Tongariro Graben will provide important implications for seismic hazard assessment in the region, which is a very popular winter and summer sport locality and site of one of the most popular alpine walkways in the country, a UNESCO World Heritage Centre hosting up to 7000 people per day in the high season [Jolly *et al.*, 2014]. Also, major transport, power distribution and power generation assets in the area are exposed to volcanic and tectonic hazards.

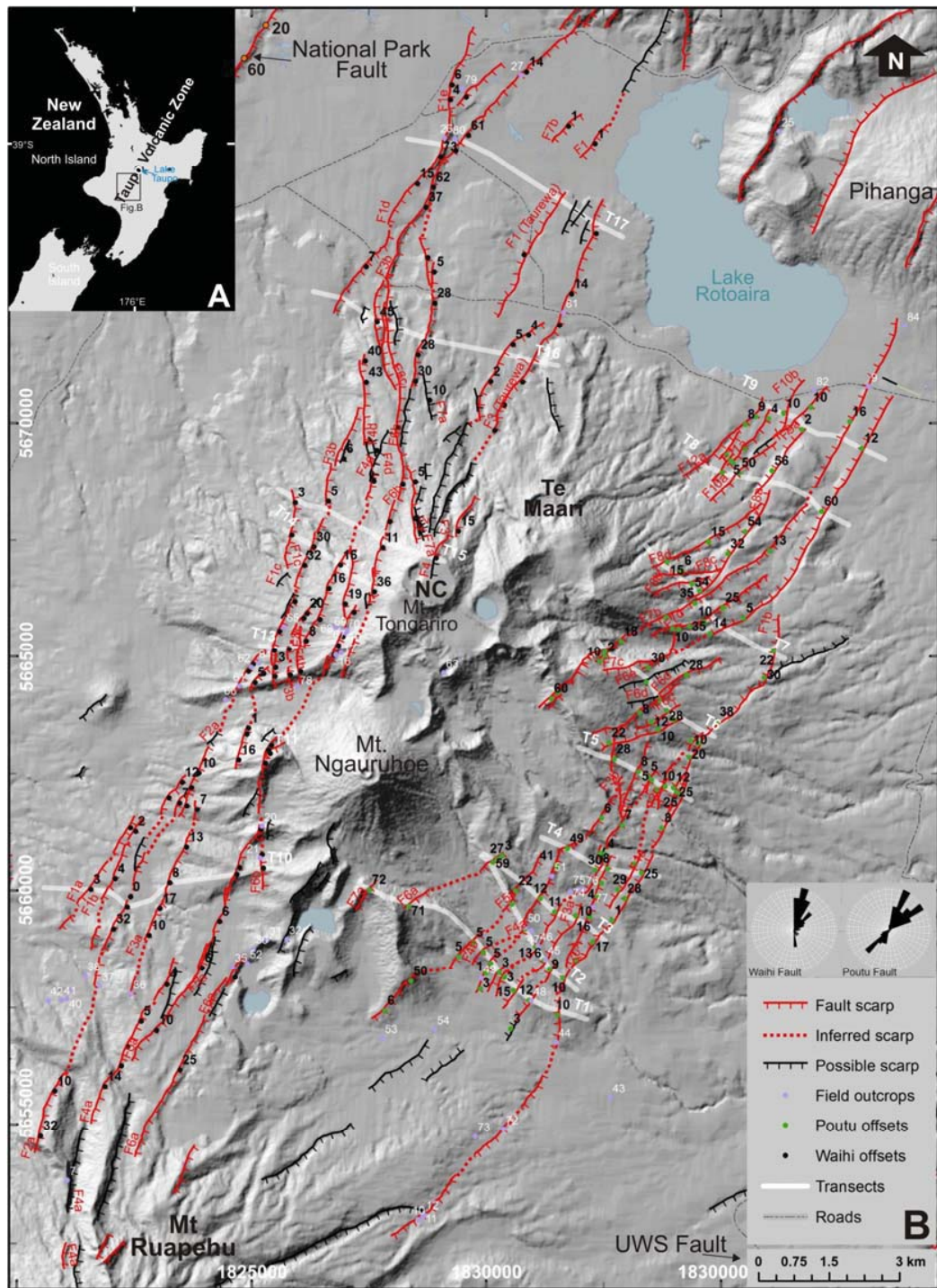


Figure 33. A, Location map of the Taupo Rift in the North Island of New Zealand. B, Location of the Tongariro Graben and the Tongariro Volcanic Complex at the southern section of the Taupo Volcanic Zone. 229 vertical fault displacements (2 northern National Park Fault, 117 Waihi Fault and 110 Poutu Fault) measured by geomorphic surfaces on transverse profiles over the faults (values in meters). Seventeen transects marked with white lines (T1-T17). Field points marked with purple dots and white numbers (referred to as Tong # in the text and figures). UWS, Upper Waikato Stream; NC, North Crater. For more details about displacements, lithology and surface ages see Chapter 5, Tables S3 and S4.

6.3 Methods

The fault geometry (azimuth and dip), movement sense and fault displacements were measured with field measurements and geomorphic analyses of the faults using ArcGIS on a 2 m resolution Digital Surface Model [S. Ashraf, methodology described in *Gómez-Vasconcelos et al.*, 2016]. 117 profiles were traced across the Waihi Fault zone and 110 across the Poutu Fault zone, perpendicular to the fault strands, at locations where the faults displace geomorphic surfaces of known ages (Fig. 33; Chapter 5). The age of stratigraphic markers and geomorphic surfaces provided a broad age control of vertical fault motion. Vertical displacements were converted to net-displacement to calculate net faults slip-rates, following the methods described by Villamor and Berryman [2001; 2006b].

Uncertainties for this data set come from the imperfection of preservation of surfaces and the lack of outcrops on the entire fault set. Some outcrops show no faulting at some time intervals while others do, which may reflect that: 1) not all strands ruptured during the same rupturing event [as observed for other normal faults; e.g. Paeroa Fault, North Taupo Rift; *Berryman et al.*, 2008]; 2) not all strands are exposed at each location along the fault (erosion); 3) not all time intervals were exposed on each of the fault exposures.

In order to calculate the slip-rates in the Tongariro Graben, vertical displacements were summed across all fault strands, to derive the mean vertical slip-rate for the entire fault zone. Earthquake moment magnitudes (M_w) were calculated using the fault-scaling relationship developed for the Taupo Volcanic Zone [*Villamor et al.*, 2007; *Stirling et al.*, 2012], based mainly on the surface-rupture length ($M_w = 4.80 + 1.33 \times \log$ [subsurface rupture length]). Fault lengths were measured in this work, based on fault displacements, geomorphology and field observations. For fault width a 15 km-thick

seismogenic crust is assumed, as suggested on previous seismic studies [Hurst and McGinty, 1999; Hayes et al., 2004; Stirling et al., 2012].

Fault recurrence interval was derived from slip-rate and single-event displacement (SED). Realistic SEDs could not be obtained from field data, so SED was derived from the fault area based on the seismic moment (M_0) by the equation of Aki and Richards [1980] ($SED = [M_0] / [fault\ area * 2.52E + 23]$). M_0 is calculated from the M_w by the equation of Hanks and Kanamori [1983].

6.4 Results

6.4.1 Fault geometry

The Waihi Fault zone comprises 19 fault strands [three of which were previously defined as Taurewa Fault; *Lecointre et al.*, 2002]. They are all NNE-oriented (average of 023°) normal faults with 1 antithetic fault (Taurewa). The fault zone width extends from ~1 km west from the Tongariro Graben axis to 5 km to the west (Fig. 33). The fault zone is at least 38 km in length, from south-western Lake Taupo to the north-western slopes of Mt. Ruapehu. The fault geometric pattern changes along the fault: the southern section has a $\sim 025^\circ$ trend, while the northern section has a $\sim 000^\circ$ trend. Some fault strands have tilted blocks [e.g., Waihi F3b to the northwest; *Miller and Williams-Jones*, 2016] and have very steep dips ($>80^\circ$), while others show en-echelon geometry, fault splaying and non-parallel faulting.

The Poutu Fault zone consists of 23 parallel NNE-oriented (average 040°) normal fault strands; 11 of them dip to the SE, while the others dip to the NW forming a graben-like structure. This fault zone width extends from ~2 km east of Ngāuruhoe and Red Crater vents to 6 km east of the Tongariro Graben axis (Fig. 33). The fault zone is at least 30 km long, extending from the northern part of Pihanga to the northeast slopes of Mt. Ruapehu. The fault geometric pattern changes along the fault: the southern section of

the fault has a $\sim 060^\circ$ trend, while the northern section has a $\sim 025^\circ$ trend. Some fault strands dip at $>70^\circ$ in the outcrops and others show en-echelon geometry, horsetail fault splaying, with soft-linked fault arrays and sometimes non-parallel faulting, especially to the north, near Lake Rotoaira.

The Waihi and Poutu fault zones converge towards the south, narrowing the graben and the limits of the volcanic vent complex. To the north, adjacent to the Te Maari vents, the graben widens slightly: Waihi Fault zone displays \sim N-trending fault strands and Poutu Fault zone displays $\sim 060^\circ$ -trending fault strands, splaying slightly outwards at the axis of the graben (Fig. 33).

6.4.2 Fault slip-rates

The spacing between single fault strands within each fault zone is between ~ 0.2 and 1 km, and thus they are likely to merge into a single fault plane at depth, as suggested by Villamor and Berryman [2001] and Nicol et al. [2010] for structures with similar fault spacing in the central TVZ. If the surface fault strands represent the whole fault, the summation of displacements on all strands characterises the total deformation of the fault. Eight transects across the Waihi Fault zone and nine across the Poutu Fault zone (Fig. 33; Tables S3 and S4; Chapter 5) were used to estimate the total deformation accommodated since <100 ka. For the Waihi Fault this amounted to an average of 28 ± 3.6 m since 20 ka and 173 ± 10.9 m since 60 ka, and for the Poutu Fault, an average of 65 ± 9.3 m since 20 ka and 178 ± 14 m since 60 ka (Table 9). This total displacement provided the basis for slip-rate calculations, leading to mean slip-rates of 2.6 ± 0.8 mm/yr and 2.2 ± 1.9 mm/yr, for the Waihi and Poutu faults, respectively (Table 9).

TABLE 9. VERTICAL DISPLACEMENTS AND SLIP-RATES SUMMARY FOR THE TONGARIRO GRABEN, FROM WAIHI AND POUTU FAULTS TRANSECTS AND RIFT-BOUNDING FAULTS

Transect number (age)	Vertical displacement measured for each fault in the transect (m)				Total offset* (only synthetic) (m)	Vertical slip-rate (only synthetic) (mm/yr)	Rift-Bounding faults Total offset (m)	West/East Tongariro Graben slip-rate (mm/yr)
	Vertical displacement ± error (fault number, age when different from transect age)	Vertical displacement ± error (fault number, age when different from transect age)	Vertical displacement ± error (fault number, age when different from transect age)	Vertical displacement ± error (fault number, age when different from transect age)				
Waihi Fault								
T 15 (12 ka)	3±1.3 (1c)	5±1.5 (3b)	5±1.5 (4d)	11±2.1 (6b)	-	24±3.5	-	-
T 10 (20 ka)	3±1.3 (1a)	4±1.4 (1b)	5±1.5 (2a)	8±1.8 (3a)	55±6.5 (5a, 200 ka)	28±3.6	20±3 [§]	2.4±0.2
T 12 (22 ka)	3±1.3 (2a)	5±1.5 (3b)	15±2.5 (3b)	12±2.2 (4b)	13±2.3 (4c, 30.6 ka)	69±5.6	-	-
T 11 (25 ka)	10±2 (2a)	16±2.6 (3b)	20±3 (5a)	15±2.5 (5a)	-	61±5.1	-	-
T 16 (40 ka)	16±2.6 (1d)	45±5.5 (3b)	28±3.8 (6b)	33±4.3 (6c)	11±2.1 (2)	160±9.4	-	-
T 13 (52.6 ka)	37±4.7 (3b)	5±1.5 (4b)	8±1.8 (4c)	40±5 (5a, 40 ka)	-	102±8.1	-	-
T 14 (59 ka)	22±3.2 (1c)	30±4 (3b)	16±2.6 (4c, 25 ka)	19±2.9 (5b, 25 ka)	36±4.6 (6b, 40 ka)	173±10.9	60±7 [§]	3.9±0.3
T 17 (85 ka)	73±8.3 (1d)	61±7.1 (3b)	15±2.5 (1T _w ** , 25 ka)	14±2.4 (3, 25 ka)	1±1.1 (7b, 3 ka)	149±11.5	-	-
Mean slip-rate						2.6±0.8		3.2±0.4
Poutu Fault								
T 5 (15 ka [†])	25±3.5(1a)	25±3.5(1b)	12±2.2(1b)	10±2(2c**)	12±2.2(2c)	79±4.7	-	-
T 9 (17.7 ka)	12±2.2 (7c)	16±2.6 (7b)	2±1.2 (9a)	10±2 (10a**)	10±2 (10b)	40±4.1	-	-
T 1 (20 ka)	10±2.0 (1a)	12±2.2 (2a)	15±2.5 (3a)	3±1.3 (3b**)	3±1.3 (3b**)	37±3.9	-	-
T 2 (20 ka)	10±2 (1a)	9±1.9 (2a)	6±1.6 (3a)	13±2.3 (3b)	6±1.6 (4a**)	38±3.9	10±2 ^{††}	3.8±0.3
T 3 (20 ka)	17±2.7 (1a)	16±2.6 (2b**)	10±2 (3a)	11±2.1 (3b)	12±2.2 (4a**)	38±4	-	-
T 7 (20 ka)	22±3.2 (1b, 36.1 ka)	14±2.4(7c)	10±2(7d**)	35±4.5 (7b** , 60 ka)	4±1.4 (8a)	41±4.2	-	-
T 4 (60 ka)	25±3.5 (1a)	27±3.7 (2c)	12±2.2 (2b**)	30±4 (3b)	49±5.9 (4a** , 97 ka)	82±6.5	30±4 ^{††}	3.5±0.2
T 6 (60 ka)	38±4.8 (1b)	29±3.9 (6b)	28±3.8 (6c)	60±7 (6d**)	10±2 (6e**)	95±7.3	-	-
T 8 (100 ka)	60±7 (7c)	13±2.3 (7b, 17.7 ka)	56±6.6 (9a)	50±6 (10a**)	10±2 (11a**)	181±12.2	-	-
Mean slip-rate						2.2±1.9		3.7±0.4

Note: T_w, Taurewa Fault. For a complete version of this table see chapter 5.

* Displacement values were converted to transect ages when the existing values were of a different age.

[§] National Park Fault.

[†] Uncertain (Anomalous data, possibly due to age uncertainties in the offset surfaces).

** Antithetic fault strands.

^{††} Upper Waikato Stream Fault (Gómez-Vasconcelos et al., 2016).

6.5 Discussion

6.5.1 Fault segmentation

To assess possible segmentation along the Waihi and Poutu faults, all displacements measured along the different traces of the faults are compared (Fig. 34). The data show that individual fault strands have variable displacements for different aged surfaces along the Waihi and Poutu fault zones. For example, displacements along the Waihi Fault increase for 20-40 ka displacements in the northern part of the fault zone. While this displacement increment in the Waihi Fault zone could be a consequence of the fault segmentation, it could simply occur because of multiple fault strands merging at this point (that is, fewer strands on the north, each accommodating more deformation; Fig. 33). The Poutu Fault zone does not show a consistent pattern of displacement variation (increase or decrease) along individual fault strands (Fig. 34).

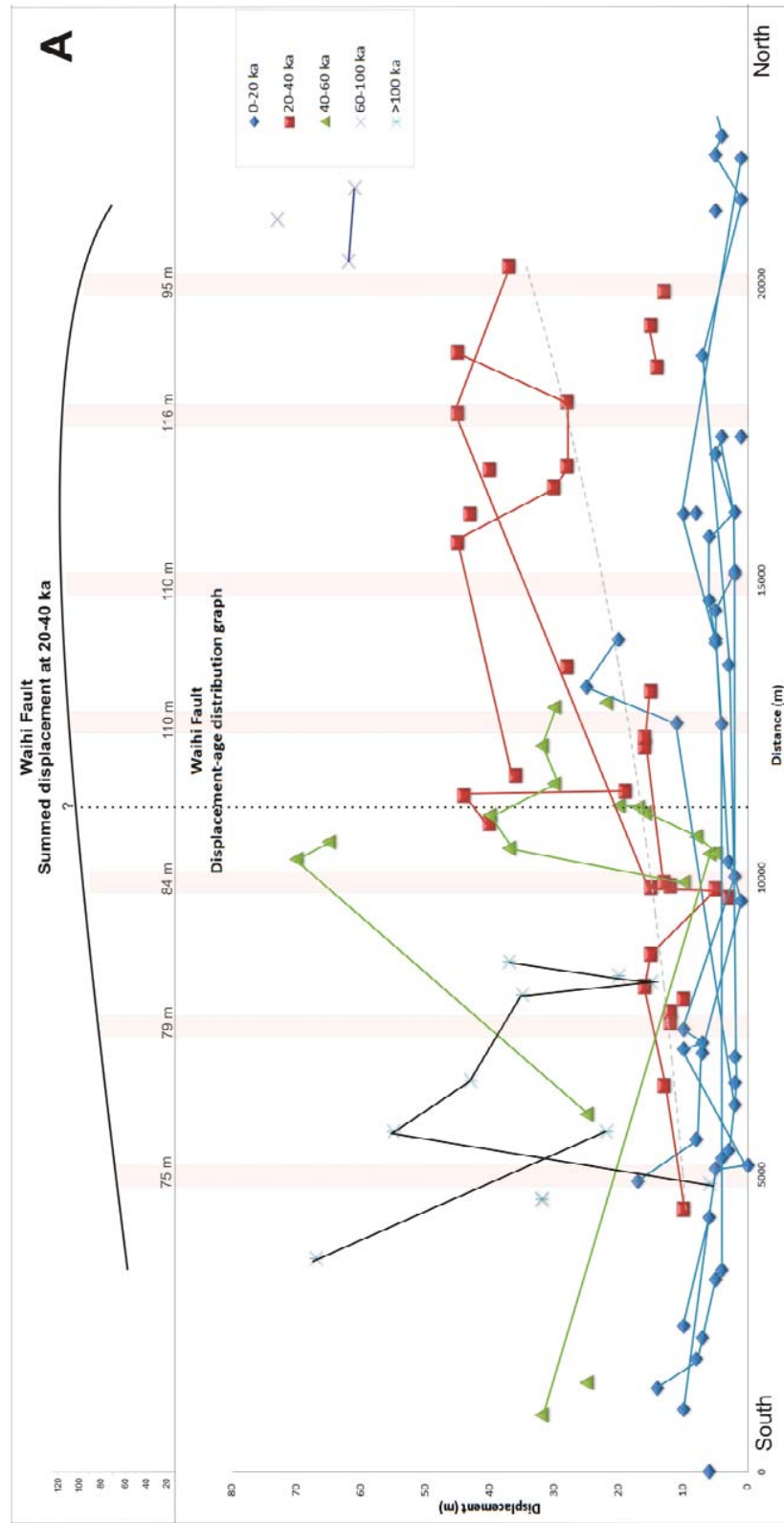
Total displacements along the Waihi and Poutu faults suggest that the faults can rupture their entire length (Fig. 34) To obtain the total displacement at several locations (slices) along the faults, measured displacements of each age along small sections of the fault zones were averaged and interpolated to 20-40 ka (for those values obtained in surfaces different to the 20-40 ka ones), and then summed across the fault zone. In general, both faults have a central higher displacement that diminishes toward the tips, displaying a bell-shaped curve, similar to that defined by Morley [2000] for normal faults. The Waihi Fault has slightly greater total displacement to the north, creating a central-north modal curve, while Poutu Fault has slightly greater displacements in the central part, creating a central-modal curve, although there is a possible sub-mode in the northern part of the fault zone. These results suggest that the increase in slip-rate for the 20-40 ka surface on the northern part of the Waihi Fault is a consequence of the presence of fewer fault strands in that area.

The lack of historic fault surface ruptures or paleoseismic trenches along the entire length of the faults, together with the complexity of their surface expression in this region, make the fault segmentation uncertain. Different possible scenarios are suggested for segmentation (surface rupture length) for each of the fault zones, based mainly on the fault strands geometry (morphometry and distribution; Fig. 35).

The whole Waihi Fault is at least 38 km in length and up to 52 km if it extends to the SW boundary of Lake Taupo, including traces mapped north of the study area [Fig. 35; *Langridge et al.*, 2016]. Based on its geometry, Waihi Fault can be divided in two (or three) segments. The Waihi South segment is 18 km long and is based on relatively continuous ~025-trending parallel fault strands. The change in fault orientation and displacement increment (Fig. 34) is used here to define the possible northern boundary of the segment. Therefore, the fault segment finishes against ~N-trending fault strands, c. 1 km north of the North Crater. The Waihi North segment is 20 km long. It starts with the ~N-trending fault strands, changing to ~025-trending rift-parallel fault strands to the north and terminating close to the southern end of Lake Taupo. The fault segment termination is based on the abrupt rift variation that occurs at the Taupo Domain [*Rowland and Sibson*, 2001], involving greater slip-rates [*Wallace et al.*, 2004] and higher heat flux [*Rowland et al.*, 2010]. If this segmentation of the Waihi Fault is correct, then there needs to be a third segment to the north, along the SW Lake Taupo shore, up to the Ōruanui collapse collar margin [*Wilson et al.*, 2006]. In this study the segment beyond the study area was not examined, because it requires understanding of the fault expression within the lake.

The whole Poutu Fault is at least 30 km in length and it can be divided in two segments. The Poutu South segment is 12 km long and is based on relatively continuous ~025-trending parallel fault strands. Although this segment is expected to be at least as long as the thickness of the seismogenic crust, which is 15 km [*Hurst and McGinty*, 1999; *Hayes et al.*, 2004]. This relationship is shown to exist for other short

faults with surface rupture expression in previous seismic hazard studies [*Stirling et al.*, 2012]. Some fault traces in this area displaced younger sediments, but did not produce a geomorphic expression [*Gómez-Vasconcelos et al.*, 2016], thus erosion likely hinders fault geomorphic expression in the southern segment of the Poutu Fault. The Poutu North segment is 18 km long. It starts with ~060-trending fault strands, changing to ~025-trending rift-parallel fault strands to the north and terminating 5 km from the southern end of Lake Taupo, north of Pihanga volcano (Fig. 35).



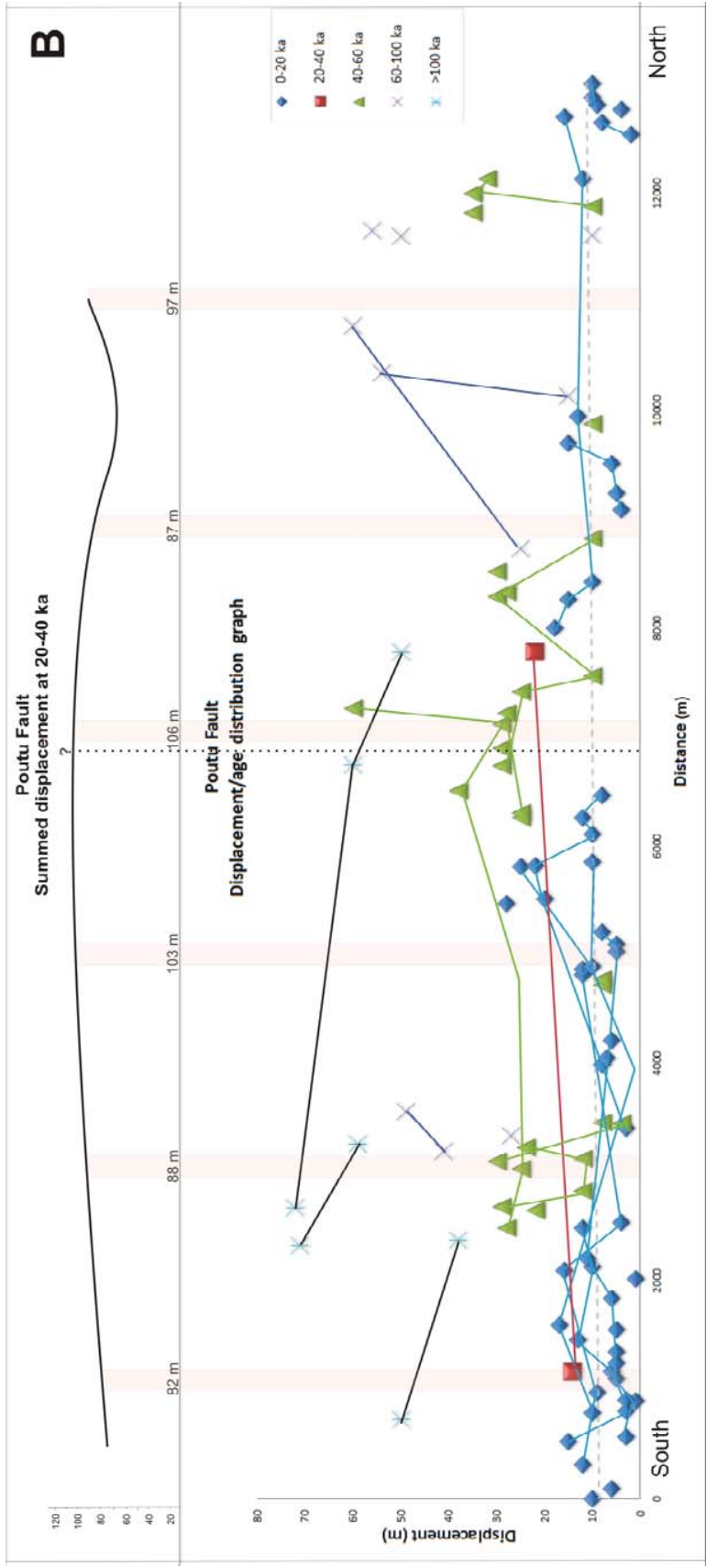


Figure 34. Measured individual fault strand displacements for different age surfaces along the strike of the Waihi (A) and Poutu (B) fault zones. Displacements for the same fault strand are connected with lines of different colours for different ages: blue for 0-20 ka, red for 20-40 ka, green for 40-60 ka, purple for 60-100 ka and black for >100 ka. To obtain the total displacement at several locations (slices) along the faults, measured displacements of each age along small sections of the fault zones were averaged and interpolated to 20-40 ka (for those values obtained in surfaces different to the 20-40 ka ones), and then summed across the fault zone. Summed values are used to evaluate the displacement variability along the faults and try to identify segmentation patterns. Dotted lines represent the suggested segmentation based on fault strands geometry (Fig. 35).

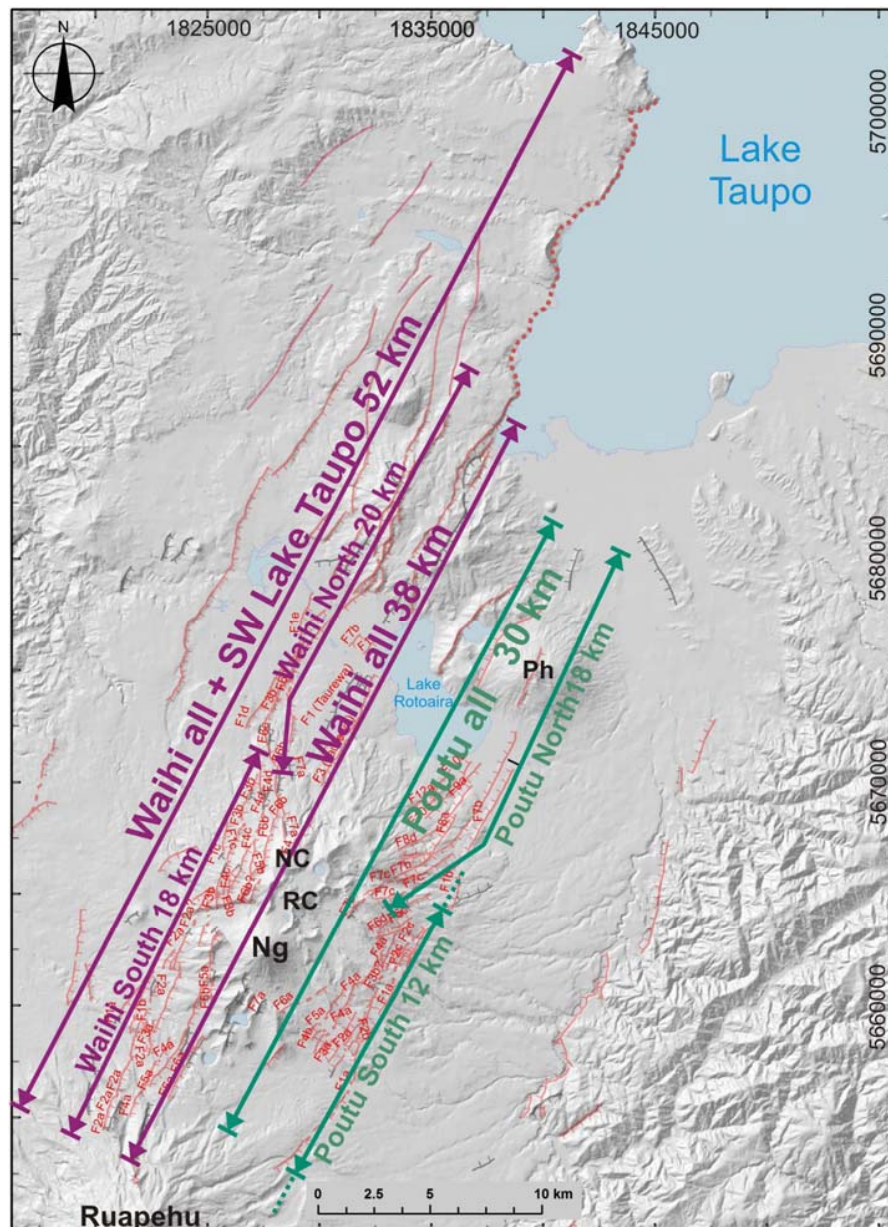


Figure 35. Potential segment surface-length rupture models for the Waihi and Poutu faults, marked with purple and green lines, respectively. Ng, Ngāuruhoe; RC, Red Crater; NC, North Crater; Ph, Pihanga.

6.5.2 Magnitude and recurrence interval of potential earthquakes

Because of the spatial coincidence between faults and volcanoes, the seismicity in this area is very complex, involving tectonic, volcano-tectonic, volcanic earthquakes and swarm activity [Hurst and McGinty, 1999; Miller and Savage, 2001; Reyners, 2010]. There have not been large main shocks with surface rupture in historic time. There was a M_w 6.3 earthquake in 1846 at the south-western edge of Lake Taupo [Hegan et al., 2001; Cooper, 2002], but there is no information about its surface rupture. Therefore, fault length data is used here for an estimation of magnitudes of future potential earthquakes (Table 10).

If the entire length of the Waihi Fault Zone (38 km) were to rupture at once this would produce a M_w 7.0 earthquake, with an average single-event displacement of 2 m. For a whole Poutu Fault Zone rupture (30 km-long), a M_w 6.9 earthquake could occur, with an average displacement of 1.6 m. The worst case scenario is a 52 km-long rupture, including the whole Waihi Fault Zone and the SW boundary of Lake Taupo, generating a M_w 7.2 earthquake, with an average single-event displacement of 2.9 m (Fig. 35; Table 10). The M_w 6.3 for short segment ruptures (Table 10), thus is in accordance with the 1846 M_w 6.3 event, which was retrospectively assigned to the Waihi Fault [Scott and Potter, 2014].

The information obtained from progressive displacements of geomorphic surfaces of different ages is not accurate enough to assess recurrence intervals. This is because there are only a few well-dated surfaces in this region and their ages have thousands of years of difference, which is a time span larger than their likely recurrence interval for fault rupture. At least 19 events were identified occurring over the last 200 ka for the Waihi Fault and at least 15 events for the Poutu Fault. This estimate of surface-rupture events is an underestimate because of the large difference in age of the chronological markers and the large progressive displacements obtained (>5 m).

Fault rupture recurrence intervals were derived from slip-rates and single-event displacements as described in the Methods section above. When slip-rates are combined with the derived average displacements, a recurrence interval of 1.0 ka and 0.9 ka for Waihi and Poutu faults is obtained, respectively (Table 10). If Waihi and Poutu faults were to rupture by segments, their recurrence intervals would be shorter. This denotes that M_w 6.3 to 6.7 earthquakes are likely to be twice as frequent as M_w 6.9 to 7.0 earthquakes in the Tongariro Graben (Table 10).

TABLE 10. MOMENT MAGNITUDE AND SINGLE-EVENT DISPLACEMENT FOR DIFFERENT FAULT LENGTHS

Fault	Segment surface length (km)	Sub-surface length (m)	Average displacement (m)	M_w	Slip-rate (mm/yr)	Recurrence interval (ka)
Poutu North segment	18	21	1	6.3	1.95±0.5	0.57
Poutu South segment	15	14	0.7	6.3	2.5±1.9	0.53
whole Poutu Fault	30	35	1.6	6.9	2.2±1.9	0.9
Waihi North segment	20	23	1.1	6.7	2.8±0.7	0.6
Waihi South segment	18	21	1	6.6	2.4±0.6	0.4
whole Waihi Fault	38	44	2	7.0	2.6±0.8	1
whole Waihi + SW Lake Taupo	52	61	2.9	7.2	-	-

Note: Estimated average single-event displacement in meters. Earthquake moment magnitude (M_w) based on Webb's equation, for a certain segment surface length (km) and fault area (as described in Villamor et al. 2007; Stirling et al. 2012). Average single event displacement (SED) was derived from the fault area based on the seismic moment (M_0) by the equation of Aki and Richards (1980). M_0 is calculated from the M_w by the equation of Hanks and Kanamori (1979) (see methods section).

6.5.3 Updating fault characterisation for seismic hazard assessment in the Tongariro area

Earlier studies on the Waihi Fault estimated a mean slip-rate of 1.1 mm/yr [Lecointre et al., 1998; Litchfield et al., 2013], a M_w 6.5 earthquake and recurrence interval of 1 ka [Stirling et al., 2012] or 2 ka [Van Dissen et al., 2003]. Earlier studies on the Poutu Fault estimated a mean slip-rate of 1.85 mm/yr [Litchfield et al., 2013], a M_w 6.6 earthquake and recurrence interval of 1 ka [Stirling et al., 2012] or 2 ka [Van Dissen et al., 2003].

The new data show that the Waihi Fault mean slip-rate value is likely to be 2.6 ± 0.8 mm/yr and the Poutu Fault mean slip-rate is 2.2 ± 1.9 mm/yr. These faults are capable of producing a M_w 7.2 earthquake, with a recurrence interval of 1.0 ka and 0.9 ka for Waihi and Poutu faults, respectively. If these faults were to rupture in segments, recurrence intervals would be shorter and magnitudes would decrease, but the short-term seismic hazard would increase. With this new data it is not possible to quantify how often the faults will rupture the entire length of the zone vs. shorter segments.

The new results yield more rapid slip-rates and greater earthquake magnitudes than earlier studies because this study adds extensive fieldwork, higher resolution maps, and better understanding of the age of geomorphic surfaces (Chapter 5), allowing better geomorphological characterization. This data increases the (short-term) seismic hazard (more rapid slip-rates) and addresses uncertainties, slip-rates, magnitudes and fault segmentation, which can be used to update the National Seismic Hazard Model for New Zealand [Stirling *et al.*, 2012; Litchfield *et al.*, 2013] and can provide a better local assessment of hazard, relevant to the population and regional infrastructure.

6.6 Conclusions

New characterisation of the faults in the Tongariro region indicates a 2.6 ± 0.8 mm/yr mean slip-rate value for the Waihi Fault and 2.2 ± 1.9 mm/yr for the Poutu Fault; these values are 19 to 136% greater than previous estimates. Waihi and Poutu faults are capable of producing M_w 7.2 and 6.9 earthquakes, with recurrence intervals of 1.0 ka and 0.9 ka, respectively. Fault strands displacements along the Tongariro Graben suggest that Waihi and Poutu faults tend to rupture as a whole structure, while fault strands geometry suggest they could rupture in segments. If these faults rupture in segments, recurrence intervals would be shorter and magnitudes would decrease, but the short-term seismic hazard would increase. Therefore, recurrence intervals, slip-

rates, magnitudes and single-event displacements will change depending on the length of the fault and the numbers of strands that rupture at once. More detailed paleoseismic studies on Waihi and Poutu faults are needed to better understand their segmentation pattern and to improve the current characterization of the seismic hazard in the region.

CHAPTER 7. Spatio-temporal associations between dike intrusions and fault ruptures in the Tongariro Volcanic Centre, New Zealand.

- 7.1 Abstract
- 7.2 Introduction
- 7.3 Tectonic and geological setting
- 7.4 Speculated volcano-tectonic interactions in the Taupo Rift
- 7.5 Methods
- 7.6 Results
 - 7.6.1 Fault slip-rate changes and volcanic activity in the TgVC
 - 7.6.2 Variability on eruptive volumes
 - 7.6.3 Spatio-temporal associations in the TgVC
 - 7.6.4 Scenarios for volcano-tectonic interactions in the TgVC
 - 7.6.5 Coulomb Stress transfer models for the scenarios observed in the TgVC
- 7.7 Discussion
 - 7.7.1 Volcano-tectonic interactions by stress transfer
 - 7.7.2 Factors controlling volcano-tectonic interactions in the TgVC
 - 7.7.3 Implications for natural hazards
 - 7.7.4 Limitations of this study
- 7.8 Conclusions

Supplementary files

Table S10. Main stratigraphic units

Table S11. Magma volumes of the Tongariro Volcanic Centre

Table S12. Co-seismic slip for the southern Taupo Rift faults

“Is this eruption related to that earthquake?”
This is a question commonly asked to volcanologists and seismologists when eruptions occur closely in time and space to large earthquakes.
Hill et al. (2002) answer this question, “Well, maybe.”
While Schminke (2004) says, “In general yes, in this particular instance maybe, but we do not know exactly how.”



Figure 36. Stormy Point look-out, Manawatu, showing sequences of river terraces from 400 to 12 ka.

Spatio-temporal associations between dike intrusions and fault ruptures in the Tongariro Volcanic Centre, New Zealand.

M. G. Gómez-Vasconcelos, P. Villamor, S. J. Cronin, A. Palmer, B. Stewart, J. Procter.

7.1 Abstract

In the southern Taupo Rift, in the Central North Island of New Zealand, crustal extension is mostly accommodated by normal faulting and occasionally by dike intrusions. Fault acceleration and deceleration apparently coincide with episodes of voluminous volcanic activity. If spatio-temporal association between volcanic eruptions and earthquakes can be expected, it will be very important for hazard assessment in this and similar regions in the world. Firstly, in order to assess if these interactions are causative or coincidental, static stress transfer models were examined. Eight faults and four dikes were modelled as the main sources of regional stress changes in the Tongariro Volcanic Centre for the last 100 ka. Integrated models were used to explain time associations and short-term variations in fault slip-rates and volcanic activity. These short-term rifting variations can be influenced by static stress transfer between adjacent faults (within <20 km from the source) and dike intrusions (within <10 km), or by fluctuations in magma input availability through time. Magma volumes and frequency of volcanic activity in the region thus must be considered to better understand the volcanic and seismic cycles in the southern Taupo Rift.

7.2 Introduction

In continental rifts, faults and volcanoes can interact with each other in many different ways, because extension is accommodated by a combination of dike intrusion and normal faulting [McCalpin, 2009]. The volume and flux of magma assisting the rifting process will influence the predominant extension mechanism and thus the predominant type of fault-volcano interaction. For example, in magma-assisted rifts, the most

common type of volcano-tectonic interaction is dike intrusion with associated surficial normal faulting above the arrested dike [e.g., Krafla and Afar: *Rubin and Pollard*, 1988; *Wright et al.*, 2006; *Ebinger et al.*, 2010]. In magma-poor rifts the main type of volcano-tectonic interaction could be through static stress transfer. In these cases, promotion of dike intrusions, or fault ruptures by other dikes or faults, occurs when magmatic systems are near a critical over-pressured state, or when faults are close to Coulomb failure [*Dmowska et al.*, 1988; *Stein et al.*, 1994; *Nostro et al.*, 1998; *Nostro et al.*, 2001; *LaFemina et al.*, 2004; *Roman*, 2005; *Walter et al.*, 2007; *Walter*, 2007; *Bonali et al.*, 2013; *Fujita et al.*, 2013; *Bagge and Hampel*, 2015; *Bonali et al.*, 2015; *Bonini et al.*, 2016].

The Taupo Rift has spatially (and probably temporally) variable levels of magma input spanning from fully magma-assisted to magma-starved situations along strike. This conditions the type of extension process and thus the type of volcano-fault interactions, as described by *Rowland et al.*, [2010]. The southern Taupo Rift (Fig. 37) is considered a magma-poor section of the rift (Chapter 5), where faulting and volcanism coexist spatially and temporally. The extensional processes in the Taupo Rift have been described as either magma-dominated [*Rowland et al.*, 2010] or tectonic-dominated with some magma input (Chapter 5). The former is based on the spatial coincidence of faults and volcanoes, as well as interpretations of paleo-rifting episodes, such as the full unzipping of the TgVC at 11 cal ka BP [*Nairn et al.*, 1998]. This unzipping model is based on a quantitative assessment of the relative contributions of dike intrusion and tectonic faulting to extension rates.

General plate tectonics reconstructions of the area suggests that extension rates across the Taupo Rift were likely constant over the last 1.5 Ma [*Nicol and Wallace*, 2007]. In the Central section of the Taupo Rift, magmatism is currently absent (between Okataina and Taupo Volcanic centres) and thus tectonic extension predominates [*Seebeck et al.*, 2010; *Villamor et al.*, 2011]. In this region, short-term

slip-rates are variable for individual faults, caused by fault-fault static stress interactions, but they smooth out over the long-term (for periods of >20 ka) to be in balance with the extension rate [Nicol *et al.*, 2006]. In the southern Taupo Rift, it is unclear whether dike intrusion and tectonic faulting is in balance with the regional extension rate in the long-term (>20 ka), or whether rifting is episodic, as suggested by Nairn *et al.* [1998]. Short-term fault slip-rate variations have been suggested to coincide with changes in regional volcanic activity during the last 100 ka [Nairn *et al.*, 1998; Villamor *et al.*, 2007; Gómez-Vasconcelos *et al.*, 2016].

This study evaluates how dikes and faults interact in a magma-poor section of the rift, with the aim of a better understanding of rifting processes. The southern Taupo Rift provides a unique place for this type of study, where volcanic activity has been present since 350 ka [Tost *et al.*, 2016] and extensive studies of volcanic eruptions have been undertaken [Topping, 1973; Cronin *et al.*, 1996b; Lecointre *et al.*, 2002; Moebis *et al.*, 2011; Pardo *et al.*, 2012]. Further, regional and local tectonic structures have been well studied through time [Hurst and McGinty, 1999; Rowland and Sibson, 2001; Acocella *et al.*, 2003; Van Dissen *et al.*, 2003; Hayes *et al.*, 2004; Villamor and Berryman, 2006b; Villamor *et al.*, 2007; Gómez-Vasconcelos *et al.*, 2016; Langridge *et al.*, 2016], allowing determination of spatio-temporal associations with volcanic activity.

While there are many causes for temporal coincidences of deceleration/acceleration of faults and dikes, processes behind their interaction are varied [e.g., Hill *et al.*, 2002]. In Chapter 5 is suggested that faulting in the southern Taupo Rift is mainly tectonic (i.e., associated with little dike intrusion). Therefore, in this case, if there are volcano-tectonic interactions, they may be associated with static stress transfer.

In this study, potential spatio-temporal associations for the southern Taupo Rift between volcano-fault, fault-fault and volcano-volcano were compiled from the literature and new mapping. Further, possible scenarios for fault slip-rate changes

coinciding with episodes of voluminous volcanic activity were described. Coulomb stress transfer models were subsequently undertaken to evaluate these scenarios and assess the possible processes behind fault slip-rate variations. Finally, an integrated model for volcano-tectonic interactions in the TgVC was developed, which builds on the understanding of extension processes in the region. Identifying the specific faults or dike intrusions that are likely to be affected by a specific fault rupture or dike intrusion, will build enhanced understanding of continental rifting and improvement of future hazard assessments in the study area.

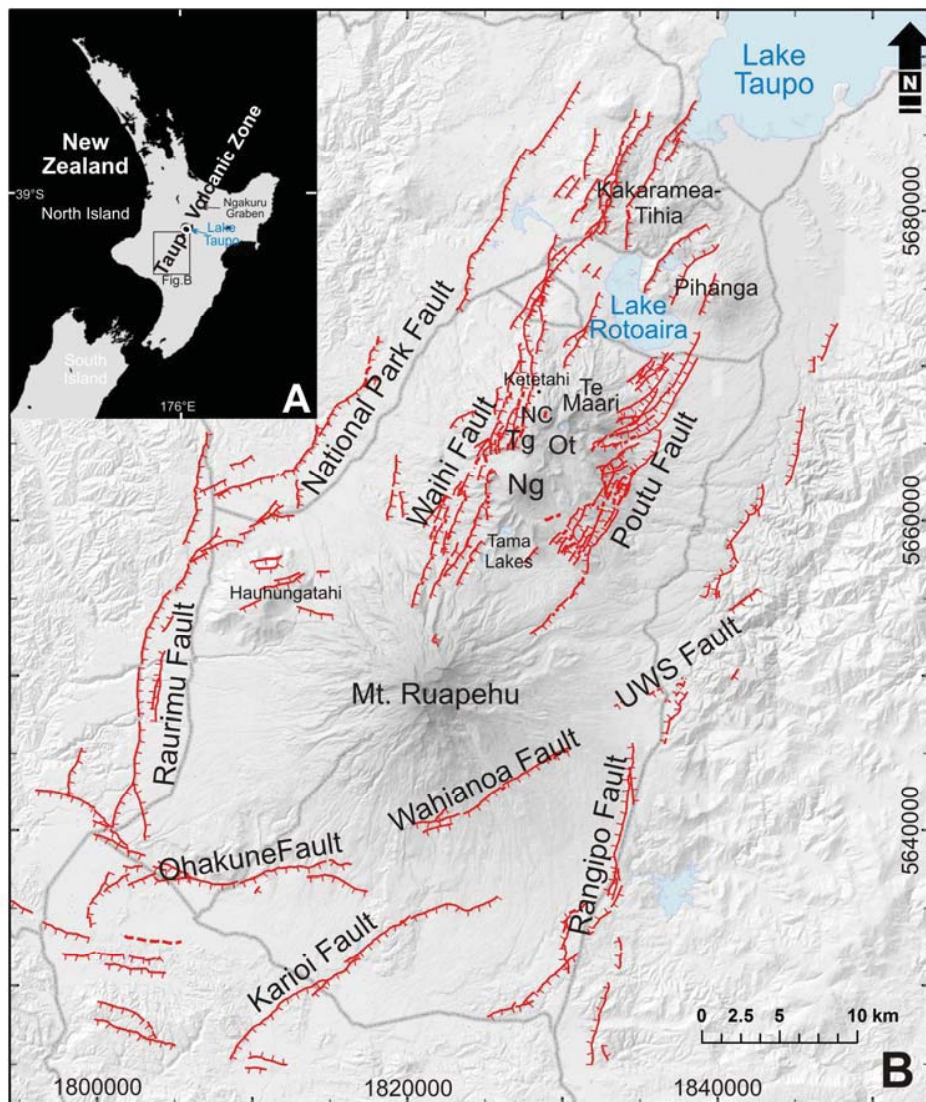


Figure 37. A, Location of the Taupo Volcanic Zone in the North Island of New Zealand. B, Tongariro Volcanic Centre in the southern sector of the Taupo Volcanic Zone. Location of the main regional volcanoes and faults (red lines) [Chapter 5; *Villamor and Berryman*, 2006b; *Langridge et al.*, 2016]. Ng, Ngāuruhoe; Tg, Mt. Tongariro; Ot, Oturere; NC, North Crater; UWS, Upper Waikato Stream.

7.3 Tectonic and geological setting

The Taupo Volcanic Zone (TVZ) is the NNE-trending Quaternary volcanic arc associated with the Hikurangi Trench, where the Pacific Plate subducts below the Australian Plate in the North Island of New Zealand. Extension within the arc is caused by the current fore arc clockwise rotation [*Wallace et al.*, 2004], as well as active slab rollback [*Seebeck et al.*, 2014; Fig. 37].

The Tongariro Volcanic Centre (TgVC) represents the southernmost volcanic centre of the TVZ, with two volcanic complexes dominating the landscape. Mt. Ruapehu and the Tongariro Volcanic Complex display a NNE-trending volcano vent corridor. Volcanic chronology in the area is achieved by a combination of direct dating of volcanic deposits, along with a well-established tephrochronology of local sourced units [*Topping*, 1973; *Cole*, 1978; *Donoghue et al.*, 1991; *Donoghue and Neall*, 2001; *Lecointre et al.*, 2004b; *Moebis et al.*, 2011; *Pardo et al.*, 2012]. Further temporal control is provided by rhyolitic tephra marker beds from the Taupo and Okataina volcanic centres to the north [*Froggatt and Lowe*, 1990; *Wilson et al.*, 1995; *Lowe et al.*, 2013]. Together, the tephra units were used to map and date sequences of volcanoclastic deposits and related landscape surfaces [*Palmer and Neall*, 1989; *Cronin and Neall*, 1997; *Donoghue and Neall*, 2001; *Lecointre et al.*, 2004a]. A summary of the main mappable deposits used in this study can be found in the data supplement (Table S10).

NNE-trending faults occur along the TgVC, on both sides of the volcanic vent corridor. These faults define the Ruapehu Graben [*Topping*, 1973; *Rowland and Sibson*, 2001;

Villamor and Berryman, 2006a] in the south, and the Tongariro Graben in the north (Chapter 5). In the Ruapehu Graben, radial extension (*Villamor and Berryman, 2006a*) is responsible for a complex fault pattern, including the ENE-trending Karioi fault set (Wahianoa Fault), the E-W Ohakune Fault, the NNE-trending Rangipo and Raurimu faults, and the NE-trending Upper Waikato Stream Fault [*Villamor and Berryman, 2006b; Gómez-Vasconcelos et al., 2016*]. Four NNE-striking parallel faults make up the Tongariro Graben, with two rift-bounding faults: the National Park Fault and the Upper Waikato Stream Fault. Within these, two intra-rift faults occur: the Waihi and the Poutu faults [Chapter 5; *Van Dissen et al., 2003; Lecointre et al., 2004b; Villamor and Berryman, 2006b; Cassidy et al., 2009*].

7.4 Speculated volcano-tectonic interactions in the Taupo Rift

In the central Taupo Rift, *Villamor et al. [2011]* and *Seebeck et al. [2010]* suggested that cold crust sections occur, where extension is tectonically controlled, as well as areas with thinner, hotter crust, where extension is controlled by dike intrusions. *Rowland et al. [2010]* proposed that rifting episodes in the rift are associated with fault ruptures and volcanic activity, especially with caldera-forming eruptions [*Gravley et al., 2007; Allan et al., 2013*]. These studies suggest that rifting mechanisms in the TVZ vary in space and time according to magmatic style.

In the northern and central Taupo Rift, analysis of historic data suggests that the 1886 Mt. Tarawera eruption was associated with fissuring along surrounding faults, but no major fault rupture occurred [*Seebeck and Nicol, 2009*]. Paleoseismic data in the central Taupo Rift (Ngakuru Graben; Fig. 37) suggest that there are temporal associations between eruptions of the Okataina Volcanic Centre and nearby faulting [*Seebeck and Nicol, 2009*]. For example, at 1315 AD, the rhyolite Kaharoa eruption [*Hogg et al., 2003*] was primed by a deep basaltic dike [*Nairn et al., 2005*]. The eruption

followed a Ngapouri Fault earthquake, but the timing relationship between the earthquake and the initial deep basaltic dike is unknown [Nairn *et al.*, 2005; Berryman *et al.*, 2006]. Berryman *et al.* [2008] and Villamor *et al.* [2011] found geometric relationships in paleoseismic trenches that show fault rupture during deposition of volcanic ash on the fault scarp. Villamor *et al.* [2011] suggested that stress transfer could encourage faulting after a dike intrusion and magma chamber inflation or deflation in the Okataina Volcanic Centre.

Past studies in the southern Taupo Rift have shown that accelerated fault movements may coincide with periods of major explosive volcanism. Villamor *et al.* [2007] postulated an association of the Bullot Formation from Mt. Ruapehu from 25 to 11 cal ka BP [Donoghue *et al.*, 1995; Pardo *et al.*, 2012] with activity on the Rangipo Fault. In the same area, Gómez-Vasconcelos *et al.* [2016] suggested that the Ōruanui eruption from Taupo caldera at 25.4 ± 0.2 cal ka BP coincided with higher slip-rates on the Upper Waikato Stream Fault. Further, it was suggested that the Pahoka-Mangamate eruptions from Tongariro at 11 cal ka BP [Nairn *et al.*, 1998] coincided with higher slip-rates on the Wahianoa Fault [Gómez-Vasconcelos *et al.*, 2016]. Nairn *et al.* [1998] also speculated that the Pahoka-Mangamate eruptions were caused by an episode of accelerated regional extension. The six ~ 0.5 - 1 km³ pyroclastic eruptions at 11 cal ka BP occurred in the brief time window of 200 to 400 years, at a far higher rate than background activity levels. The Pahoka-Mangamate tephras are interbedded with two rhyolite tephras from Taupo caldera, located ~ 50 km to the north, suggesting that the rifting event must have been of regional extent [Rowland *et al.*, 2010]. However, despite these suggestions, no fault slip-rate variability has been reported for this event.

Gerst and Savage [2004], and Johnson *et al.* [2011] studied the anisotropy changes after an eruption from Mt. Ruapehu, suggesting that magma intrusions can encourage fault ruptures by stress changes in the crust. On the northern Waihi Fault, at the southwestern edge of Lake Taupo, a M_w 6.3 earthquake in May 1846 was responsible for

disastrous landslides [Hegan *et al.*, 2001; Cooper, 2002]. In the same month, an eruption at Ketetahi may have occurred, suggesting a possible connection with the Waihi Fault earthquake [Scott and Potter, 2014].

7.5 Methods

Paleoseismic and volcanic activity data of previous studies was reviewed to examine scenarios for potential spatial and temporal associations between volcanic and seismic activity. Paleoseismic data used consisted mainly of slip-rate variations on the main faults in the southern TVZ over the last 100 ka, age of the Oturere lava flows, in the eastern Tongariro Graben [Hobden *et al.*, 1996]. Fault slip-rates were reconstructed after the evaluation of progressive displacements from field outcrops, trenches and geomorphic displacements [Van Dissen *et al.*, 2003; Lecointre *et al.*, 2004b; Villamor and Berryman, 2006b; Villamor *et al.*, 2007; Gómez-Vasconcelos *et al.*, 2016]. Coulomb stress models are created for those scenarios to assess whether they can be explained by changes in the crustal stresses. The Coulomb failure criterion (CFC; equation 1) is used to calculate the co-seismic ("static") stress changes on pre-defined fault planes, computed with Okada's equations [1992], in which failure is promoted when the Coulomb stress change (ΔCFC ; equation 2) is positive [King *et al.*, 1994; Nostro *et al.*, 1997]. For the stress calculations the numerical modelling software developed by the USGS "Coulomb 3.3.01" [Lin and Stein, 2004; Toda *et al.*, 2005] is used.

$$CFC = |\tau| + \mu(\sigma_n + \rho) \quad (1)$$

Where μ is the friction coefficient, ρ is the pore fluid pressure, τ is the shear stress and σ_n is the normal stress.

$$\Delta CFC = \Delta\tau + \mu(\Delta\sigma_n + \Delta\rho) \quad (2)$$

Where $\Delta\tau$ is the change in shear stress, $\Delta\sigma_n$ is the change in normal stress and Δp is the change in pore pressure.

Coulomb software calculates the stress changes produced by a “source” fault rupture or dike intrusion on a “receiver” fault or dike (that is a dike with a specific strike, dip and depth) in the surrounding region. A positive stress change (red area; unclamping positive) implies that the earthquake brought the receiver fault closer to failure, while a negative value (blue area) indicates a delay of the next earthquake. Negative normal stresses (tensile) was considered here as positive. The input file uses the fault location, azimuth, area, dip and slip. The fault location and azimuth are compiled from this and other studies [Villamor and Berryman, 2006b; Villamor et al., 2007; Stirling et al., 2012]. The fault area is calculated with the fault length, fault dip and thickness of the seismogenic crust. A best estimate dip of 70° at the surface and 60° at seismogenic depth was used, as observed in the field and suggested by studied faults within the Taupo Rift [Villamor and Berryman, 2001; Nicol et al., 2006; Mouslopoulou et al., 2008]. For the fault width, a 15 km-thick seismogenic crust was assumed, as suggested by previous seismic studies [Hurst and McGinty, 1999; Hayes et al., 2004; Stirling et al., 2012]. The co-seismic slip depends on the magnitude and fault length; therefore, each fault will have a different slip (Table S12). Observations in the TgVC and TVZ are of near-vertical dikes with an average 1-m-wide of co-intrusive opening [Cole and Hunt, 1968; Hobden, 1997]. Historic and prehistoric eruptions have shown distances between co-eruptive vents of no more than 2 km-long (e.g. in the Pahoka-Mangamate series of eruptions, Nairn et al., 1998), which is used here as a conservative estimate of the dike intrusion length.

Crustal rheology parameters used were the Young’s modulus (80 GPa), Poisson’s ratio (0.25) and Friction coefficient (0.4). The friction coefficient calculated for Ngāuruhoe by Nairn and Self [1978] is 0.4.

A fault rupture in association with moderate to large earthquakes could be promoted when positive stress changes happen between the middle and upper crust [Huc *et al.*, 1998], thus a calculation depth of 7.5 km was used. The nucleation depth used for a dike intrusion beneath the Tongariro Volcanic Complex is 10 km, and 5 km for Mt. Ruapehu [Ingham *et al.*, 2009]. This assumes that dike intrusions beneath the Tongariro Volcanic Complex come straight from the brittle-ductile boundary at 10-15 km-depth and Mt. Ruapehu dike intrusions derive from 5-7 km-depth [Nakagawa *et al.*, 1999; Miller and Savage, 2001]. The depths reflect also the petrological understanding of magmas erupted at these two volcanoes, with deeper basaltic-andesite magmas at the Tongariro Volcanic Complex and a shallow plexus of dikes and sills modifying andesitic magmas at Mt. Ruapehu [Hobden *et al.*, 1999; Gamble *et al.*, 2003; Price *et al.*, 2005]. Positive stress changes at the magma storage depths can promote a dike intrusion. It is important to note that magma chamber inflation or deflation also causes stress changes in the crust that can promote localised fault rupture; however, such modeling was not undertaken in this study.

Assuming that the extension is radial at Mt. Ruapehu, as previously proposed, dike intrusions could occur in any direction. Three possible directions were modelled here: (1) NNE-SSW, which is represented by the present-day structure of the rift [e.g., Darby and Meertens, 1995; Acocella *et al.*, 2003], (2) N-S, which is represented by the mean trend of the prominently exposed Mead's Wall dike on the northern flanks of Mt. Ruapehu (this study), and (3) E-W, which is represented by the Ohakune Fault trend and the volcanic craters associated with it in the lower southern flanks of Mt. Ruapehu [Villamor and Berryman, 2006a].

7.6 Results

7.6.1 Fault slip-rate changes and volcanic activity in the TgVC

Short-term (<45 ka) slip-rates summed across the Tongariro Graben tend to be constant in time (Waihi + Poutu faults; Fig. 38), although they are highly variable for individual faults in the TgVC (Fig. 39). There was a general fault slip-rate acceleration in the Tongariro Graben between 25 to 20 cal ka BP and ca. 90 ka (Fig. 38).

Average slip-rates of 2.9 ± 0.6 mm/yr on the Waihi Fault occurred between 85 (Tongariro – Oturere lava flow) and 25 ka and of 2.2 ± 0.7 mm/yr thereafter to the present day (Chapter 5). At the Poutu Fault the slip-rate was 1.6 ± 0.3 mm/yr from 100 (Mangahouhounui lavas) to 60 ka, and 2.2 ± 0.9 mm/yr thereafter to the present day (Chapter 5). On the Rangipo Fault Villamor et al. [2007] calculated slip-rates of 1.8 mm/yr from 25.4 to 13.6 cal ka BP, and of 0.24 mm/yr from 13.6 cal ka BP to the present day. Along the Upper Waikato Stream Fault, slip-rates of 0.45 mm/yr occurred between 45 and 36.1 cal ka BP, 1.5 mm/yr between 36.1 and 23.7 cal ka BP, and 0.26 mm/yr between 23.7 cal ka BP and the present day [Gómez-Vasconcelos et al., 2016]. For the Wahianoa Fault, slip-rates of <0.1 mm/yr occurred between 45 and 15 cal ka BP, of 5 mm/yr from 15 to 10 cal ka BP, and of >0.55 mm/yr from 10 cal ka BP to the present day [Gómez-Vasconcelos et al., 2016].

Slip-rate variation in the Tongariro Graben

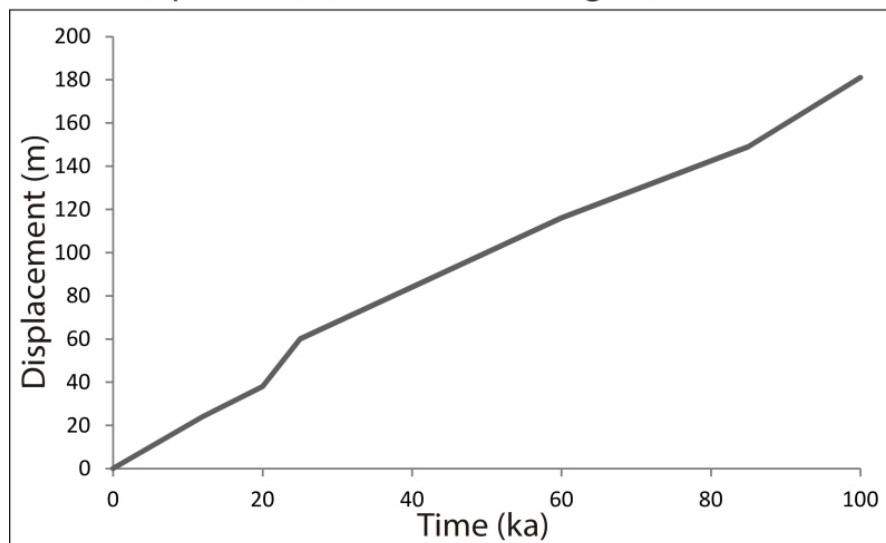


Figure 38. Summed vertical displacements across the Tongariro Graben for the last 100 ka (Waihi and Poutu faults).

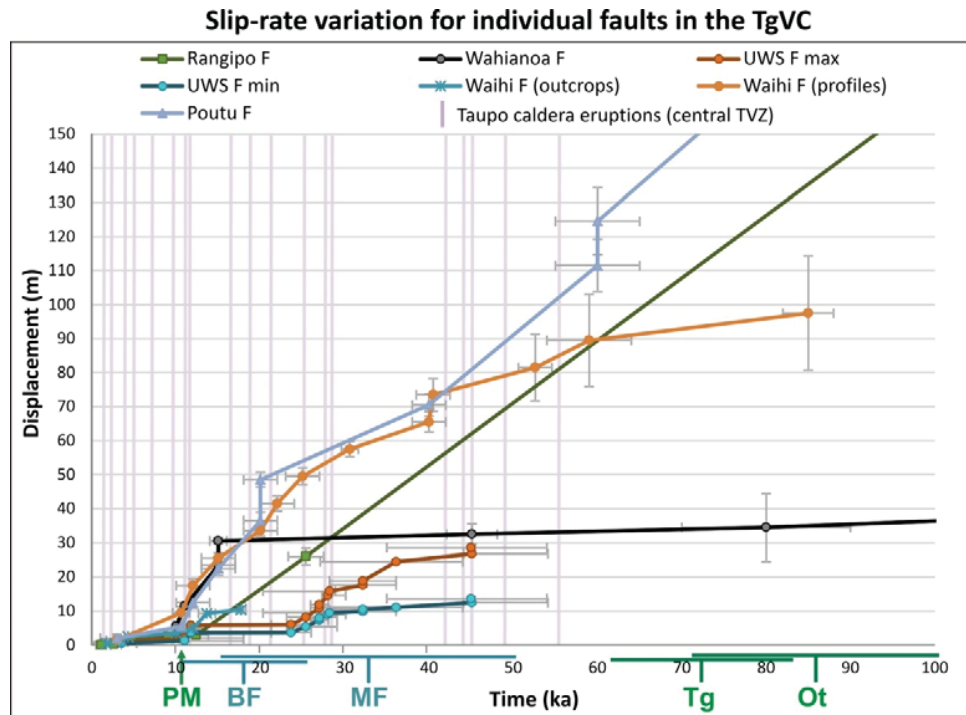


Figure 39. Variations in short-term fault slip-rates for various faults in the TgVC from 100 ka to the present day (zero), showing a temporal association with regional volcanic activity and Taupo caldera eruptions [Hajdas *et al.*, 2006; Wilson *et al.*, 2009; Hogg *et al.*, 2011; Lowe *et al.*, 2013; Vandergoes *et al.*, 2013]. UWS, Upper Waikato Stream Fault; TVZ, Taupo Volcanic Zone; PM, Pahoka-Mangamate sequence at ~11 cal ka BP; BF, Bullot Formation; MF, Mangawhero Formation; Tg, Mt. Tongariro; Ot, Oturere lavas.

7.6.2 Eruption volumes

Volumes of erupted magmas over the last ~250 ka in the TgVC were compiled from various literature sources (Fig. 40 and Table S11). These are likely to be large underestimates due to the bulk of the volume of stratovolcanoes being contained within volcanoclastic deposits in the ring plain [e.g., Zernack *et al.*, 2011]. Ring plain volumes are expected to be at least twice as the total volume of the stratovolcanoes (>350 km³; Fig. S11). For the Mt. Ruapehu, the largest components of the current volcanic edifice include lava flows [e.g., Wahianoa Formation, 45 to 74 km³; Gamble *et al.*, 2003; Conway *et al.*, 2016]. Large volumes of erupted magma are contained within tephra fall

deposits which have only been calculated well over the last ~25 ka. Some periods show high rates of eruption [e.g., Pahoka-Mangamate sequence, where 7 km³ was likely erupted at 11 cal ka BP; *Nairn et al.*, 1998]. Volume estimates for the ring plain are however more difficult, with single large debris avalanches and debris flows having estimated volumes between 1 and 2 km³ [e.g., Whangaehu Formation, 1 km³; R11 lahars, 1 km³; *Cronin et al.*, 1996b; *Keigler et al.*, 2011]. At the Tongariro Volcanic Complex, similar uncertainties in volume estimates occur due to the vast and poorly constrained volumes of volcanoclastic deposits on the ring plain, aside from one or two single collapse events that are well studied [e.g., Te Whaiiau Formation, 0.5 km³; *Lecointre et al.*, 2002].

Recognising the imperfections in estimating eruption volumes over time, it appears that magma input rates in the TgVC are variable over time, and some volcanoes have been more active than others during specific periods (Fig. 40). For example, Mt. Ruapehu magma input was higher during emplacement of the Wahianoa Formation from 180 to 119 ka [*Tost and Cronin*, 2015], while the Tongariro Volcanic Complex had low rates of volcanic activity between ~60 and 17 ka.

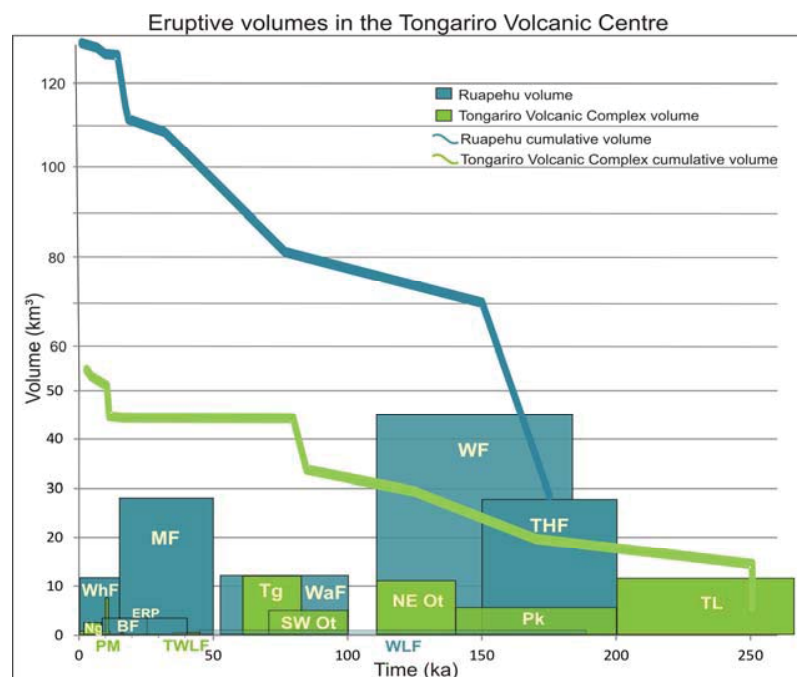


Figure 40. Eruptive volumes of the main tephras and lava flows in the Tongariro Volcanic Centre (Table S11). Mt. Ruapehu sourced deposits in blue and Tongariro Volcanic Complex in green. Ng, Ngāuruhoe [Moebis *et al.*, 2011]; PM, Pahoka-Mangamate sequence [Nairn *et al.*, 1998]; WhF, Whakapapa Formation [Conway *et al.*, 2016]; BF, Bullot Formation [Pardo *et al.*, 2012]; ERP, Eastern Ring Plain [Cronin *et al.*, 1996b]; MF, Mangawhero Formation [Conway *et al.*, 2016]; TWLF, Te Whaiau Laharic Formation [Lecointre *et al.*, 2002]; WLF, Whangaehu Laharic Formation [Keigler *et al.*, 2011]; Tg, Mt. Tongariro [Hobden *et al.*, 1996]; Ot, Oturere [Hobden *et al.*, 1996]; WF, Wahianoa Formation [Gamble *et al.*, 2003; Tost and Cronin, 2015]; WaF, Waimarino Formation [Lecointre *et al.*, 1998]; Pk, Pukekaikiore [Hobden *et al.*, 1996]; THF, Te Herenga Formation [Conway *et al.*, 2016]; TL, Tama Lakes [Hobden *et al.*, 1996].

7.6.3 Spatio-temporal associations in the TgVC

Correspondence between fault slip-rate variations (Fig. 39) and the rough estimate of volumetric eruption rates over time (Figs. 40 and S11) were evaluated for six periods, based on the volcanic activity variation in the last 250 ka (Fig. 41). The 45-11 ka period represents a time of moderate to high rates of explosive volcanism at Mt. Ruapehu [Cronin *et al.*, 1996b]. This period was divided in two: (1) the 45-25 ka period, which deposits were eroded during the Last Glacial Maximum. Evidence of this can be found in the north-eastern ring plain of Ruapehu. And (2) the 25-11 ka period, which deposits are preserved and grouped within the Bullot Formation from Mt. Ruapehu [Donoghue *et al.*, 1995; Pardo *et al.*, 2012]. While the 11-10 ka period represents a large burst of pyroclastic eruptions [Nairn *et al.*, 1998].

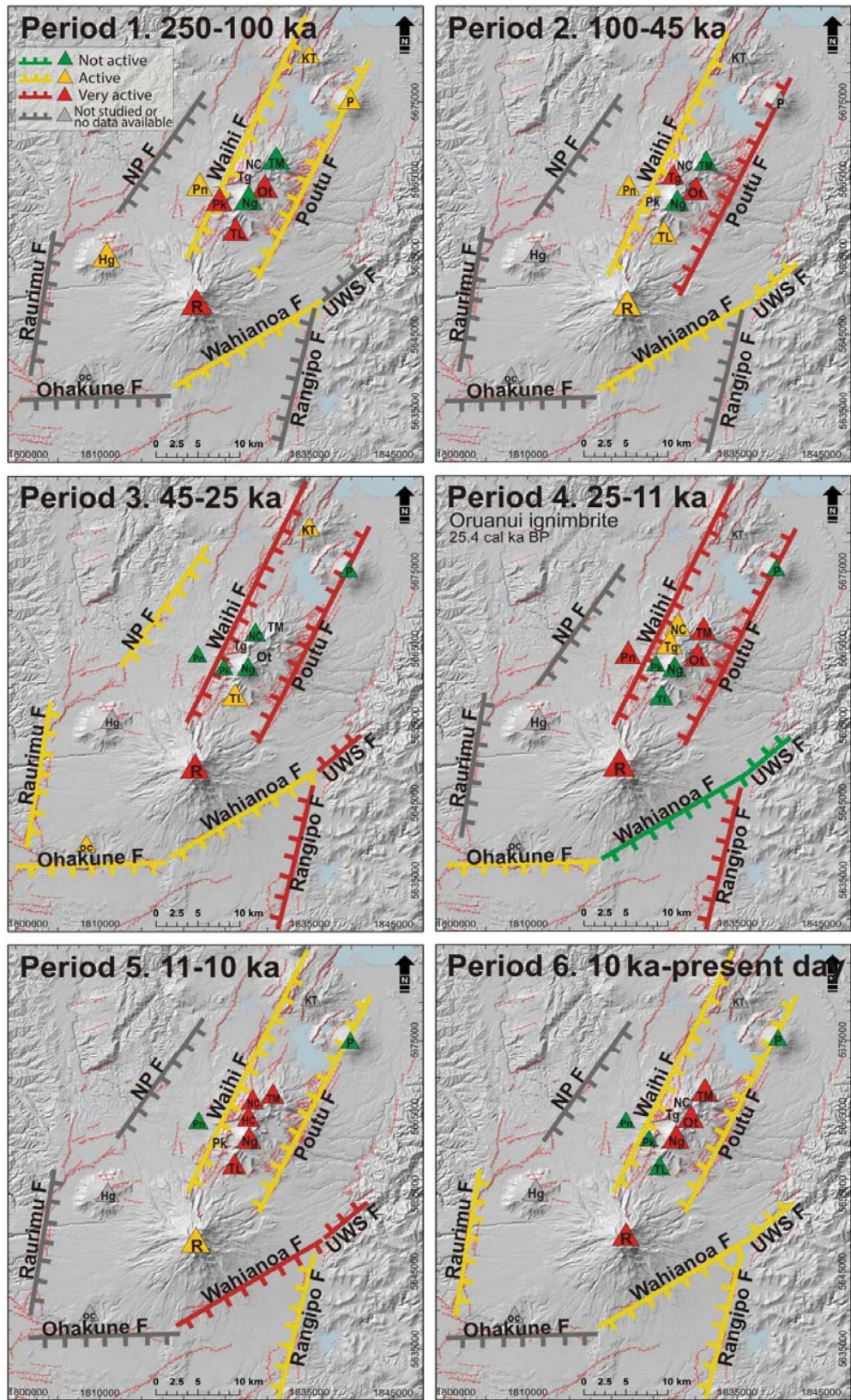


Figure 41. Spatio-temporal associations for the Tongariro Volcanic Centre from known paleo-earthquakes (fault slip-rates and events) and volcanic eruptions for six different periods, showing their variation in activity for the last 250 ka. The triangles are the volcanic vents and the lines are the faults. R, Ruapehu; TL, Tama Lakes; Ng, Ngāuruhoe; Tg, Mt. Tongariro; Ot, Oturere; NC, North Crater; TM, Te Maari; Pk, Pukekaikiore; Pn, Pukeonake; P, Pihanga; KT, Kakaramea-Tihia; Hg, Hauhungatahi; OC, Ohakune Craters; HC, Half Cone; NP F, National Park Fault; UWS F, Upper Waikato Stream Fault. At time 4 there was a major caldera forming eruption at Taupo caldera: the Ōruanui ignimbrite at 25.4 cal ka BP [Wilson, 2001].

7.6.4 Scenarios for volcano-tectonic interactions in the TgVC

Based on the spatio-temporal associations for the TgVC of Figure 41, 187 possible scenarios could be considered. Up to 56% of the scenarios are possible dike-fault or fault-dike interactions, 39% are dike-dike interactions, and 5% are fault-fault interactions (Fig. 42).

7.6.5 Coulomb stress transfer models

To evaluate the possible interactions between fault ruptures and dike intrusions, fault-fault and/or dike-dike interactions in the TgVC, static stress transfer models were generated for eight faults and four dikes (volcanic vents) as the main sources of regional stress changes, only the main models are shown here (Figs. 43-45). The Coulomb stress changes were calculated on specific receiver faults and normal stress changes were calculated on specific receiver dikes. The resultant stress changes are superimposed on a 3D Google image. A positive stress change (red area) for the region, where the fault or dike is located, leads to a possible scenario for fault-dike, dike-fault, fault-fault or dike-dike interactions, while a negative stress change (blue area), leads to a non-likely scenario for volcano-tectonic interactions.

From the stress change models (Figs. 43-45), 64 positive stress transfer scenarios could be identified, where 47% are dike-dike interactions, 38% are dike-fault or fault-dike interactions, and 15% are fault-fault interactions (Fig. 46).

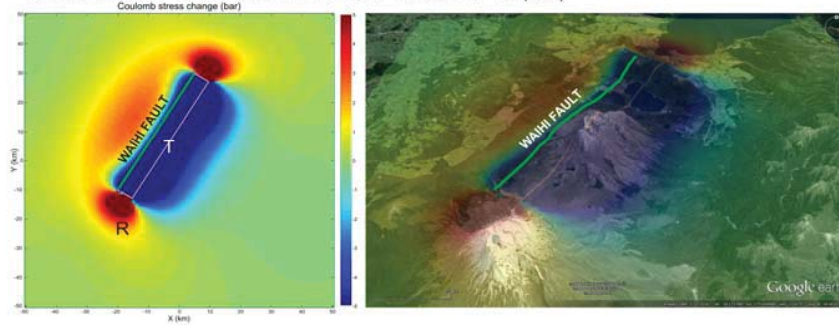
After running a sensitivity analysis, we deduce that resultant stress change models rely on the Coulomb software input parameters, which should be as close as possible to real conditions. Nevertheless, every model has uncertainties, not only due to measurement and data errors but also to assumptions on parameters and features such as constant conditions (probably not close to reality). For example, the Coulomb software only considers the co-seismic or co-intrusive stress change, but does not consider the background stress, in cases where the fault is close to the Coulomb failure or the magmatic system is in an over-pressured state.

There are other types of volcano-tectonic interactions that have not been examined, because of their complexity. Static stress was examined, but not dynamic stress. Static stress changes decay rapidly ($1/r^3$, where r is the distance from the earthquake epicentre), within hours to months from the initial earthquake, and they are limited to

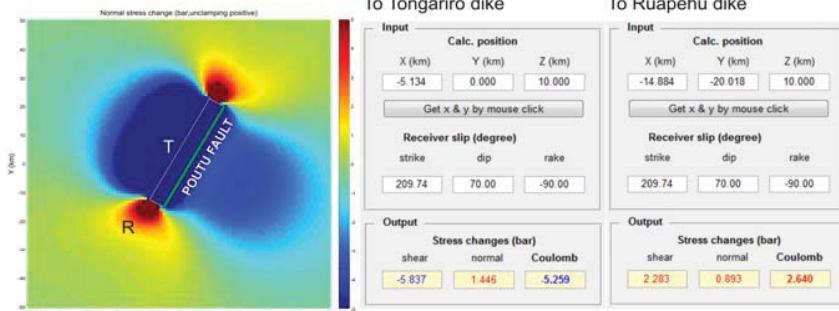
distances of just a few fault lengths [*Hill et al.*, 2002; *Manga and Brodsky*, 2006]. Dynamic stress changes decay more slowly ($1/r$), within years to centuries, and on longer distances from the rupture zone (up to ~ 1000 km) [*Manga and Brodsky*, 2006; *Hill*, 2008; *Watt et al.*, 2009]. Further, stress changes due to magma chamber inflation or deflation were not modelled, which could also cause stress changes in the crust around it and could promote fault ruptures; however, at the TgVC dike intrusion is likely to be the dominant mode.

Figure 43 (next page). Stress change models with different source faults. Red areas are positive, where the stress changes are likely to encourage a fault rupture or a dike intrusion on the receiver fault or dike. Green lines represent faults on surface and red lines represent faults at depth. A, Negative normal stress change on Ngāuruhoe and other dikes in the Tongariro Volcanic Complex, and positive normal stress change on Mt. Ruapehu after a Waihi Fault rupture (2 m slip). B, Positive normal stress change on the Tongariro Volcanic Complex dikes and Mt. Ruapehu after a Poutu Fault rupture (1.6 m slip). C and D, Positive Coulomb stress change on Rangipo, Upper Waikato Stream (UWS) and Ohakune faults after a Wahianoa Fault rupture (1 m slip). E, Negative normal stress change on Mt. Ruapehu after a Wahianoa Fault rupture (1 m slip).

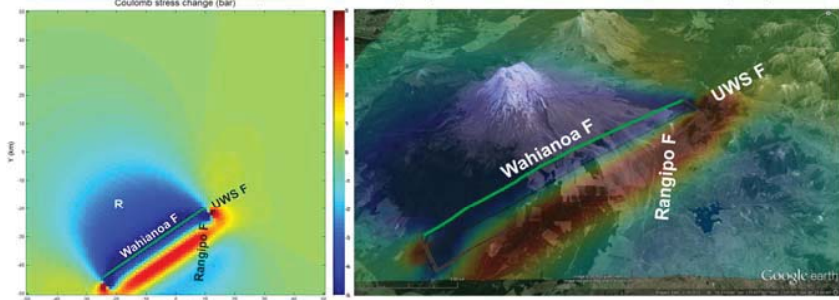
A. WAIHI FAULT TO PARALLEL DIKES, AT 10 KM DEPTH (030)



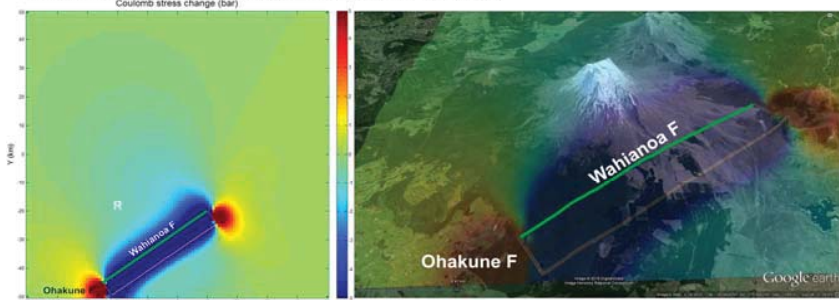
B. POUTU FAULT (210) TO DIKES (030)



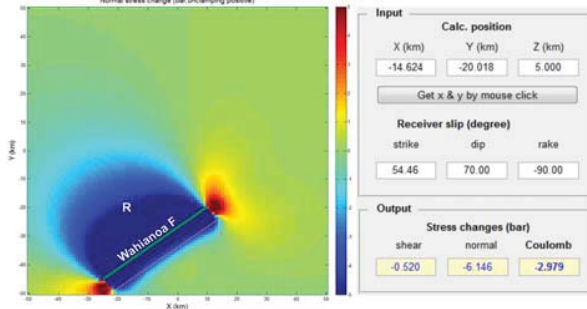
C. WAHIAHOA FAULT (054) TO RANGIPO (185) AND UPPER WAIKATO STREAM (229) FAULTS



D. WAHIAHOA FAULT (054) TO OHAKUNE FAULT (090)



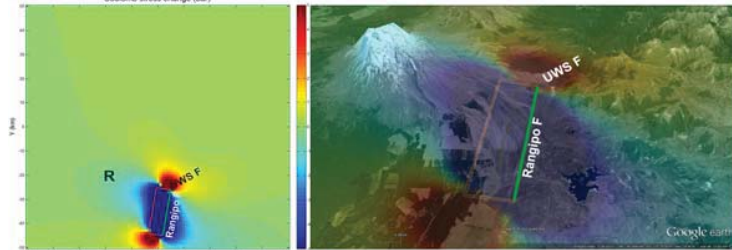
E. WAHIAHOA FAULT (054) TO RUAPEHU DIKE (030)



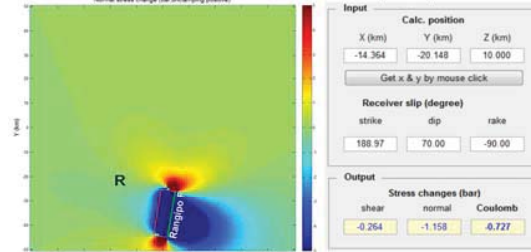
A. RANGIPO FAULT (185) TO WAHIANOA FAULT (054)



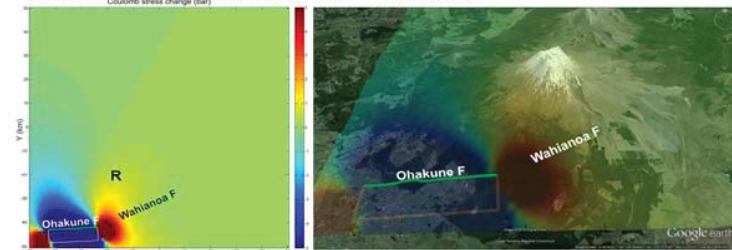
B. RANGIPO FAULT (185) TO UPPER WAIKATO STREAM FAULT (229)



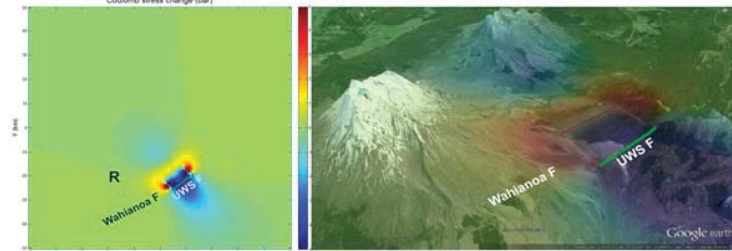
C. RANGIPO FAULT (185) TO RUAPEHU DIKE (030/90)



D. OHAKUNE FAULT (087) TO WAHIANOA FAULT (054)



E. UPPER WAIKATO STREAM FAULT (229) TO WAHIANOA FAULT (054)



F. UPPER WAIKATO STREAM FAULT (229) TO RANGIPO FAULT (185)

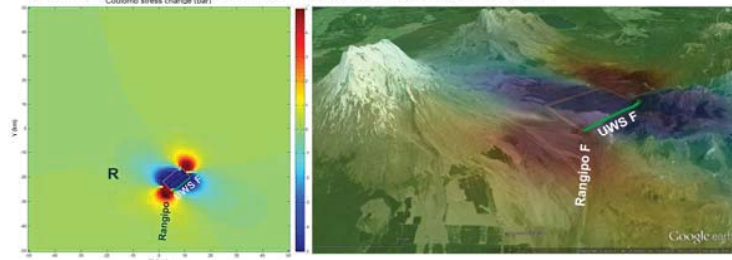


Figure 44. Stress change models from different source faults. A and B, Positive Coulomb stress change on Wahianoa and Upper Waikato Stream (UWS) faults after a Rangipo Fault rupture (1 m slip). C, Negative normal stress change on Mt. Ruapehu dike after a Rangipo Fault rupture (1 m slip). D, Positive Coulomb stress change on Wahianoa Fault after an Ohakune Fault rupture (1.2 m slip). E, Positive Coulomb stress change on the Wahianoa Fault after an Upper Waikato Stream Fault rupture (0.8 m slip). F, Positive Coulomb stress change on the Rangipo Fault after an UWS Fault rupture (0.8 m slip).

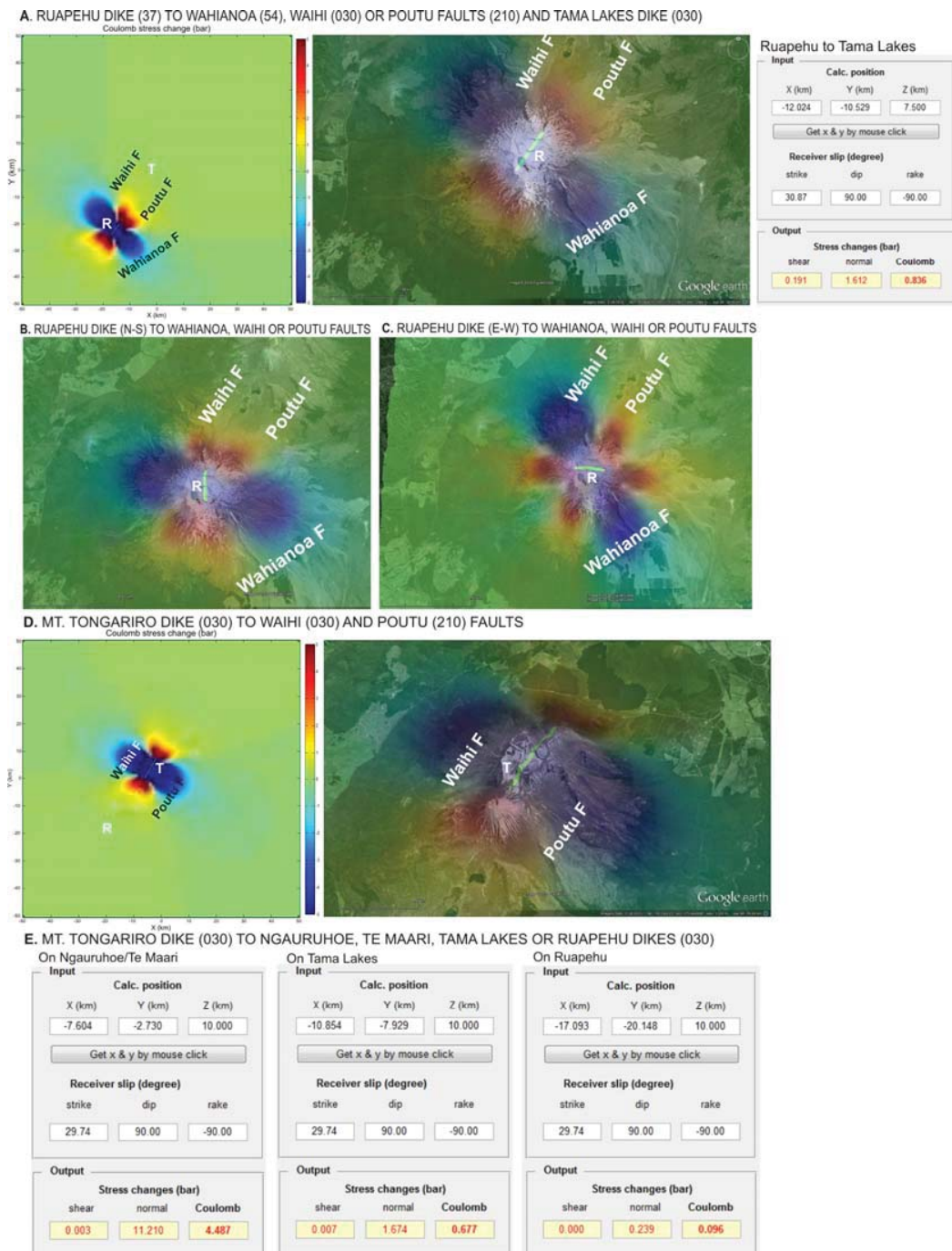


Figure 45. A, Negative Coulomb stress change on Wahianoa and southern Waihi faults, and positive stress change on southern Poutu Fault and Tama Lakes dikes after a NNE-SSW Ruapehu dike intrusion (1 m-wide). B, Positive stress change on southern Waihi and Poutu faults, southern Wahianoa Fault and Tama Lakes dikes, and negative stress change on northern Wahianoa Fault after a N-S Mt. Ruapehu dike intrusion. C, Positive stress change on Poutu Fault and Tama Lakes dikes, and negative stress change on Waihi and Wahianoa faults after an E-W Mt. Ruapehu dike intrusion. D, Positive Coulomb stress change on Waihi and Poutu faults after a NNE-SSW Tongariro Volcanic Complex dike intrusion (1 m-wide). E, Positive normal stress change on Ngāuruhoe, Te Maari, Tama Lakes and Ruapehu dikes after a Mt. Tongariro dike intrusion (1 m-wide).

		Receiver																		
		Dike						Receiver		Fault										
		Tongariro Volcanic Complex						Waihi whole	Waihi segment	Poutu whole	Poutu segment	Wahianoa	UWS	Raurimu	Ohakune	National Park	Rangipo			
		Ruapehu	Tama Lakes	Ngauruhoe	North Crater	Te Maari	Tongariro - Oturere	Pukekaikiore	Pukeonake	Waihi whole	Waihi segment	Poutu whole	Poutu segment	Wahianoa	UWS	Raurimu	Ohakune	National Park	Rangipo	
Source	Dike	Ruapehu																		
		Tama Lakes																		
		Ngauruhoe																		
		North Crater																		
		Te Maari																		
		Tongariro - Oturere																		
		Pukekaikiore																		
		Pukeonake																		
	Fault	Waihi whole																		
		Waihi segment																		
		Poutu whole																		
		Poutu segment																		
		Wahianoa																		
		UWS																		

Figure 46. Possible scenarios for dike-fault, dike-dike and fault-fault interactions by stress transfer in the Tongariro Volcanic Centre for the last 100 ka after evaluating the Coulomb and normal stress change models (Figs. 43-45), where the red colour denotes a positive stress change and the blue colour a negative stress change. See more information about the Waihi and Poutu faults segmentation in Chapter 6.

7.7 Discussion

In this section, possible integrated scenarios for volcano-tectonic interactions are presented, and an integrated model to explain rifting variations over the last ~100 ka in the TgVC is proposed.

7.7.1 Volcano-tectonic interactions by stress transfer

Specific periods with temporal associations between volcanic and tectonic activity in the TgVC include the following:

45-25 cal ka BP

There is a period of low volcanic activity (or small scale eruptions) in the Tongariro Volcanic Complex (Fig. 40). Mainly Mt. Ruapehu was active over this period [Cronin *et al.*, 1996b; Cronin and Neall, 1997]. This could be explained by a higher seismic activity, where the faults in the Tongariro Graben (Waihi, Poutu and Upper Waikato Stream faults) might have accommodated most of the extension for this period (Fig. 41). Another possible explanation for the low volcanic activity could be data scarcity, because there are many tephra in the eastern side of Mt. Ruapehu that have not been studied [Cronin and Neall, 1997; Gómez-Vasconcelos *et al.*, 2016]. The main problem in this time frame is that intense erosion during the Last Glacial Maximum eroded tephra from most parts of the ring plain, with a few remaining locations preserved (Cronin *et al.*, 1996). There could have been adjustment along the Waihi and Poutu faults as the Taupo system prepared for the Ōruanui eruption.

Mt. Ruapehu was very active in this period, which coincides with deceleration on the Wahianoa Fault, and acceleration on the Upper Waikato Stream and Rangipo faults (Fig. 41). Negative Coulomb stress changes suggest that Mt. Ruapehu dike intrusions

could stop or delay Wahianoa Fault ruptures (Figs. 45 and 46). Therefore Mt. Ruapehu, together with the Upper Waikato Stream and Rangipo faults, might have accommodated most of the extension in the Ruapehu Graben from 45 to 25 cal ka BP.

25-11 cal ka BP

Large eruptions from Mt. Ruapehu between 25-11 ka BP [Bullock Formation; 0.1 to 0.6 km³ of eruptive material each and >3 km³ in total; Fig. 40; *Pardo et al.*, 2012] are associated with deceleration of the Wahianoa and Upper Waikato Stream faults [*Gómez-Vasconcelos et al.*, 2016], and acceleration of the Rangipo Fault [Fig. 39; *Villamor et al.*, 2007]. Coulomb stress change models (Fig. 45) suggest negative stress should occur at the Wahianoa Fault after NNE-SSW and E-W dike intrusions from Mt. Ruapehu, which could delay or decelerate fault ruptures on this fault. So it is possible that during periods of cyclic large eruptions from Mt. Ruapehu, activity on the Wahianoa Fault is inhibited or slowed down. However, dike intrusions at Mt. Ruapehu do not decelerate the Upper Waikato Stream Fault nor accelerate the Rangipo Fault, because they are too far from Mt. Ruapehu (>15 km). Other causes need to be found to address the temporal associations between Mt. Ruapehu and these two faults.

In terms of fault-fault interactions, ruptures on the Rangipo Fault could promote ruptures on the Wahianoa and Upper Waikato Stream faults (Fig. 44A and 44B). However, in the 25-11 ka BP period, acceleration on the Rangipo Fault coincides with deceleration of the Wahianoa and Upper Waikato Stream faults (Fig. 39). Thus, the coincidence of acceleration of the Rangipo and deceleration of the Wahianoa and Upper Waikato Stream faults could be coincidental, or due to other processes.

To assess why the Rangipo Fault was accelerating during the 25-11 ka BP period, Coulomb stress change models were examined in the southernmost part of the rift. These models show a possible fault-fault interaction by static stress transfer between

the Ohakune, Wahianoa, Karioi, Upper Waikato Stream and Rangipo faults, where a rupture of any of these faults could promote rupture in any of the other faults, within <20 km (Figs. 43 and 44). There is not enough data to understand if other faults such as the Raurimu Fault were decelerating during this period. However, given the fault-fault interactions described for other sections of the rift [e.g., central Taupo Rift; Nicol *et al.*, 2010], it is possible that activity could migrate between faults so that certain faults can dominate during some periods, while others dominate in other periods. More paleoseismic data is needed to resolve this.

Mt. Ruapehu's greater volcanic activity during the 25-11 ka BP period also shows a temporal relationship with acceleration on the Waihi and Poutu faults (Fig. 39). This volcano-tectonic interaction could be explained by Coulomb stress transfer models (Fig. 45A, B and C), with a positive stress change from Mt. Ruapehu dike intrusions promoting ruptures on Waihi and Poutu faults, and vice versa. The Tongariro Volcanic Complex vents were less active in this period although large-volume eruptions from this centre are known between ~26 and 16.6 ka BP (Shane *et al.*, 2008). Static stress models suggest that while dike intrusions on Mt. Ruapehu could promote dike intrusion on the Tongariro Volcanic Complex vents, ruptures of Waihi and Poutu faults would inhibit them (Figs. 43 and 45). It is possible that the Waihi and Poutu faults dominated the crustal stress state during that period (and kept the dikes closed), or that magma was only available sporadically along the Tongariro Volcanic Complex at that time. Magma availability and state of unrest is another important control of the process that will dominate extension during different periods.

In summary, Mt. Ruapehu had high rates of explosive activity from 45 to 11 ka, helped by increased crustal stresses caused by the Waihi and Poutu faults, but also likely due to high rates of magma supply. Mt. Ruapehu dike intrusions negatively influenced the Wahianoa Fault, which had slow slip-rates during this period. Mt. Ruapehu high activity also coincides with high slip-rates on the Rangipo Fault. This relationship is not clear,

because Mt. Ruapehu is too far from the Rangipo Fault to influence each other's state of stress, thus any temporal association is likely to be coincidental, or it could relate to broader rift processes. Thus, Mt. Ruapehu and Rangipo Fault accommodated most of the extension at the Ruapehu Graben for this period.

Ground deformation or stress changes in the TgVC may be also caused by dike intrusions or magma chamber inflation or deflation from the Taupo caldera, ~50 km to the north. Evidence of these are the extensional fissures found in the Upper Waikato Stream [Donoghue *et al.*, 1995; Gómez-Vasconcelos *et al.*, 2016] and near Lake Rotoaira in the Poutu canal [Topping, 1973]. After a Taupo caldera dike intrusion, rupture of Waihi and Poutu faults could be promoted by positive Coulomb stress changes, similar to the fault-dike interactions suggested by Villamor *et al.* [2011] in the Okataina Volcanic Centre. Slip-rate acceleration on the Waihi and Poutu faults from 25 to 20 ka (Fig. 38) could have followed the caldera-forming Ōruanui eruption from Taupo caldera at 25.4 cal ka BP, to compensate for the sudden and significant regional rift extension.

While more field information and appropriate modelling of crustal stress changes associated with the Ōruanui eruption are needed, there seem to be volcano-tectonic interactions for this period following its eruption. In addition to the extension associated with the large eruptive volume of the Ōruanui, plus unknown arrested dikes, large crustal stress changes south of Lake Taupo, promoted rupture of the Waihi and Poutu faults for at least 5 ka after the eruption (Fig. 38). The Tongariro Graben faults slip-rate decelerated slightly but continued at elevated rates until 11 ka. Therefore, the Waihi and Poutu faults accommodated most of the extension in the Tongariro Graben from 25 to 11 cal ka BP. The high slip-rate of the Waihi and Poutu faults could have inhibited eruptions along the Tongariro Volcanic Complex, and/or there was not enough magma available along this section of the rift. The Upper Waikato Stream Fault showed slower

slip-rates during this period, probably because Waihi and Poutu faults were already accommodating most of the extension rate.

11-10 cal ka BP

During the Pahoka-Mangamate (PM) explosive eruption sequence at 11 cal ka BP [Nairn *et al.*, 1998], several vents in the Tongariro Volcanic Complex became active at the same time (Mt. Ruapehu, Tama Lakes, proto-Ngāuruhoe, Half Cone, North Crater and Te Maari; Fig. 41). These eruptions extruded a large volume of magma [at least 7 km³ during a period of 200 to 400 years; Fig. S11; Nairn *et al.*, 1998]. Nairn *et al.* [1998] inferred a period of accelerated regional extension due to the synchronous activity in the TgVC with a Taupo sourced rhyolitic eruption at 11.2 cal ka BP [Poronui tephra; Hajdas *et al.*, 2006]. This synchronous volcanic activity could be explained by stress transfer, where positive normal stress changes will occur at the tips of intruding dikes promoting adjacent dike intrusions of similar azimuth (Fig. 45). This could unzip the whole TgVC dike system, if there were magma available and the magmatic system was already over-pressured.

The PM volcanic sequence coincides with a slight deceleration in the Waihi and Poutu faults (Fig. 41). This interaction could be explained by Coulomb stress changes, as dike intrusions along the whole length of the TgVC will produce negative stress changes in these two faults. While individual dikes (e.g., intrusion of just the Mt. Tongariro dike; Fig. 45E) may cause positive stress at some areas along the fault planes, the unzipping of the whole TgVC would have a summed effect of causing negative stress in Waihi and Poutu faults (Figs. 43, 45 and 46). It seems that during this period, the Tongariro Volcanic Complex volcanism accommodated a larger percentage of the extension of the Tongariro Graben compared to other periods (note that fault slip-rate may still account for the largest component of the total extension).

Despite a potential trigger of Mt. Ruapehu dike intrusion from intrusions north of it during the Pahoka-Mangamate volcanic sequence, Mt. Ruapehu was not very active in this period, instead it marks the cessation of large-volume explosive eruptions at this centre and a transition to smaller-scaled events [e.g., *Donoghue and Neall, 2001; Moebis et al., 2011*]. This could be related to scarce magma availability or to a change in the conduit/vent dynamics, with Pardo et al. [2014] showing a shallowing of the magma system, followed by a move to a new southern vent (the current Crater Lake). A lack of high-magnitude explosive volcanic activity at Mt. Ruapehu coincides with acceleration in Wahianoa and Upper Waikato Stream faults (Fig. 41). Coulomb stress change models show a possible explanation for this, where a negative normal stress change suggests that Wahianoa Fault ruptures could stop or delay dike intrusions in Mt. Ruapehu (Figs. 43E and 46). Therefore, Wahianoa and Upper Waikato Stream faults might have accommodated a large part of the extension at this latitude along the Ruapehu Graben from 11 to 10 cal ka BP.

Historic cases

The normal stress change models show that a rupture of the entire Waihi Fault would not promote a dike intrusion in the Tongariro Volcanic Complex (Fig. 43A). However, if the Waihi Fault ruptures only in one segment, it might promote a dike intrusion in the Tongariro Volcanic Complex dikes north or south of the rupture (Fig. 46). This could have been manifest in the case of an eruption report at the Ketetahi area on northern Mt. Tongariro after the 1846 M_w 6.3 earthquake on Waihi Fault [*Scott and Potter, 2014*], a magnitude which is consistent with a single segment rupture of the fault [e.g., *Villamor et al., 2007; Stirling et al., 2012*].

Explosive eruptions from Ngāuruhoe in 1975 were associated with release of high-gas overpressures and large atmospheric shock waves [*Nairn and Self, 1978*], although it

did not promote a fault rupture or dike intrusion in the TgVC. This probably shows that the nearby faults and dike intrusions were not close to Coulomb failure or in an over-pressured state at that time.

7.7.2 Factors controlling volcano-tectonic interactions in the TgVC

Simultaneous short-term variations in tectonic (fault slip-rates) and volcanic activity in the TgVC could be influenced by two main factors: (1) stress transfer between adjacent faults and dike intrusions, or (2) fluctuations in magma input through time:

- 1) After an earthquake, the static stress changes in the neighboring 20 km could promote a new fault movement, if the receiver faults are close to the Coulomb failure threshold. Similarly, a dike intrusion could induce a dike intrusion within a 10-km radius, if the magma system was primed. For example, if an increase on the slip-rate of a fault is sustained during a certain period, stress changes around that fault may cause a sustained increase or decrease in dike intrusion rate (fault-dike interactions) or fault slip-rate of a nearby fault (fault-fault interaction).
- 2) The availability and overpressure state of magma will determine whether a dike will intrude into the crust and/or erupt. Dike intrusion or fault rupture in the vicinity can promote this dike to intrude (dike-dike and dike-fault interactions) if magma is available at the base or within the crust. Availability of magma in the TgVC will be strongly influenced by processes occurring in the mantle wedge of the subducting zone. The opening of a dike due to extension and promotion by nearby faults and dikes can bring magma to unrest, or allow magma already stored in crustal reservoirs to intrude and erupt. However, the process controlling the availability of that magma needs to be more deeply explored.

In the last 1.5 Ma, regional crustal extension in the Taupo Rift has been constant [Nicol and Wallace, 2007]. In tectonic sections of the rift, fault-fault stress interactions have been invoked to explain short-term variability of fault slip-rate [e.g., Mouslopoulou et al., 2009; Nicol et al., 2010]. This fault slip-rate becomes near-constant when summed across all faults of that section of the rift and for periods that are longer than 20 ka [Nicol et al., 2010]. However, in sections of the rift where extension is also accommodated by dike intrusion, the magma input and magma volume emplaced has varied through time. In volcanically active sections, such as the TgVC, tectonic input must adapt, explaining the acceleration or deceleration on some faults during a certain period (Fig. 47).

As suggested in Chapter 5, extension in the Tongariro Graben is almost entirely driven by tectonic faulting and normal faults accommodate 78-95% of extension. It is probable that this percentage varies in time depending on magma input availability (Fig. 47).

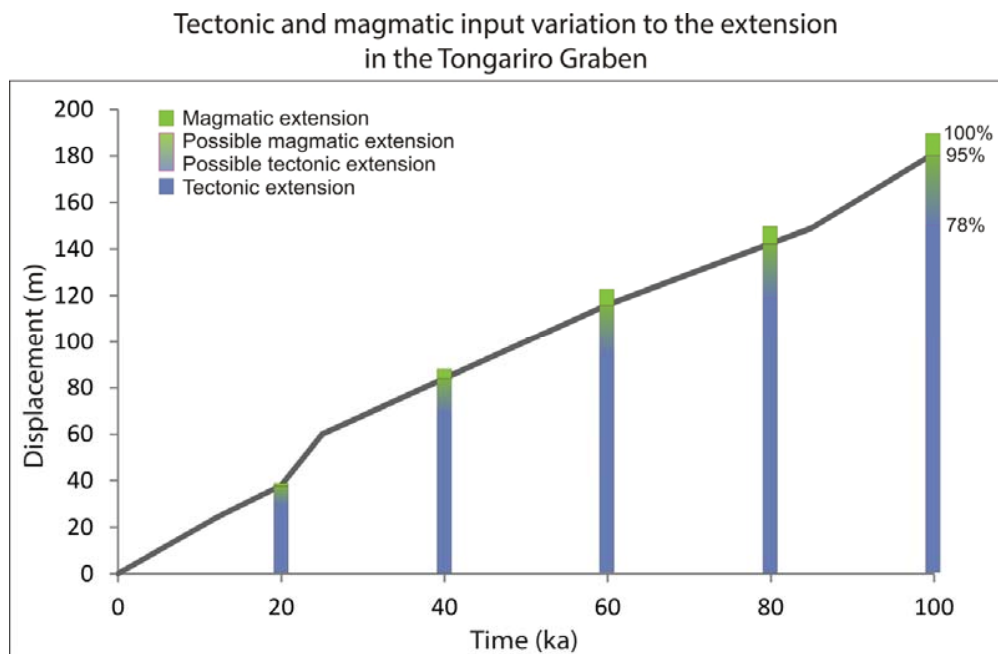


Figure 47. Combination of tectonic and magmatic extension in the Tongariro Graben. Fault slip-rate variation could be explained by different tectonic and magmatic input to the total extension. Input can fluctuate through time but total extension remains constant. Magmatic input could vary from 22 to 5% and tectonic input from 95 to 78% of the total extension (Chapter 5).

Rowland et al. (2010) suggested that in the TgVC seismic cycles are not periodic and hence unpredictable. Here it is proposed that cycles could be defined by the recurrence of magma input (magma availability) into the system (here defined by volcanic eruptions and possibly non-eruptive dike intrusions). A better understanding of the predictability of this magma input can help to assess the balance between tectonics and volcanism at different periods, and representative modes of fault-volcano interactions.

In this study, a great acceleration is shown on the Waihi and Poutu faults around 25 cal ka BP in association with the voluminous ($>500 \text{ km}^3$) Ōruanui eruption from the nearby Taupo caldera [Wilson et al., 2006]. In the periods between such major rhyolitic eruptions, variability may be influenced solely by availability of comparatively small volumes ($<1 \text{ km}^3$) of andesitic magma, thus, the variability of slip-rates may be small or short-lived. For the periods in between the huge rhyolitic eruptions, brief pulses of high magmatic supply rates at both TgVC and Taupo caldera, could explain coincident pulses of activity, e.g., the Pahoka-Mangamate + Poronui sequence (unzipping event, see below), that need to be taken into account in seismic-magmatic cycles.

In summary, to better understand tectono-volcanic cycles in the TgVC, improved information on eruptive volumes and event frequency are needed. Volcanic eruptions that could influence TgVC faults can include: (1) small to moderate eruptions from the Tongariro Volcanic Complex and Mt. Ruapehu with local impacts, (2) many large eruptions in a short period that combined form an “unzipping event”, and (3) extremely large-volume (major) eruptions from Taupo Caldera. The mean long-term magma extrusion rate in the TgVC is $\sim 0.8 \text{ km}^3/\text{ka}$ (Chapter 5) to $1 \text{ km}^3/\text{ka}$ [Cronin et al., 1996b]. An average volume for small to moderate eruptions in the Tongariro Volcanic Centre is around 0.2 km^3 (Hobden et al., 1999; Moebis et al., 2011; Pardo et al., 2012; Topping et al., 1973), leading to a recurrence rate of ~ 4 to 5 eruptions per thousand years. An unzipping event may produce larger volumes, e.g, 7 km^3 [Nairn et al., 1998] or 10 km^3

[Hobden *et al.*, 1996]. Therefore, an unzipping event could occur every ~10 to 15 ka. Major eruptions like the Taupo eruption at 1.7 cal ka BP [Hogg *et al.*, 2011], with a volume of ~105 km³ [~35 km³ dense-rock equivalent; Wilson *et al.*, 2009] or Ōruanui eruption from Taupo caldera at 25.4 cal ka BP [Vandergoes *et al.*, 2013], with a volume of ~500 km³ [Wilson *et al.*, 2006], could occur every 25 to >50 ka.

7.7.3 Implications for natural hazards

The resultant possible scenarios for volcano-tectonic interactions could be considered as possible cascading effects after a volcanic eruption, or an earthquake in the TgVC, which would pose an important hazard to this region. Historical examples of these are the 1846 M_w 6.3 earthquake in the northern Waihi Fault, which caused landslides in the SW shore of Lake Taupo [e.g., Little Waihi village landslides in 1846 and 1910; Hegan *et al.*, 2001; Cooper, 2002], and possibly a small eruption in Ketetahi [Scott and Potter, 2014].

A potential future case could be a Mt. Ruapehu dike intrusion (NNE-oriented dike), promoting a dike intrusion in the Tongariro Volcanic Complex, with volcanic unrest or an eruption. A Mt. Ruapehu dike intrusion could promote a fault rupture in the Waihi or Poutu faults, which could trigger landslides. Another potential case could be a Wahianoa Fault rupture, which can promote ruptures in the Rangipo, Upper Waikato Stream and Ohakune faults, at a worst case, generating a M_w ~7.0 earthquake [Gómez-Vasconcelos *et al.*, 2016].

7.7.4 Limitations of this study

The main limitations of this study are the temporal resolution, completeness of eruptive volume information and paleoseismic data. Reflecting on this, the following limitations of the results must be considered:

- A fault rupture may promote a dike intrusion, which may be arrested or erupt. Prehistoric arrested dikes cannot be quantified, because they are not in the geological record.
- Not all the volcanic eruptions are dated and mapped (nor even equally preserved on the ring plain due to variations in physical weathering in relation to paleoclimatic variations). Further, not all paleoseismic events are well constrained in time or space.
- Magma volumes are not always well known, and some lava formations (e.g., Wahianoa Formation) imply large magma volumes ($>45 \text{ km}^3$) over very long periods (e.g., $>50 \text{ ka}$), which adds imprecision to the analysis.
- Differences between Mt. Ruapehu and the Tongariro Volcanic Complex were not addressed. The Tongariro Volcanic Complex shows linear extension with parallel faults, while Mt. Ruapehu shows radial extension and different fault orientations (NNE-SSW, N-S or NE-SW and E-W). Also, Mt. Ruapehu's volcanic load [large dimension and density, $>110 \text{ km}^3$; *Gamble et al.*, 2003] could modify the local stress field, the fault orientation and magma ascent beneath the volcano.
- The location of the magma source is not well constrained. Petrological and seismic studies suggest that there is a shallow magma chamber beneath Mt. Ruapehu at ~ 5 to 7 km depth [*Nakagawa et al.*, 1999; *Miller and Savage*, 2001]. The magma supply of the Tongariro Volcanic Complex could be between 10 and 15 km depth, at the lower limit of the seismogenic crust [*Hurst and McGinty*, 1999; *Hayes et al.*, 2004; *Stirling et al.*, 2012], with a range of magma supply depths between 5 and 15 km . However, between these depth ranges the stress changes are highly variable (Fig. 48). These uncertainties make it difficult to define if a dike intrusion would be promoted by stress changes in nearby structures.

- Taupo caldera or other calderas north of the study area were not modelled because more data were needed, but they are certainly relevant to understand the cycles in the TgVC. The interactions mentioned between the TgVC and Taupo caldera were inferred via coincident timing of events alone.

7.8 Conclusions

Short-term variations for the last 100 ka in fault slip-rates and volcanic activity in the TgVC could be influenced by static stress transfer between adjacent faults (within <20 km from the source) and dike intrusions (within <10 km), or by fluctuations in magma input availability through time. Fault slip-rates in the TgVC are near-constant when all the faults are summed across a section of the rift, but individual fault slip-rates are very variable, especially in sections of the rift where extension is also accommodated by dike intrusion because of the magma input variation. In those sections, such as the TgVC, in order to keep the extension constant in the long-term the tectonic input has to adapt, explaining the acceleration or deceleration in some faults during a certain period. The amount of magma assisting the rifting process will condition the predominant extension mechanism and thus the predominant type of fault-volcano interaction. Therefore, magma volumes and their frequency have to be considered to better understand the volcanic and seismic cycles.

A high slip-rate period between 25 and 11 cal ka BP in the Waihi and Poutu faults could have been promoted by stress transfer after the Ōruanui eruption at 25.4 cal ka BP. This accelerated period could have reduced volcanic activity in the Tongariro Volcanic Complex vents by normal stress changes. During this period, the Upper Waikato Stream Fault was slow, therefore Waihi and Poutu faults probably accommodated most of the extension of the Tongariro Graben during that period.

Mt. Ruapehu had high rates of activity from 45 to 11 ka, possibly helped by increased crustal stresses caused by the Waihi and Poutu faults. At the same time, Mt. Ruapehu dike intrusions influenced negatively the Wahianoa Fault. Therefore, Mt. Ruapehu and Rangipo Fault may have accommodated most of the extension during this period.

At 11 cal ka BP, several vents in the Tongariro Volcanic Complex became active at the same time (unzipping event), coinciding with deceleration in the Waihi and Poutu faults, possibly caused by negative stress changes from the dike intrusions. Here it is considered that the Tongariro Volcanic Complex volcanism accommodated a larger percentage of the extension of the Tongariro Graben, compared to other periods. Despite a potential trigger of Mt. Ruapehu eruptions from intrusions north of it during this period, it was not very active and instead went into a period of rapidly declining size and volume of eruptions, along with a vent system change. The Wahianoa and Upper Waikato Stream faults might have accommodated a large part of the extension of the Ruapehu Graben from 11 to 10 cal ka BP.

The resultant possible fault-fault, dike-fault and dike-dike interactions in the southern Taupo Rift could be considered as possible cascading effects after a certain volcanic eruption or an earthquake in the TgVC, which would pose an important hazard to the region.

CHAPTER 8. CONCLUSIONS:

Understanding mechanical coupling between volcanic unrest and large earthquakes in the Tongariro Volcanic Centre

This chapter presents a synthesis of the thesis, and revisits the findings of the research in relation to the aims expressed in Chapter 1. The distinctive characteristics of this work have been to elucidate aspects of the southern Taupo Rift and apply a range of methods to answer questions around volcano-tectonic interactions that are important from a hazard perspective, but very difficult to quantify with precision.

8.1 Summary

The southern Taupo Rift, represented by the Tongariro Volcanic Centre, hosts both andesitic and basaltic volcanoes coexisting with normal faults of the Ruapehu and Tongariro grabens. The Ruapehu Graben is located at the southernmost part of the rift, where Mt. Ruapehu occupies the axis of the graben, surrounded by faults with N-S, E-W, NE-SW and NNE-SSW strikes. To the north, the Tongariro Graben contains the NNE-aligned volcanic vents from the Tongariro Volcanic Complex at the axis of the graben, closely bounded by parallel inward-dipping faults.

This thesis extends the mapping of active faults in the Tongariro Volcanic Centre and adds information on fault characterisation for hazard assessment. For the first time, the Upper Waikato Stream, Wahianoa, Waihi and Poutu faults rupture histories are studied. Specifically results allow updates of potential earthquake rupture scenarios for the National Seismic Hazard Model of New Zealand:

- The Upper Waikato Stream Fault is a 15-km-long NNE-striking normal fault downthrown to the NW, and a previously unrecognised seismogenic source at the eastern boundary of the Ruapehu Graben. This fault is capable of producing

a M_w 6.5 earthquake, with a recurrence interval between 1.6 and 3.5 ka, and a mean slip-rate of 0.5 ± 0.06 mm/yr in the last 45 ka.

- The Wahianoa Fault is a 15-km-long NE-striking normal fault downthrown to the SE, located at the southeastern flank of Mt. Ruapehu. This system is capable of producing a M_w 6.8 earthquake if it ruptures together with the Upper Waikato Stream Fault, with a recurrence interval between 2.4 and 13.6 ka, and a mean slip-rate of 0.2 ± 0.3 mm/yr in the last 133 ka.
- A conceivable 43-km-long rupture in this region could involve the Rangipo, Upper Waikato Stream and Kaimanawa faults moving together. Such a scenario would be capable of producing a M_w 7.1 earthquake with a single-event displacement of 2.4 m.
- The Waihi Fault is a 38-km-long NNE-striking normal fault downthrown to the SE, at the western flanks of the Tongariro Volcanic Complex. This large system is capable of producing a M_w 7.0 earthquake, with a recurrence interval of 1.0 ka, and has displayed a mean slip-rate of 2.6 ± 0.8 mm/yr in the last 85 ka. A potential 52-km-long rupture involves the Waihi Fault, together with the fault at the southwestern boundary of Lake Taupo. This combined rupture is capable of producing a M_w 7.2 earthquake with a single-event displacement of 2.9 m. The Waihi Fault could also rupture in two possibly separate segments: the northern segment is 20 km long (M_w 6.6); and the southern segment is 18 km long (M_w 6.7).
- The Poutu Fault is a 30-km-long NNE-striking normal fault downthrown to the NW, at the eastern flanks of the Tongariro Volcanic Complex. It is capable of producing a M_w 6.9 earthquake, with a recurrence interval of 0.9 ka, and has displayed a mean slip-rate of 2.2 ± 1.9 mm/yr over the last 100 ka. The Poutu Fault may also rupture in two independent segments: the northern segment is 18 km long (M_w 6.3) and the southern segment is 15 km long (M_w 6.3).

The co-location of faults and volcanoes in the Tongariro Volcanic Centre has always raised the question of their possible interactions. This thesis provides a step towards the understanding of volcano-tectonic interactions in this area. An attempt was made to quantify the magmatic and tectonic contribution to the regional extension and to analyse the potential link between them. This part of the study found:

- All the faults in the Tongariro Volcanic Complex are of tectonic origin and are not likely to be dike-extension driven faults. However, stress transfer in this system could trigger a new fault rupture after a dike intrusion within 20 km, if the fault is close to Coulomb failure. Conversely, a new fault rupture could trigger an intrusion within 10 km if the magmatic system is in an over-pressured state.
- Fluctuations in magma volumes (input) through time could modify the magmatic and tectonic contribution to the total crustal extension, changing the natural behaviour of seismic and volcanic cycles in the Tongariro Volcanic Centre. In the Tongariro Graben, individual fault slip-rates are very variable in the last 100 ka, with event recurrence intervals between 0.7 and 3.8 ka, and a co-seismic slip between 1 and 73 m.
- Of the total geodetic extension in the Tongariro Graben (7.4 mm/yr), it has been calculated that 78 to 95% is accommodated by normal faulting and only 5 to 22% by dike intrusions. Of the intrusion-based extension, 4 to 5% results in volcanic eruptions and the remaining 18 to 19% are probably arrested dike intrusions. Some of this extension could also be hybrid, involving both arrested magma and eruptions.

Volcano-tectonic settings are complex, not least due to the difficulty of gaining precise data on fault motion events, volumetric eruption rates and eruption ages. This work has shown, despite some uncertainties in the data, that static stress transfer can be of great importance in volcanic and seismic unrest in continental rifts. Here the ideas

developed about these interactions help to visualize and understand spatio-temporal associations between tectonic and volcanic activity, both locally and globally.

8.2 Tongariro and Ruapehu grabens

Ruapehu and Tongariro grabens are located at the southernmost end of a rift, where extension gives way to compression. Their geomorphology is similar to other magmatic rifts, but their main surface expression has been shown to be essentially tectonic. These grabens differ from other sections of the Taupo Rift in having intermediate rates (see below) of magma intrusion, while other segments are non-magmatic or involve large magma volumes and caldera systems.

- (1) The Tongariro Volcanic Centre is located at the southern termination of the Taupo Rift, where extension decreases to zero and gives way to compression only ~20 km to the south [Wallace *et al.*, 2004]. The southernmost volcano of the Taupo Volcanic Zone is Mt. Ruapehu, a stratovolcano surrounded by faults in almost every direction, because the extension is radial [Villamor and Berryman, 2006a]. This process can be explained by rapid tectonic block rotation and the transition from subduction to collision [Wallace *et al.*, 2005]. The subducting Pacific Plate, at the Hikurangi Margin, collides with the Chatham Rise (continental fragment), creating a rotating axis and ending the subduction process at the southern Taupo Rift [Wallace *et al.*, 2005].
- (2) The Tongariro Volcanic Complex comprises NNE-aligned vents bounded by parallel faults. The faults initiate scarcely ~2 km from the axis of the Tongariro Graben. Normally when they are so close to the volcanic vents, they are connected and normal faulting can be the reflection of repeated dike intrusions [e.g., Opheim and Gudmundsson, 1989; Stein *et al.*, 1991; Wright *et al.*, 2006], but in the Tongariro Graben, faulting appears from the results presented here,

to be the result of pure tectonic or hybrid extension. Hybrid extension is a tectonic rupture associated with large earthquakes, but promoted by deeply arrested dikes (Chapter 5).

- (3) Another distinctive characteristic of the southern Taupo Rift is how the volcanic style and tectonic regime vary over only a very short distance. In the central TVZ the seismogenic crust is only 6-10 km thick and large calderas occur [Bryan *et al.*, 1999]. There are also areas with cold crust, where extension is mainly controlled by tectonic faults, and areas with hot crust, where extension is mainly controlled by dike intrusions. In the southern Taupo Rift, south of Lake Taupo, the seismogenic crust is 15 km thick [Hurst and McGinty, 1999]. Here, hot and cold crust co-exists at the same latitude, but the extension is mainly tectonically controlled. In the TVZ, extension decreases gradually to the south [Wallace *et al.*, 2004]. Changes in volcanic and tectonic styles happen at accommodation zones along the rift [Rowland *et al.*, 2010], together with extension rate changes .

8.3 Methodologies used: advantages and disadvantages

A variety of methods were used for this study to gather quantitative data for comparison of volcanic and tectonic information; some were more successful than others.

Terrestrial Laser Scanning (TLS)

In the Upper Waikato Stream TLS techniques were used (Chapter 4) to measure the displacements of almost every single deposit along a long sequence of semi-continuous outcrops in fine detail, including places difficult to reach by foot. TLS allows

creation of 3D models and rich data sets of the study location, which are very useful to measure subtle changes in the morphology. A TLS survey is relatively fast, depending on the resolution, but is not a method suitable for regional studies. To scan a 20 x 60 m area, ~1 hour is needed to produce point clouds at 2 and 4 cm spacing at c. 30 m distance, giving a 0.03 m resolution DEM. A further disadvantage of using this technique is that it is very expensive and a specialist is needed to process the data.

Real Time Kinematic (RTK) GPS

RTK GPS is a widespread precision positioning technique for simple and accurate fault scarp measurements; it is lightweight to carry in the field and now corrected positions can be accessed via cell phone signal without the need for base-station setup. The measurements are more accurate than hand-held GPS and data can be exported very easily to a computer in almost any file type. This technique was used in the Tongariro Graben (Chapters 5 and 6) and its only limitation is in areas where cell phone signal is unobtainable.

Coulomb software

Coulomb modelling was very useful in this study to help to understand the static stress changes in the crust and to investigate possible scenarios for volcano-tectonic associations by stress transfer. The software used is a free application and runs with Matlab. It is easy to use and interesting 3D models can be created with it. However, like any model, many assumptions have to be made, the most important of which is assuming a homogeneous crust or that constant parameters exist in the modelled areas, which do not represent real conditions (Chapter 7).

Volcanic Paleoseismology using geomorphic displacements and field outcrops

Without a high density of fault plane outcrops, or paleoseismic trenches, surface deformation of dated landscape surfaces is needed to quantify fault displacements, particularly if different deposits of variable age are transected by faults. Uncertainties of this method are high depending on the precision of the age determinations of the surfaces (which are sometimes highly approximate), and the topographic information used to measure the offsets. In this study, a 2-m resolution digital surface model was used, thus the measurement error is not very large, but the age information is sometimes of low quality.

Identifying scarp profiles accurately also depends on the age of the displaced surface, the erosion and depositional processes, recurrence of seismic activity and regional evolution. To understand the morphology and take advantage of it as a paleoseismic tool requires detailed morphological observations.

8.4 Fulfilment of study objectives and additional contributions

Specific contributions

The findings of this thesis help to improve the current characterization of seismic and volcanic potential of active faults in the southern Taupo Rift (addressing objective VIII):

- A summary of volcanic activity, magma volumes and frequency of volcanic activity for the last 100 ka is presented, addressing objective I. This work compiles literature on the volcanic history in the TgVC (Table S10), and evaluates the location, frequency and volume of volcanism. Dike intrusions are also revised; their dimension, frequency and potential deformation at the surface are evaluated (chapters 5 and 7). An average dike size of 2-km-long and 1-m-wide is estimated from historic and prehistoric eruptions in the TVZ. If

the intrusive to extrusive magma volume ratio of 5 to 1 [*White et al.*, 2006] is applied to the Tongariro Volcanic Complex dikes, there would be 4 eruptions and 20 arrested intrusions per thousand years.

- This work improves the Quaternary tectonic history of the faults in the southern TVZ, addressing objective II. The paleoseismic history of the Wahianoa, Upper Waikato Stream (Chapter 4), Waihi, and Poutu faults (Chapter 5) is reconstructed using paleoseismological and tectonic geomorphology methods. New and existing structural data are compiled: rupture histories and fault slip-rates of the main faults are revised for the last 100 ka (Chapter 7).
- An improved fault database and map of the southern Taupo Rift was created, addressing objective II, where regional faults were identified, mapped, described and classified (supplementary file). The Upper Waikato Stream Fault and many fault strands of the Waihi and Poutu faults were identified as new seismic sources that can be added to the National Seismic Hazard Model. Also, the new and updated fault slip-rates can be used to update the current National Seismic Hazard Model (objective V).
- Spatio-temporal associations between fault ruptures and volcanic eruptions are studied, addressing objectives III and IV. Variations in magma volume, recurrence and location are compared with seismic displacement, slip-rate, magnitude, recurrence and location (Chapter 7). Possible scenarios for volcano-tectonic interactions from field data are identified and compared to theoretical models to explain these interactions. Static stress changes after a dike intrusion could promote a new fault rupture <20 km from the source, if the fault is close to Coulomb failure. Conversely faults could generate nearby (<10 km) magma intrusions if the magma is in a ready state. Stress transfer in the crust might be responsible, at least in part, for the variations in tectonic and magmatic rates observed in the last 100 ka for the Tongariro Volcanic Centre (Chapter 7). Input of magma from processes in the mantle wedge of the

subduction zone is acknowledged as a further strongly controlling factor on spatio-temporal associations between fault ruptures and volcanic eruptions. However, this could not be addressed by the present study. Rifting processes tend to be episodic, where the amount of magma assisting the rifting process will condition the predominant extension mechanism and thus the predominant type of fault-volcano interaction. Therefore, magma volumes and their frequency have to be considered to better understand the volcanic and seismic cycles.

- Faults in the TgVC are evaluated for tectonic or magmatic origin, addressing objectives II and III. This is of importance for seismic hazard evaluation (objective V), because the seismic hazard can be overestimated in dike intrusion related faults. Displacements along faults associated with shallow arrested dikes do not follow the traditional scaling relationships [e.g., *Wells and Coppersmith*, 1994], as they display large offsets for small earthquakes. However, in the TgVC, the seismic hazard is probably underestimated, because faults are not associated with shallow arrested dikes, but are of tectonic origin. Long-term surface displacement presented by the TgVC faults is associated with tectonic faulting, either pure tectonic or hybrid extension. The term hybrid extension is defined here for seismogenic fault ruptures that are promoted by deeply arrested dikes. Dikes intruding at 15 to 10 km depth could generate positive Coulomb stress changes above them and promote tectonic faulting (Chapter 5). Therefore, to assess seismic hazard in the region, tectonic and hybrid extension have to be taken into account.
- The extension accommodated by normal faults and by dike intrusions is evaluated, addressing objective III. The total present-day geodetic extension [7.4 mm/yr; *Wallace et al.*, 2004] is compared with the geological extension rate at seismogenic depth in the Tongariro Graben (7 ± 1.2 mm/yr; this study). Normal faults accommodate 78-95% (5.8-7.0 mm/yr) of the total extension and

dike intrusions 5-22% (0.4-1.6 mm/yr), from which 4-5% is of volcanic eruptions and 18-19% of arrested dike intrusions (Chapter 5).

8.5 Future challenges

Volcanic and seismic activity in the TgVC and the southern Taupo Rift poses many additional questions and areas of study.

- It is important to clarify the exact vent location of certain eruptions, the creation (and extinction) of volcanic vents, and/or the reactivation of older volcanic systems in order to understand spatio-temporal fault-volcano interactions.
- Improving the knowledge of the dimensions of intruding dikes in this area would tell us how much extension is achieved by dike intrusion. Also, it would improve the results of the stress transfer models, since dike width is one of the input parameters.
- It would be very helpful to know if there is a relationship between eruptive volume and amount of extension, or the influence of volcanic load in vent or fault location in the TgVC.
- The 2-m resolution digital surface model (DSM) used in this study is adequate, but vegetated areas proved problematic. There are still some faults (Raurimu and National Park faults) and volcanoes (Pihanga, Kakaramea-Tihia) that are poorly studied, mainly because of the vegetation in the western and northern parts of the TgVC. Also, the DSM is not precise enough to measure scarps <2 m high. LiDAR data could be used to solve this problem.
- Geodetic extension values taken from Wallace et al. [2004] have not been updated with slip-rates for the TVZ. Therefore, new geodesy data are needed (e.g., InSAR) together with geodynamic modelling to improve the modelling results.

- Coulomb models are used to evaluate the static stress changes in the TgVC, which is just one type of volcano-tectonic interaction. Dynamic or quasi-static stress changes should be also considered, which are likely to act on longer timescales and on longer distances from the source.
- The normal stress on faults is unknown (Coulomb failure criterion), as well as magma pressure states in the critical areas of the crust in this region that influence tectonic motion or dike rise.
- More paleoseismic trenches are needed in the southern Taupo Rift in order to have a more complete seismic history and assess fault segmentation and particularly to address the transition between the Tongariro Graben and the major caldera system to the north.

REFERENCES



- A., T. R. G. D. V. P. R. C. R. (2004), Incipient rifting at the southern termination of the Taupo volcanic zone from gravity data., *Geological Society of New Zealand Miscellaneous Publication*, 117A: 106.
- Abdallah, A., V. Courtillot, M. Kasser, A.-Y. Le Dain, J.-C. L epine, B. Robineau, J.-C. Ruegg, P. Tapponnier, and A. Tarantola (1979), Relevance of Afar seismicity and volcanism to the mechanics of accreting plate boundaries, *Nature*, 282(5734), 17-23.
- Acocella, V., and M. Neri (2009), Dike propagation in volcanic edifices: overview and possible developments, *Tectonophysics*, 471(1), 67-77.
- Acocella, V., K. Spinks, J. Cole, and A. Nicol (2003), Oblique back arc rifting of Taupo Volcanic zone, New Zealand, *Tectonics*, 22(4).
- Aki, K., and P. Richards (1980), *Quantitative Seismology—Theory and Methods* Freeman, New York.
- Allan, A. S., D. J. Morgan, C. J. Wilson, and M.-A. Millet (2013), From mush to eruption in centuries: assembly of the super-sized Oruanui magma body, *Contributions to Mineralogy and Petrology*, 166(1), 143-164.
- Anderson, E. M. (1905), The dynamics of faulting, *Transactions of the Edinburgh Geological Society*, 8(3), 387-402.
- Bacon, C. R. (1982), Time-predictable bimodal volcanism in the Coso Range, California, *Geology*, 10(2), 65-69.
- Baer, G., Y. Hamiel, G. Shamir, and R. Nof (2008), Evolution of a magma-driven earthquake swarm and triggering of the nearby Oldoinyo Lengai eruption, as resolved by InSAR, ground observations and elastic modeling, East African Rift, 2007, *Earth and Planetary Science Letters*, 272(1), 339-352.
- Bagge, M., and A. Hampel (2015), Three-dimensional finite-element modelling of coseismic Coulomb stress changes on intra-continental dip-slip faults, *Tectonophysics*.
- Barrientos, S. E. (1994), Large thrust earthquakes and volcanic eruptions, in *Shallow Subduction Zones: Seismicity, Mechanics and Seismic Potential*, edited, pp. 225-237, Springer.
- Beanland, S. (1995), The North Island dextral fault belt, Hikurangi subduction margin, New Zealand, *Unpublished PhD thesis, Victoria University of Wellington, Wellington, New Zealand*.

- Beanland, S., K. R. Berryman, and G. H. Blick (1989), Geological investigations of the 1987 Edgecumbe earthquake, New Zealand, *New Zealand Journal of Geology and Geophysics*, 32(1), 73-91.
- Bebbington, M., S. J. Cronin, I. Chapman, and M. B. Turner (2008), Quantifying volcanic ash fall hazard to electricity infrastructure, *Journal of Volcanology and Geothermal Research*, 177(4), 1055-1062.
- Benedetti, L., I. Manighetti, Y. Gaudemer, R. Finkel, J. Malavieille, K. Pou, M. Arnold, G. Aumaître, D. Bourlès, and K. Keddadouche (2013), Earthquake synchrony and clustering on Fucino faults (Central Italy) as revealed from in situ ³⁶Cl exposure dating, *Journal of Geophysical Research: Solid Earth*, 118(9), 4948-4974.
- Benoit, J. P., and S. R. McNutt (1996), Global volcanic earthquake swarm database and preliminary analysis of volcanic earthquake swarm duration.
- Berryman, K., P. Villamor, and R. V. Dissen (2006), Volcano-tectonic interactions in a rhyolite domain: the Taupo Volcanic Zone, New Zealand, paper presented at Geophysical Research Abstracts.
- Berryman, K., P. Villamor, I. Nairn, R. Van Dissen, J. Begg, and J. Lee (2008), Late Pleistocene surface rupture history of the Paeroa fault, Taupo rift, New Zealand, *New Zealand Journal of Geology and Geophysics*, 51(2), 135-158.
- Bibby, H., T. Caldwell, F. Davey, and T. Webb (1995), Geophysical evidence on the structure of the Taupo Volcanic Zone and its hydrothermal circulation, *Journal of volcanology and geothermal research*, 68(1), 29-58.
- Biggs, J., F. Amelung, N. Gourmelen, T. H. Dixon, and S.-W. Kim (2009), InSAR observations of 2007 Tanzania rifting episode reveal mixed fault and dyke extension in an immature continental rift, *Geophysical Journal International*, 179(1), 549-558.
- Blake, S. (1984), Magma mixing and hybridization processes at the alkalic, silicic, Torfajökull central volcano triggered by tholeiitic Veidivötn fissuring, south Iceland, *Journal of volcanology and geothermal research*, 22(1), 1-31.
- Bonali, F., A. Tibaldi, and C. Corazzato (2015), Sensitivity analysis of earthquake-induced static stress changes on volcanoes: the 2010 Mw 8.8 Chile earthquake, *Geophysical Journal International*, 201(3), 1868-1890.
- Bonali, F., A. Tibaldi, C. Corazzato, D. Tormey, and L. Lara (2013), Quantifying the effect of large earthquakes in promoting eruptions due to stress changes on magma pathway: the Chile case, *Tectonophysics*, 583, 54-67.
- Bonini, M., M. L. Rudolph, and M. Manga (2016), Long- and short-term triggering and modulation of mud volcano eruptions by earthquakes, *Tectonophysics*, 672, 190-211.
- Borgia, A. (1994), Dynamic basis of volcanic spreading, *Journal of Geophysical Research: Solid Earth*, 99(B9), 17791-17804.
- Borgia, A., J. Burr, W. Montero, L. D. Morales, and G. E. Alvarado (1990), Fault propagation folds induced by gravitational failure and slumping of the central Costa Rica volcanic range: Implications for large terrestrial and Martian volcanic edifices, *Journal of Geophysical Research: Solid Earth*, 95(B9), 14357-14382.

- Briggs, R. (1983), Distribution, form, and structural control of the Alexandra Volcanic Group, North Island, New Zealand, *New Zealand Journal of Geology and Geophysics*, 26(1), 47-55.
- Bryan, C., S. Sherburn, H. Bibby, S. Bannister, and A. Hurst (1999), Shallow seismicity of the central Taupo Volcanic Zone, New Zealand: its distribution and nature, *New Zealand Journal of Geology and Geophysics*, 42(4), 533-542.
- Buck, W. R., P. Einarsson, and B. Brandsdóttir (2006), Tectonic stress and magma chamber size as controls on dike propagation: Constraints from the 1975–1984 Krafla rifting episode, *Journal of Geophysical Research: Solid Earth (1978–2012)*, 111(B12).
- Bursik, M., and K. Sieh (1989), Range front faulting and volcanism in the Mono Basin, eastern California.
- Cashman, K. (1979), Evolution of Kakaramea and Maungakatote Volcanoes, Tongariro Volcanic Centre, New Zealand: A Thesis Submitted for the Degree of Master of Science with Honours (Geology) at Victoria University of Wellington, Victoria University of Wellington.
- Cassidy, J., M. Ingham, C. A. Locke, and H. Bibby (2009), Subsurface structure across the axis of the Tongariro Volcanic Centre, New Zealand, *Journal of volcanology and geothermal research*, 179(3), 233-240.
- Chesley, C., P. C. LaFemina, C. Puskas, and D. Kobayashi (2012), The 1707 Mw8.7 Hōei earthquake triggered the largest historical eruption of Mt. Fuji, *Geophysical Research Letters*, 39(24).
- Chouet, B. A. (1996), Long-period volcano seismicity: its source and use in eruption forecasting, *Nature*, 380(6572), 309-316.
- Cole, J. (1978), Andesites of the Tongariro Volcanic Centre, North Island, New Zealand, *Journal of volcanology and geothermal research*, 3(1), 121-153.
- Cole, J. (1990), Structural control and origin of volcanism in the Taupo volcanic zone, New Zealand, *Bulletin of volcanology*, 52(6), 445-459, doi:10.1007/BF00268925.
- Cole, J., and T. Hunt (1968), Basalt dikes in the Tarawera volcanic complex, New Zealand, *New Zealand Journal of Geology and Geophysics*, 11(5), 1203-1206.
- Conway, C. E., G. S. Leonard, D. B. Townsend, A. T. Calvert, C. J. Wilson, J. A. Gamble, and S. R. Eaves (2016), A high-resolution $^{40}\text{Ar}/^{39}\text{Ar}$ lava chronology and edifice construction history for Ruapehu volcano, New Zealand, *Journal of Volcanology and Geothermal Research*.
- Conway, C. E., D. B. Townsend, G. S. Leonard, C. Wilson, A. Calvert, and J. A. Gamble (2015), Lava-ice interaction on a large composite volcano: a case study from Ruapehu, New Zealand, *Bulletin of Volcanology*, 77(3), 1-18.
- Cooper, L. (2002), Hipaua Steaming Cliffs and Little Waihi Landslide, edited, Citeseer.
- Corazzato, C., L. Francalanci, M. Menna, C. Petrone, A. Renzulli, A. Tibaldi, and L. Vezzoli (2008), What controls sheet intrusion in volcanoes? Structure and petrology of the Stromboli sheet complex, Italy, *Journal of Volcanology and Geothermal Research*, 173(1), 26-54.

- Cowie, P. A., G. P. Roberts, J. M. Bull, and F. Visini (2012), Relationships between fault geometry, slip rate variability and earthquake recurrence in extensional settings, *Geophysical Journal International*, 189(1), 143-160.
- Cronin, S. J., K. Hodgson, V. Neall, A. Palmer, and J. Lecointre (1997a), 1995 Ruapehu lahars in relation to the late Holocene lahars of Whangaehu River, New Zealand, *New Zealand Journal of Geology and Geophysics*, 40(4), 507-520.
- Cronin, S. J., V. Neall, J. Lecointre, M. Hedley, and P. Loganathan (2003), Environmental hazards of fluoride in volcanic ash: a case study from Ruapehu volcano, New Zealand, *Journal of Volcanology and Geothermal Research*, 121(3), 271-291.
- Cronin, S. J., V. Neall, J. Lecointre, and A. Palmer (1997b), Changes in Whangaehu River lahar characteristics during the 1995 eruption sequence, Ruapehu volcano, New Zealand, *Journal of volcanology and geothermal research*, 76(1), 47-61.
- Cronin, S. J., V. Neall, and A. Palmer (1997c), Lahar history and hazard of the Tongariro River, northeastern Tongariro Volcanic Centre, New Zealand, *New Zealand Journal of Geology and Geophysics*, 40(3), 383-393.
- Cronin, S. J., V. Neall, A. Palmer, and R. Stewart (1997d), Methods of identifying late Quaternary rhyolitic tephra on the ring plains of Ruapehu and Tongariro volcanoes, New Zealand, *New Zealand Journal of Geology and Geophysics*, 40(2), 175-184.
- Cronin, S. J., and V. E. Neall (1997), A late Quaternary stratigraphic framework for the northeastern Ruapehu and eastern Tongariro ring plains, New Zealand, *New Zealand Journal of Geology and Geophysics*, 40(2), 185-197.
- Cronin, S. J., V. E. Neall, J. A. Lecointre, and A. S. Palmer (1996a), Unusual "snow slurry" lahars from Ruapehu volcano, New Zealand, September 1995, *Geology*, 24(12), 1107-1110.
- Cronin, S. J., V. E. Neall, and A. S. Palmer (1996b), Geological history of the northeastern ring plain of Ruapehu volcano, New Zealand, *Quaternary international*, 34, 21-28.
- Cronin, S. J., V. E. Neall, R. B. Stewart, and A. S. Palmer (1996c), A multiple-parameter approach to andesitic tephra correlation, Ruapehu volcano, New Zealand, *Journal of volcanology and geothermal research*, 72(3), 199-215.
- Danišík, M., P. Shane, A. K. Schmitt, A. Hogg, G. M. Santos, S. Storm, N. J. Evans, L. K. Fifield, and J. M. Lindsay (2012), Re-anchoring the late Pleistocene tephrochronology of New Zealand based on concordant radiocarbon ages and combined $^{238}\text{U}/^{230}\text{Th}$ disequilibrium and (U-Th)/He zircon ages, *Earth and Planetary Science Letters*, 349, 240-250.
- Darby, D. J., and C. M. Meertens (1995), Terrestrial and GPS measurements of deformation across the Taupo back arc and Hikurangi forearc regions in New Zealand, *Journal of Geophysical Research: Solid Earth*, 100(B5), 8221-8232.
- De Chabaliér, J.-B., and J.-P. Avouac (1994), Kinematics of the Asal Rift (Djibouti) determined from the deformation of Fieale Volcano, *SCIENCE-NEW YORK THEN WASHINGTON*, 1677-1677.
- de Vries, B. v. W., and O. Merle (1996), The effect of volcanic constructs on rift fault patterns, *Geology*, 24(7), 643-646.

- DeMets, C., R. G. Gordon, D. F. Argus, and S. Stein (1994), Effect of recent revisions to the geomagnetic reversal time scale on estimates of current plate motions, *Geophysical Research Letters*, 21(20), 2191-2194.
- Dmowska, R., J. R. Rice, L. C. Lovison, and D. Josell (1988), Stress transfer and seismic phenomena in coupled subduction zones during the earthquake cycle, *J. geophys. Res.*, 93, 7869-7884.
- Donoghue, S., V. Neall, and A. Palmer (1995), Stratigraphy and chronology of late Quaternary andesitic tephra deposits, Tongariro Volcanic Centre, New Zealand, *Journal of the Royal Society of New Zealand*, 25(2), 115-206.
- Donoghue, S., R. Stewart, and A. Palmer (1991), Morphology and chemistry of olivine phenocrysts of Mangamate tephra, Tongariro Volcanic Centre, New Zealand, *Journal of the Royal Society of New Zealand*, 21(3), 225-236.
- Donoghue, S. L. (1991), Late quaternary volcanic stratigraphy of the southeastern sector of the Mount Ruapehu ring plain New Zealand: a thesis presented as partial fulfilment of the requirements for the degree of Doctor of Philosophy in Soil Science.
- Donoghue, S. L., and V. E. Neall (2001), Late Quaternary constructional history of the southeastern Ruapehu ring plain, New Zealand, *New Zealand Journal of Geology and Geophysics*, 44(3), 439-466.
- Eaves, S. (2015), The glacial history of Tongariro and Ruapehu volcanoes, New Zealand.
- Eaves, S. R., A. N. Mackintosh, B. M. Anderson, A. M. Doughty, D. B. Townsend, C. E. Conway, G. Winckler, J. M. Schaefer, G. S. Leonard, and A. T. Calvert (2016), The Last Glacial Maximum in the central North Island, New Zealand: palaeoclimate inferences from glacier modelling, *Climate of the Past*, 12(4), 943-960.
- Ebinger, C., A. Ayele, D. Keir, J. Rowland, G. Yirgu, T. Wright, M. Belachew, and I. Hamling (2010), Length and timescales of rift faulting and magma intrusion: The Afar rifting cycle from 2005 to present, *Annual Review of Earth and Planetary Sciences*, 38, 439-466.
- Ebinger, C., D. Keir, A. Ayele, E. Calais, T. Wright, M. Belachew, J. Hammond, E. Campbell, and W. Buck (2008), Capturing magma intrusion and faulting processes during continental rupture: seismicity of the Dabbahu (Afar) rift, *Geophysical Journal International*, 174(3), 1138-1152.
- Ewart, A., W. Hildreth, and I. Carmichael (1975), Quaternary acid magma in New Zealand, *Contributions to mineralogy and petrology*, 51(1), 1-27.
- Ferry, M., M. Meghraoui, N. A. Karaki, M. Al-Taj, and L. Khalil (2011), Episodic behavior of the Jordan Valley section of the Dead Sea fault inferred from a 14-ka-long integrated catalog of large earthquakes, *Bulletin of the Seismological Society of America*, 101(1), 39-67.
- Fleming, C. A. (1953), *The Geology of Wanganui Subdivision: Waverly and Wanganui Sheet Districts (N137 and N138)*, Owen, Government printer.
- Fontijn, K., D. Delvaux, G. G. Ernst, M. Kervyn, E. Mbede, and P. Jacobs (2010), Tectonic control over active volcanism at a range of scales: Case of the Rungwe

Volcanic Province, SW Tanzania; and hazard implications, *Journal of African Earth Sciences*, 58(5), 764-777.

Froggatt, P. C., and D. J. Lowe (1990), A review of late Quaternary silicic and some other tephra formations from New Zealand: their stratigraphy, nomenclature, distribution, volume, and age, *New Zealand Journal of Geology and Geophysics*, 33(1), 89-109.

Fujita, E., T. Kozono, H. Ueda, Y. Kohno, S. Yoshioka, N. Toda, A. Kikuchi, and Y. Ida (2013), Stress field change around the Mount Fuji volcano magma system caused by the Tohoku megathrust earthquake, Japan, *Bulletin of volcanology*, 75(1), 1-14.

Gamble, J. A., R. C. Price, I. E. Smith, W. C. McIntosh, and N. W. Dunbar (2003), 40 Ar/39 Ar geochronology of magmatic activity, magma flux and hazards at Ruapehu volcano, Taupo Volcanic Zone, New Zealand, *Journal of volcanology and geothermal research*, 120(3), 271-287, doi:10.1016/S0377-0273(02)00407-9.

Gerst, A., and M. K. Savage (2004), Seismic anisotropy beneath Ruapehu volcano: A possible eruption forecasting tool, *Science*, 306(5701), 1543-1547.

Gómez-Vasconcelos, M., P. Villamor, S. Cronin, J. Procter, G. Kereszturi, A. Palmer, D. Townsend, G. Leonard, K. Berryman, and S. Ashraf (2016), Earthquake history at the eastern boundary of the South Taupo Volcanic Zone, New Zealand, *New Zealand Journal of Geology and Geophysics*, doi:10.1080/00288306.2016.1195757.

Graham, I., J. Cole, R. Briggs, J. Gamble, and I. Smith (1995), Petrology and petrogenesis of volcanic rocks from the Taupo Volcanic Zone: a review, *Journal of volcanology and geothermal research*, 68(1), 59-87.

Gravley, D., C. Wilson, G. Leonard, and J. Cole (2007), Double trouble: Paired ignimbrite eruptions and collateral subsidence in the Taupo Volcanic Zone, New Zealand, *Geological Society of America Bulletin*, 119(1-2), 18-30.

Gregg, D. (1960), *The geology of Tongariro subdivision*, RE Owen, Govt. Printer.

Gregg, D. (1964), Letter to the term: The term "Taupo Volcanic Zone", *New Zealand Journal of Geology and Geophysics*, 7(2), 397-397, doi:10.1080/00288306.1964.10420186.

Grindley, G. (1960), Sheet 8 Taupo-Geological Map of New Zealand 1: 250,000, *Department of Scientific and Industrial Research, Wellington, New Zealand*.

Grindley, G. W., H. J. Harrington, and B. L. Wood (1961), *The geological map of New Zealand 1: 2,000,000*, New Zealand Department of Scientific and Industrial Research.

Guba, I., and H. Mustafa (1988), Structural control of young basaltic fissure eruptions in the plateau basalt area of the Arabian Plate, northeastern Jordan, *Journal of volcanology and geothermal research*, 35(4), 319-334.

Gudmundsson, A. (1983), Form and dimensions of dykes in eastern Iceland, *Tectonophysics*, 95(3), 295-307.

Gudmundsson, A. (1995), Infrastructure and mechanics of volcanic systems in Iceland, *Journal of Volcanology and Geothermal Research*, 64(1), 1-22.

- Gudmundsson, A. (2002), Emplacement and arrest of sheets and dykes in central volcanoes, *Journal of Volcanology and Geothermal Research*, 116(3), 279-298.
- Gudmundsson, A. (2003), Surface stresses associated with arrested dykes in rift zones, *Bulletin of Volcanology*, 65(8), 606-619.
- Gudmundsson, A. (2006), How local stresses control magma-chamber ruptures, dyke injections, and eruptions in composite volcanoes, *Earth-Science Reviews*, 79(1), 1-31.
- Gudmundsson, A. (2009), Toughness and failure of volcanic edifices, *Tectonophysics*, 471(1), 27-35.
- Gudmundsson, A. (2011), Deflection of dykes into sills at discontinuities and magma-chamber formation, *Tectonophysics*, 500(1), 50-64.
- Gudmundsson, A., and S. L. Brenner (2004), How mechanical layering affects local stresses, unrests, and eruptions of volcanoes, *Geophysical Research Letters*, 31(16).
- Gudmundsson, A., L. B. Marinoni, and J. Marti (1999), Injection and arrest of dykes: implications for volcanic hazards, *Journal of Volcanology and Geothermal Research*, 88(1), 1-13.
- Gudmundsson, A., T. H. Simmenes, B. Larsen, and S. L. Philipp (2010), Effects of internal structure and local stresses on fracture propagation, deflection, and arrest in fault zones, *Journal of Structural Geology*, 32(11), 1643-1655.
- Hackett, W., and B. Houghton (1989), A facies model for a Quaternary andesitic composite volcano: Ruapehu, New Zealand, *Bulletin of volcanology*, 51(1), 51-68, doi:10.1007/BF01086761.
- Hackett, W. R., S. M. Jackson, and R. P. Smith (1996), Paleoseismology of volcanic environments, *International Geophysics*, 62, 147-181.
- Hajdas, I., D. J. Lowe, R. M. Newnham, and G. Bonani (2006), Timing of the late-glacial climate reversal in the Southern Hemisphere using high-resolution radiocarbon chronology for Kaipo bog, New Zealand, *Quaternary Research*, 65(2), 340-345.
- Hayes, G., M. Reyners, and G. Stuart (2004), The Waiouru, New Zealand, earthquake swarm: Persistent mid crustal activity near an active volcano, *Geophysical Research Letters*, 31(19).
- Head, J. W., L. Wilson, and D. K. Smith (1996), Mid-ocean ridge eruptive vent morphology and substructure: Evidence for dike widths, eruption rates, and evolution of eruptions and axial volcanic ridges, *Journal of Geophysical Research: Solid Earth (1978–2012)*, 101(B12), 28265-28280.
- Hegan, B., J. Johnson, and C. Severne (2001), Landslide risk from the Hipaua geothermal area near Waihi village at the southern end of Lake Taupo, paper presented at Engineering and Development in Hazardous Terrain: New Zealand Geotechnical Society 2001 Symposium, Christchurch, August 2001, Institution of Professional Engineers New Zealand.
- Hill, D. P. (2008), Dynamic stresses, Coulomb failure, and remote triggering, *Bulletin of the Seismological Society of America*, 98(1), 66-92.

- Hill, D. P., F. Pollitz, and C. Newhall (2002), Earthquake-volcano interactions, *Physics Today*, 55(11), 41-47.
- Hitchcock, D., and J. Cole (2007), Potential impacts of a widespread subplinian andesitic eruption from Tongariro volcano, based on a study of the Poutu Lapilli, *New Zealand Journal of Geology and Geophysics*, 50(2), 53-66.
- Hobden, B. (1997), Modelling magmatic trends in time and space: eruptive and magmatic history of Tongariro volcanic complex, *Unpublished PhD thesis, University of Canterbury*.
- Hobden, B., B. Houghton, J. Davidson, and S. Weaver (1999), Small and short-lived magma batches at composite volcanoes: time windows at Tongariro volcano, New Zealand, *Journal of the Geological Society*, 156(5), 865-868.
- Hobden, B., B. Houghton, M. Lanphere, and I. Nairn (1996), Growth of the Tongariro volcanic complex: New evidence from K-Ar age determinations, doi:10.1080/00288306.1996.9514701.
- Hochstein, M. (1995), Crustal heat transfer in the Taupo Volcanic Zone (New Zealand): comparison with other volcanic arcs and explanatory heat source models, *Journal of Volcanology and Geothermal Research*, 68(1), 117-151.
- Hochstein, M., S. Sherburn, and J. Tikku (1995), Earthquake Swarm Activity Beneath the Tokaanu-Waihi Geothermal System, Lake Taupo, New Zealand *Rep.*, Geothermal Institute and Geology Department, University of Auckland, NZ, IGNS, Wairakei, NZ.
- Hodgson, K. A. (1993), Late quaternary lahars from Mount Ruapehu in the Whangaehu River, North Island, New Zealand: a thesis presented in partial fulfilment of the requirements for the degree of Doctor of Philosophy in Soil Science at Massey University.
- Hodgson, K. A., J. A. Lecointre, and V. E. Neall (2007), Onetapu formation: the last 2000 yr of laharc activity at Ruapehu volcano, New Zealand, *New Zealand Journal of Geology and Geophysics*, 50(2), 81-99.
- Hogg, A., T. Higham, D. Lowe, J. Palmer, P. Reimer, and R. Newnham (2003), Wiggle-match date for Polynesian settlement layer (Kaharoa Tephra) of New Zealand: Antiquity.
- Hogg, A., D. J. Lowe, J. Palmer, G. Boswijk, and C. B. Ramsey (2011), Revised calendar date for the Taupo eruption derived by 14C wiggle-matching using a New Zealand kauri 14C calibration data set, *The Holocene*, 0959683611425551.
- Holden, L., L. Wallace, J. Beavan, N. Fournier, R. Cas, L. Ailleres, and D. Silcock (2015), Contemporary ground deformation in the Taupo Rift and Okataina Volcanic Centre from 1998 to 2011, measured using GPS, *Geophysical Journal International*, 202(3), 2082-2105.
- Houghton, B., C. Wilson, M. McWilliams, M. Lanphere, S. Weaver, R. Briggs, and M. Pringle (1995), Chronology and dynamics of a large silicic magmatic system: central Taupo Volcanic Zone, New Zealand, *Geology*, 23(1), 13-16.

- Huc, M., R. Hassani, and J. Chéry (1998), Large earthquake nucleation associated with stress exchange between middle and upper crust, *Geophysical Research Letters*, 25(4), 551-554.
- Hurst, A., and P. McGinty (1999), Earthquake swarms to the west of Mt Ruapehu preceding its 1995 eruption, *Journal of Volcanology and Geothermal Research*, 90(1), 19-28.
- Hurst, T., A. D. Jolly, and S. Sherburn (2014), Precursory characteristics of the seismicity before the 6 August 2012 eruption of Tongariro volcano, North Island, New Zealand, *Journal of volcanology and geothermal research*, 286, 294-302.
- Ingham, M., H. Bibby, W. Heise, K. Jones, P. Cairns, S. Dravitzki, S. Bennie, T. Caldwell, and Y. Ogawa (2009), A magnetotelluric study of Mount Ruapehu volcano, New Zealand, *Geophysical Journal International*, 179(2), 887-904.
- Ishihara, Y. (2003), Major existence of very low frequency earthquakes in background seismicity along subduction zone of south-western Japan, paper presented at AGU Fall Meeting Abstracts.
- Jellinek, A. M., and D. J. DePaolo (2003), A model for the origin of large silicic magma chambers: precursors of caldera-forming eruptions, *Bulletin of Volcanology*, 65(5), 363-381.
- Johnson, J. H., M. K. Savage, and J. Townend (2011), Distinguishing between stress-induced and structural anisotropy at Mount Ruapehu Volcano, New Zealand, *Journal of Geophysical Research: Solid Earth*, 116(B12).
- Johnston, D. M., B. F. Houghton, V. E. Neall, K. R. Ronan, and D. Paton (2000), Impacts of the 1945 and 1995–1996 Ruapehu eruptions, New Zealand: an example of increasing societal vulnerability, *Geological Society of America Bulletin*, 112(5), 720-726.
- Jolly, A., P. Jousset, J. Lyons, R. Carniel, N. Fournier, B. Fry, and C. Miller (2014), Seismo-acoustic evidence for an avalanche driven phreatic eruption through a beheaded hydrothermal system: An example from the 2012 Tongariro eruption, *Journal of volcanology and geothermal research*, 286, 331-347.
- Kanamori, H. (1983), Magnitude scale and quantification of earthquakes, *Tectonophysics*, 93(3-4), 185-199.
- Kear, D. (1964), Volcanic alignments north and west of New Zealand's central volcanic region, *New Zealand Journal of Geology and Geophysics*, 7(1), 24-44.
- Kear, D. (1993), Reflections on major North Island basement rock assemblages and on megafaults, *Journal of the Royal Society of New Zealand*, 23(1), 29-41.
- Keigler, R., J.-C. Thouret, K. A. Hodgson, V. E. Neall, J. A. Lecointre, J. N. Procter, and S. J. Cronin (2011), The Whangaehu Formation: Debris-avalanche and lahar deposits from ancestral Ruapehu volcano, New Zealand, *Geomorphology*, 133(1), 57-79.
- Kilgour, G., V. Manville, F. Della Pasqua, A. Graettinger, K. Hodgson, and G. Jolly (2010), The 25 September 2007 eruption of Mount Ruapehu, New Zealand: directed ballistics, surtseyan jets, and ice-slurry lahars, *Journal of Volcanology and Geothermal Research*, 191(1), 1-14.

- King, G. C., R. S. Stein, and J. Lin (1994), Static stress changes and the triggering of earthquakes, *Bulletin of the Seismological Society of America*, 84(3), 935-953.
- Koyama, M. (2002), Mechanical Coupling Between Volcanic Unrests and Large Earthquakes, *Journal of Geography (Chigaku Zasshi)*, 111(2), 222-232.
- Kumagai, H., B. A. Chouet, and M. Nakano (2002), Temporal evolution of a hydrothermal system in Kusatsu-Shirane Volcano, Japan, inferred from the complex frequencies of long-period events, *Journal of Geophysical Research: Solid Earth (1978–2012)*, 107(B10), ESE 9-1-ESE 9-10.
- Kurokawa, K., K. Otsuki, and T. Hasenaka (1995), Tectonic stress field and fractal distribution of volcanoes in the Michoacan-Guanajuato region of the Mexican Volcanic Belt.
- LaFemina, P. C., C. B. Connor, B. E. Hill, W. Strauch, and J. A. Saballos (2004), Magma–tectonic interactions in Nicaragua: the 1999 seismic swarm and eruption of Cerro Negro volcano, *Journal of Volcanology and Geothermal Research*, 137(1), 187-199.
- LaFemina, P. C., T. H. Dixon, R. Malservisi, T. Árnadóttir, E. Sturkell, F. Sigmundsson, and P. Einarsson (2005), Geodetic GPS measurements in south Iceland: Strain accumulation and partitioning in a propagating ridge system, *Journal of Geophysical Research: Solid Earth*, 110(B11).
- Lamarche, G., P. M. Barnes, and J. M. Bull (2006), Faulting and extension rate over the last 20,000 years in the offshore Whakatane Graben, New Zealand continental shelf, *Tectonics*, 25(4).
- Langridge, R., W. Ries, N. Litchfield, P. Villamor, R. Van Dissen, D. Barrell, M. Rattenbury, D. Heron, S. Haubrock, and D. Townsend (2016), The New Zealand Active Faults Database, *New Zealand Journal of Geology and Geophysics*, 59(1), 86-96.
- Lecointre, J., K. Hodgson, V. Neall, and S. Cronin (2004a), Lahar-triggering mechanisms and hazard at Ruapehu volcano, New Zealand, *Natural Hazards*, 31(1), 85-109.
- Lecointre, J. A., V. E. Neall, and A. S. Palmer (1998), Quaternary lahar stratigraphy of the western Ruapehu ring plain, New Zealand, *New Zealand Journal of Geology and Geophysics*, 41(3), 225-245.
- Lecointre, J. A., V. E. Neall, C. R. Wallace, and W. M. Prebble (2002), The 55-to 60-ka Te Whaiu Formation: a catastrophic, avalanche-induced, cohesive debris-flow deposit from Proto-Tongariro Volcano, New Zealand, *Bulletin of volcanology*, 63(8), 509-525.
- Lecointre, J. A., V. E. Neall, R. C. Wallace, M. B. Elliot, and R. Sparks (2004b), Late Quaternary evolution of the Rotoaira Basin, northern Tongariro ring plain, New Zealand, *New Zealand Journal of Geology and Geophysics*, 47(3), 549-565.
- Lee, J., K. Bland, D. Townsend, and P. Kamp (2011), Geology of the Hawke's Bay area, *Institute of Geological and Nuclear Sciences*, 1(250,000).
- Leonard, G., J. Begg, and C. Wilson (2010), Geology of the Rotorua Area, QMAP 1: 250000 Geological Map, *GNS Science, Lower Hutt, New Zealand*, 102.

- Leonard, G., D. Townsend, C. Wilson, D. Gravley, A. Calvert, J. Begg, D. Downs, C. Deering, and M. Rosenberg (2014), Forensic analysis of caldera volcanism: Integrating geomorphology, geochemistry, physical volcanology and geochronology to map and refine the history of Taupo Volcanic Zone., in *International Course & Workshop on Collapse Calderas.*, edited.
- Lin, J., and R. S. Stein (2004), Stress triggering in thrust and subduction earthquakes and stress interaction between the southern San Andreas and nearby thrust and strike-slip faults, *Journal of Geophysical Research: Solid Earth*, 109(B2).
- Lipman, P. W., J. P. Lockwood, R. T. Okamura, D. t. Swanson, and K. Yamashita (1985), Ground deformation associated with the 1975 magnitude-7.2 earthquake and resulting changes in activity of Kilauea volcano, Hawaii.
- Litchfield, N., R. Van Dissen, R. Sutherland, P. Barnes, S. Cox, R. Norris, R. Beavan, R. Langridge, P. Villamor, and K. Berryman (2013), A model of active faulting in New Zealand, *New Zealand Journal of Geology and Geophysics*, 57(1), 32-56.
- Lowe, D. J., M. Blaauw, A. G. Hogg, and R. M. Newnham (2013), Ages of 24 widespread tephra erupted since 30,000 years ago in New Zealand, with re-evaluation of the timing and palaeoclimatic implications of the Lateglacial cool episode recorded at Kaipo bog, *Quaternary Science Reviews*, 74, 170-194.
- Lowe, D. J., P. A. Shane, B. V. Alloway, and R. M. Newnham (2008), Fingerprints and age models for widespread New Zealand tephra marker beds erupted since 30,000 years ago: a framework for NZ-INTIMATE, *Quaternary Science Reviews*, 27(1), 95-126.
- Lube, G., E. C. Breard, S. J. Cronin, J. N. Procter, M. Brenna, A. Moebis, N. Pardo, R. B. Stewart, A. Jolly, and N. Fournier (2014), Dynamics of surges generated by hydrothermal blasts during the 6 August 2012 Te Maari eruption, Mt. Tongariro, New Zealand, *Journal of volcanology and geothermal research*, 286, 348-366.
- Lube, G., S. J. Cronin, and J. N. Procter (2009), Explaining the extreme mobility of volcanic ice-slurry flows, Ruapehu volcano, New Zealand, *Geology*, 37(1), 15-18.
- MacKinnon, T. C. (1983), Origin of the Torlesse terrane and coeval rocks, South Island, New Zealand, *Geological Society of America Bulletin*, 94(8), 967-985.
- Magee, C. (2011), Emplacement of sub-volcanic cone sheet intrusions, University of Birmingham.
- Mahony, S., L. Wallace, M. Miyoshi, P. Villamor, R. Sparks, and T. Hasenaka (2011), Volcano-tectonic interactions during rapid plate-boundary evolution in the Kyushu region, SW Japan, *Geological Society of America Bulletin*, 123(11-12), 2201-2223.
- Manconi, A., T. Walter, and F. Amelung (2007), Effects of mechanical layering on volcano deformation, *Geophysical Journal International*, 170(2), 952-958.
- Manga, M., and E. Brodsky (2006), Seismic triggering of eruptions in the far field: volcanoes and geysers, *Annu. Rev. Earth Planet. Sci.*, 34, 263-291.
- McCalpin, J. (1996), 1996, *Paleoseismology*, edited, San Diego, Academic Press.
- McCalpin, J. P. (2009), *Paleoseismology*, Academic press.

- Michetti, A. M. (2002), Stratigraphic evidence of coseismic faulting and aseismic fault creep from exploratory trenches at Mt. Etna volcano (Sicily, Italy), *Ancient Seismites*, 359, 49.
- Miller, C. A., and G. Williams-Jones (2016), Internal structure and volcanic hazard potential of Mt Tongariro, New Zealand, from 3D gravity and magnetic models, *Journal of Volcanology and Geothermal Research*, 319, 12-28.
- Miller, V., and M. Savage (2001), Changes in seismic anisotropy after volcanic eruptions: evidence from Mount Ruapehu, *Science*, 293(5538), 2231-2233.
- Miyaji, N., A. Kan'no, T. Kanamaru, and K. Mannen (2011), High-resolution reconstruction of the Hoei eruption (AD 1707) of Fuji volcano, Japan, *Journal of Volcanology and Geothermal Research*, 207(3), 113-129.
- Moebis, A., S. J. Cronin, V. E. Neall, and I. E. Smith (2011), Unravelling a complex volcanic history from fine-grained, intricate Holocene ash sequences at the Tongariro Volcanic Centre, New Zealand, *Quaternary international*, 246(1), 352-363, doi:10.1016/j.quaint.2011.05.035.
- Monaco, C., S. Catalano, O. Cocina, G. De Guidi, C. Ferlito, S. Gresta, C. Musumeci, and L. Tortorici (2005), Tectonic control on the eruptive dynamics at Mt. Etna Volcano (Sicily) during the 2001 and 2002–2003 eruptions, *Journal of Volcanology and Geothermal Research*, 144(1), 211-233.
- Moran, S., S. Stihler, and J. Power (2002), A tectonic earthquake sequence preceding the April–May 1999 eruption of Shishaldin Volcano, Alaska, *Bulletin of volcanology*, 64(8), 520-524.
- Morley, C., and N. Wonganan (2000), Normal fault displacement characteristics, with particular reference to synthetic transfer zones, Mae Moh mine, northern Thailand, *Basin Research*, 12(3-4), 307-327.
- Mortimer, N. (2004), New Zealand's geological foundations, *Gondwana Research*, 7(1), 261-272.
- Mortimer, N., R. Herzer, P. Gans, C. Laporte-Magoni, A. Calvert, and D. Bosch (2007), Oligocene–Miocene tectonic evolution of the South Fiji Basin and Northland Plateau, SW Pacific Ocean: evidence from petrology and dating of dredged rocks, *Marine Geology*, 237(1), 1-24.
- Mouslopoulou, V., A. Nicol, J. Walsh, D. Beetham, and V. Stagpoole (2008), Quaternary temporal stability of a regional strike-slip and rift fault intersection, *Journal of Structural Geology*, 30(4), 451-463.
- Mouslopoulou, V., J. J. Walsh, and A. Nicol (2009), Fault displacement rates on a range of timescales, *Earth and Planetary Science Letters*, 278(3), 186-197.
- Nairn, I., and S. Self (1978), Explosive eruptions and pyroclastic avalanches from Ngauruhoe in February 1975, *Journal of Volcanology and Geothermal Research*, 3(1-2), 39-60.
- Nairn, I., P. Shane, J. Cole, G. Leonard, S. Self, and N. Pearson (2004), Rhyolite magma processes of the ~ AD 1315 Kaharoa eruption episode, Tarawera volcano, New Zealand, *Journal of Volcanology and Geothermal Research*, 131(3), 265-294.

- Nairn, I. A., J. W. Hedenquist, P. Villamor, K. R. Berryman, and P. A. Shane (2005), The~ AD1315 Tarawera and Waioatapu eruptions, New Zealand: contemporaneous rhyolite and hydrothermal eruptions driven by an arrested basalt dike system?, *Bulletin of Volcanology*, 67(2), 186-193.
- Nairn, I. A., T. Kobayashi, and M. Nakagawa (1998), The~ 10 ka multiple vent pyroclastic eruption sequence at Tongariro Volcanic Centre, Taupo Volcanic Zone, New Zealand:: Part 1. Eruptive processes during regional extension, *Journal of volcanology and geothermal research*, 86(1), 19-44.
- Nakagawa, M., K. Wada, T. Thordarson, C. Wood, and J. Gamble (1999), Petrologic investigations of the 1995 and 1996 eruptions of Ruapehu volcano, New Zealand: formation of discrete and small magma pockets and their intermittent discharge, *Bulletin of Volcanology*, 61(1-2), 15-31.
- Nakamura, K. (1975), Volcano structure and possible mechanical correlation between volcanic eruptions and earthquakes, *Bull. Volcanol. Soc. Jpn*, 20, 229-240.
- Nakamura, K. (1977), Volcanoes as possible indicators of tectonic stress orientation—principle and proposal, *Journal of Volcanology and Geothermal Research*, 2(1), 1-16.
- Neall, V. E., and B. Alloway (2004), *Quaternary Geological Map of Taranaki, 1: 100 000*, Institute of Natural Resources, Massey University.
- Nicol, A., and L. Wallace (2007), Temporal stability of deformation rates: Comparison of geological and geodetic observations, Hikurangi subduction margin, New Zealand, *Earth and Planetary Science Letters*, 258(3), 397-413.
- Nicol, A., J. Walsh, K. Berryman, and P. Villamor (2006), Interdependence of fault displacement rates and paleoearthquakes in an active rift, *Geology*, 34(10), 865-868.
- Nicol, A., J. Walsh, P. Villamor, H. Seebeck, and K. Berryman (2010), Normal fault interactions, paleoearthquakes and growth in an active rift, *Journal of Structural Geology*, 32(8), 1101-1113.
- Nostro, C., M. Cocco, and M. E. Belardinelli (1997), Static stress changes in extensional regimes: an application to southern Apennines (Italy), *Bulletin of the Seismological Society of America*, 87(1), 234-248.
- Nostro, C., A. Piersanti, and M. Cocco (2001), Normal fault interaction caused by coseismic and postseismic stress changes, *Journal of Geophysical Research: Solid Earth (1978–2012)*, 106(B9), 19391-19410.
- Nostro, C., R. S. Stein, M. Cocco, M. E. Belardinelli, and W. Marzocchi (1998), Two-way coupling between Vesuvius eruptions and southern Apennine earthquakes, Italy, by elastic stress transfer, *Journal of Geophysical Research*, 103(24), 487-424.
- Okada, Y. (1992), Internal deformation due to shear and tensile faults in a half-space, *Bulletin of the Seismological Society of America*, 82(2), 1018-1040.
- Opheim, J. A., and A. Gudmundsson (1989), Formation and geometry of fractures, and related volcanism, of the Krafla fissure swarm, northeast Iceland, *Geological Society of America Bulletin*, 101(12), 1608-1622.
- Pallister, J. S., J. J. Major, T. C. Pierson, R. P. Hoblitt, J. B. Lowenstern, J. C. Eichelberger, L. Lara, H. Moreno, J. Muñoz, and J. M. Castro (2010), Interdisciplinary

studies of eruption at Chaitén Volcano, Chile, *Eos, Transactions American Geophysical Union*, 91(42), 381-382.

Palmer, B. A., and V. E. Neall (1989), The Murimotu Formation—9500 year old deposits of a debris avalanche and associated lahars, Mount Ruapehu, North Island, New Zealand, *New Zealand Journal of Geology and Geophysics*, 32(4), 477-486.

Paquet, F., O. Dauteuil, E. Hallot, and F. Moreau (2007), Tectonics and magma dynamics coupling in a dyke swarm of Iceland, *Journal of Structural Geology*, 29(9), 1477-1493.

Pardo, N., S. J. Cronin, K. Németh, M. Brenna, C. I. Schipper, E. Breard, J. D. White, J. Procter, B. Stewart, and J. Agustín-Flores (2014), Perils in distinguishing phreatic from phreatomagmatic ash; insights into the eruption mechanisms of the 6 August 2012 Mt. Tongariro eruption, New Zealand, *Journal of volcanology and geothermal research*, 286, 397-414.

Pardo, N., S. J. Cronin, A. S. Palmer, and K. Németh (2012), Reconstructing the largest explosive eruptions of Mt. Ruapehu, New Zealand: lithostratigraphic tools to understand subplinian–plinian eruptions at andesitic volcanoes, *Bulletin of volcanology*, 74(3), 617-640.

Patterson, D. B., and I. J. Graham (1988), Petrogenesis of andesitic lavas from Mangatepopo valley and Upper Tama lake, Tongariro volcanic centre, New Zealand, *Journal of volcanology and geothermal research*, 35(1), 17-29.

Payne, S., R. McCaffrey, R. King, and S. Kattenhorn (2012), A new interpretation of deformation rates in the Snake River Plain and adjacent basin and range regions based on GPS measurements, *Geophysical Journal International*, 189(1), 101-122.

Phillips, W. (1974), The dynamic emplacement of cone sheets, *Tectonophysics*, 24(1), 69-84.

Pillans, B., B. P. Kohn, G. Berger, P. Froggatt, G. Duller, B. Alloway, and P. Hesse (1996), Multi-method dating comparison for mid-Pleistocene Rangitawa tephra, New Zealand, *Quaternary Science Reviews*, 15(7), 641-653.

Price, R. C., J. A. Gamble, I. E. Smith, R. Maas, T. Waight, R. B. Stewart, and J. Woodhead (2012), The anatomy of an Andesite volcano: a time–stratigraphic study of andesite petrogenesis and crustal evolution at Ruapehu Volcano, New Zealand, *Journal of Petrology*, egs050, doi:10.1093/petrology/egs050.

Price, R. C., J. A. Gamble, I. E. Smith, R. B. Stewart, S. Eggins, and I. C. Wright (2005), An integrated model for the temporal evolution of andesites and rhyolites and crustal development in New Zealand's North Island, *Journal of Volcanology and Geothermal Research*, 140(1), 1-24.

Price, R. C., R. George, J. A. Gamble, S. Turner, I. E. Smith, C. Cook, B. Hobden, and A. Dosseto (2007), U–Th–Ra fractionation during crustal-level andesite formation at Ruapehu volcano, New Zealand, *Chemical Geology*, 244(3), 437-451.

Price, R. C., S. Turner, C. Cook, B. Hobden, I. E. Smith, J. A. Gamble, H. Handley, R. Maas, and A. Möbis (2010), Crustal and mantle influences and U–Th–Ra disequilibrium in andesitic lavas of Ngauruhoe volcano, New Zealand, *Chemical Geology*, 277(3), 355-373.

- Procter, J., S. Cronin, I. Fuller, M. Sheridan, V. Neall, and H. Keys (2010a), Lahar hazard assessment using Titan2D for an alluvial fan with rapidly changing geomorphology: Whangaehu River, Mt. Ruapehu, *Geomorphology*, 116(1), 162-174.
- Procter, J., S. J. Cronin, I. C. Fuller, G. Lube, and V. Manville (2010b), Quantifying the geomorphic impacts of a lake-breakout lahar, Mount Ruapehu, New Zealand, *Geology*, 38(1), 67-70.
- Procter, J., A. Zernack, K. Nemeth, S. Cronin, A. Patra, G. Leonard, G. Jolly, H. Keys, and M. Sheridan (2013), Titan2d Computer simulation and geomorphic analysis of the eruptive vents, landslide and debris flows of the 2012 Te Maari eruption from Mt. Tongariro, New Zealand, paper presented at EGU General Assembly Conference Abstracts.
- Reyners, M. (2010), Stress and strain from earthquakes at the southern termination of the Taupo Volcanic Zone, New Zealand, *Journal of Volcanology and Geothermal Research*, 190(1), 82-88.
- Roman, D. C. (2005), Numerical models of volcanotectonic earthquake triggering on non-ideally oriented faults, *Geophysical Research Letters*, 32(2).
- Roman, D. C., and K. V. Cashman (2006), The origin of volcano-tectonic earthquake swarms, *Geology*, 34(6), 457-460.
- Rössler, M. (2006), World heritage cultural landscapes: a UNESCO flagship programme 1992–2006, *Landscape Research*, 31(4), 333-353.
- Rowland, J., and R. Sibson (2001), Extensional fault kinematics within the Taupo Volcanic Zone, New Zealand: soft-linked segmentation of a continental rift system, *New Zealand Journal of Geology and Geophysics*, 44(2), 271-283.
- Rowland, J. V., C. J. Wilson, and D. M. Gravley (2010), Spatial and temporal variations in magma-assisted rifting, Taupo Volcanic Zone, New Zealand, *Journal of Volcanology and Geothermal Research*, 190(1), 89-108.
- Rubin, A. M. (1992), Dike-induced faulting and graben subsidence in volcanic rift zones, *Journal of Geophysical Research: Solid Earth (1978–2012)*, 97(B2), 1839-1858.
- Rubin, A. M., and D. D. Pollard (1988), Dike-induced faulting in rift zones of Iceland and Afar, *Geology*, 16(5), 413-417.
- Sanderson, R. W., J. Johnson, and J. Lees (2010), Ultra-long period seismic signals and cyclic deflation coincident with eruptions at Santiaguito volcano, Guatemala, *Journal of Volcanology and Geothermal Research*, 198(1), 35-44.
- Scholz, C. H. (2002), *The mechanics of earthquakes and faulting*, Cambridge university press.
- Scott, B. J., and S. H. Potter (2014), Aspects of historical eruptive activity and volcanic unrest at Mt. Tongariro, New Zealand: 1846–2013, *Journal of Volcanology and Geothermal Research*, 286, 263-276.
- Seebeck, H., and A. Nicol (2009), Dike intrusion and displacement accumulation at the intersection of the Okataina Volcanic Centre and Paeroa Fault zone, Taupo Rift, New Zealand, *Tectonophysics*, 475(3), 575-585.

- Seebeck, H., A. Nicol, T. Stern, H. Bibby, and V. Stagpoole (2010), Fault controls on the geometry and location of the Okataina Caldera, Taupo Volcanic Zone, New Zealand, *Journal of Volcanology and Geothermal Research*, 190(1), 136-151.
- Seebeck, H., A. Nicol, P. Villamor, J. Ristau, and J. Pettinga (2014), Structure and kinematics of the Taupo Rift, New Zealand, *Tectonics*, 33(6), 1178-1199.
- Shane, P., S. Martin, V. Smith, K. Beggs, M. Darragh, J. Cole, and I. Nairn (2007), Multiple rhyolite magmas and basalt injection in the 17.7 ka Rerewhakaaitu eruption episode from Tarawera volcanic complex, New Zealand, *Journal of Volcanology and Geothermal Research*, 164(1), 1-26.
- Shane, P., I. A. Nairn, V. C. Smith, M. Darragh, K. Beggs, and J. W. Cole (2008), Silicic recharge of multiple rhyolite magmas by basaltic intrusion during the 22.6 ka Okareka Eruption Episode, New Zealand, *Lithos*, 103(3), 527-549.
- Skinner, D. (1986), Neogene volcanism of the Hauraki volcanic region, *Royal society of New Zealand bulletin*, 23, 21-47.
- Spinks, K. D., V. Acocella, J. W. Cole, and K. N. Bassett (2005), Structural control of volcanism and caldera development in the transtensional Taupo Volcanic Zone, New Zealand, *Journal of Volcanology and Geothermal Research*, 144(1), 7-22.
- Stein, R. S., P. Briole, J. C. Ruegg, P. Tapponnier, and F. Gasse (1991), Contemporary, Holocene, and Quaternary deformation of the Asal Rift, Djibouti: Implications for the mechanics of slow spreading ridges, *Journal of Geophysical Research: Solid Earth*, 96(B13), 21789-21806.
- Stein, R. S., G. C. King, and J. Lin (1994), Stress triggering of the 1994 M= 6.7 Northridge, California, earthquake by its predecessors, *SCIENCE-NEW YORK THEN WASHINGTON-*, 1432-1432.
- Stipp, J. J. (1968), *The geochronology and petrogenesis of the Cenozoic volcanics of North Island, New Zealand*, Australian National University.
- Stirling, M., G. McVerry, M. Gerstenberger, N. Litchfield, R. Van Dissen, K. Berryman, P. Barnes, L. Wallace, P. Villamor, and R. Langridge (2012), National seismic hazard model for New Zealand: 2010 update, *Bulletin of the Seismological Society of America*, 102(4), 1514-1542.
- Stock, J., and P. Molnar (1982), Uncertainties in the relative positions of the Australia, Antarctica, Lord Howe, and Pacific plates since the Late Cretaceous, *Journal of Geophysical Research B*, 87(B6), 4697-4714.
- Sutherland, R. (1999), Cenozoic bending of New Zealand basement terranes and Alpine Fault displacement: a brief review, *New Zealand Journal of Geology and Geophysics*, 42(2), 295-301.
- Sykes, L. R., and M. L. Sbar (1973), Intraplate earthquakes, lithospheric stresses and the driving mechanism of plate tectonics, *Nature*, 245, 298-302.
- Tait, S., C. Jaupart, and S. Vergnolle (1989), Pressure, gas content and eruption periodicity of a shallow, crystallising magma chamber, *Earth and Planetary Science Letters*, 92(1), 107-123.

- Taylor, J. R. (1982), An introduction to error analysis: the study of uncertainties in physical measurements, *Herndon, VA: University Science*.
- Tibaldi, A. (1995), Morphology of pyroclastic cones and tectonics, *Journal of Geophysical Research: Solid Earth (1978–2012)*, 100(B12), 24521-24535.
- Toda, S., R. S. Stein, K. Richards-Dinger, and S. B. Bozkurt (2005), Forecasting the evolution of seismicity in southern California: Animations built on earthquake stress transfer, *Journal of Geophysical Research: Solid Earth*, 110(B5).
- Topping, W. (1973), Tephrostratigraphy and chronology of late Quaternary eruptives from the Tongariro Volcanic Centre, New Zealand, *New Zealand Journal of Geology and Geophysics*, 16(3), 397-423.
- Tost, M., and S. Cronin (2015), Linking distal volcanoclastic sedimentation and stratigraphy with the development of Ruapehu volcano, New Zealand, *Bulletin of Volcanology*, 77(11), 1-17.
- Tost, M., S. Cronin, J. Procter, I. Smith, V. Neall, and R. Price (2015), Impacts of catastrophic volcanic collapse on the erosion and morphology of a distal fluvial landscape: Hautapu River, Mount Ruapehu, New Zealand, *Geological Society of America Bulletin*, 127(1-2), 266-280.
- Tost, M., R. Price, S. Cronin, and I. Smith (2016), New insights into the evolution of the magmatic system of a composite andesite volcano revealed by clasts from distal mass-flow deposits: Ruapehu volcano, New Zealand, *Bulletin of Volcanology*, 78(5), 1-22.
- Townend, J., S. Sherburn, R. Arnold, C. Boese, and L. Woods (2012), Three-dimensional variations in present-day tectonic stress along the Australia–Pacific plate boundary in New Zealand, *Earth and Planetary Science Letters*, 353, 47-59.
- Townsend, D., A. Nicol, V. Mouslopoulou, J. Begg, R. Beetham, D. Clark, M. Giba, D. Heron, B. Lukovic, and A. McPherson (2010), Palaeoearthquake histories across a normal fault system in the southwest Taranaki Peninsula, New Zealand, *New Zealand Journal of Geology and Geophysics*, 53(4), 375-394.
- Townsend, D., A. Vonk, and P. Kamp (2008), Geology map of the Taranaki area: scale 1: 250 000, *Three maps and notes (36 pp.)*. Institute of Geological and Nuclear Sciences: Lower Hutt.
- Trippanera, D., J. Ruch, V. Acocella, and E. Rivalta (2015), Experiments of dike-induced deformation: Insights on the long-term evolution of divergent plate boundaries, *Journal of Geophysical Research: Solid Earth*, 120(10), 6913-6942.
- Van Dissen, R., K. Berryman, T. Webb, M. Stirling, P. Villamor, P. Wood, S. Nathan, A. Nicol, J. Begg, and D. Barrell (2003), An interim classification of New Zealand's active faults for the mitigation of surface rupture hazards, paper presented at proceedings, Pacific Conference on Earthquake Engineering, Citeseer.
- Vandergoes, M. J., A. G. Hogg, D. J. Lowe, R. M. Newnham, G. H. Denton, J. Southon, D. J. Barrell, C. J. Wilson, M. S. McGlone, and A. S. Allan (2013), A revised age for the Kawakawa/Oruanui tephra, a key marker for the Last Glacial Maximum in New Zealand, *Quaternary Science Reviews*, 74, 195-201.

- Villamor, P., and K. Berryman (2001), A late Quaternary extension rate in the Taupo Volcanic Zone, New Zealand, derived from fault slip data, *New Zealand Journal of Geology and Geophysics*, 44(2), 243-269.
- Villamor, P., and K. Berryman (2006a), Evolution of the southern termination of the Taupo Rift, New Zealand, *New Zealand Journal of Geology and Geophysics*, 49(1), 23-37.
- Villamor, P., and K. Berryman (2006b), Late Quaternary geometry and kinematics of faults at the southern termination of the Taupo Volcanic Zone, New Zealand, *New Zealand Journal of Geology and Geophysics*, 49(1), 1-21.
- Villamor, P., K. Berryman, I. Nairn, K. Wilson, N. Litchfield, and W. Ries (2011), Associations between volcanic eruptions from Okataina volcanic center and surface rupture of nearby active faults, Taupo rift, New Zealand: Insights into the nature of volcano-tectonic interactions, *Geological Society of America Bulletin*, 123(7-8), 1383-1405.
- Villamor, P., R. Van Dissen, B. V. Alloway, A. S. Palmer, and N. Litchfield (2007), The Rangipo fault, Taupo rift, New Zealand: An example of temporal slip-rate and single-event displacement variability in a volcanic environment, *Geological Society of America Bulletin*, 119(5-6), 529-547.
- Walcott, R. (1987), Geodetic strain and the deformational history of the North Island of New Zealand during the late Cainozoic, *Philosophical Transactions of the Royal Society of London A: Mathematical, Physical and Engineering Sciences*, 321(1557), 163-181.
- Wallace, L. M., J. Beavan, R. McCaffrey, and D. Darby (2004), Subduction zone coupling and tectonic block rotations in the North Island, New Zealand, *Journal of Geophysical Research: Solid Earth (1978–2012)*, 109(B12).
- Wallace, L. M., R. McCaffrey, J. Beavan, and S. Ellis (2005), Rapid microplate rotations and backarc rifting at the transition between collision and subduction, *Geology*, 33(11), 857-860.
- Walter, T., R. Wang, V. Acocella, M. Neri, H. Grosser, and J. Zschau (2009), Simultaneous magma and gas eruptions at three volcanoes in southern Italy: An earthquake trigger?, *Geology*, 37(3), 251-254.
- Walter, T., R. Wang, M. Zimmer, H. Grosser, B. Lühr, and A. Ratdomopurbo (2007), Volcanic activity influenced by tectonic earthquakes: static and dynamic stress triggering at Mt. Merapi, *Geophysical Research Letters*, 34(5).
- Walter, T. R. (2007), How a tectonic earthquake may wake up volcanoes: Stress transfer during the 1996 earthquake–eruption sequence at the Karymsky Volcanic Group, Kamchatka, *Earth and Planetary Science Letters*, 264(3), 347-359.
- Walter, T. R., and F. Amelung (2006), Volcano-earthquake interaction at Mauna Loa volcano, Hawaii, *Journal of Geophysical Research: Solid Earth (1978–2012)*, 111(B5).
- Walter, T. R., and V. R. Troll (2003), Experiments on rift zone evolution in unstable volcanic edifices, *Journal of Volcanology and Geothermal Research*, 127(1), 107-120.

- Watt, S. F., D. M. Pyle, and T. A. Mather (2009), The influence of great earthquakes on volcanic eruption rate along the Chilean subduction zone, *Earth and Planetary Science Letters*, 277(3), 399-407.
- Weldon, R., K. Scharer, T. Fumal, and G. Biasi (2004), Wrightwood and the earthquake cycle: What a long recurrence record tells us about how faults work, *GSA today*, 14(9), 4-10.
- Wells, D. L., and K. J. Coppersmith (1994), New empirical relationships among magnitude, rupture length, rupture width, rupture area, and surface displacement, *Bulletin of the seismological Society of America*, 84(4), 974-1002.
- White, S. M., J. A. Crisp, and F. J. Spera (2006), Long-term volumetric eruption rates and magma budgets, *Geochemistry, Geophysics, Geosystems*, 7(3).
- Wilson, C. (1993), Stratigraphy, chronology, styles and dynamics of late Quaternary eruptions from Taupo volcano, New Zealand, *Philosophical Transactions of the Royal Society of London A: Mathematical, Physical and Engineering Sciences*, 343(1668), 205-306.
- Wilson, C., S. Blake, B. Charlier, and A. Sutton (2006), The 26· 5 ka Oruanui eruption, Taupo volcano, New Zealand: development, characteristics and evacuation of a large rhyolitic magma body, *Journal of Petrology*, 47(1), 35-69.
- Wilson, C., D. Gravley, G. Leonard, and J. Rowland (2009), Volcanism in the central Taupo Volcanic Zone, New Zealand: tempo, styles and controls, *Studies in Volcanology: The Legacy of George Walker. Special Publications of IAVCEI*, 2, 225-247.
- Wilson, C., B. Houghton, M. McWilliams, M. Lanphere, S. Weaver, and R. Briggs (1995), Volcanic and structural evolution of Taupo Volcanic Zone, New Zealand: a review, *Journal of volcanology and geothermal research*, 68(1), 1-28.
- Wilson, C., A. Rogan, I. Smith, D. J. Northey, I. Nairn, and B. Houghton (1984), Caldera volcanoes of the Taupo volcanic zone, New Zealand, *Journal of Geophysical Research: Solid Earth*, 89(B10), 8463-8484.
- Wilson, C. J. (2001), The 26.5 ka Oruanui eruption, New Zealand: an introduction and overview, *Journal of Volcanology and Geothermal Research*, 112(1), 133-174.
- Woods, A. W., and D. M. Pyle (1997), The control of chamber geometry on triggering volcanic eruptions, *Earth and planetary science letters*, 151(3), 155-166.
- Wright, I. (1993), Pre-spread rifting and heterogeneous volcanism in the southern Havre Trough back-arc basin, *Marine Geology*, 113(3), 179-200.
- Wright, T. J., C. Ebinger, J. Biggs, A. Ayele, G. Yirgu, D. Keir, and A. Stork (2006), Magma-maintained rift segmentation at continental rupture in the 2005 Afar dyking episode, *Nature*, 442(7100), 291-294.
- Yamamoto, T., Y. Nakamura, and H. Glicken (1999), Pyroclastic density current from the 1888 phreatic eruption of Bandai volcano, NE Japan, *Journal of volcanology and geothermal research*, 90(3), 191-207.
- Zernack, A., S. Cronin, V. Neall, and J. Procter (2011), A medial to distal volcanoclastic record of an andesite stratovolcano: detailed stratigraphy of the ring-plain succession

of south-west Taranaki, New Zealand, *International Journal of Earth Sciences*, 100(8), 1937-1966.

APPENDICES

A CD accompanies the thesis and is stored in a pocket at the rear. The CD contains the following files:

Appendix A. Supplementary data

- A1. Fault Database and ArcMap shapefile
- A2. Supplementary figures
- A3. Supplementary tables
- A4. Journal publication
- A5. Extended abstract

Appendix B. Statements of contribution

This thesis contains two chapters that were published as journal articles (Chapters 4 and 5). This appendix contains two “Statements of contribution to doctoral thesis containing publications”, form DRC 16.



Figure 48. Mt. Ruapehu volcano from Waihohonu moraine (June 2014 by Agnes Samper).